No. d'ordre: 2011ISAL0048 **Année 2011**

THESE

Présentée devant

(INSTITUT NATIONAL DES SCIENCES APPLIQUEES DE LYON)

Pour obtenir

LE GRADE DE DOCTEUR

Ecole Doctorale des Sciences de l'Ingénieur de Lyon:

Mécanique, Energétique, Génie civil, Acoustique (MEGA)

Spécialité:

MECANIQUE – GENIE MECANIQUE

Par

Syed Mushtaq Ahmed SHAH

PREDICTION OF RESIDUAL STRESSES DUE TO GRINDING WITH PHASE TRANSFORMATION

Thèse soutenue le 20 juin 2011 devant la commission d'examen

Rapporteurs :

Joël RECH,	Maître de Conférences/HDR (ENISE, France)
Claire LARTIGUE ,	Professeur des Universités IUT de Cachan, Université Paris-Sud XI

Examinateurs :

Michel CORET	Maître de Conférences (INSA de Lyon, France)
Jean François RIGAL	Professeur des Universités (INSA de Lyon, France)
Pierre LAGARRIGUE	Professeur des Universités (JFC Albi France)

Directeur de thèse :

Daniel NELIAS	Professeur des Universités (INSA de Lyon, France)

LaMCoS, INSA-Lyon, CNRS UMR5259, F69621.
(Laboratoire de Mécanique des Contacts et des Structures)
20, Av. Albert Einstein, 69621 Villeurbanne Cedex, France.

INSA Direction de la Recherche-Ecoles Doctorales-Quadriennal 2011

SIGLE	ECOLE DOCTORALE	NOM ET COORDONNEES DU RESPONSABLE
CHIMIE	**CHIMIE DE LYON** **http://sakura.cpe.fr/ED206** M. Jean Marc LANCELIN Insa : R. GOURDON	M. Jean Marc LANCELIN Université Claude Bernard Lyon 1 Bât CPE 43 bd du 11 novembre 1918 69622 VILLEURBANNE Cedex Tél : 04.72.43 13 95 Fax : lancelin@hikari.cpe.fr
E.E.A.	**ELECTRONIQUE, ELECTROTECHNIQUE, AUTOMATIQUE** **http://www.insa-lyon.fr/eea** eea@ec-lyon.fr Secrétariat : M.C. HAVGOUDOUKIAN AM. 64.43 – Fax : 64.54	Gérard SCORLETTI Ecole Centrale de Lyon Bâtiment H9 36 avenue Guy de Collongue 69134 ECULLY Tél : 04.72.18 60 97 Fax : 04 78 43 37 17 Gerard.scorletti@ec-lyon.fr
E2M2	**EVOLUTION, ECOSYSTEME, MICROBIOLOGIE, MODELISATION** **http://biomserv.univ-lyon1.fr/E2M2** Insa : H. CHARLES	Gundrun BORNETTE CNRS UMR 5558 Université Claude Bernard Lyon 1 Bât G. Mendel 43 bd du 11 novembre 1918 69622 VILLEURBANNE Cédex Tél : 04.72.43.12.94 e2m2@biomserv.univ-lyon1.fr
EDISS	**INTERDISCIPLINAIRE SCIENCES-SANTE** Sec : Safia Boudjema M. Didier REVEL Insa : M. LAGARDE	M. Didier REVEL Hôpital Cardiologique de Lyon Bâtiment Central 28 Avenue Doyen Lépine 69500 BRON Tél : 04.72.68 49 09 Fax :04 72 35 49 16 Didier.revel@creatis.uni-lyon1.fr
INFOMATHS	**INFORMATIQUE ET MATHEMATIQUES** http://infomaths.univ-lyon1.fr Secrétariat : C. DAYEYAN	Johannes KELLENDONK Université Claude Bernard Lyon 1 LIRIS - INFOMATHS Bâtiment Nautibus 43 bd du 11 novembre 1918 69622 VILLEURBANNE Cedex Tél : 04.72. 43.19.05 - Fax : 04 72 43 13 10 infomaths@bat710.univ-lyon1.fr
Matériaux	**MATERIAUX DE LYON** Secrétaire : Mériem LABOUNE	Pr. Jean-Yves BUFFIERE INSA de Lyon MATEIS Bâtiment Blaise Pascal 7 avenue Jean Capelle 69621 VILLEURBANNE Cédex Tel : 04 72 43 71 70 Fax : 04 72 43 72 37 ed.materiaux@insa-lyon.fr
MEGA	**MECANIQUE, ENERGETIQUE, GENIE CIVIL, ACOUSTIQUE** Secrétariat : M. LABOUNE PM : 71.70 –Fax : 87.12	Pr. Philippe BOISSE INSA de Lyon Laboratoire de Vibrations et Acoustique Bâtiment Antoine de Saint Exupéry 25 bis avenue Jean Capelle 69621 VILLEURBANNE Cedex Tél :04.72.18.71.70 Fax : 04 72 43 72 37 mega@insa-lyon.fr Site web : http://www.ed-mega.com
ScSo	**ScSo*** M. OBADIA Lionel Insa : J.Y. TOUSSAINT	M. OBADIA Lionel Université Lyon 2 86 rue Pasteur 69365 LYON Cedex 07 Tél : 04.78.69.72.76 Fax : 04.37.28.04.48 Lionel.Obadia@univ-lyon2.fr

*ScSo : Histoire, Geographie, Aménagement, Urbanisme, Archéologie, Science politique, Sociologie, Anthropologie

To my beloved late Daughter Fatima

Acknowledgments

Taking first foot steps towards presenting new understandings is a worthy experience. The dream of this lifetime experience can not be seen without the help and support of some earnest people. I would like to express my deepest gratitude to the project director Pr. Daniel Nélias for his support, contribution and enthusiasm for this work. Indeed, I feel honoured to remain under his learned supervision. None of this would have been possible without his consistent help and valuable guidance.

I am extremely grateful to Prof. Claire LARTIGUE and Dr. Joël RECH and for accepting to be the Reviewers and dedicating their valuable time for this dissertation. I would express my appreciation for Prof Pierre LAGARRIGUE, Prof. Jean François RIGAL and Dr. Michel CORET who took interest in evaluating this work.

I owe my sincere thanks to Dr. Tarek Mubrouki and Dr. M. Zain for their generous help and fruitful suggestions during my thesis.

I would also like to express my indebtedness to Mr. Yancheng Zhang, Dr. M. A. Khan, Dr M. Asad, Dr. V. Boulcly, Dr Tanveer, Dr. Zahoor Dr. Razzaq and all others for sharing their knowledge and extending their assistance in completing this task.

I would like to acknowledge the financial assistance provided by Higher Education Commission (HEC) of Pakistan in collaboration with Government of France through an Overseas Research Scholarship Program.

I owe my appreciation to the humble favour and cooperation shown by BUET Khuzdar

Finally, I would like to take this opportunity to express my heartfelt thanks to my wife Dr. Rakhshinda for her constant encouragement cooperation and sacrifice throughout my studies. Thanks to my family members for their moral support and constant encouragement. Thanks to my beloved daughter Alvina and love to my newborn son Muhammad.

I will not say I failed 1000 times, I will say that I discovered 1000 ways that can cause failure.

Thomas Alva Edison

Abstract

Grinding is a commonly used finishing process to produce components of desired shape, size and dimensional accuracy. The ultimate goal is to have the maximum workpiece quality, minimum machining time and high economic efficiency by making a selective adaptation of the possible process strategy and chosen parameter selection. The focus of this study arose from a limitation that challenges the grinding industry. The production rate of the ground parts is generally constrained by surface topography and subsurface damage appearing as residual tensile stress, localized burns, and phase transformation induced micro and macro-cracking. This damage may reduce the life of critical components that are often subjected to severe working conditions with repeated loading and vibrations. To explore the influence of the grinding conditions and workmaterial properties on the nature of residual stresses, a full understanding of the grinding stress history in relation to the grinding parameters and the workpiece properties is required. This motivates the need for a reliable numerical modelling to simulate the grinding process. The numerical model sought should be able to predict not only the required grinding residual stresses but also the deformation history, because irreversible strains are caused by the coupling of: (1) material non-linearity (i.e. stress-strain and/or strain rate relations), (2) geometrical non-linearity due to large strains, (3) non-linearity introduced by the contact between the grinding wheel and the workpiece, and (4) the dependence of material properties on temperature.

The objective of this thesis is to build up a reliable finite element model for grinding-induced residual stress analysis and thus to explore thoroughly the mechanisms in terms of grinding conditions. Specifically, the following points are taken into consideration:

1. investigate the grinding temperature in relation to thermal grinding parameters and thermal workmaterial properties (for AISI 52100 bearing steel here),
2. predict different phase transformations at a given temperature history
3. study the residual stresses due to thermal loading including the effect of phase change,
4. analyze the mechanically induced residual stresses under iso-thermal grinding conditions,
5. couple individual effects involved in grinding and

6. discuss the favourable grinding conditions for beneficial residual stresses.

To overcome the mathematical modelling difficulties, a model buidt with Abaqus®/Standard, a well-known finite element method commercial package, is developped to account for various physics involved in the simulation of the grinding process. Material behavior is defined in various user subroutines such as: PHASE, PROP, UEXPAN and UMAT. UMAT and UEXPAN are special purpose user sub-routines available in Abaqus for defining the materials constitutive behaviour and expansion coefficient, respectively; PHASE and PROP have been written separately to calculate the time and temperature dependent phase proportions and their effects on the thermo-mechanical properties, respectively. The temperature field arising due to the moving heat source are obtained with the user subroutine DFLUX which is used to predict phase transformations and subsequently the martensite depth. In order to solve the non-linear problem arising from the contact between the grinding wheel and the workpiece an equivalent grinding contact traction profile with a normal pressure and a tangential shear stress are applied through the Abaqus® /Standard user subroutines DLOAD and UTRACLOAD, respectively. To simplify the problem a step by step procedure is followed for the analysis where each phenomenon involved in the grinding process (thermal, phase transformation and mechanical) is described separately and then sequentially coupling of the three is presented at the end. The variations of the residual stresses and strains at integration points have been examined, and the effects of the friction coefficient (μ), Peclet number (Pe), non dimensional heat transfer coefficient (H) and different magnitudes of input heat flux (Q) on both the microstructure and the residual stress state are analyzed. Finally, based on the new findings in this research, a more comprehensive methodology is suggested for further study.

Keywords: Grinding process, modelling and simulation, finite element, thermal analysis, mechanical analysis, phase transformation, grinding parameters, residual stress, umat user subroutine, AISI 52100 (100Cr6) steel.

Résumé

La rectification est un procédé couramment utilisé dans l'industrie pour la finition des surfaces. L'optimisation du procédé consiste à trouver un compromis entre la qualité des pièces, minimiser les temps d'usinage et augmenter l'efficacité énergétique grâce au choix judicieux des paramètres de rectification. Par ailleurs le taux de production des pièces rectifiées est souvent limité par des contraintes sur la topographie de la surface et des problèmes liés à l'apparition de brûlures de rectification ou de micro-fissures à la surface des pièces. Ces défauts d'aspect engendrent généralement, lorsqu'ils concernent une surface fonctionnelle, une réduction de la durée de vie du composant ainsi rectifié.'effet des conditions de rectification et des propriétés des matériaux sur la nature des contraintes résiduelles a été analysé par modélisation numérique. Le modèle élément finis permet la prédiction non seulement des contraintes résiduelles, mais aussi des phases en présence et des déformations associées. Ces déformations sont induites par un couplage entre quatre phénomènes : (1) la non linéarité du comportement du matériau (viscoélastoplasticité), (2) la non linéarité géométrique en raison des grandes déformations locales, (3) la non linéarité introduite par le contact entre la meule et la pièce, et (4) la dépendance des propriétés des matériaux à la température. L'objectif de cette étude est de construire un modèle numérique fiable en se basant sur la méthode des éléments finis pour analyser les contraintes résiduelles induites par la rectification et d'explorer, par conséquent, les mécanismes en termes de conditions de rectification. Plus précisément, les points suivants sont abordés :

2 étudier la distribution de la température en fonction des paramètres thermiques liés au procédé de rectification et des propriétés thermiques du matériau rectifié (100Cr6 ici),

3 prédire les différentes transformations de phase en fonction de l'histoire thermique vue par le matériau (en chaque point),

4 étudier les contraintes résiduelles pour les conditions de chargement thermique, y compris en présence de changement de phase,

5 analyser les contraintes résiduelles induites mécaniquement sous des conditions isothermes de rectification,

6 couplage des effets thermiques, mécaniques et métallurgiques dans la prédiction des contraintes résiduelles et

7 proposer les conditions optimales pour la rectification, notamment en terme de contraintes résiduelles.

Le modèle éléments finis a été construit avec le logiciel commercial, Abaqus ® / Standard. Le comportement du matériau étudié (100Cr6) a été défini dans les routines utilisateurs PHASE, PROP, UEXPAN et UMAT. Les routines UMAT et UEXPAN sont disponibles de base dans Abaqus. Elles permettent de définir la loi de comportement des matériaux et le coefficient de dilatation thermique, respectivement. Les routines utilisateurs PHASE et PROP ont été développées pour calculer la proportion des phases en fonction du temps et de la température et leurs effets sur les propriétés thermomécaniques, respectivement. Les températures dues à une source de chaleur en mouvement sont obtenues avec la sub-routine utilisateur DFLUX qui est exploitée pour prévoir la transformation de phase et ensuite la profondeur de la couche martensitique. Afin de simplifier le problème de non linéarité provenant du contact de la meule avec la pièce, un chargement normal et tangentiel de type contact de Hertz a été ajouté aux travers des routines DLOAD et UTRACLOAD. Pour simplifier le problème, deux étapes ont été adoptées. La première consiste à suivre une procédure étudiant séparément les trois phénomènes apparaissant dans le processus de rectification (effets thermiques, les transformations de phase et les effets mécaniques). Les effets ont ensuite été couplés.

La variation des contraintes résiduelles et des déformations aux points d'intégration a été analysée. Les effets du coefficient de frottement (μ), du nombre de Peclet (Pe), de la conductance de paroi (H) et du flux de chaleur (Q) sur la microstructure et l'état de contraintes résiduelles ont été analysés. Enfin, sur la base des nouveaux résultats de ce travail de recherche, une méthodologie plus complète est proposée pour la suite.

Mots clefs : Rectification, simulation numérique, éléments finis, analyse thermique, analyse mécanique, transformation de phase, paramètres de rectification, contraintes résiduelles, subroutine utilisateur UMAT, acier AISI 52100 (100Cr6)

Contents

List of figures

List of tables

Nomenclature

Grinding parameters

Symbol	*Units*	*Significance*
a_p	[m]	Depth of cut
b	[m]	Width of cut
D_e	[m]	Equivalent diameter
D_s	[m]	Diameter of grinding wheel
D_w	[m]	Diameter of workpiece (for cylindrical grinding)
F_t	[N]	Tangential force
F_t'	[N/m]	Specific tangential force
F_{t_o}'	[N/m]	Specific tangential force for h_{eq}=1
F_n	[N]	Normal force
F_n'	[N/m]	Specific Normal force
f	[m/sec]	Feed
h_{eq}	[m]	Equivalent chip thickness
L_c	[m]	Length of grinding zone /Contact length
N_s	[Rev/min]	Grinding wheel rotational velocity
N_w	[Rev/min]	Workpiece rotational velocity (cylindrical grinding)
n	-	Exponent of h_{eq}
V_c	[m/sec]	Cutting speed
V_f	[m/sec]	Feed rate
V_s	[m/sec]	Grinding wheel velocity
V_w	[m/sec]	Workpiece velocity
Z	[mm^3/sec]	Chip depostion
Z′	[mm^2/sec]	Specific chip deposition

Thermal Parameters

Symbol	*Units*	*Significance*
α_w	[m^2/sec]	thermal diffusivity of the work material
c_p	[J/kg-°C]	specific heat capacity
h_{conv}	[W/m^2-°C]	Convective heat transfer coefficient
K	[W/m-°C]	thermal conductivity
k_w	-	heat intensity distribution factor
k_v	-	energy dissipation
T	[°C]	temperature
T_o	[°C]	Ambient temperature
T_{ref}	[°C]	reference temperature
T_{max}	[°C]	Maximum surface temperature
ζ_{fact}		Temperature softening multiplier

Mechanical Parameters

Symbol	*Units*	*Significance*
E	[GPa]	Young's Modulus
σ	[MPa]	stress
σ_y^g	[MPa]	Global yield stress of the material
ε		Strain
$\dot{\varepsilon}$		Strain rate
μ		Friction coefficient
υ		Poisson's coefficient

Metallurgical Parameters

Symbol	*Units*	*Significance*
α_α	-	thermal expansion coefficient of alpha phase
α_γ	-	thermal expansion coefficient of gamma phase
β	-	material constant
ε_α^{th}	-	thermal strain of alpha phase
ε_γ^{th}	-	thermal strain of gamma phase
$\Delta\varepsilon_{\alpha\gamma}^{25°C}$	-	thermal strain difference between two phases
C_{z_i}	[N/m^2]	Strength multiplier of the phase *i*
κ_i	-	Empirically obtained constant for the phase *i*
M_s	[°C]	martensite start temperature
n_i	-	Empirically obtained constant for the phase *i*
σ_y^α	[N/m^2]	Yield stress of alpha (ferrite) phase
σ_y^γ	[N/m^2]	Yield stress of gamma (austenite) phase
T_s	[°C]	Transformation start temperature for a phase consitituent
T_f	[°C]	Transformation finish temperature for a phase consitituent
$\dot{T}_L^i$	[°C]	Lower critical cooling rate of phase *i*
$\dot{T}_U^i$	[°C]	Upper critical cooling rate of phase *i*
$\dot{T}$	[°C/sec]	Cooling rate
T_{aus}	[°C]	Austenizing temperature
t_o	[*sec*]	Equivalent transformation time
t_s	[*sec*]	Time when an assumed small portion of phase has transformed
t_e	[*sec*]	Time when assumed equivalent proportion of phase has transformed
z		Phase fraction
z_i		Average phase fraction of constituent *i*
z_i^{eq}		Equilibrium fraction of phase *i* that is achieved after an infinite long time
z_γ		Austenite phase fraction
z_M		Martensite phase fraction

Numerical simulations

Symbol	*Units*	*Significance*
d	$[m]$	specimen depth related to y direction
E^{thm}		thermal strain
ε_{xx}		Longitudinal strain
$(\varepsilon_{xx})_T$		Longitudinal thermal strain
$\dot{\varepsilon}_{ij}^{e}$		Elastic strain rate
$\dot{\varepsilon}_{ij}$		Total strain rate
$\dot{\varepsilon}_{ij}^{p}$		Plastic strain rate
$\bar{\varepsilon}^{pl}$		Equivalent plastic strain
$\dot{\bar{\varepsilon}}^{pl}$		Equivalent plastic strain rate
m		Strain rate sensitivity factor
H_m		Hardening parameter
P	[N/m²]	Normal distributed pressure applied through subroutine DLOAD on the workpiece
P_α	[N/m²]	Tangential traction applied through subroutine UTRACLOAD on the surface of the workpiece
σ_{xx}		Longitudinal stress MPa
x ,y		x and y coordinates fixed to workpiece

Non-dimensional parameters

Pe	Peclet Number	$Pe = \frac{V_w L_c}{4\alpha_w}$
H	Non-dimensional heat transfer coefficient	$H = \frac{2h\alpha_w}{KV_w}$
T′	Non-dimensional Temperature	$T' = \frac{T}{\left(\frac{QL_c}{2K}\right)}$
t′	Non-dimensional time	$t' = \frac{V_w^2 t}{2\alpha}$
	Non-dimensional longitudinal distance along workpiece	$= \frac{2x}{L_c}$
	Non-dimensional distance along depth of the workpiece	$= \frac{2y}{L_c} = \frac{2d}{L_c}$

CHAPTER 1

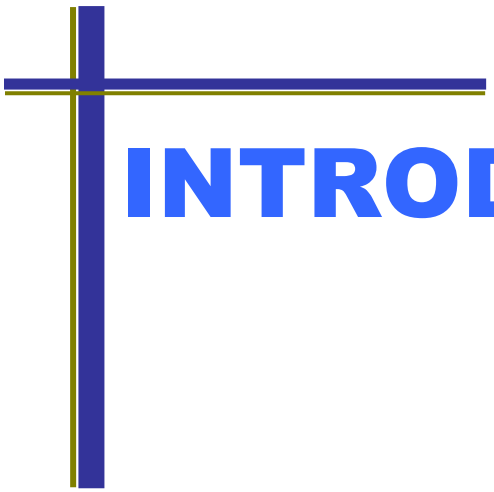

INTRODUCTION

1

1.1 Introduction

May be due to the complex nature of grinding process the literary phrases like “To put your nose to the grind stone”, or “It was a real grind at work today” or may be “To grind to a halt” are came into daily usage, well this is exactly what this thesis is all about; “Grinding”. Grinding as defined by the Webster’s dictionary is “To reduce to small fragments by friction”, but this type of material removal process is not small in a commercial sense, as it is a billion dollar growth industry that accounts for approximately 25% of all machining operations in manufacturing [MALK89]. Grinding is a commonly used finishing process to produce components of desired shape, size and dimensional accuracy where the ultimate goal is to have the maximum workpiece quality, minimum machining time and high energetic efficiency by making a selective adaptation of the possible process strategy and chosen parameter selection. The focus of this study arose from a limitation that challenges the grinding industry. The production rate of ground parts is generally constrained by surface topography and surface and near surface damages such as burns and micro and macro-cracking induced by phase transformations and residual stresses. These types of damage may reduce the life of critical components that are often subjected to severe working conditions with repeated loading and vibrations. Subsurface damage is termed in industry as *“thermal damage”*. In 1960 term *“surface integrity”* was coined by Field [FIEL64] to describe the overall condition of the surface and this sentence includes both surface topography and subsurface or near-surface damage.

The importance of surface integrity depends upon its impact on the product performances [SHAW96] such as: fracture strength, fatigue strength, corrosion rate, stress corrosion cracking, wear, magnetic properties, dimensional stability and so on. Surface integrity includes all aspects related to the quality of surfaces such as surface finish, metallurgical damage, and residual stresses [FIEL64]. The importance of surface integrity may arise, for instance, in some

applications in which the orientation of the grinding scratches relative to the loading of the surface plays an important role in the fracture strength of the ground surface. For example, a tensile loading stress across the loading direction brings about lower fracture strength compared with that along the loading direction. As a second aspect of the surface integrity, metallurgical damage is characterized by change of microstructure, change in surface hardness, and the presence of micro cracks in very brittle material or by change in fatigue strength, fracture strength, stress corrosion cracking, or the rate of wear. One cause of the change of surface hardness is due to phase transformation under a critical temperature history. For instance, phase transformation may be formed by austenizing and quenching of steel ground components. The third aspect of surface integrity, i.e. residual stresses, is related to fracture strength, fatigue strength, corrosion resistance, wear resistance and dimensional stability, and is coupled with metallurgical characteristics of the workpiece material. Therefore, the development of residual stress in ground components must be fully understood.

1.2 Causes of Residual Stresses Induced by Grinding

In general, ground components, such as gears, bearings and cams, are subjected to external loads of thermal and mechanical origins during grinding, resulting in residual stresses. The nature of the residual stresses depends to a great extent on the manufacturing processes required to produce the final product.

To achieve final dimensional accuracy, unwanted material needs to be ground and thus removed. As a final material removal process, a grinding operation involves abrasive grains and workpiece interaction, which results in contact forces that lead to different deformation mechanisms such as (1) work material removal characterized by separation of surface layers and formation of chips, (2) ploughing of the ground surface recognized as the generation of grooves and side ridges and (3) surface rubbing. The details of the interaction forces between the grinding wheel and the workpiece are reflected by the grinding conditions described by dimensional and non-dimensional parameters such as grinding wheel speed, table speed, depth of cut and thus the apparent inter contact zone between the grinding wheel and the workpiece.

In contrast to other material removal processes, a grinding operation requires more energy to remove the same material volume and thus has a higher specific energy. This indeed results in high generation of heat energy. The level of heat generated depends not only on the interaction forces within the grinding zone but also on the plastic deformation mechanism associated with the material removal process, the table speed and the grinding wheel speed. Consequently, the workpiece temperature rises to a level governed by its thermal properties and the grinding conditions. As the workpiece moves with table speed, the grinding temperature starts to decrease due to the cooling effect and thermal energy diffusion into the workpiece. As a result, the workpiece experiences complex thermal strains and stresses; the level of which may result in critical effective stresses above which the workpiece may undergo plastic strain.

With a critical grinding temperature history, phase transformation may be initiated. To be more specific, phase transformation in steel may take place if the is austenitized and cooled very rapidly. For a given steel alloy, the austenitizing temperature and the critical cooling rate associated with phase change are mainly workpiece composition dependent. Phase transformation is characterized by volume growth and hardness increase the mechanisms of which are related to workmaterial composition and the cooling rate of the grinding temperature history. The surface volume growth may result in compressive residual stresses while the hardness increase leads to higher levels of residual stresses in grinding.

Phase transformation is usually associated with thermal and plastic strains. The mechanical residual stresses are dominant in iso-thermal grinding processes or when the grinding temperature is relatively low. Thermal residual stresses, on the other hand, are mainly generated when the specific energy of material removal is very high as for grinding conditions with very high wheel speed and very low depth of cut. The combined effects of the residual stress sources may arise in some grinding conditions characterized by medium depth of cut, high wheel and table speed. It should be noted that the nature of residual stresses depends to a great extent, on the mechanisms of residual stresses and workmaterial properties.

In summary, the key causes of residual stress mechanisms are (1) residual stresses induced under iso-thermal mechanical grinding conditions, (2) residual stresses due to the grinding zone heat energy and temperature rise, and (3) residual stresses associated with phase transformation due to critical grinding temperature history.

1.3 Determination of Grinding Residual Stresses

Various methods for determining residual stresses have been developed over the last few decades and can be classified as destructive methods, such as the indentation hardness test, semi-destructive methods such as the combined layer removal and the X-ray diffraction measurement, and non-destructive methods such as X-ray and acoustic emission (AE) methods. The destructive methods are easy to implement. However they can only be used to estimate the maximum fatigue load of a ground part. Added to this, the tested element cannot be of further practical use. Non-destructive methods, on the other hand, are more powerful in terms of their accuracy and speed and more economical in the light of production strategies as they produce damage free tested workmaterial. Unfortunately, the limitation of the above methods in surface residual stresses measurement needs to be resolved by improving the available techniques for a more reliable residual stresses determination.

Although the above methods are useful practical tools for residual stress investigation they cannot explore the residual stress mechanisms, therefore they are said to be post-grinding measurement techniques. Hence predictive techniques are required to analyze the mechanical and/or the thermal deformation associated with a grinding process thus providing in advance useful guidelines for controlling and minimization of severe residual stress effect on ground products. This needs careful theoretical simulation of a given grinding operation in terms of grinding conditions and workmaterial properties by suitable numerical methods such as the finite element method (FEM) and the finite difference method (FDM). However, due to the nature of deformation mechanisms and the workmaterial properties associated with grinding mechanisms, the finite element method is found to be one of the best modelling tools. Therefore most of the mathematical models used were based on FEM.

The complex force interaction between the grinding wheel and the workpiece makes the grinding process very difficult to be modelled. Added to that, temperature rise during grinding chip formation is also difficult to control and thus the introduction of a suitable cooling (and lubricating) fluid becomes demanding.

The above complexity indicates that much attention should be paid to the following aspects: (1) grinding temperature, (2) modelling of the heat source generated by grinding, (3) modelling of cooling and (4) modelling of associated phase transformations due to high temperature rise, (5) modelling of the contact mechanism between the grinding wheel and the workpiece. The last can be simplified by removing the grinding wheel and substituting an equivalent grinding force profile. By this the non-linearity problem arising from the contact of the grinding wheel and workpiece can be resolved.

1.4 Aims and objectives of the thesis

As discussed before, in order to meet the requirement of smooth surfaces (as far as possible) or accurate dimensions in applications, machine elements need to be ground but at the cost of an unavoidable residual stress formation. To explore the influence of grinding conditions and workmaterial properties on the nature of residual stresses, a full understanding of the grinding stress history in relation to the grinding parameters and the workpiece properties is required. This motivates the need for a reliable mathematical modelling to simulate the grinding processes. The mathematical models sought should be able to predict not only the required grinding residual stresses but also the strain history, because irreversible strains are caused by the coupling of: (1) material non-linearity (i.e. stress-strain and/or strain rate relations), (2) geometrical non-linearity due to large strain, (3) non-linearity introduced by the boundary conditions characterized by the mutual contact between the grinding wheel and the workpiece, and (4) the dependence of material properties on temperature.

The objective of this thesis is to build up a reliable finite element model for grinding-induced residual stress analysis and thus to explore thoroughly the mechanisms in terms of grinding conditions. Specifically, it will

1. investigate the grinding temperature in relation to thermal grinding parameters and thermal workmaterial properties,
2. predict different phase transformations at a given temperature history
3. study the thermal residual stresses including the effect of phase change,
4. analyze the mechanically induced residual stresses under iso-thermal grinding conditions,
5. combine the individual effects of grinding condition coupling on residual stress distributions and
6. discuss the favourable grinding conditions for beneficial residual stresses.

To overcome the mathematical modelling difficulties, Abaqus® /Standard, a well-known finite element method commercial package, will be implemented to account for numerical calculations and associated solution convergence. Material behavior will be defined in subroutines, PHASE, PROP, UEXPAN and UMAT. Moreover, UMAT and UEXPAN are special purpose routines available in Abaqus for defining materials constitutive behavior and user expansion coefficient respectively; however PHASE and PROP are written separately to calculate time and temperature dependent phase proportions and their effect on thermo-mechanical properties respectively. The temperatures arising due to moving heat source are obtained with user subroutine DFLUX which are used to predict the phase transformation and subsequently martensite depth. In order to resolve the non-linearity problem arising from the contact of the grinding wheel and workpiece an equivalent grinding force profile and a tangential stress traction are substituted through the Abaqus® /Standard user subroutines DLOAD and UTRACLOAD respectively.

1.5 Dissertation – At a glance

For clear and comprehensive presentation of the work, manuscript is organized in six chapters as outlined succinctly in the following:

Chapter 1 describes the context and the historical background of the problem under investigation. The development of residual stresses in the ground components is explained. A

brief introduction is given about the motive and need for a reliable mathematical modelling to simulate the grinding process.

Chapter 2 reviews some basic concepts of grinding process and provide a literature review on grinding process and the finite element modelling of grinding process.

Chapter 3 gives an account of the review on phase transformation phenomena. Various phase transformation models, several multiphase models are introduced in details. A multiphase transformation model, formulated in Abaqus® /Standard via a user subroutine PHASE to study the multiphase transformation during heating and cooling is also presented to verify the metallurgical model to be used for subsequent grinding process modeling.

Chapter 4 discusses the development of Finite Element (FE) models. Coupled thermal-displacement analyses are performed to simulate grinding process. Heat source models are defined to integrate the heat flux. Simulations to study thermal, mechanical and phase transformation effects on residual stresses and the simulations involving coupled phenomena are performed.

Chapter 5 outlines the interpretation and discussion of the numerical simulations. Based on numerical results, the development and distribution of residual stresses including phase transformations are described. Effect of different grinding parameters on temperature histories, phase transformation, and the subsequent effects on surface integrity of the material are described.

Chapter 6 summarizes a general conclusion outlining the major points of this dissertation and a discussion of possible avenues in future as a continuation of this research work.

CHAPTER 2

GRINDING FROM CRAFT TO SCIENCE

2

2.1 Grinding from craft to science

Grinding is a common collective name for machining which utilizes hard abrasive particles as cutting medium. The grinding process of shaping materials is probably the oldest in existence and can be traced back in Neolithic times [WOOD59] when man found that he could sharpen his tools by rubbing them against gritty rocks. The grinding wheel originated in ancient Egypt in association with the beginnings of metallurgy [MALK89]. Early concepts of grinding machine appear in the drawings of Leonardo Da Vinci dating from about the year 1500 and it took another 300-400 years until some of the grinding machine concepts envisioned by Leonardo Da Vinci were put into practice [MALK89].

Despite the fact that this process is known for a long time, its industrial application as it exists today has emerged in the late nineteenth century. The 20th century saw the burgeoning of grinding as a modern process. Seminal publications by Alden and Guest started the process of bringing the art of grinding into a scientific basis [ALDE14] [GUES15].

Modern Technology has brought about innovative changes in grinding process. Faster grinding wheel speeds and improved grinding wheel technology have allowed greatly increased removal rates. New grinding fluids and method of delivering fluids have also been introduced to achieve higher removal rates while maintaining quality. With all its technological advancements grinding is not a process without its share problems. Problems experienced may include thermal damage, rough surfaces, surface integrity problems etc. Overcoming these problems quickly and efficiently is helped by a correct understanding of the interplay of factors in grinding, which is the main theme of this manuscript.

2.2 Definition

Grinding is a process which utilizes various tiny and hard abrasive particles formed in a binder as a multitude of cutting edges to continuously remove unwanted material on a workpiece at very high speeds. The chips produced by grinding are therefore very small, by about two orders of magnitude smaller compared to other cutting operations [KALP97]. That's why grinding is considered as a major process which has the advantage over most precision machining operations in the production of components requiring smooth surfaces and fine tolerances [KALP97] [MALK89] [SHAW96]. Most grinding processes are similar; however, the operation may vary according to the wheel shape, motions, etc. During the process an abrasive surface is pressed against the workpiece and then, by moving either the abrasive surface or the workpiece, material is removed by mechanical action of irregularly shaped abrasive grains in all grinding operations. **Figure 2.1** illustrates the basic grinding operation. Six basic elements are involved [MARI07]:

- The workpiece: material, shape hardness, speed, stiffness, thermal and chemical properties
- The Abrasive tool: structure, hardness, speed, stiffness, thermal and chemical properties, grain size, and bonding
- The geometry and motions governing the engagement between the abrasive tool and the workpiece (kinematics)
- The process fluid: flow rate, velocity, pressure physical, chemical and thermal properties
- The atmospheric environment
- The machine accuracy, stiffness, temperature, stability, vibrations

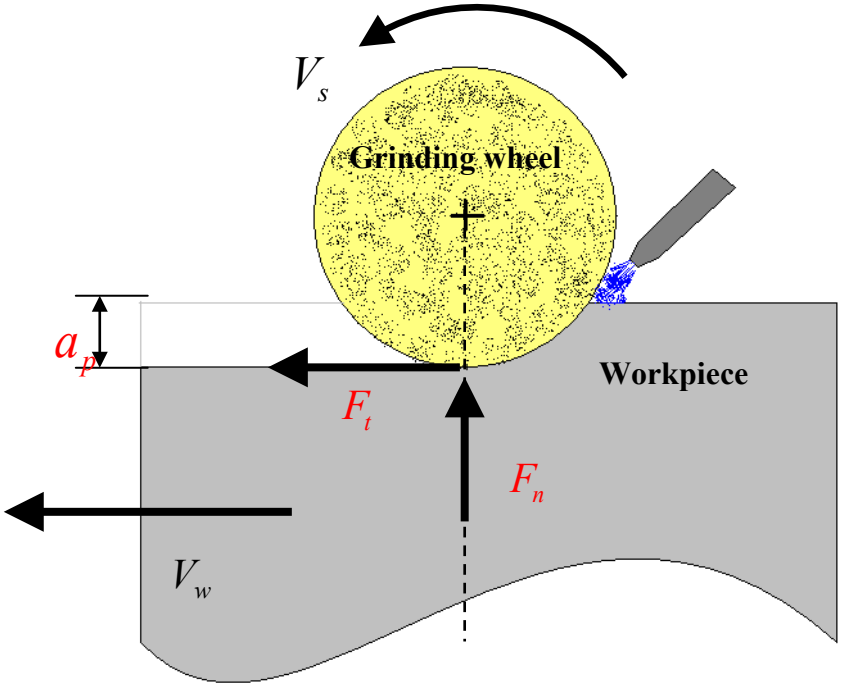

Figure 2.1 Basic grinding elements

2.3 Four Basic Grinding operations:

Four basic grinding processes are illustrated in **Figure 2.2** which shows examples of peripheral grinding of flat and cylindrical surfaces. A full description of grinding operations commonly employed is rather more complex and for details the reader is referred to [MARI07]. In **Figure 2.2** (a) distinction is drawn between grinding with the face of the grinding wheel, known as face grinding and grinding with the periphery of the wheel known as peripheral grinding. Surface grinding usually refers to grinding flat or profiled surfaces with linear motion. Cylindrical grinding refers to grinding a rotating workpiece. Cylindrical grinding may be employed internally or externally. In practice, the range of possible grinding process is large and includes number of profiles generating operations, viz. slitting and grooving. Profiling processes include grinding spiral flutes, screw threads, spur gears and helical gears using methods similar to gear cutting, shaping, planing or hobbing with cutting tools. In this manuscript, only the surface grinding is discussed. The main parameters are shown in **Figure 2.1**. In surface grinding the workpiece is usually fixed on the table of the grinding machine which performs a translational motion as shown in **Figure 2.1**. In this work, a particular case is dealt where the wheel is large compared to the workpiece.

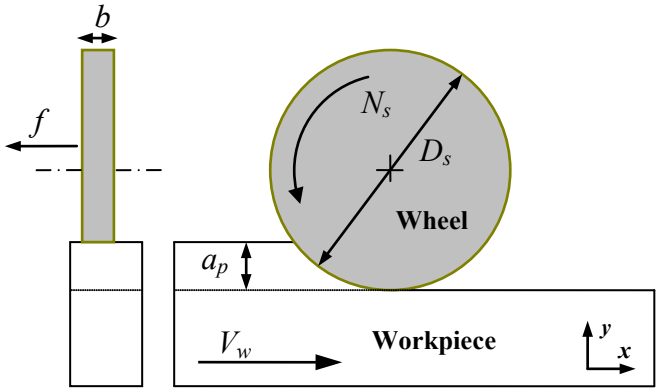

(a) Peripheral surface grinding

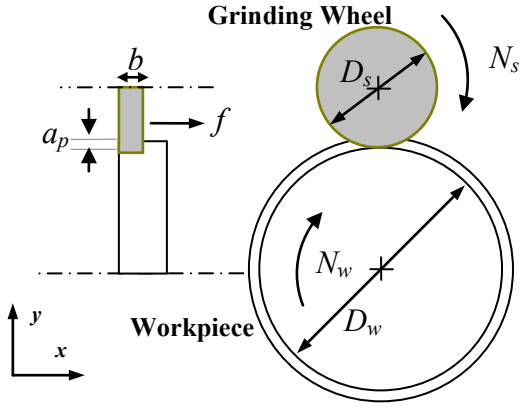

(b) Peripheral cylindrical grinding

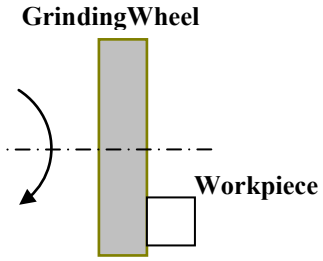

(c) Face surface grinding

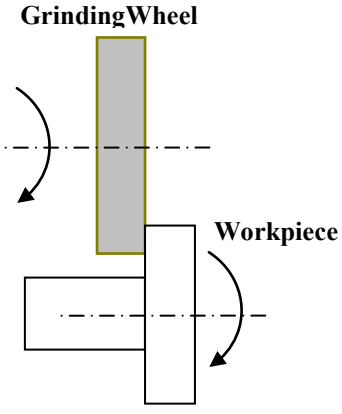

(d) Face cylindrical grinding

Figure 2.2 Examples of four grinding operations using straight wheels

2.4 Process Parameters:

This section aims at presenting all the parameters appearing in grinding process and many of them will be used frequently in the subsequent discussion. These parameters are very well developed in previous works [TANG85] [MALK89] [HAMD00] and can be classified as:

- *main parameters or machine parameters* - that can be directly controlled by the operator
- *secondary parameters or calculated* – which are derived directly by calculating main parameters.
- *Random parameters* - which are difficult to control and may affect the surface integrity of workpiece.

The main parameters that can be found in **Figure 2.1** are as under

- Grinding wheel speed $V_s = \pi.N_s.D_s$ $[m.s^{-1}]$;
- Grinding wheel peripheral speed N_s $[Rev.s^{-1}]$
- Workpiece speed V_w $[m.s^{-1}]$; often given in $[m.min^{-1}]$;
- Workpiece peripheral speed (for cylindrical grinding) N_w $[Rev.s^{-1}]$
- Depth of cut a_p $[m]$; often given in $[mm]$ or $[\mu m]$;
- Width of cut b $[m]$;
- Feed f $[m.s^{-1}]$. It is often customary to give in $[mm.min^{-1}]$ or $[mm.revolution^{-1}]$ depending on grinding type
- Type of work given as up or down grinding. A grinding process can be classified as either an up- or down-grinding according to the moving direction of the grinding wheel relative to the workpiece. When the wheel peripheral velocity, N_s, opposes the workpiece velocity, V_w the process is said to be an 'up-grinding', otherwise it is called a 'down-grinding' as shown in the **Figure 2.3**

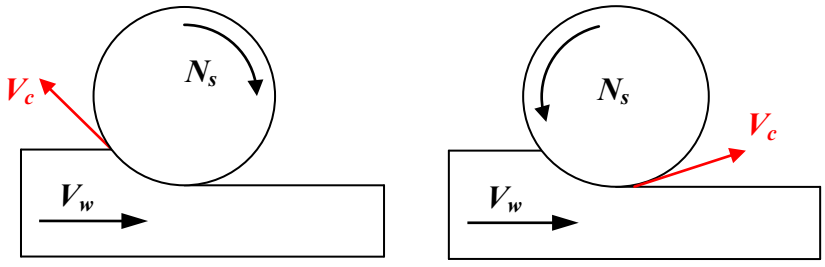

(a) Up-grinding (b) Down-grinding

Figure 2.3 Modes of grinding

We can now cite a list of some common parameters calculated from machine parameters

- Equivalent diameter $D_e\,[m]$: $D_e = D_s$ for plane grinding and $D_e = \frac{D_s.D_w}{D_s + D_w}$ for cylinderical grinding;
- Cutting speed $V_c\ [m.s^{-1}] : V_c = V_s \pm V_w$
- Contact length $L_c\,[m]$ the contact length may be evaluated geometrically by the relation $L_c = \sqrt{a_p.D_e}$ defined by Malkin [MALK89] where D_e is the equivalent diameter. This relationship is not valid in the case of high pressure because of the elasticity of the wheel which changes the contact geometry;
- Feed rate V_f ;
- Chip deposition $Z\,[mm^3.min^{-1}] : Z = a_p.b.V_w$;
- Specific chip deposition Z' : is the chip deposition per unit active width $Z' = \frac{Z}{b}$;
- Equivalent chip thickness $h_{eq}\,[m]$ it can be defined as theoretical chip thickness given by the relation $h_{eq} = \frac{a_p.V_w}{V_s}$ [HAMD00];
- Wear factor G : ratio between the volume of the ground material and volume of the abrasive consumed
- Ratio of the desired material removed and the material actually removed
- Maximum chip thickness $e_m\,[m]$ it can be estimated geometrically by the relation $e_m = \frac{2.L_c.V_w}{V_s}.\sqrt{\frac{a_p}{D_e}}$

There are also other important grinding parameters that may affect the surface integrity of the ground workpiece. The operator's experience and the rigidity of the machine are examples. However, these parameters are somewhat manageable, but it is difficult to quantify them. Finally, lubrication is also a major parameter to ensure the surface integrity of ground parts.

2.5 Historical Account of Grinding Process Modeling:

Tönshoff [TÖNS92] defined that "a model is the summary of representation of a process that serves to connect causes and effects. Thus, it is understandable that a model is intended to establish a relationship between the input and output parameters of a process with a view to predict the results in advance. In grinding, the input data are the parameters as described

previously, where the output data is vast: it may be the quality of the surface - roughness, dimensions - or integrity - residual stresses, thermal effects. Whatever may be these quantities they are derived directly from the forces as well as the maximum temperature reached during the process. Over the years many different scientific approaches to the solution of this problem were developed. A detailed account of these approaches is presented by Brinksmeier et al. [BRINK06]. These approaches include: (**Figure 2.4**)

- Empirical process models
- Physical process models
- Heuristic process models (rule based models)

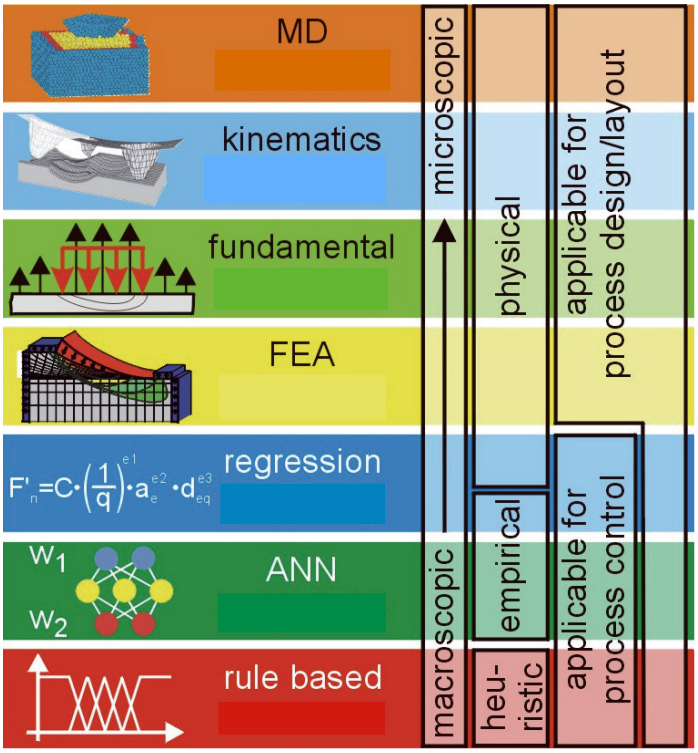

Figure 2.4 Categories of models and their application areas for simulation [BRINK06]

These models comprise the process characteristics like grinding force and temperatures and the results like surface topography or integrity were the major topics of the discussion. Empirical models based on experimental approach [ARRA05] [BELA91] aims at finding a correlation between grinding conditions and surface layer parameters. Depending on the model parameters, a test campaign in the form of experimental design is implemented. Then

on the basis of recorded input and output parameters the correlation is established. This is a relatively simple method with some disadvantages. Experimental works are usually time- and capital-consuming which limits their application. Moreover, there is a limited possibility to extrapolate the experimental results on different grinding methods and grinding conditions. Even if analytical models can be used as a basis to further calculate forces and grinding energy, the modelling of physical process data is certainly a domain of the Finite Element Analysis (FEA).

The analytical approach [BADG00] [BECK04] aims to develop predictive models that are derived from basic physical interrelationships. Based on the knowledge of a process and the selection of appropriate physical quantities, physical models can be developed using mathematical formulations. In this method thermal effects are usually described. On the basis of the calculations of temperature distribution in the workpiece, such changes in surface layer like micro-hardness, residual stresses, microstructure, etc. are estimated [BECK04]. Such an approach is very promising but at the present stage it is limited to theoretical investigations because of complex calculations and still limited knowledge about material behaviour in extreme grinding conditions.

Heuristic process models or Rule based models (RB) can help to model the human reasoning process, especially when it comes to ill-defined or difficult problems. Within the field of grinding processes a variety of approaches are employed for many possible classifications of artificial intelligence methodologies. Often used approaches are knowledge based systems and fuzzy logic systems. For a realistic modelling a sophisticated knowledge base is important to achieve good predictions for the quality of the output parameters. The simulation quality is high for specific applications, but difficult to transfer to other grinding processes. Furthermore rule based models are well suited for combinations with other model approaches for improving the effectiveness.

2.6 A Thermo-metallo-mechanically coupled Phenomenon

Grinding requires an extremely high energy input per unit volume of material removal compared with other machining processes, and almost all of the energy is converted into heat which is concentrated in the grinding zone where the wheel interacts with the workpiece. This leads to the generation of non-uniform high temperatures which can affect the metallurgical micro-structure and then the hardness distribution, and create a heat affected zone (HAZ) along with residual stresses,, thermal shrinkage, thermal cracking, and chemical modifications

of the material as described in [ANON60] [LEBL85] [LITT67] [SNOE78]. These effects are collectively termed as *surface integrity* problems as described in chapter 1.

Phase transformations in most steels introduce volumetric changes, transformation plasticity and changes in mechanical properties and consequently bring changes in the stress field. Local plastic flow may also occur when the effective stress exceeds the yield strength. All these factors interact with each other and cause a continuously changing internal stress/strain field. Therefore grinding process simulation requires understanding and modeling three types of phenomena: the thermal, metallurgical and mechanical which essentially implies that there are various thermal, metallurgical and mechanical processes happening simultaneously during grinding process throughout the heating and cooling phases.

In order to capture the residual stress state and resulting distortions, it is, therefore, necessary to model all these phenomena as accurately as possible. However, depending upon the type of material, certain simplifications may be adopted at this stage. For example, during a process where temperature values are high enough, certain steels show phase transformations in solid state and if the cooling rate is very high, the only phase obtained after complete cooling is martensite while some other alloys do not show any change of phase in solid state. Similarly if pressure has not being taken into account then the transformation plasticity phenomenon may be ignored. **Figure 2.5** presents the interaction and coupling of thermal, metallurgical and mechanical aspects of the process.

The thermal effect may also induce mechanically an intrinsic dissipation corresponding to an evolution of irreversible strains such that the internal hardening variables dissipate energy in the form of heat. This rise in temperature due to mechanical work done is often trivial as compared to the increase in temperature due to the heat energy produced during grinding. Therefore in our case it is ignored for the sake of simplicity. The thermal modelling aspects are discussed in the preceding sections while metallurgical and mechanical modelling aspects are described in detail in chapter 3 and chapter 4, respectively.

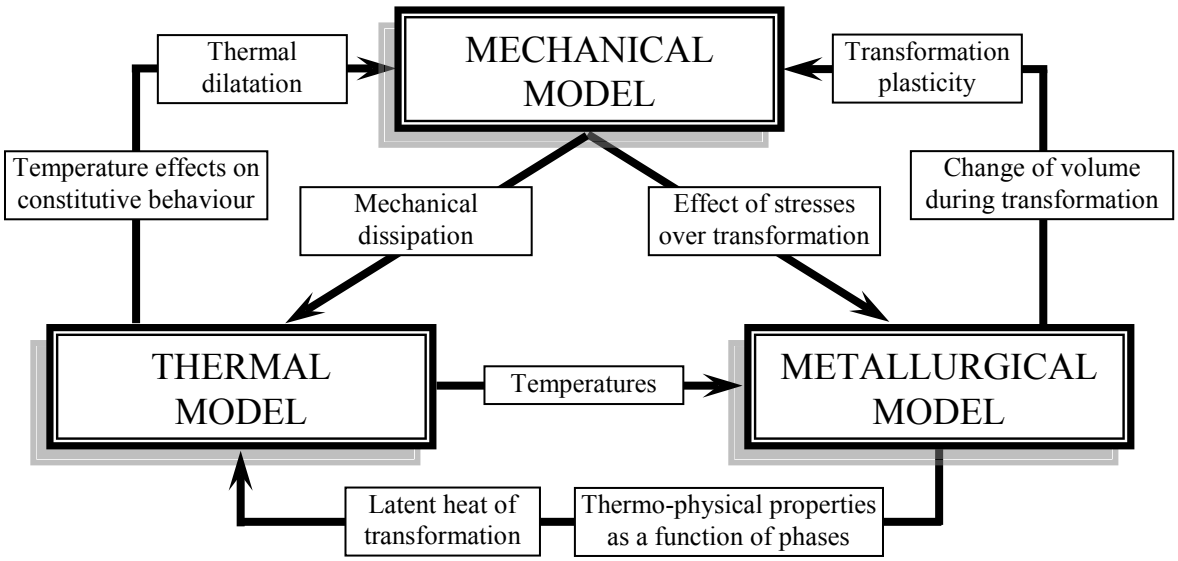

Figure 2.5 Coupling of physical phenomena in grinding [INOU85]

2.7 Thermal modelling

2.7.1 The importance of thermal modelling for grinding

As noted previously grinding is a machining process that requires an extremely high level of energy per unit volume of material removal, as opposed to other machining operations. Virtually all of this energy is dissipated as heat, leading to extremely high temperatures at the grinding zone. Many problems developed in grinding are caused by excessive heat or thermal damage, which can lead to undesirable side effects such as the appearance of burn marks and cracks on the surface, softening (tempering) and rehardening of the surface material, accompanied by unwanted residual stresses leading to reduced fatigue strength of the component. Dimensional accuracy may also be difficult to obtain because of thermal expansion and distortion of the workpiece during grinding.

Thermal damage to the workpiece is often the main factor influencing grinding input parameters. When burning occurs, it generally becomes necessary to reduce the grinding power by lowering the removal rate, by using a coarser dressing condition, or by changing to a softer grade wheel, which all adds costs to the finished product. Therefore, an understanding of the processes is needed to develop a thermal model for grinding. Analysis of the grinding

temperatures and control of thermal damage requires a detailed knowledge about the grinding energy, and its distribution along the grinding zone.

The heat in grinding is generated in the contact zone between the grinding wheel and the workpiece as well as immediately under this zone due to the plastic strain that is caused by the passing grains and to a lesser extent the bond of the grinding wheel. Heat penetration into the workpiece generates a temperature field with an extremely high temperature gradient in the sub surface layer, which decreases further down into the material. An illustration of the heat generated is shown in **Figure 2.6**.

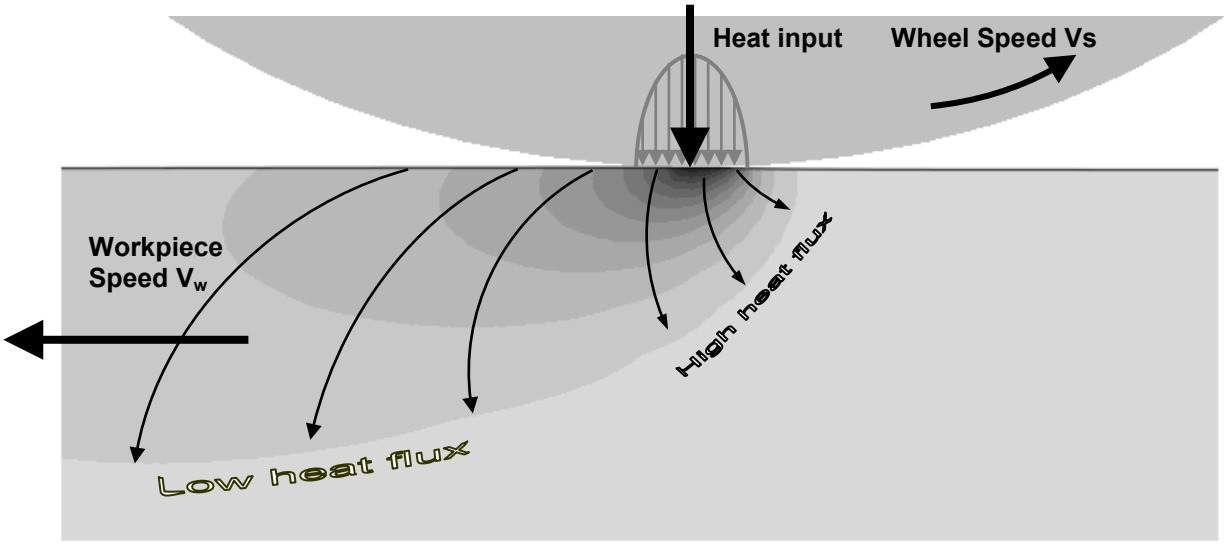

Figure 2.6 Illustration of the heat generated at the grinding wheel contact zone

2.7.2 Previous development of thermal grinding models

Considerable research has been directed to both analytical and experimental aspects of heat transfer in grinding [MALK89] [LIND71] [SNOE78] [KIMN97] [ROWE91] [BALI98] [SAUE72] [SATO61] [LAVI91] [SHAW93]. The majority of the thermal grinding models developed to date are based on the pioneering work of Jaeger's [JAEG42] two dimension moving band heat source theory from 1942. Due to the importance of the Jaeger's model it was felt that special attention should be given to it, and this is described below:

2.7.3 Jaeger's moving band heat source model

Jaeger's model is based on an analytical description of the temperature distribution in a workpiece if a heat source of defined intensity is moved along its surface. The temperature field is considered to arise from a plane heat source moving along the surface of a semi-infinite body whose thermal conductivity and specific heat are independent of the temperature. The assumptions of the model are that the flat heat source is a constant and has an equally distributed heat flux density and that the entire heat input stays in the process. In many cases a two dimensional model can be used, provided that the grinding wheel radius is large compared to the wheel workpiece contact length. An illustration of the process is shown in **Figure 2.7**.

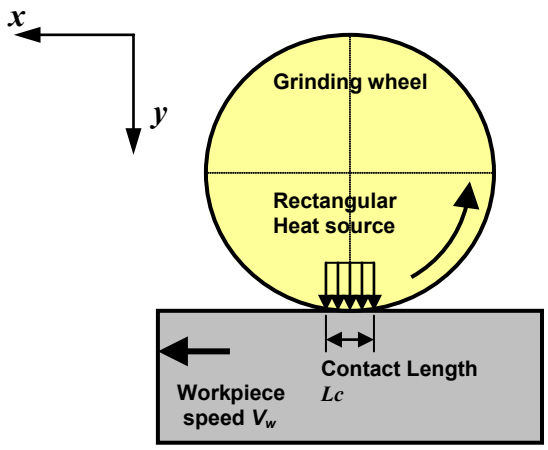

Figure 2.7 An illustration of Jaeger's moving heat source theory for grinding

Jaeger's model also works for cylindrical grinding with the additional condition that the contact length is small with respect to the workpiece circumference [MALK74], which in most cases it is, since the cylindrical workpiece is generally much bigger then the dimensions of the grinding zone [SNOE78]. Jaeger's equation for the amount of heat generated on the surface of the workpiece during grinding is:

$$T'_{\max} = \left(\frac{\pi K v}{2\alpha q}\right) T_{\max} = 3.543 B^{\frac{1}{2}} \qquad (2.1)$$

where $B = \dfrac{vL_c}{2\alpha}$ for B > 5

$T'_{\max}$ = maximum dimensionless surface temperature

K = thermal conductivity ($Wm^{-1}\,°C^{-1}$)

v = velocity of the heat source equivalent to workpiece velocity (m/s)

α = thermal diffusivity (m^2/s)

q = specific heat flux ($Jm^{-2}\,s^{-1}$)

T_{max} = maximum temperature (°C)

L_c = length of heat source (m)

2.7.4 Review of the thermal modelling process

In order to calculate the grinding temperature at the surface, it is necessary to specify certain assumptions concerning Jaeger's model. There are a number of variables that need to be taken into account, such as the total heat flux distribution and how it is modelled (rectangular or triangular), the energy partition values, the thermal characteristics of the workpiece, the geometry of the grinding wheel-workpiece interface and so on. All of these will be covered in the following sections. Rowe [ROWE91] has researched many thermal grinding models and developed several of his own. Rowe believes thermal models to predict the onset of burn proceed in three stages:

1. Determination of the energy applied at the grain-workpiece interface
2. The energy at the grain workpiece interface is partitioned between the grains of the grinding wheel and the workpiece.
3. The determination of the controlling temperature in the grinding zone as seen by the workpiece and the evaluation of the critical specific energy at the critical temperature for onset of thermal damage.

Snoeys [SNOE78] also shares a common view on the modelling process as he states that

"*The two dimensional model is defined by three sets of fundamental physical quantities. The first is the heat input into the workpiece and its distribution over the contact area. The second is the real contact length. And the third is the thermal characteristics of the metal (conductivity, specific heat per unit volume)*"

Past development of thermal grinding models appears to proceed in a systematic order. Therefore the research of thermal grinding models can be summarised and reviewed into five logical stages as follows:

1. The amount of energy entering the grinding system that is converted to heat (energy partitioning)
2. The amount of heat entering the workpiece (heat partitioning).
3. The type of heat source being modelled
4. Distribution of the heat flux over the work-wheel interface
5. The mathematical modelling process (Physical characteristics)

2.7.4.1 Energy partitioning

The amount of energy entering the grinding system has been cited by numerous researchers [KIMN97] [ROWE90,92] [COSM84] [MALK78] [ESHG68] as an important starting point for any thermal model to be established. Malkin [MALK74] has outlined the significance of the entering energy of the system by stating "*The temperature of the workpiece surface where the greatest heat is generated is determined by the distribution of the energy over the grinding area and what fraction of the energy is conducted as heat into the workpiece."*

Initial investigations by Shaw and Outwater [OUTW52] assumed that all of the grinding energy went into chip formation. Shaw used the assumption that the shear strains involved in chip formation tend to be much larger in grinding then in other metal cutting operations, which results in larger chip formation energy, but neglected any frictional rubbing forces that might occur. Cook's [COOK71] findings later showed that typically 75 percent of the total chip formation energy goes into shearing, with the balance associated with friction. It was also established by Cook that melting would occur if the specific shearing energy per unit volume exceeded the energy required to melt a unit volume of workpiece material. The shearing grinding energy entering the workpiece was therefore limited to the melting temperature that placed an upper bound condition on thermal model development with no more heat being able to be consumed by the workpiece. This was also confirmed later by Malkin's [MALK89] findings. Malkin then showed that the total grinding energy entering the system is consumed by three components: chip formation, ploughing and sliding. Malkin determined that almost all of the energy required for sliding and ploughing is converted to heat, which differs slightly to his earlier work in 1974 [MALK74] where only 75 percent of the ploughing energy was stated to be converted to heat. With the use of calorimetric methods Malkin also found that 55% of the chip-formation energy is also converted to heat.

Several other researchers [LEED71] [MARR77] [BALI98] [SAUE72] [SATO61] [KOHL95] indicated heat measurements to be around 60 – 95% of the consumed energy into the workpiece. Rowe et al [ROWE88] on the other hand has based the development of thermal models on the fact that all of the grinding energy entering the system is transformed into heat.

From the previous studies, there are differing views on how heat is transformed from the energy input of the grinding system. But the majority of researchers are in agreement, emphasizing that a high proportion of the energy that enters the grinding system is converted to heat, with several researchers indicating that all entering energy is transformed into heat [ROWE88] [COSM84].

2.7.4.2 The amount of heat entering the workpiece (heat partitioning)

With knowledge of the amount of energy entering the grinding system that is converted to heat, it now becomes important to know how much of that heat is actually consumed by the surface of the workpiece where thermal damage is likely to occur. Shaw and Outwater's [OUTW52] previously noted sliding source shear plane model estimated that 35 percent of the energy from the grinding process would be conducted as heat into the workpiece due to the shearing of the chips.

Shaw's and Outwater's heat theory was later disproved by Sato [SATO61] who showed that approximately 85 percent of the grinding energy is consumed as heat into the workpiece. Of the remaining heat, 4 percent is conducted into the chips and 12 percent into the wheel. Sato noted this was quite an opposite to a milling operation where about 80 percent of the total heat is carried off by the chips, and the heat entering the workpiece is only about 10 percent. Sato's research showed that the heat entering the workpiece also increases with the depth of cut of the grinding wheel and increases with a decrease in work speed.

Malkin [MALK74] believes that approximately 84 percent of the energy entering the system is converted to heat into the workpiece. Malkin's model assumes that all heat generated is converted into heat in the workpiece, and does not apportion any heat from the grinding zone to the grinding wheel, grinding fluid, or the chips produced. Malkin's heat model uses the same principles as Hahn's model in 1962 [HAHN62] where the heat generated is due to the wear flats of the grains which discounts the shear plane theory of Shaw and Outwater [OUTW52].

Rowe and co-workers [ROWE88, 95, 96] showed that there are four heat flux components that make up the grinding process: the heat flux carried away with the coolant, the grinding chips,

the grinding wheel and the workpiece (an illustration of the four heat partitioning elements are shown in **Figure 2.8**). Rowe showed that the workpiece consumes about 85 percent of the heat generated and is constant along the grinding zone.

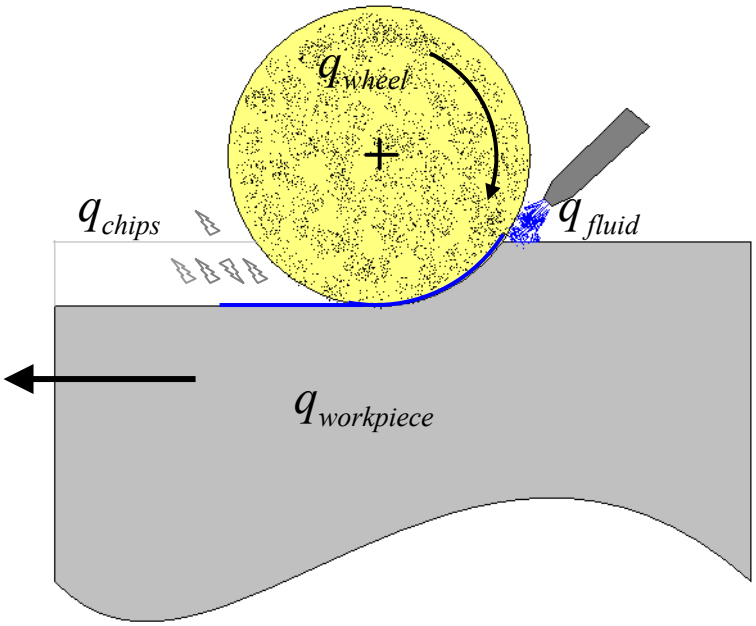

Figure 2.8 Rowe's four heat partitioning elements of grinding

When discussing the amount of energy applied to the grinding process that is converted to heat in the workpiece surface, the models show quite similar results. Peters [PETE83] assumes that 80% of the energy goes directly into the workpiece. Malkin's [MALK89] results presume that 84% of the entering energy is converted to heat into the workpiece, which is nearly identical to Rowe's 85% prediction [ROWE95].

2.7.4.3 The type of heat source being considered

Hahn's research in the 1960's [HAHN62] showed that it exists two important temperatures to be considered in the grinding zone. The first is the maximum workpiece background temperature or average temperature, which is at the surface of the workpiece as a result of all the cutting grains. The second is a high localised temperature of short duration, which is the heat generated from an individual grain-workpiece interface.

Subsequent authors have also reached the same conclusions to that of Hahn [DESR70] [MALK74] on the existence of the two different temperatures, but also mentioned a third, which is the bulk heat component of the workpiece. Malkin [MALK89] states that the average bulk temperature rise is only a small fraction of the rise in the grinding zone temperature and dismisses it as having any significant effect on the thermal heat generated on the surface.

Analysis by Des Ruisseaux and Zerkle [DESR70] showed that the high temperature at the grain wear flat exists for too short a time to induce the diffusion-driven damage, typically found in ground surfaces. Snoeys and co-workers [SNOE78] also concluded that the extreme temperatures during the short duration are localised on the shear planes and agreed with Hahn [HAHN62] that the average temperature was primarily responsible for thermal damage of the workpiece.

2.7.4.4 Distribution of the heat flux over the work-wheel interface

It now becomes necessary from Jaeger's model to determine how the heat is distributed into the workpiece. It has been determined by Jaeger [JAEG42] and other researchers [MARR77] [SAUE71] that there exist two primary solutions in determining the distribution of the heat flux into the workpiece; the total heat flux distribution can be modelled as either rectangular (uniform) or triangular. The rectangular distribution modelled, shown in **Figure 2.9 (a)**, assumes a uniform heat flux field and that the temperature is constant over the workpiece. The triangular distribution method **Figure 2.9 (b)** applies a higher heat flux value to an area of the contact length in a triangular pattern.

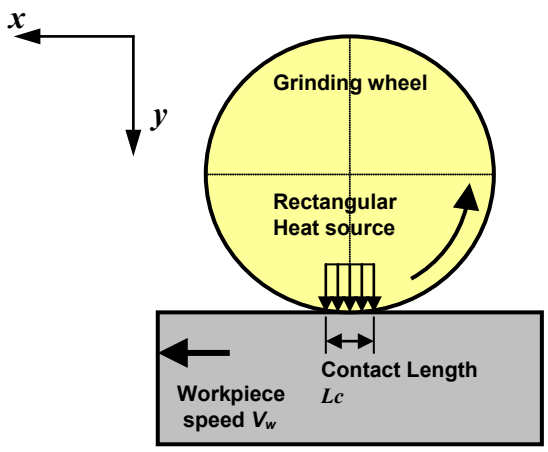

(a) Rectangular distribution theory

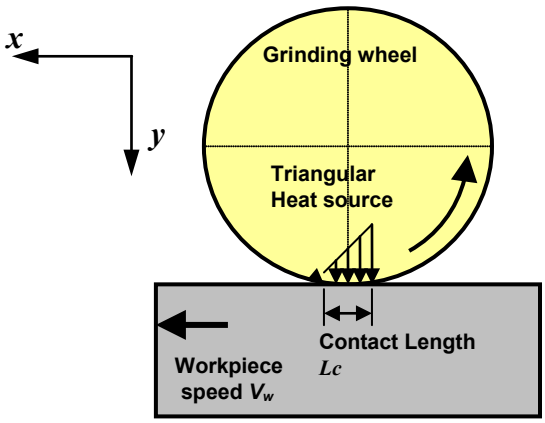

(b) Triangular distribution theory

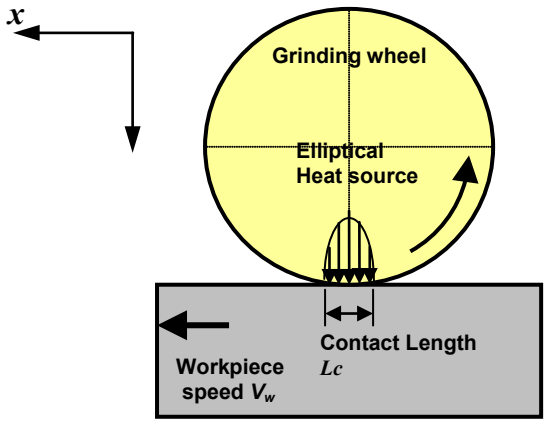

(c) Elliptical distribution theory

Figure 2.9 Different heat source profiles

There are differing views amongst researchers on which distribution method is best to use for grinding. Some [SATO61] [MALK74] [DESR70] use a rectangular (uniform) distribution, mostly to simplify subsequent calculations. However, due to the localised "spike" temperatures of a very short time as previously discussed, some researchers [SNOE78, DEDE72, MARR77] have argued that the assumption of a uniform heat flux field may not lead to accurate predictions. Snoeys [SNOE78] has commented that the heat flux distribution has a second order effect upon the maximum temperature. The layers only a few microns below the ground surface are the most affected by the shape of the flux distribution. The work by Snoey [SNOE78] suggests that the heat flux distribution, e.g. how the heat is distributed into the depth of the workpiece, is closer to the triangular distribution method than to the rectangular distribution method, which

supports Dederichs [DEDE72] and Marris [MARR77] experimental findings and that the assumption of a triangular heat distribution across the grinding zone, leads to more accurate solutions. Snoey also determined that heat is mainly generated by the friction with an increasing normal force on the grain. One drawback of the models discussed is that, all of them have ignored the contact problem between wheel and workpiece during grinding process and in some cases it is replaced by a normal force and a tangential traction. Recall the Hertzian contact theory where theoretically the pressure distribution between two contacting surfaces is given by an elliptical profile and accordingly the heat source should have an elliptically distributed profile for wheel and workpiece contact. Keeping in view the Hertzian contact an elliptical heat source model will be assumed for all major simulations in this manuscript.

2.7.4.5 The mathematical modelling process (Physical characteristics)

The physical attributes of the thermal process are now expressed as mathematical expressions in the formation of the thermal models. This generally includes some type of thermal variables for the workpiece and grinding wheel (conductivity, specific heat per unit volume, etc). A number of different thermal models [SNOE78] [SAUE72] [SATO61] [MALK74] [MARR77] [ROWE88] [PETE83] [TAKA72]… etc have been developed so far. The purpose of modelling the thermal problem is to calculate the temperature histories associated with the work piece. This calculation consists of resolving the heat equation while considering the thermal loading and boundary conditions. For a large class of grinding operations, temperature distribution in the workmaterial may be calculated by solving the heat-conduction equation, subject to the geometrical and temperature boundary conditions. In general, the grinding temperature distribution, T, will depend on time, t. Accordingly, the temperature distribution may be expressed as follows:

$$T = T(x, y, z ; t)$$

where (x,y,z) denote rectangular Cartesian coordinates and t denotes time. For a given time t, the above equation defines the grinding temperature distribution as a function of coordinates (x,y,z). For plane strain problems, the grinding temperature can be expressed as

$$T = T(x, y ; t)$$

By the theory of heat conduction [CARS65], the temperature, T, at a point in the workpiece is determined by the partial differential equation:

$$\frac{\partial}{\partial x}\left(K(T)\frac{\partial T}{\partial x}\right)+\frac{\partial}{\partial y}\left(K(T)\frac{\partial T}{\partial y}\right)+Q_w=\rho(T)C_p(T)\frac{\partial T}{\partial t} \quad (2.2)$$

with, ρ density in kg.m^{-3},

C_p specific heat capacity in J.kg^{-1}.°C^{-1},

K thermal conductivity in W.m^{-1}.°C^{-1},

T temperature in °C.

Q_w heat flux in W.m^{-2}

Heat transfer takes place by means of conduction, convection and radiation. During grinding the work piece gets heated due to friction between wheel and workpiece on the surface and then this heat is transferred within the workpiece by conduction of heat energy, while heat loss in the surrounding environment takes place through convection. Additional amount of heat loss may also take place when coolants are used. The heat transfer phenomena as general boundary condition is described in the following equation:

$$q_{conv}=h_{conv}(T)(T-T_0) \quad (2.3)$$

with,

$h_{conv}(T)$ convective heat transfer coefficient as a function of temperature in W.m^{-2}.°C^{-1},

T_0 ambient temperature in °C,

T temperature of the component being ground in °C,

2.8 Force Modeling

The grinding stresses rely on the complex nature of the contact mechanisms between a grinding wheel and a workpiece, it is therefore important to consider different grinding tractions and their related stresses. It has been demonstrated in the literature [BRAK88][ONOK61] that the forces generated in grinding contribute greatly to the finished product. They can affect the surface finish, the part dimensions of the ground workpiece, and lead to higher cycle times of the grinding operation. To overcome these problems an understanding of the grinding forces, and more importantly how to predict these forces, is required to optimise the process.

It has been shown that the true input to the grinding process is the normal force developed at the wheel work interface [HAHN71]. Unlike other metal cutting processes, the magnitude of the normal forces produced is substantially higher, due to the unique machining characteristics of the operation. The cutting grits on the grinding wheels are randomly placed with varying cutting angles relative to the surface that can produce high force bearing negative rake angles [KOMA71]. These randomly placed grits may also contain wear flats that produce high rubbing and ploughing forces [MALK89a]. When the grinding wheel engages the workpiece, forces are developed; the degree of force produced depends on a number of input variables in the grinding process, such as work speeds, dressing speeds, wheel specification, coolant used, etc. There have been many models developed over the years to predict the grinding forces. A critical review of theses models analysing their attributes follows.

2.8.1. Past force grinding models

Past development of models to predict the forces generated in grinding can be categorised into two main branches of study: macro-level and micro-level. On the macro-level we have the basic requirements for grinding, such as the grinding wheel, the workpiece and the machine. The grinding models and relationships are then developed as a complete system.

The micro-level bases more of the modelling on the mechanisms of the cutting process and through the topography of the grinding wheel, with particular emphasis on the grits of the grinding wheel ploughing into the workpiece and forming chips. They consider parameters such as the number of cutting grains, grain spacing, the real contact length etc. A critical review of both types of models follows.

2.8.1.1 The macro force grinding models

As stated previously the macro force models are based on the complete grinding system. There have been a number of significant models developed to analyse the overall grinding forces in this way. The most significant are based on the work conducted by Hahn and Lindsey [HAHN66,71,86] [LIND71a,75,86].

Hahn and Lindsay describe the force component to be an independent input into the grinding system from which all other parameters are determined. Their research shows that the forces generated in grinding comprises of three components: rubbing, ploughing and cutting. This is in agreement with other work by Okumura [OKAM67] and Busch [BUSC68]. Hahn and Lindsay have experimentally determined and plotted the force and material removal relationships, linking them to the three force components as a wheel-work characteristic chart (**Figure 2.10**).

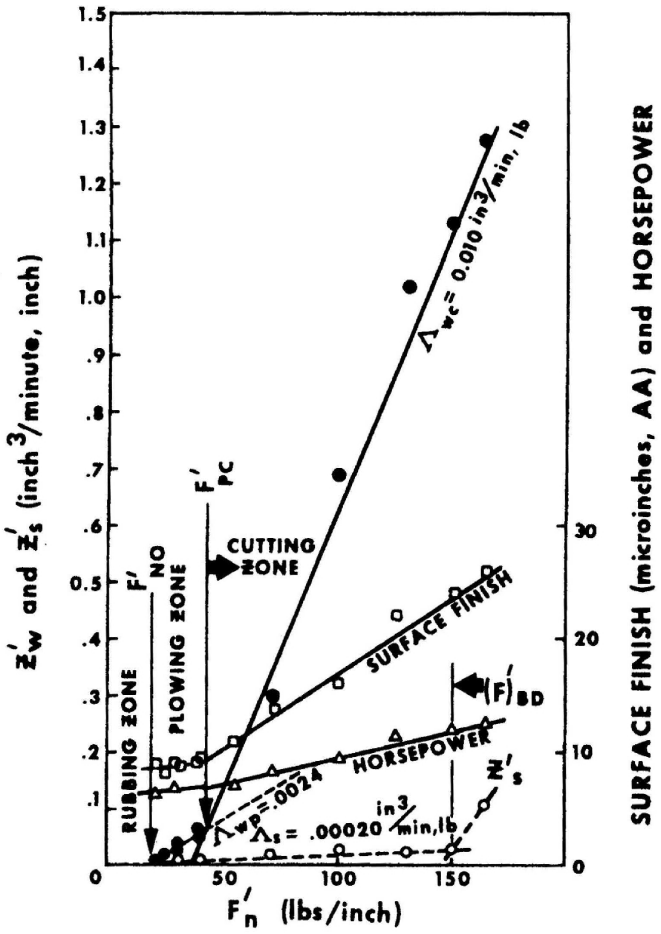

Figure 2.10 The Hahn and Lindsay wheel-work characteristic chart

This graph illustrates the three different grinding zones of the individual force components. Lindsey states [LIND86] that the threshold force (rubbing) occurs where no material is removed below this value. Between the ploughing transition value, both rubbing and ploughing will take place, and above this value rubbing, ploughing, and cutting will take place.

Hahn and Lindsay determined that if the threshold force is known, or the grinding operation has become a steady state, a linear relationship exists between the force and stock removal rate with the slope being the work removal parameter. The mathematical relationship for this is shown in Equation 2.4. This work removal parameter lays the foundation for the subsequent force modelling equations.

$$WRP = \frac{R_q}{F_n} \tag{2.4}$$

where

WRP = work removal parameter (m^3 /sec. N)

R_q = Volumetric removal rate (m^3 /sec)

F_n = normal force (N)

Peters' chip thickness model [PETE80][SNOE74] has also shown potential for a practical model to predict grinding forces. The equivalent chip force model is based on the thickness of a continuous layer of material (chip) being removed at a volumetric rate per unit width by the grinding wheel. It has been shown that the chip thickness has a controlling influence on the forces produced in grinding [BACK52][REIC56][SNOE71]. Peters uses this parameter to develop a force grinding model as follows:

$$F'_n = F'_{t_o} .h^n_{eq} \tag{2.5}$$

$$h_{eq} = \frac{V_w a_p}{V_s} \tag{2.6}$$

where h_{eq} is the equivalent chip thickness F'_{t_0} and n are coefficients to be determined and F'_n is the normal force (N)

The equivalent chip thickness model correlates fairly well, not only with the grinding forces and energy, but also with other performance characteristics, including surface roughness and wheel wear. However, this model has limited practical use for predicting grinding forces because the constants F'_{t_0} and n depend on the particular wheel, workpiece, grinding fluid, and dressing conditions, as well as on the accumulated stock removal.

A similar model for approximating forces is presented by Tanguy [TANG85] and is given by Equation 2.7. Some of values of the constants F'_{t_0} and n for this model are alos presented in Table 2.1.

$$F'_t = F'_{t_0} .h^n_{eq} \tag{2.7}$$

where h_{eq} is the equivalent chip thickness F'_{t_0} and n are coefficients to be determined and F'_t tangential force defined by

$$F'_t = \frac{F_t}{b}$$

Table 2.1 Examples of the data for force model equation 2.7 [TANG85]

Material	Grinding wheels	Modulus of Elasticity [GPa]	μ	$F_{t_0}^{'}$	n
100Cr6 at 62-63 HRc	2A60I6V	40	0,38	13	0.55
100Cr6 at 62-63 HRc	2A60K6V	47	0,40	20	0.65
100Cr6 at 62-63 HRc	2A60M6V	56	0,41	23	0.72
100Cr6 at 62-63 HRc	2A80J6V	40	0,40	14	0.59
100Cr6 at 62-63 HRc	2A80K6V	45	0,40	20	0.65
100Cr6 at 62-63 HRc	2A80M6V	52	0,43	35	0.75

Once defined by specific measured or modelled cutting forces, it is easy to obtain the power absorbed then the specific energy E_{sp} by equation 2.8.

$$E_{sp} = \frac{P}{Z} = \frac{F_t.V_c}{Z} \approx \frac{F_t.V_s}{Z} = \frac{F_t^{'}V_s}{Z^{'}} = \frac{F_t^{'}}{h_{eq}} \tag{2.8}$$

By inserting the equation. 2.7 into equation. 2.8, then we can redefine the specific energy as:

$$E_{sp} = F_{t_0}^{'}.h_{eq}^{n-1} \tag{2.9}$$

Finally, it is necessary to determine the coefficients $F_{t_0}^{'}$ and n for grinding condition data to obtain a force model. These parameters can easily be measured through dynamometers but unfortunately the extrapolation for the conditions outside the experimental measurement domain are not evident to take into account the strong non linearity of the process. Moreover some studies have attempted to generalize the choice of parameters by fuzzy logic approaches [ALI97], [NAND04].

2.8.1.2. The micro force grinding models

As previously mentioned the micro force models take into consideration the microstructure of the grinding wheel's topographical surface and are otherwise known as topographical surface force modelling. The models predominately predict the forces that will develop from a engaged cutting grit of the grinding wheel cutting into the workpiece, as shown in **Figure 2.11.**

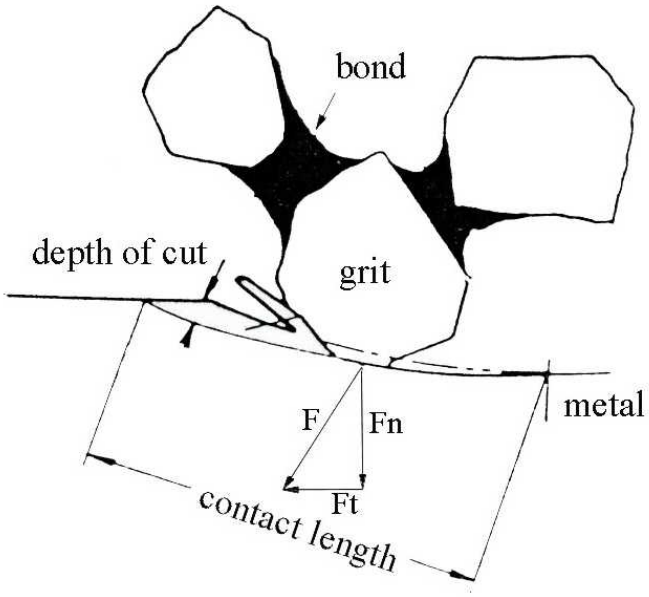

Figure 2.11 Illustration of a grinding wheel grit cutting into the workpiece

The forces obtained from the theoretical models will vary depending on the assumptions the models have made with regard to the mechanics of grinding and their interpretations of it. It also depends on how they have applied geometrical and known grinding relationships in the formation of the finished models.

In general, the cutting forces in grinding are influenced by several parameters; the type of material being machined, the material removal rate, the density of active grits n_g, the geometry of the grits, lubricant. . . etc. From an analytical point of view, the cutting forces are transmitted to wheel-workpiece interface through the grits in contact. For the sake of simplicity, it can then be reduced initially to study the single grain contact. In this case, the mechanical and thermal cutting processes such as turning or milling and grinding are comparable and are from the same phenomena.

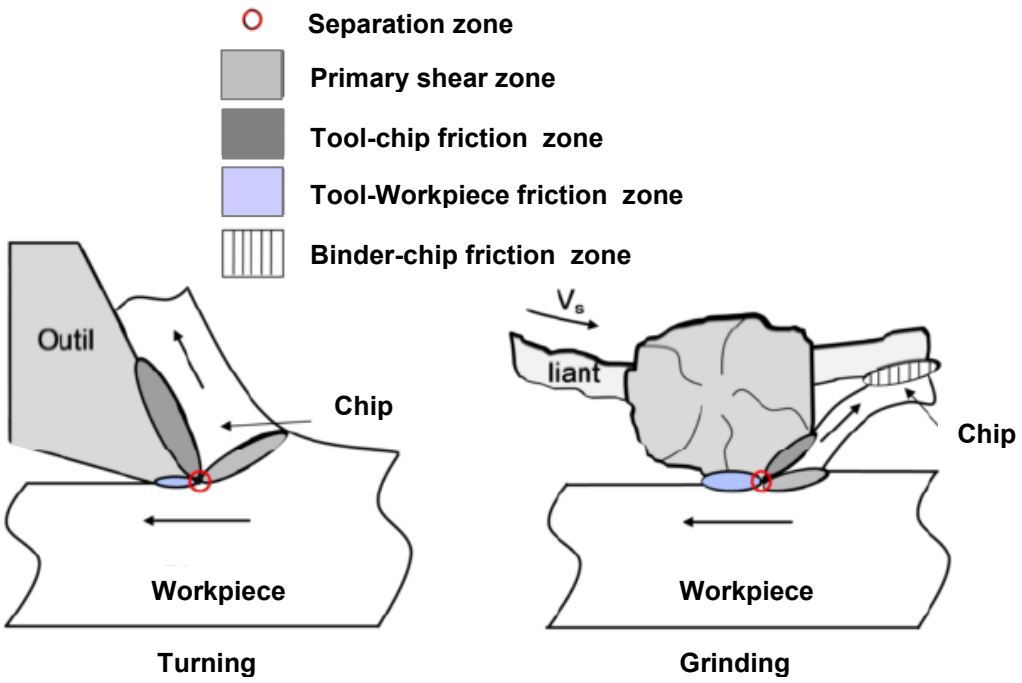

Figure 2.12 Comparison of the zones of contact and friction in turning and grinding [BROS09]

Figure 2.12 presents a comparison of friction and shear zones during the process of turning and grinding of grit. It is clear that the phenomena involved are comparable, yet magnitudes are different. In fact, the size of an abrasive grain in grinding is about 100 µm while a turning tool is measuring a few millimetres. In addition, the grinding contact is not continuous but divided on a few grits which indicate active locally high contact pressures. The specific energy E_{sp} for example is much higher in grinding than turning. Table 2.2 presents a comparison of these key variables.

Table 2.2 [BROS09]

Parameters	**Turning**	**Grinding**
Specific Energy [$J.mm^{-3}$]	1-2	20-100
Dimensional Precision [*mm*]	0,1-1	0,01-0,1
Roughness of the Machined surface Ra [*µm*]	1-2	0.1-0.2

The earliest creation of a force model involving the microstructure of the grinding wheel was by Salje [SALJ53] in 1953. Salje's model considered the shear strength as a specific parameter. The model consisted of a speed grinding ratio, a working grit engagement area (real contact length), an equivalent diameter, a constant for the grit size and a grinding constant for the grinding wheel and workpiece interface. The constant is determined from a set of known experimental grinding graphs where the particular wheel and work combination is being modelled. The model was a good first attempt in predicting the forces produced by the cutting action of the grits of the grinding wheel, but was limited due it being based on an unchanging and time dependent surface and sharpness of the cutting grit. Werner's research [WERNE71] discounted the theory that all the forces are due to shearing, and proposed that the forces are due only to a small amount from shearing with the rest caused by friction between the rubbing of the grit and the workpiece material.

Reichenbach, Shaw, and Mayer [REIC56] extended the Salje grinding model by considering the grinding wheel topography in a two dimensional form. The model considered the cutting characteristics of each grain and determined the amount of force developed by the amount of cutting grains in the cutting zone. Most grit force models subsequently developed adapted this form of two dimensional modelling approach.

Malkin and Cook [MALK71] then experimentally determined that the forces developed at the grit interface were the sum of the cutting force due to chip formation and a sliding force due to rubbing between the wear flats and the workpiece (Equation 2.10). This pioneering work was instrumental in developing future force topographical grinding models, as it recognised the fact that there are different types of mechanisms in generating the overall forces at the grit work interface. $F_n = F_{nc} + F_{ns}$ (2.10)

where,

F_{nc} = normal force due to chip formation (N)

F_{ns} = normal force due to friction (N)

The application of the micro models that take the microstructure of the wheel into account are hampered due to the high measuring efforts required. The equations that contain empirical constants require extensive testing to experimentally estimate the model parameters. This is particularly the case for the more complex equations subsequently developed where two or more unknown constants exist.

Regardless of the type of grinding, the global cutting force can be simply defined as the result of wheel action on the workpiece. This force can be resolved in terms of wheel in two

directions: normal and tangential directions giving the tangential and normal forces F_n and F_t respectively (**Figure 2.13**).

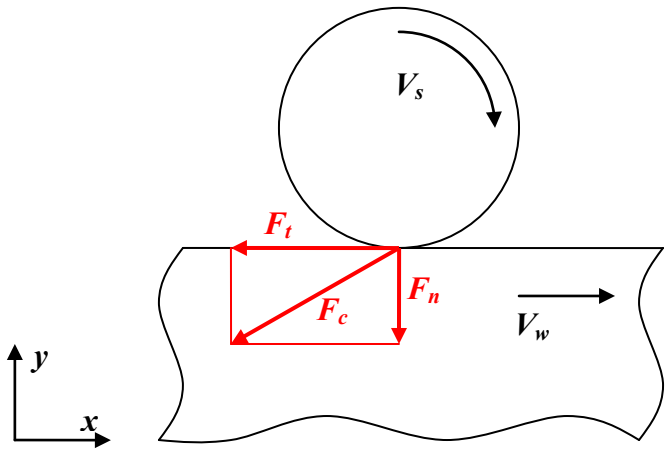

Figure 2.13 Forces in Grinding

The ratio $\mu = \frac{F_t}{F_n}$ can then be defined as the macroscopic coefficient of friction between grinding wheel and the workpiece. The value of μ generally ranges from 0.3 for hard materials to 0.6 for soft materials. Thus, each of these two forces is important to determine for obvious reasons: the tangential force will allow the calculation of the absorbed power $P_o = F_t.V_c$ while the normal force of penetration is important for the rigidity of the assembly. In short, even if analytical force models are determined for a single grit in a similar manner that obtained for turning, it becomes very difficult to obtain them globally because of the dependency on many parameters. Thus, while some authors work on modelling statistical grain distribution [HOU03], the majority of work encountered are based on an experimental approach to stress measurement [TÖNS80, COUE05, KWAK06, LIU08] with some even taking into account the vibration phenomena [ORYN99, DREW01]. Finally, if the cutting forces are very important for the determination of power absorbed, they have a small influence on the surface integrity of the final part. Indeed, it is commonly accepted [TANG85, MALK89] that the most important part of the energy is transformed into thermal energy upon contact. It is then distributed between the workpiece, the grinding wheel, chips, lubricant and the environment [ROWE97].

Finally, it is obvious that these temperatures may cause the possible damage to the surface of the workpiece it is important to study them.

2.9 Phase Transformation

The rapid heating and cooling in a grinding process may cause phase transformations, thermal strains and plastic strains simultaneously in a workpiece and in turn introduce substantial residual stresses. When phase transformation occurs, the properties of the workpiece material will change. The extent of such change depends on the temperature history experienced and the instantaneous thermal stresses developed. To carry out a reliable residual stress analysis, therefore, a comprehensive modelling technique and a sophisticated computational procedure that can accommodate the property change with the metallurgical change of material need to be developed. It was felt that a detailed description of phase transformation and related modelling should be included in dissertation. The detailed metallurgical modelling is described in chapter 3.

2.10 FEA Modelling

Many physical processes are described by differential equations such as the differential equations of Lamé's elasticity theory. For these models the numerical methods such as the Finite Differences Method (FDM) or the FEA are applied. In both, the FDM and the FEA, the real process is transformed into a model with finite elements. These finite elements are bounded by element nodes. In the FDM the concerned area is divided into a lattice structure.

The partial differential equations are solved by a system of equations accumulated through the substitution of the differential quotients with functional values on the lattice points. One disadvantage is the difficult application of the FDM for complex shaped geometries. Another disadvantage is that a local refining of the lattice structure is not possible, only the complete structure can be refined. For specific problems the FDM can be a suitable tool for analyzing the heat conduction in grinding [HONG00] [TSAI98] [STAR03] [GUOC95]. In the FEA the differential equations are solved by applying so called "shape functions" or "interpolation functions" which lead to a system of linear equations. Additionally the workpiece properties and the thermal or mechanical load must be known. The stiffness depends on the material properties and on the workpiece geometry. One advantage of the FEA is the possibility of creating irregular meshes for complex structures. The mesh can also be adapted locally, which is especially useful for large models. Generally, FEA models for the simulation of grinding processes can be separated into macroscopic and microscopic concepts.

2.10.1 Macroscopic FEA Modeling Concept

Macro-scale models are intended to capture the aggregate effects of the abrasive wheel on the workpiece. In most cases the macroscopic simulation is applied in order to calculate the influences of heat and mechanical surface pressure on the complete workpiece in terms of temperature distribution or form deviation. The calculations are mainly based on thermo-mechanical and elasto-mechanical material characteristics. The plastic material behaviour and the chip formation are not considered. The macro-scale grinding FE models reviewed are categorized as

Thermal models: based on the theory by Carslaw/Jaeger [CARS59] these models predict the temperature distribution within the work-piece [LOWI80] [DESR70] [MAHD95] [PAUL95] [MAMA03] [MALK89] [WANG03] [BIER97] [AGUI05] [WEBE99] [JINT99] [ANDE08]

Mechanical models: these models determine the mechanical strains and resulting stresses [KIMP00] [LIUW02] [WARN99]

Coupled models: coupled models determine the resulting total stress from both thermal and mechanical loads. [HAMD04][MAHD97,98,99,00][MOUL01][YUXX94] [ZHAN95].

Each model is either two-dimensional (2D) or three-dimensional (3D) and uses an elastic, elastoplastic, or thermo-elastoplastic material model.

2.10.2 Microscopic FEA Modeling Concept

In contrast to macroscopic models, microscopic simulation is restricted to analyses of the working zone. Thus, mostly a minor section of the workpiece and one contacted grain is modelled. The microscopic simulation is the most detailed approach of the real grinding process to date. For a realistic simulation an elasto-plastic material behaviour is considered as well as chip formation. But for chip formation the exact material behaviour for high strain rates must be known. Furthermore, current computer power is not sufficient to develop a comprehensive model of an entire grinding wheel in microscopic simulations or to consider the chip formation in macros

Summary

In this chapter the grinding process as a whole is discussed and a global description of the process with different physics involved in the process are explained. Two critical points

appear in the literature about the surface integrity of ground workpieces: the occurrence of metallurgical transformations and the presence of either compressive (beneficial) or tensile (detrimental) residual stresses on the surface of the workpiece. The temperature thus reached during grinding may be considered as the critical point of the process affecting the surface integrity of ground parts. It was found that grinding forces can be divided into two separate groups, macro modelling and micro modelling. The macro force models, in particular Hahns and Lindsay's WRP approach, provide a practical method to predict grinding forces in a production environment, but require a series of different calculations over a time period. It was also shown that a great deal of research was conducted into micro force modelling of the topographical forces produced by the grinding wheel. From the modelling point of view, a review of different analytical and numerical modelling approaches mostly addressing the thermal aspects of grinding process is presented. In this regard, the modelling of the contact between the grinding wheel and the workpiece and the resultant energy dissipation in the form of heat are found to be one of major difficulties to address in the modelling of the process. From the literature review it was found that predictive techniques like numerical simulations are regarded as the most useful tool to analyze the mechanical and/or the thermal strains and subsequent residual stresses associated with a grinding process thus providing in advance useful guidelines for defining the optimum grinding parameters.

CHAPTER 3

PHASE TRANSFORMATION

3

3.1 Introduction

One key point for the prediction of grinding residual stresses is the modelling of phase transformation kinetics and their consequences on the thermo-mechanical behaviour of the material. A detailed review of the phase transformation modelling is presented here in order to develop an understanding for incorporating phase transformation in modelling and simulation of grinding process. For a better understanding, it may be interesting to present a summary of some basic understanding about metallurgy of the materials. This section therefore generalizes on steel metallurgy and more specific details on the material studied are presented.

3.2 Phase transformation in steel

At high temperatures (austenitizing temperature), steel atoms are arranged according to a crystal lattice form known as austenite (FCC structure, **Figure 3.1**). As steel cools, austenite changes into pearlite, ferrite, bainite or martensite, which have a different lattice structure (BCC structure, **Figure 3.1**). A schematic diagram of phase transformation of steel under heating and cooling conditions is given in **Figure 3.2**. A transition like this, from one type of lattice to another, is referred to as a phase transformation. Solid-state phase transformation causes the macroscopic geometric change because these different types of crystalline structures have different densities, which eventually leads to the so-called transformation-induced volumetric strain. The crystalline states are functions of the temperature, the level and the stress type. The phase transformations of steels are often studied by using the system of iron-carbon. **Figure 3.3** shows the equilibrium diagram for combinations of carbon in a solid solution of iron.

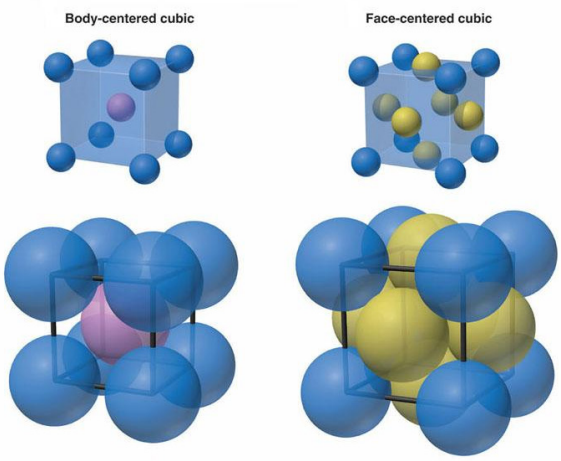

Figure 3.1 Crystal lattice structure of BCC and FCC

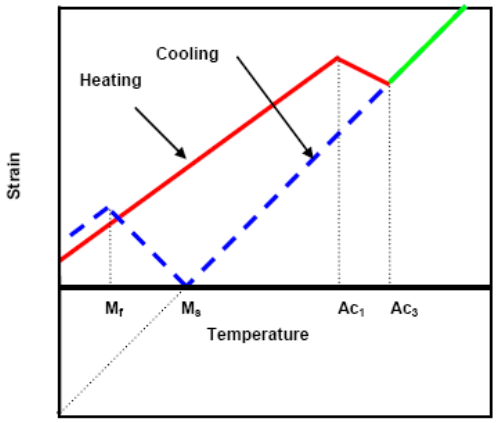

Figure 3.2 Schematic diagram of phase transformation under heating and cooling conditions

A study of the constitution and structure of all steels and irons must first start with the iron-carbon equilibrium diagram. Many of the basic features of this system **(Figure 3.3)** influence the behaviour of even the most complex alloy steels. The addition of Carbon strongly influences the allotropic changes of the material and therefore mechanical behaviour is directly related to the phases present in the material. Therefore it is important to study these phases and how they are influenced by temperature. The iron-carbon (Fe-C) diagram is a map that can be used to chart the proper sequence of operations for thermo-mechanical and thermal treatments of given steel. The art and science of steel processing is based on the existence of the austenite phase field in the Fe-C system. Controlled transformation of austenite to other phases on cooling is responsible for the great variety of microstructures and properties attainable by heat treatment of steels.

The transformation of austenite-ferrite does not follow a general rule. Moreover austenite is the densest stable phase at high temperatures. The ferritic transformation is dictated by the magnetic properties of the Fe-C system and not only by thermal agitation. Phase transformations are accompanied by a contraction of material during cooling and an expansion during heating. The decomposition of austenite into other phases is cooling rate dependent, and different cooling rates give different phase structures: for slow cooling rates it gives a mixture of ferrite and Cementite, bainite for high cooling rates and martensite for very high cooling rates.

The transformations during cooling are not only dependent on cooling rate but also on alloying element composition, and are generally different from one another. Many diagrams based on experimental data have been produced in order to understand the thermal influence on different steels. On a time-temperature graph, the starting and finishing points of phase transformation are indicated and generally accompanied by the mid points of transformation. These diagrams are of two types. The TTT diagrams (Time Temperature Transformation) also known as isothermal transformation (IT) diagrams **(Figure 3.4)**, measure the rate of transformation at a constant (isothermal) temperature. In other words, once a part is austenitized, it is rapidly cooled to a lower temperature and held at that temperature while the rate of transformation is measured. The different types of microstructures produced (ferrite, pearlite, bainite, martensite) are then indicated on the diagram together with the holding times required for each transformation to begin and end. The CCT (Continuous Cooling Transformation) diagrams also known as cooling transformation (CT) diagrams **(Figure 3.5)**, measure the degree of transformation as a function of time for a constantly changing (decreasing) temperature. In other words, a sample is austenitized and then cooled at a predetermined rate, and the degree of transformation is measured using techniques such as dilatometry, magnetic permeability or other physical methods.

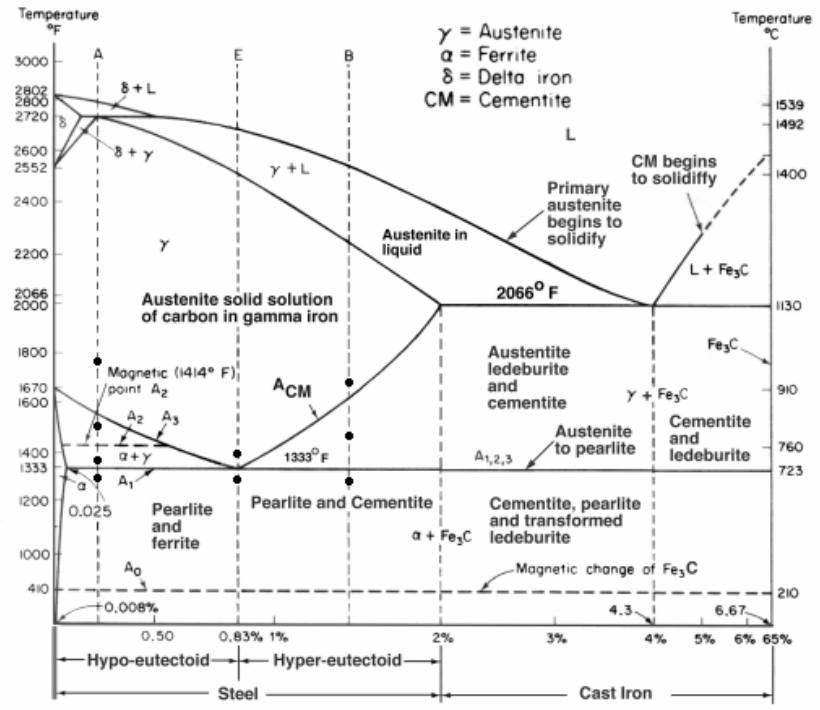

Figure 3.3 Iron Carbon phase diagram [MARU01]

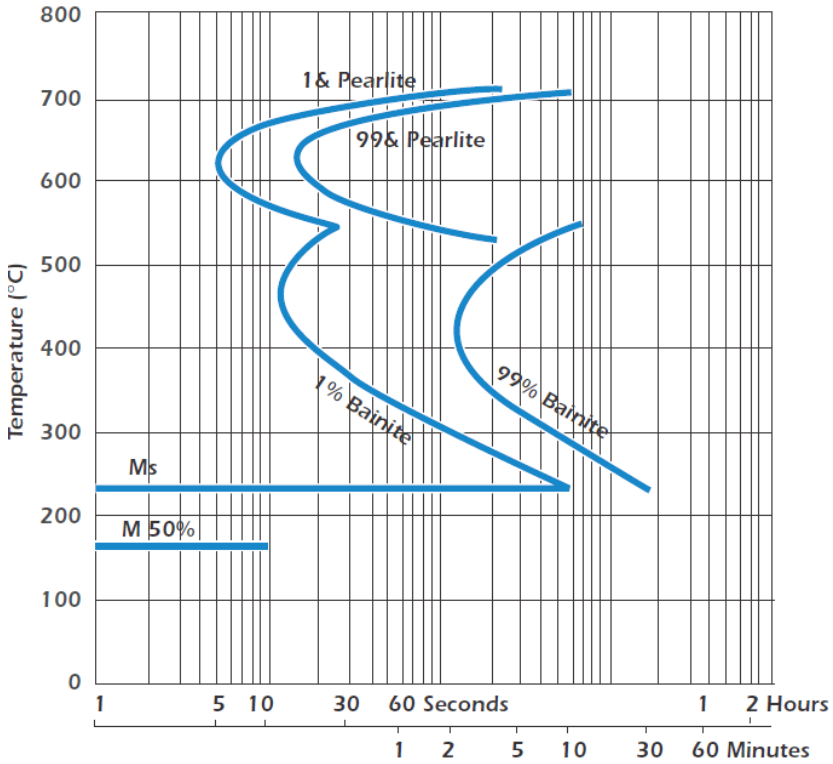

Figure 3.4 TTT diagram AISI 52100 (100Cr6) steel [OVAKO]

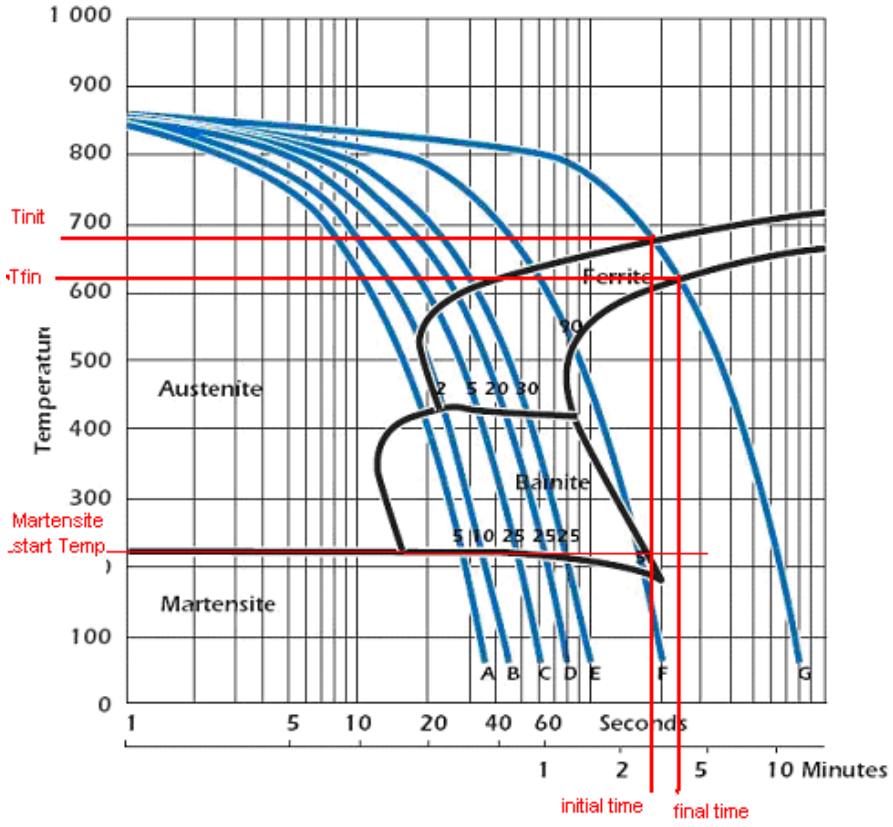

Figure 3.5 CCT diagram of AISI 52100 (100Cr6) steel [OVAKO]

3.2.1 Critical Temperatures

The transformation temperatures are often referred to as critical temperatures and are observed by measuring changes in heat transfer or volume as specimens are heated or cooled. On heating, heat is absorbed and specimen contraction occurs as ferrite and cementite are replaced by the close-packed structure, austenite. On cooling, heat is released and specimen expansion occurs as austenite transforms to ferrite and cementite. The absorption or release of heat during phase transformation produces a change in slope, or "arrest," on a continuous plot of specimen temperature versus time. The letter "**A**" is the symbol for the thermal arrests that identify critical temperatures.

There are three critical temperatures of interest in the heat treatment of steel: $\mathbf{A_1}$, which corresponds to the boundary between the ferrite cementite field and the fields containing austenite and ferrite or austenite and cementite; $\mathbf{A_3}$, which corresponds to the boundary between the ferrite-austenite and austenite fields; and $\mathbf{A_{cm}}$, which corresponds to the boundary between the cementite-austenite and the austenite fields. These temperatures assume equilibrium conditions — that is, extended periods of time at temperature or extremely slow

heating or cooling rates. Sometimes $\mathbf{A_1}$, $\mathbf{A_3}$, and $\mathbf{A_{cm}}$ are designated as $\mathbf{A_{e1}}$, $\mathbf{A_{e3}}$, and $\mathbf{A_{ecm}}$, respectively, the letter "e" indicating assumed equilibrium conditions.

The transformations that occur at $\mathbf{A_1}$, $\mathbf{A_3}$, and $\mathbf{A_{cm}}$ are diffusion controlled. Therefore, the critical temperatures are sensitive to composition and to heating and cooling rates. Rapid heating allows less time for diffusion and tends to increase the critical temperatures above those associated with equilibrium. Likewise, rapid cooling tends to lower the critical temperatures. The effect of heating or cooling rate is defined practically by a new set of critical temperatures designated "**Ac**" or "**Ar**" (for the arrests on heating or cooling, respectively). The terminology was developed by the French metallurgist Osmond, [OSMO1888]. **Ac** stands for *arrêt chauffant* and **Ar** for *arrêt refroidissant*. As a result of heating and cooling effects, therefore, there are two other sets of critical temperatures: ($\mathbf{Ac_1}$, $\mathbf{Ac_3}$, and $\mathbf{Ac_{cm}}$), and ($\mathbf{Ar_1}$, $\mathbf{Ar_3}$, and $\mathbf{Ar_{cm}}$). These sets of critical temperatures are shown schematically in **Figure 3.6**.

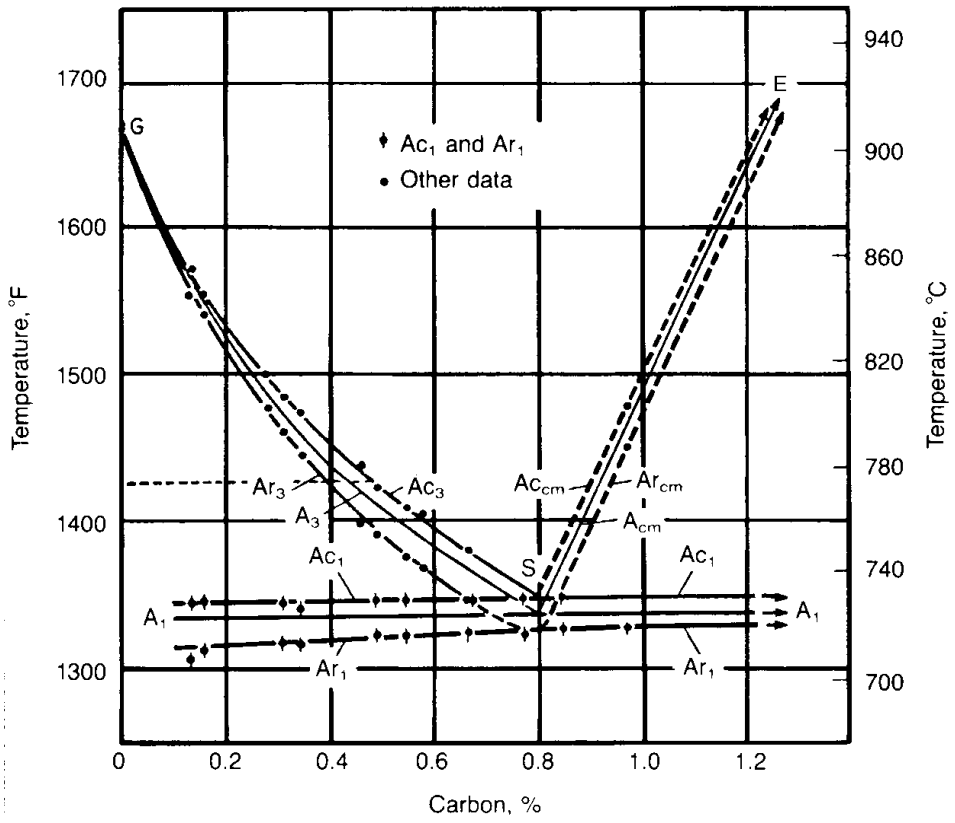

Figure 3.6 Cooling (Ar), heating (Ac) and equilibrium (A) temperatures in Fe-C alloys. Heating and cooling at 0.125 °C/min. [BAIN61]

Generally, the critical temperatures for a given steel are determined experimentally. However, some empirical formulas that show the effects of alloying elements on the critical temperatures have been developed by regression analysis of large amounts of experimental data. For example the following formulas for $\mathbf{Ac_1}$ and $\mathbf{Ac_3}$ (in degrees Celsius) have been developed by [ANDR65]:

$$Ac3 = 910 - 203\sqrt{C} - 15.2Ni + 44.7Si + 104V + 31.5\,Mo + 13.1W$$

$$Ac1 = 723 - 10.7Mn - 16.9Ni + 29.1Si + 16.9Cr + 290As + 6.38W$$

These formulas present another way of describing the effect of alloying elements on both the Fe-C diagram and the transformation behaviour of steels. Elements that stabilize austenite diminushes the arrest temperatures Ac3 and Ac1 as evidenced by their negative contributions in the corresponding equation, whereas elements that stabilize ferrite or carbide increase Ac3 and Ac1. The effect of alloying elements on Ac3 temperature has also been determined by thermodynamic calculations [KIRK78].

3.2.2 Austenitic Phase transformation during heating

When the austenitization is processed at a sufficiently slow heating rate, the initial and end temperatures of transformation are respectively noted $\mathbf{Ac_1}$ and $\mathbf{Ac_3}$ **(Figure 3.6)**. When the heating rate is faster, then the initial and end temperatures of transformation are moved towards higher values still noted $\mathbf{Ac_1}$ and $\mathbf{Ac_3}$ but which correspond to an extended domain of transformation. Thus, the heating rate influences both the kinetics of transformation and the beginning and end points of transformation.

During the austenitization, two other parameters play an essential role: the maximum temperature reached and the duration of the maintain period at this temperature. These two parameters determine the parameter of austenitization which leads to a balance between time and temperature. The higher value of this parameter means the larger size of the austenitic grain. The size of the austenitic grain has an influence on the transformations during cooling. All transformations carry out nucleation and growth. Nucleation is done preferably on discontinuities of the reticulum and for this reason the grain boundaries represent a privileged place. A change of the austenitic grain size affects the spatial distribution of the grain boundaries and thus influences the kinetics of transformation during cooling. In steels, austenite can decompose into a large variety of microstructures that are distinguished by the atomic mechanism of transformation **(Figure 3.7)**.

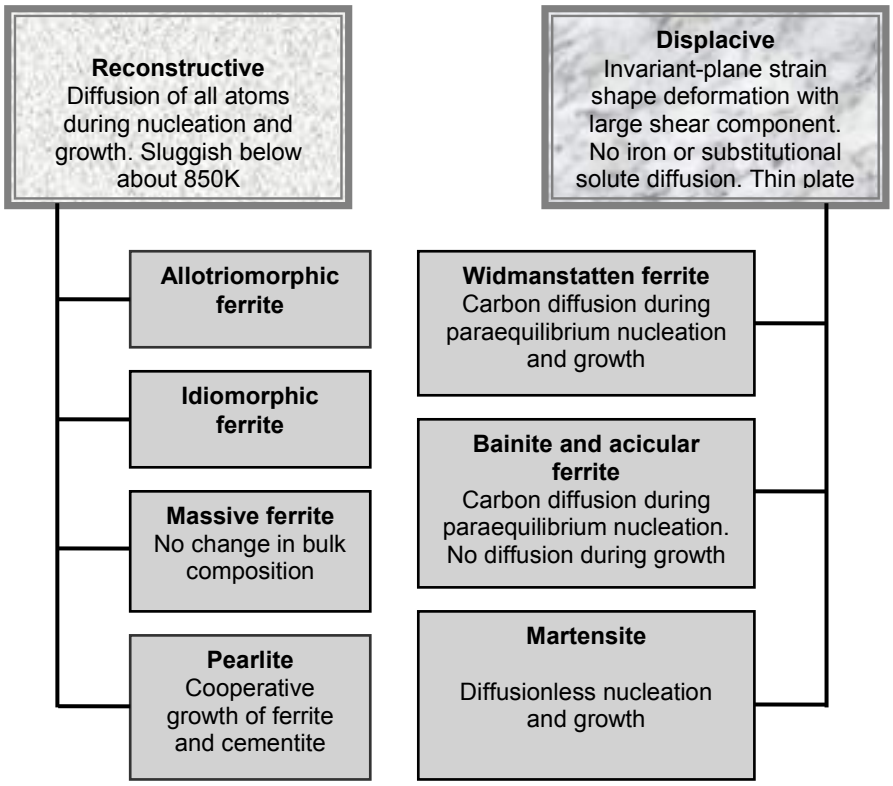

Figure 3.7 Transformation products of austenite [BHAD01]

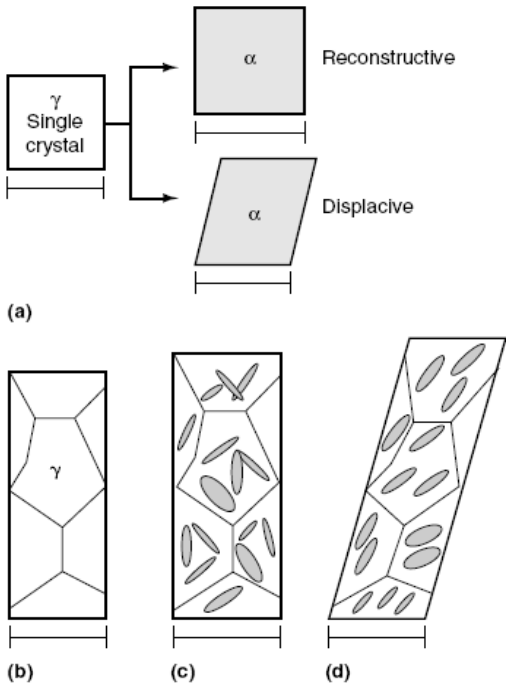

Figure 3.8 Shape changes accompanying unconstrained transformation [BHAD01]

In a displacive transformation, the change in crystal structure is achieved by a deformation of the parent structure. A reconstructive transformation is one in which the change in structure is

achieved by a flow of matter, which occurs in such a way that strains are minimized. All the transformations cause changes in shape **(Figure 3.8(a)),** which for reconstructive transformations simply reflects the change in density. Note that the horizontal scale bars are all the same length. Two kinds of shape changes may occur when a single crystal of austenite transforms to a single crystal of ferrite, as shown in **Figure 3.8(a)**. **Figure 3.8 (b)** shows a polycrystalline sample of austenite, and **Figure 3.8(c)** a sample that has been partially transformed by a reconstructive transformation mechanism into a random set of ferrite plates. Similarly polycrystalline sample of austenite that has partially transformed by a displacive transformation mechanism into an organized set of ferrite plates is shown in **Figure 3.8(d).**

3.2.3 Ferritic and Pearlitic Transformations

Pearlite is formed when the concentration of carbon in austenite reaches the eutectoid 0.76% of carbon. The austenite is decomposed simultaneously into ferrite and cementite. This is called eutectoid transformation; by the equilibrium condition there is no mother phase left after the phase transformation. Steels in which the carbon content is lower than 0.76% are called hypoeutectoids; they contain free ferrite in addition to pearlite. When the carbon content is more than 0.76% steels are called hypereutectoid; they contain free cementite. The ferritic transformation is accompanied by a distribution of carbon in ferrite and austenite; the driving force must be enough to provide energy for the diffusion of carbon. The driving force must reach a certain value to start the transformation, which explains that the transformation always takes place at a temperature lower than indicated by the equilibrium diagram. Nevertheless, ferritic transformation and pearlitic transformations are close to thermodynamic equilibrium. These changes are limited by the carbon diffusion kinetics. When the cooling becomes too fast as compared to the time for diffusion of these elements, the phase transformation stops. The austenite is then stabilized, and reaches a temperature well below the equilibrium temperature where the other types of transformations take place.

3.2.4 Martensitic Transformation

The martensitic transformation occurs very far from the thermodynamic equilibrium. When austenite is cooled very quickly, carbon does not have time to diffuse and ferrite cannot appear. Transformation occurs at temperatures well below eutectoid temperature and occurs extremely fast, i.e. at the speed of sound. Just like ferrite and pearlite, martensite is formed by a mechanism of nucleation and growth. The martensitic transformation is with characteristics

of instantaneousness nucleation, quick growth with limited size of martensitic plate, and the process is mostly due to the formation of new martensitic plates than on growth of old martensitic plates. New martensitic plates often appear on the boundaries between new phase (martensite) and old phase (austenite). It means that nucleation sites are located inside the grains, conversely to the diffusion transformation , for which nucleation occurs at the grain boundaries **(Figure 3.9)**. During martensitic transformation, there is no diffusion, and the transformation progresses through local atomic rearrangement. It stops transforming remaining austenite when the supplied energy becomes insufficient. Under anisothermal conditions, and for fast cooling rates, the ferritic diffusion transformation is stopped. Contrary to the bainitic transformation, the martensitic transformation occurs at higher cooling rate. However, in some specific martensitic steels, when the austenite is cooled, only martensitic transformation occurs at low temperatures, whereas no phase transformation happens at high temperature or mesothermal state [ZHOU04] [QIAO00]. In steels, martensite exists in many forms, according to different morphological characteristics and sub-structure, namely: lath martensite, flake martensite, butterfly shaped martensite, thin sliced martensite and thin plate martensite, etc. The lath martensite and flake martensite are often observed. Usually, the former appears with substructure of high-density dislocations, and the substructure of the latter is twin crystal.

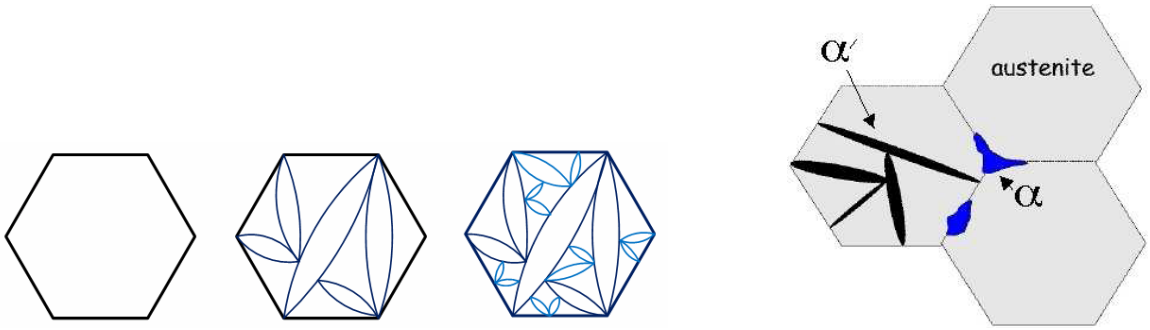

Martensite (α') is hindered by austenite grain boundaries whereas allotriomorphic ferrite (α) is not

Figure 3.9 Schematics for the formation of martensite plates

3.2.5 Bainitic Transformations

Bainitic transformation is an intermediate transformation between pearlite and martensite transformation and is the product of intermediate cooling rates. It had been postulated that the

transformation involves the formation of flat plates of supersaturated ferrite along certain crystallographic planes of the austenite grain. The ferrite was then supposed to decarburise by rejecting carbon at a rate depending on temperature, leading to the formation of carbide particles which are quite unlike the lamellar cementite phase associated with pearlite. The mechanism of transformation is shown in **Figure 3.10**. Bainite can be obtained by isothermal transformation at all temperatures where formation of pearlite and proeutectoid ferrite is sluggish, and also at temperatures below the martensite-start temperature. In steels where the transformation to bainite could be carried out without interference from other reactions, experiments demonstrated that the degree of transformation to the bainite decreases (ultimately to zero) and that the time to initiate the reaction increases rapidly when increasing the isothermal transformation temperature. This led to the definition of a bainite-start temperature (Bs) above which there is no reaction. This temperature was always found to lie well within the (metastable) $\alpha + \gamma$ phase field. Other transformations could follow bainite but in all cases rapid growth of bainite stops prematurely before the complete transformation of austenite into other phases.

Bainite grows in the form of clusters of thin lenticular plates or lathes, known as sheaves. The plates within a sheaf are known as sub-units. The growth of each sub-unit is accompanied by an invariant-plane strain shape change with a large shear component. The sub-units are to some extent separated from each other by films of residual phases such as austenite or cementite, so that the shape strain of the sheaf as a whole tends to be much smaller than that of an isolated sub-unit. The plates within any given sheaf tend to adopt almost the same crystallographic orientation and have identical shapes. Because of the relatively high temperatures at which bainite grows (where the yield stresses of ferrite and austenite are reduced), the strain causes plastic strain which in turn leads to a relatively large dislocation density in both the parent and product phases; other kinds of defects, such as twinning and faulting are also found in the residual austenite. This plastic accommodation of the shape change explains why each sub-unit grows to a limited size which may be far less than the austenite grain size.

The growth of bainitic ferrite undoubtedly occurs without any redistribution of iron or substitutional solute atoms, even on the finest conceivable scale at the transformation interface. Although some access carbon is retained in solution in the bainitic ferrite after transformation, most of it is partitioned into the residual austenite. This redistribution of carbon could of course occur after the diffusionless growth of bainitic ferrite.

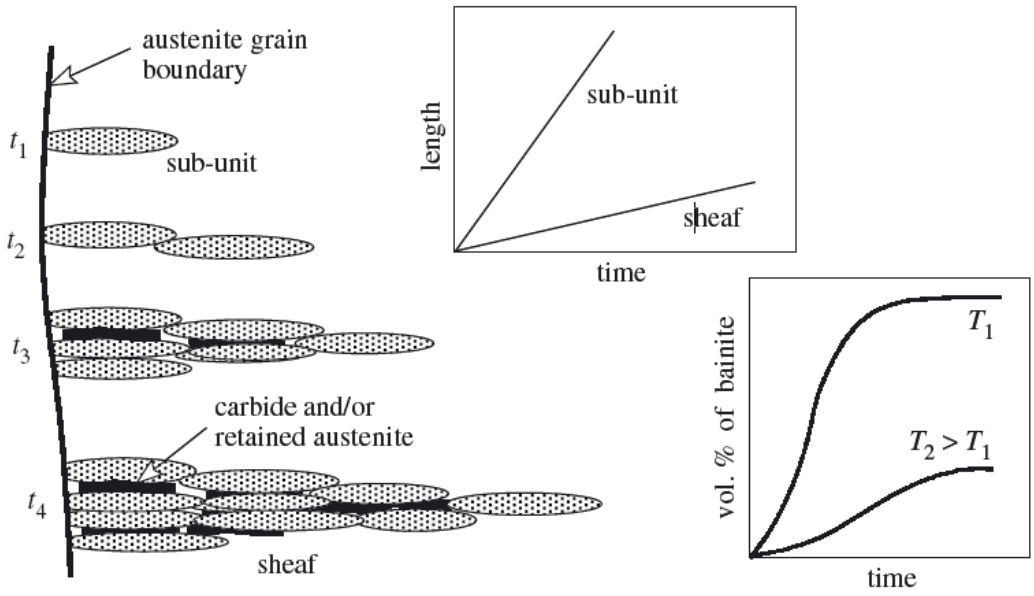

Figure 3.10 The microstructural features relevant in the kinetic description of a bainitic microstructure.

There is the lengthening of sub-units (individual platelets) and of sheaves (clusters of platelets), the latter by the repeated nucleation of sub-units, the precipitation of carbides and the change in volume fraction as a function of time and temperature [BHAD01]

3.2.6 Factors effecting phase transformation

3.2.6.1 Thermal Effect

In terms of thermal effect on phase transformation, there are four factors that should be taken into account: the heating rate, the highest temperature reached, of the dwell time at high temperature and the cooling rate. The phase transformation strongly depends on the cooling rate and the composition of alloying elements. Two types of diagrams are used to represent in a comprehensive manner transformations that occur during a given heat treatment: Time-temperature transformation (TTT) diagrams are obtained by fast cooling of austenite followed by a dwell-time at a constant temperature; and continuous cooling transformation (CCT) diagrams that describe the transformations during cooling at constant speed.

It is known that the decomposition of austenite happens in anisothermal conditions and more or less coarse mixture of ferrite-cementite, bainite and martensite according to the speed of cooling. The physical mechanism during the nucleation of the new phases depends on the start temperature of transformation, which is a function of the cooling rate. At higher cooling speeds, the initial transformation temperature is lower.

Improving the top temperature increases the grain size of austenite and the stability of austenite. The heating rate influence on the austenite transformation is shown in **Figure 3.11**. For a very slow heating rate, there is enough time to make the austenite fraction to reach equilibrium state for each temperature. For an increasing heating rate, it starts moving away from equilibrium state, and the increase in austenite fraction is slower and with hysteresis effect [LEBL84, 85]. This is well in accordance with physical reality.

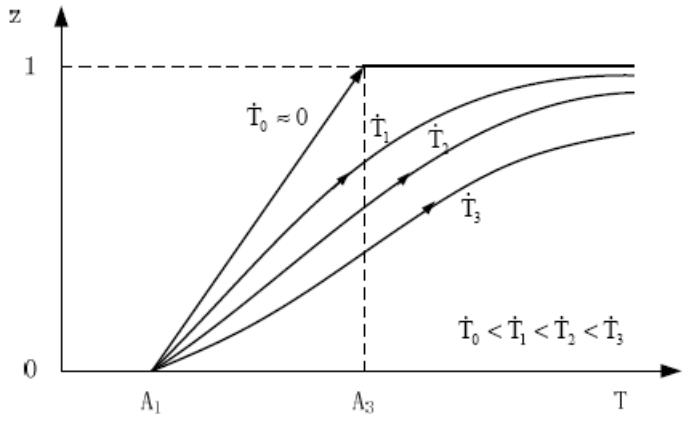

Figure 3.11 Schematic diagram of heating rate influence on austenite phase transformation [LEBL84]

3.2.6.2 Austenite Grain size

The austenite grain size plays an important role in the transformations during cooling. Several authors [CONS92][MART99], evaluated the influence of the austenite grain size on the transformations during cooling. These studies show that the grain size not only modifies the thermodynamic equilibrium but the kinetics as well.

3.2.6.3 Effect of alloying elements

To understand the metallurgy of steels, attention is to be paid to the effects that the key alloying elements have on phase stability and properties. Supermartensitic stainless steels and martensitic precipitation hardening stainless steels are essentially alloys based on iron but containing chromium and nickel. They owe their name to their room temperature martensitic microstructure. To understand the metallurgy of this family of steels, attention is paid to the effects that the key alloying elements have on phase stability and properties.

- *Carbon and nitrogen*

The transformations of phase are related to the possibility of diffusing carbon, and the carbon concentration modifies the transformations of phase. Carbon and nitrogen are strong austenite stabilisers in Fe-Cr alloys. Higher carbon content leads to more ferrite to be formed in the ferrite steel. Martensite hardness increases sharply with carbon concentration and therefore raises the probability of sulfide stress corrosion-cracking and hydrogen-induced cold-cracking.

- *Chromium*

Chromium is a ferrite stabiliser. Low carbon Fe-Cr stainless steels have a ferritic or martensitic, possibly semi-ferritic, microstructure depending on composition. When the chromium content is below approximately 12 wt%, it is possible to obtain a martensitic microstructure since the steel can be fully austenitic at elevated temperatures. Such steels solidify as δ-ferrite and are completely transformed to austenite (γ) at high temperature, after rapid cooling non-equilibrium martensite can be formed. A chromium content greater than approximately 14 wt% gives a completely ferritic stainless steel over the whole temperature range corresponding to the solid state and hence cannot be hardened on quenching. Between the austenite phase field and the fully ferritic domain, there is a narrow range of compositions which defines the semi-ferritic alloys, with a microstructure consisting partly of δ-ferrite which remains unchanged after solidification, the remainder being martensite **(Figure 3.12 a)**.

- *Nickel*

Austenite can be stabilised using substitution solutes. Nickel has the strongest effect in this respect **(Figure 3.12 b)** and also a tendency to improve toughness. Nickel influences also Ms (martensite-start temperature) as shown in **Figure 3.13**. Cr, Ni and Mo concentrations influence the boundaries of the austenite, ferrite and martensite phases **(Figure 3.14)**.

In addition, other elements have their own functions in metallurgy, for example, manganese and copper are austenite stabilising elements whereas silicon and titanium are ferrite stabilising elements. For the sake of completeness, the synthesis of [MARU01] about the role of elements is given in **table 3.1**

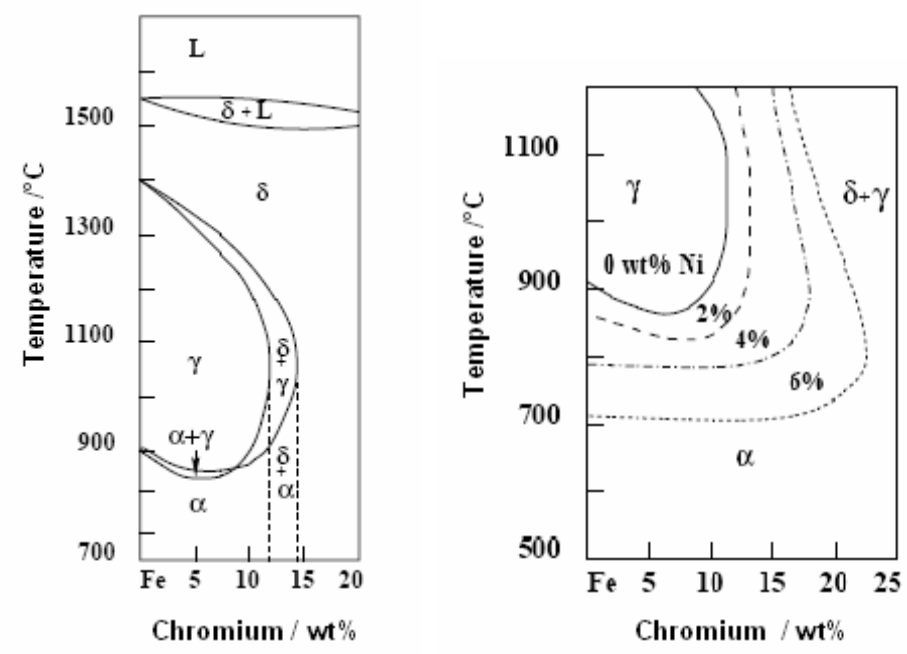

Figure 3.12 Influence of Nickel on Phase field

Figure 3.12 (a) Range of liquid, austenite and ferrite (α and δ) phase in the iron-chromium constitution diagram with a carbon content below 0.01 wt%.

Figure 3. 12 (b) Influence of nickel on the range of the austenite phase field in the iron-chromium system [FOLK88].

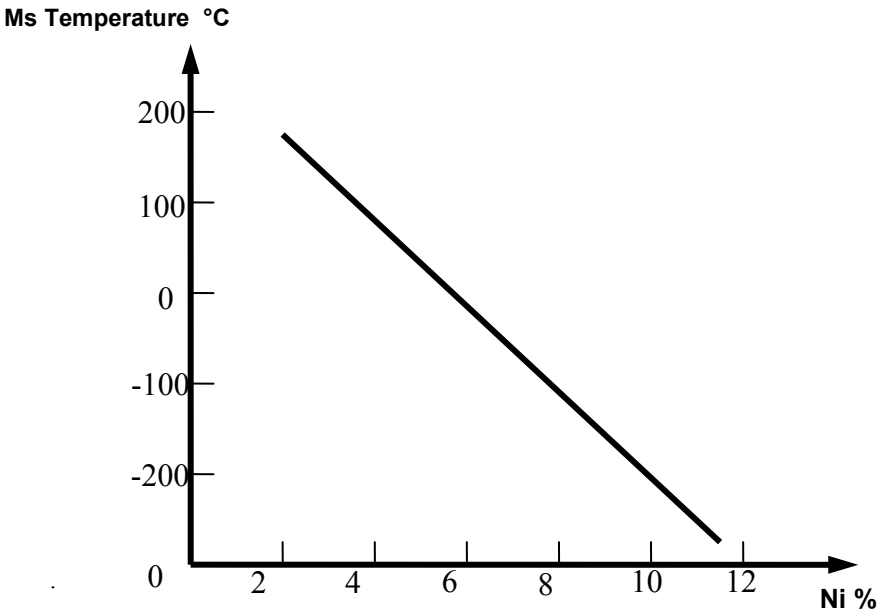

Figure 3.13 Martensite start temperature (Ms) plotted against Nickel content for 18 Cr wt%-0.04C Wt% steel [LACO93]

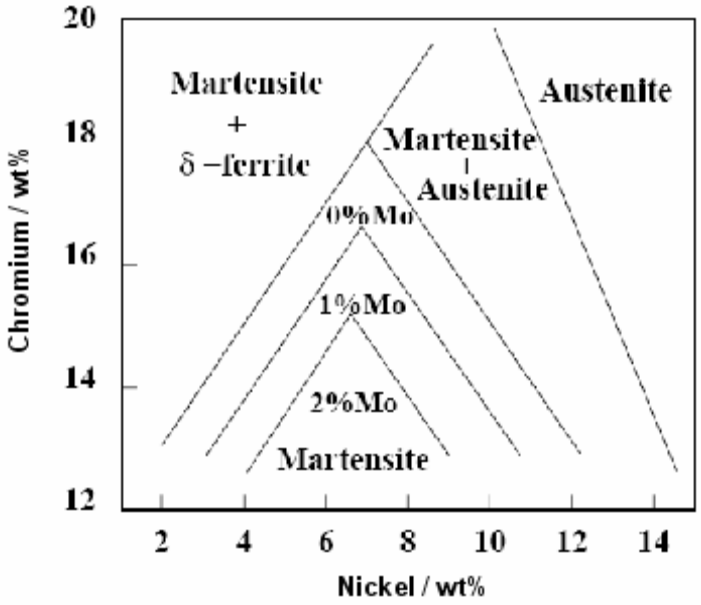

Figure 3.14 Experimental diagram showing the boundaries of the austenite, ferrite and Martensite phases as a function of Cr Ni and Mo concentration for 0.01 wt% C after austenization at 1050 °C and air cooling [KOND99]

Table 3.1 Effects of Alloying elements [MARU01]

ELEMENT	MERITS	DEMERITS
B	Improve creep strength and quench hardenability. Stabilize M23C6 particles and delay their coarsening.	Reduce impact toughness.
C	Necessary to make M23C6 and NbC.	
Co	Suppress δ-ferrite. Decrease D.	
Cr	Improve oxidation resistance. Lower Ms. Raise A1. Main element of M23C6.	Increase D.
Cu	Suppress δ-ferrite. Promote precipitation of Fe2M	
Mn		Increase D and reduce creep strength. Lower A1. Promote M23C6.
Mo	Lower Ms. Raise A1. Solid solution hardening.	Accelerate growth of M23C6.
N	Necessary to make VN.	
Nb	Form MX and contribute to strengthening	Promote precipitation of z phase.
Ni		Increase D and reduce creep strength. Lower A1.
Re	Prevent the loss of creep rupture strength. Lower Ms.	Lower A1.
Si	Improve oxidation resistance.	Increase D and reduce creep strength.
V	Form MX and contribute to strengthening.	
W	Lower Ms. Raise A1. Delay coarsening of M23C6 particles. Solid solution hardening	

3.2.6.4 Stress

The influence of stress on the transformations of phases is obvious. Applied stress modifies the energy stored in material and many work shows that the mechanisms of nucleation are most affected [DENG87] [DENS87] [GAUT94]. The applied stress is either hydrostatic or uniaxial. On one hand, only extremely high value of hydrostatic pressure (a few hundreds of MPa) can have a remarkable influence on transformation kinetics, and on the other hand, slight or moderate uniaxial stress may affect the transformation. Thus Gautier [GAUT94] showed that the time of beginning and end of transformation depend on the applied pressure in the case of an isothermal transformation in eutectoid steel. In the same way, Patel [PATE53] studied the influence of applied stresses on the martensite start temperature. Hydrostatic pressure delays the transformation whereas compression or tensile stresses make the transformation to start earlier. However, in the case of the transformations with continuous cooling, if the cooling rate is relatively high (> 1°C/s), it seems that low uniaxial stress has a little influence on the transformation kinetics.

3.4 Phase transformations and Residual Stresses

Strains due to phase transformations modify residual stresses and strains. It is well known that the martensitic transformation of carburized steels puts the surface under compression. It is argued that this is because of the expansion at the surface due to formation of the lower-density martensite from austenite. Phase transformation can also compensate for stress. Greenwood and Johnson [JOHN62][GREE69] showed that when a phase change is accompanied by a change in volume, the tensile strain expected when transformation occurs under the influence of a tensile stress σ is given by:

$$\varepsilon = \frac{5}{6}\frac{\Delta V}{V}\frac{\sigma}{\sigma_Y} \tag{3.1}$$

where σ_Y is the yield stress of the weaker phase and $\frac{\Delta V}{V}$ is the transformation volume strain.

The role of shear strains associated with transformation has been emphasized in later work by Magee and Paxton [MAGE70], and subsequently by Fischer [FISC90], Leblond et al. [LEBL89], and Bhadeshia et al. [BHAD91]. Not only does transformation affect stress, but the latter

modifies the development of microstructure. The microstructure tends to be more organized when transformation occurs in a stress's parent phase, because the stress favours the formation of certain orientations relative to others. This is illustrated schematically in **Figure 3.8 (b) to (d)**.

There is little doubt that transformations in steel play a major role in the development of residual stresses. For reconstructive transformations (for example, pearlite), it is the difference in density between the parent and product phases that contributes to transformation plasticity. The plasticity can be much larger for displacive transformations (Widmanstatten ferrite, bainite, martensite) because of the large shear component in the deformed shape when these transformation products form [BHAD01]. These are quite sophisticated effects which, with few exceptions, are not incorporated in most residual stress analyses.

3.5 Phase Transformation Models

3.5.1 Kinetic models

The first model for phase transformation was proposed by Johnson and Mehl [JOHN39], then Avrami [AVRA39,40], in order to predict the evolution of the proportions of pearlite.

$$z = 1 - e^{\frac{\pi}{3} N G^3 t^4} \tag{3.2}$$

with

z : voluminal proportion of phase transformed

N : rate of nucleation

G : rate of growth

t : time

or in a more simplified form

$$z = z_{eq}(1 - \exp -(t / \tau(T))^n \tag{3.3}$$

where

$z_{eq}(T)$: voluminal proportion of phase in equilibrium

$\tau(T)$: constant of time

n : Empirically obtained constants for the phase

These models suppose that the pearlite appears through nucleation then growth, depending on austenite. If the mechanisms are different, these models are used for the transformation of ferrite and bainite [BHAD01] [WEBS01]. The equation of Johnson-Mehl-Avrami is written for isothermal transformation, whereas the demand in calculation comes mainly from heat treatments, which are anisothermal. That's why some authors propose modifications of the preceding model to take into account anisothermal effects, see Inoue [INOU78] and further models by [FERN85] [HABR92] [SJOS85]. These models considered not only the effects of anisothermal treatments but also the role of applied stress and percentage of carbon. When the temperature is not constant a derivative form of the Johnson-Mehl-Avrami equation is used:

$$\frac{dz}{dt} = n\left(\frac{z_{eq}(T) - z}{\tau(T)}\right).\left(\ln\left(\frac{z_{eq}(T)}{z_{eq}(T) - z}\right)\right)^{(n-1)/n} \tag{3.4}$$

The martensitic transformations are treated separately, because considered as independent of time. The empirical law of Koistinen and Marburger [KOIS59] gives the volume fraction of martensite according to the temperature. The theoretical justification of this equation was given by Magee [MAGE70]

$$z_\alpha = z_\gamma(1 - e^{\beta<Ms-T>}) \tag{3.5}$$

where z_α and z_γ are volume proportion of martensite and austenite respectively; Ms is the martensite start temperature; β a coefficient material dependent; and T the temperature.

3.5.2 Phenomenological models

The generalization of the models based on the Johnson-Mehl-Avrami laws was done on phenomenological considerations and therefore lack physical bases. Their principal disadvantage comes from the fact that they can only describe single type of transformations. However in the case of heat treatments or welding, a same structure is prone to various transformations. Other types of purely phenomenological models were developed. Thus Leblond [LEBL84,85] proposed a model based on a law of simplified evolution utilizing a proportion of transformed phase in equilibrium and a constant of time

$$\dot{z} = \frac{z_{eq}(T) - z}{\tau(T)} \tag{3.6}$$

where z : volume proportion of new phase

$z_{eq}(T)$: volume proportion of phase in equilibrium

$\tau(T)$: constant of time

This model, identified from CCT diagram, gives good results for the ferritic and perlitic transformations but it is not ready to reproduce the faster transformations correctly. Leblond introduced a dependence on *dT/dt*, which enables to use the model for bainitic and martensitic transformations. However, the principal difficulty resides in the identification of the constants.

Therefore, Waeckel [WAEK94,96] proposed another model with easily identifiable parameters starting from CCT diagram and able to reproduce thermal histories of welding. The following law of evolution is proposed:

$$\dot{\underline{z}} = f(T, \dot{T}, \underline{z}, d) \tag{3.7}$$

with $\underline{z}$: proportion of phase considered

d : grain size of austenite

Conversely to the model of Leblond, in the model of Waeckel, $\dot{T}$ is an internal variable, which better fits the physics of the transformation since the kinetics is anisothermal. It should be also noted that the temperature Ms is not a metallurgical state, since it can vary during transformation. It was blended in the metallurgical variables. Moreover the volume proportion of martensite is treated separately and follows the equation of Koistinen and Marburger [KOIS59]. The grain size of austenite becomes a parameter of the model and not a variable. The function f is known in a certain number of states, and one can deduce the volume fractions of the phases by linear interpolation. This model describes well the transformations of phases during cooling at a constant rate.

3.6 Mechanical calculations with phase transformation:

It is a well known fact that structural transformations in steel as described in the previous section induce anomalous plastic behaviour which has been explained in details by several authors and a series of articles is devoted to the modeling of this phenomenon. Many models have been proposed by INPL (Institut Polytechnique de Loraine) covering a broad field of plastic [DENI87][HABR92][SJOS85] or viscoplastic [ALIA98][DENI87][GAUT94] behaviours, which can be coupled with the metallurgy and the concentration of carbon or grain size of austenite. The behaviour of material is described by aggregate variables and the parameters of the

behaviour law are calculated by a linear mixture of phases [ALIA98] [COLO92] [DENI87]. Another type of model was also developed where a particular evolution law of the plastic flow for each phase was considered and the plastic strain for all the phases was supposed to be the same [DENI96][GAUT94][LIEB88].

Two aspects can be distinguished in the plastic behavior during metallurgical transformations:

(i) Classical plasticity, i.e. response of the material (mixture of the two phases) to variations of the applied stress or the temperature;

(ii) Transformation plasticity, i.e. response of the material to a variation of phase proportions.

This phenomenon is a plastic flow occurring when an external load (even small regarding the yield stress of the weaker phase) is applied during transformation. Greenwood and Johnson [GREE65] and Magee [MAGE70] give two complementary explanations to this phenomenon:

- orientation of the local plastic flow due to phase volume incompatibility by external loading (Greenwood and Johnson mechanism)
- Preferred orientation of the martensite plates arising from the external loading (Magee mechanism)

From the metallurgical point of view the Greenwood and Johnson mechanism is related to diffusional transformation and Magee effect is related to displacive transformation occurring for martensitic transformations.

Different kinds of empirical models have been proposed for plastic behaviour during phase transformation, using simply ordinary plasticity models integrating the effect of transformation plasticity through an artificial lowering of the yield stress during the transformation and by distinguishing between classical and transformation plasticity (e.g. [LEBL85]).

Leblond [LEBL84] has conducted a theoretical study of the problem by supposing that all the phases have the same thermo elastic characteristics. He showed that the macroscopic strain rates may be expressed in the following form:

$$\dot{E}^t = \dot{E}^e + \dot{E}^{thm} + \dot{E}^p \tag{3.8}$$

Or

$$E^t = E^e + E^{thm} + E^p \tag{3.9}$$

where E^e is the macroscopic elastic strain, E^{thm} is the macroscopic thermo metallurgical strain and E^p is total plastic strain. The rates of elastic strain $\dot{E}^e$ and $\dot{E}^{thm}$ follow usually a linear mixture law. A general expression for the total plastic strain $\boldsymbol{E^p}$ has been given by Leblond [LEBL85]. The general form of the time derivative of these equations is as follows:

$$\dot{E}^p = \dot{E}^{cp} + \dot{E}^{tp} \tag{3.10}$$

$\dot{E}^{cp}$ = (term proportional to $\sum$) + (A term proportion to $\dot{T}$)

$\dot{E}^{tp}$ = (term proportional to $\dot{z}$)

Where $\sum$ is the macroscopic stress, T is the temperature and z the volume proportion of the phase α formed by the transformation.

3.6.1 The macroscopic thermo-metallurgical strain:

Solid-state phase changes are characterized by geometric transformations of the crystal lattice. Austenite is a solid solution inserted in γ iron, whereas the ferritic phases are solid carbon solutions inserted in α iron. Due to their geometrical characteristics, these two types of crystalline structures have different densities which result, on the macroscopic level, in a so-called transformation-induced volumetric strain. This volume change associated with thermal dilatation and contraction defines the so-called thermo-metallurgical transformation strain. The thermo-metallurgical transformation strains are usually determined from free dilatometer tests [VINC02] [CORE01].

$$E^{thm}(T,z) = (1-z)\,\varepsilon_\gamma^{th}(T) + z\cdot\varepsilon_\alpha^{th}(T) \tag{3.11}$$

$$\varepsilon_\alpha^{th}(T) = \alpha_\alpha \cdot \left[T - T_{ref}\right]$$

$$\varepsilon_\gamma^{th}(T) = \alpha_\gamma \cdot \left[T - T_{ref}\right] - \Delta\varepsilon_{\alpha\gamma}^{25°C}$$

where

T_{ref} is the reference temperature

$\Delta\varepsilon_{\alpha\gamma}^{25°C}$ is the thermal strain difference between the two phases

α_γ is the thermal expansion coefficient of the austenite phase

α_α is the thermal expansion coefficient of the ferrite phase

3.6.2 Classical plastic strain and transformation-induced plasticity:

The transformation plasticity is generally described by an expression of Greenwood-Johnson type. To represent the transformation process we can use the general form as:

$$\varepsilon^{tp} = k \cdot f(z) \cdot \sigma \tag{3.12}$$

where σ is the applied stress; *f(z)* is a formula describing the evaluation of the transformation plasticity depending on the amount z of the formed phase and many expressions are presented in the literature for *f(z)*

$$f(z) = z(2-z) \tag{3.13}$$ [DENI87]

$$f(z) = z\left[1-\ln(z)\right] \tag{3.14}$$ [LEBL85]

$$f(z) = 3z - 2z^{3/2} \tag{3.15}$$ [LEBL85]

$$f(z) = \sin(0.5\pi z) \tag{3.16}$$ [BESS93]

$$f(z) = \ln\left(1+\frac{z}{\varepsilon}\right)^2 \tag{3.17}$$ [FISC90]

By definition *f(z)* = 0 for *z* = 0 and *f(z)* = 1 for *z* = 1. *k* is the transformation plasticity parameter given by the general form of equation:

$$k = c\frac{1}{\sigma_\gamma^y}\frac{\Delta V}{V} \tag{3.18}$$ [DALG08]

where ***c*** is a factor ranging between 0.66 and 0.83 [DALG08] $\frac{\Delta V}{V}$ is the change of the volume due to transformation; σ_γ^y is the yield strength of austenite at the actual temperature.

3.7 Proposed Model for Phase Transformation:

The metallurgical history of a point depends mainly on its thermal history. This dependency is described by a CCT diagram. This diagram gives the start and end of transformation temperatures, either according to cooling rate, or according to cooling time. For the metallurgical evolution of the material i.e. the phase proportion evolution is determined using the equations proposed in the subsequent paragraph. The CCT diagrams obtained experimentally for AISI 52100 steel in the work of various researchers will be used to determine model parameters. This is done by aligning the data of the CCT diagram of AISI 52100 steel as closely as possible with the predictions provided by the suggested models. This identification consequently involves executing successive tests with the numerical model for

different parameters, then selecting those which provide results comparable with those of the experimental diagrams.

In case of diffusion-controlled transformations, the metallurgical transformation kinetics during a heating/continuous cooling process is determined using the isothermal transformation kinetics for the material studied. The transformed fraction of phase ***i***, z_i is calculated based on the Avrami [AVRA39] type model designed to compute phase transformation kinetics during heating and cooling. The proposed model is expressed as:

$$z_i = z_i^{eq}\left[1-\exp\left\{-\kappa_i(T).(t)^{m_i(T)}\right\}\right] \tag{3.19}$$

where z_i is the average phase fraction of constituent i at time t

and z_i^{eq} is the maximum or equilibrium fraction of phase i that a phase can achieve after an infinitely long time determined from the equilibrium phase diagram with known temperature and chemical composition, and κ_i and m_i are empirically obtained constants for the phase i. From the previous investigations, the constant κ_i generally depends on temperature, chemical compositions, and prior austenite grain size. Conversely, the parameter n_i is usually known to be constant over the range of temperature and transformation conditions and according to Christian, the suggested value may range between 1 and 4.

The Avrami [AVRA39] equation was originally proposed for an isothermal condition, thus the equation cannot be directly utilized for non-isothermal cases such as transformation during heating or cooling. For non-isothermal transformation kinetics, it is assumed that heating or cooling curves can be divided into small time intervals within which the kinetics is isothermal. This method is called rule of additivity by Scheil where the temperature-time curve is discretized in a series of isothermal steps. On each step the volume fraction of new phase formed is calculated by using isothermal transformation kinetics. The principle of transition from isothermal step n to next step n+1 is based on the introduction of an equivalent time t_o for each transformation, as illustrated in **Figure 3.15**. z_i is the proportion of austenite formed at the end of step n. At the beginning of step n+1, the phase proportion z_i allows to determine the equivalent time t_o from isothermal kinetics defined for the step n+1.

$$z_{i,n+1} = z_{i,n+1}^{eq}\left[1-\exp\left\{-\kappa_i(T).(t_o+\Delta t)^{m_i(T)}\right\}\right] \tag{3.20}$$

$$t_o = \left(-\frac{1}{\kappa_i}\ln\left(1-\frac{z_{i,n}}{z_i^{eq}}\right)\right)^{\frac{1}{m_i}} \tag{3.21}$$

The parameters $\kappa_i(T)$ and $m_i(T)$ are obtained as follows.

At each temperature the coefficients $\kappa_i(T)$ and $m_i(T)$ may be calculated by assuming two points corresponding to a given percentage of the phase formed, for example assuming that the transformation curves of a continuous cooling transformation (CCT) diagram gives the start time t_S when a small proportion (e.g. 1%) of the new phase is formed and the end time t_E when 99% of the equilibrium phase fraction z_i^{eq} is formed at constant temperature T

$$\left.\begin{aligned} 1-\exp\left\{-\kappa_i(T).(t_S)^{m_i(T)}\right\} &= 0.01 \\ 1-\exp\left\{-\kappa_i(T).(t_E)^{m_i(T)}\right\} &= 0.99 z_i^{eq} \end{aligned}\right\} \qquad (3.22)$$

The transformation parameters $\kappa_{i(T)}$ and $m_{i(T)}$ are obtained by solving eq. (3.22):

$$\kappa_i(T) = -\frac{1}{(t_E)^{m_i(T)}}\ln(1-0.99 z_i^{eq}) \qquad (3.23)$$

$$m_i(T) = \frac{1}{\ln\left(\frac{t_S}{t_E}\right)}\ln\left[\frac{\ln(1-0.01)}{\ln(1-0.99 z_i^{eq})}\right] \qquad (3.24)$$

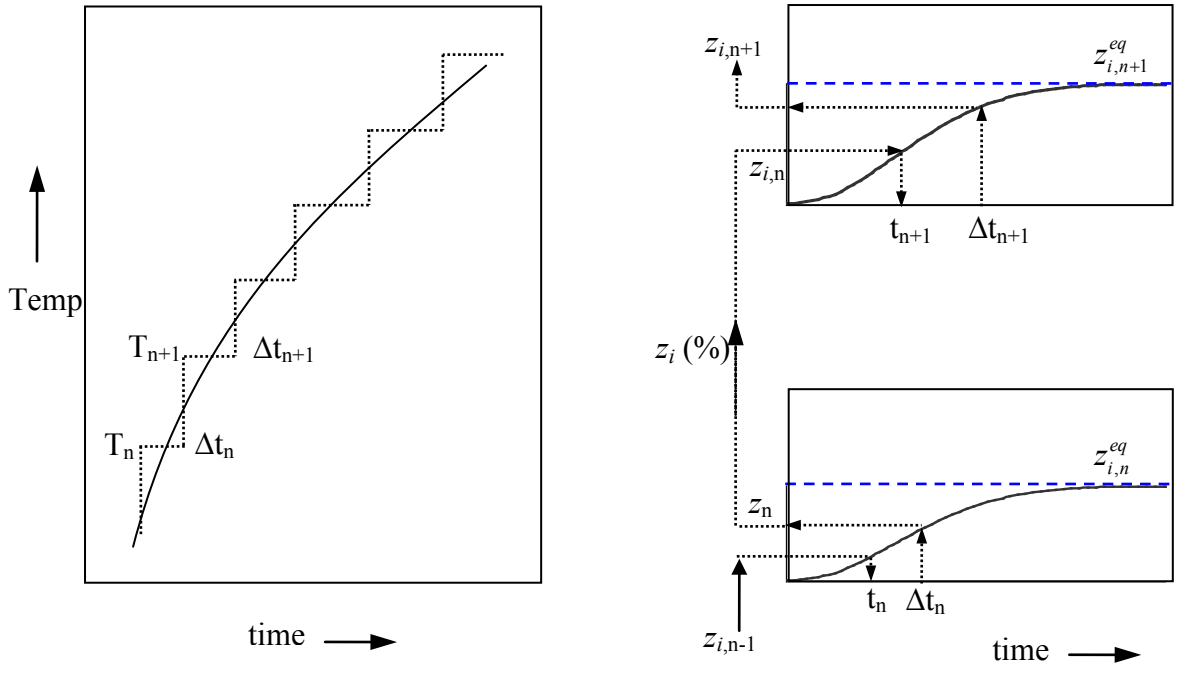

Figure 3.15 Schematic representation of computation of new phase formed

3.7.1 Heating

For heating process the model is based on the knowledge of the Isothermal Transformation diagram during heating. For example, the material under investigation (AISI 52100 / 100Cr6 steel) is a hypereutectoid carbon steel with a carbon content C >0.8 (**Figure 3.16**) and an initial ferrite-cementite structure. The time-temperature-austenitization (TTA) diagram taken for the model is shown in **Figure 3.17**.

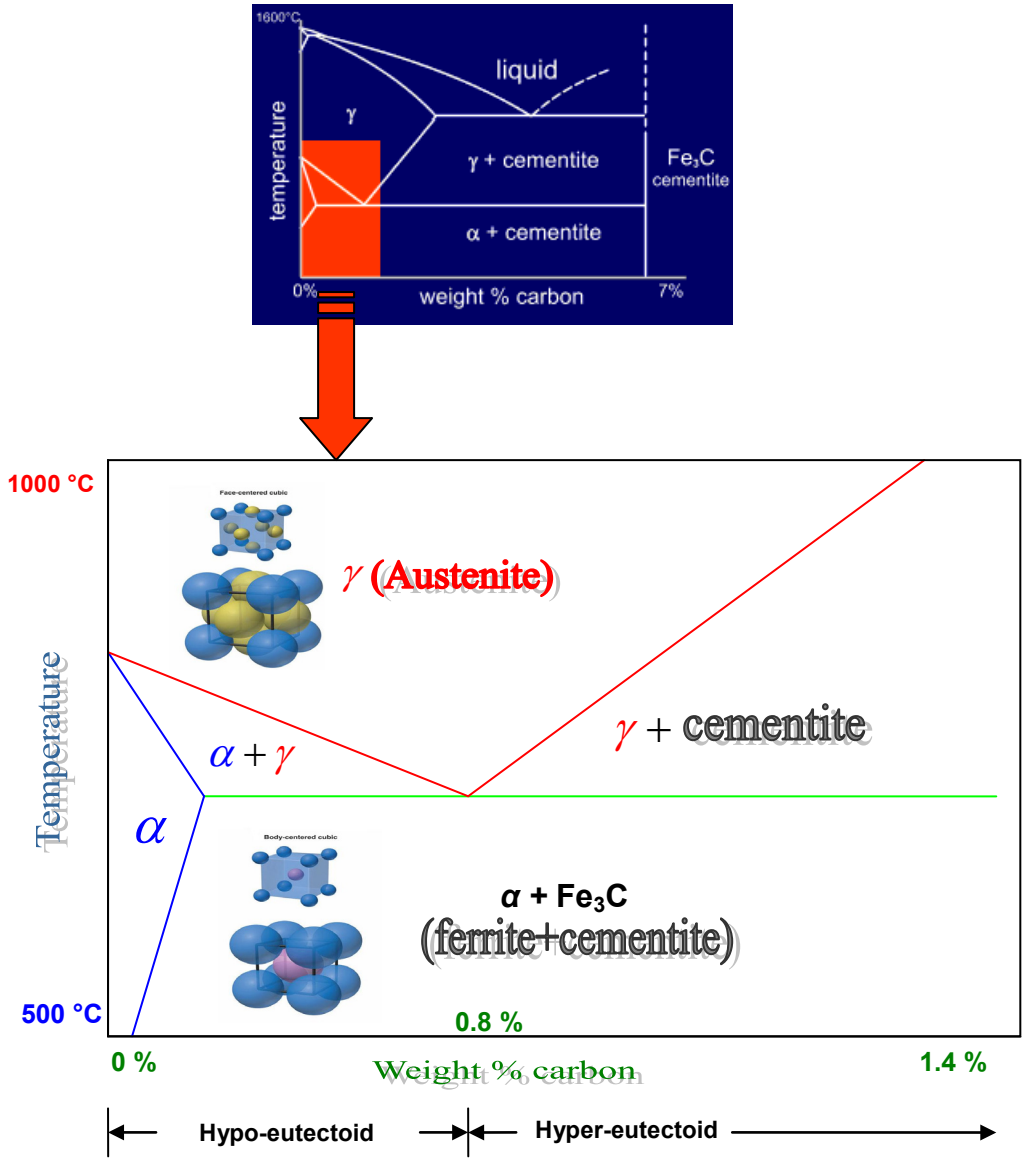

Figure 3.16 Iron Carbon diagram

The Austenite appears instantaneously from the pearlite, between temperatures Ac1 and Ac3, until complete dissolution of pearlite has occurred (curve 1, **Figure 3.17**). The percentage of austenite formed z^{eq} can be determined from CCT diagram (**Figure 3.5**). The end of

transformation is defined by curve 2 in Figure 3.17. Above the temperature Ac3, curve 2 represents the time required for the complete dissolution of both pearlite and ferrite. After this time the structure is totally austenitic.

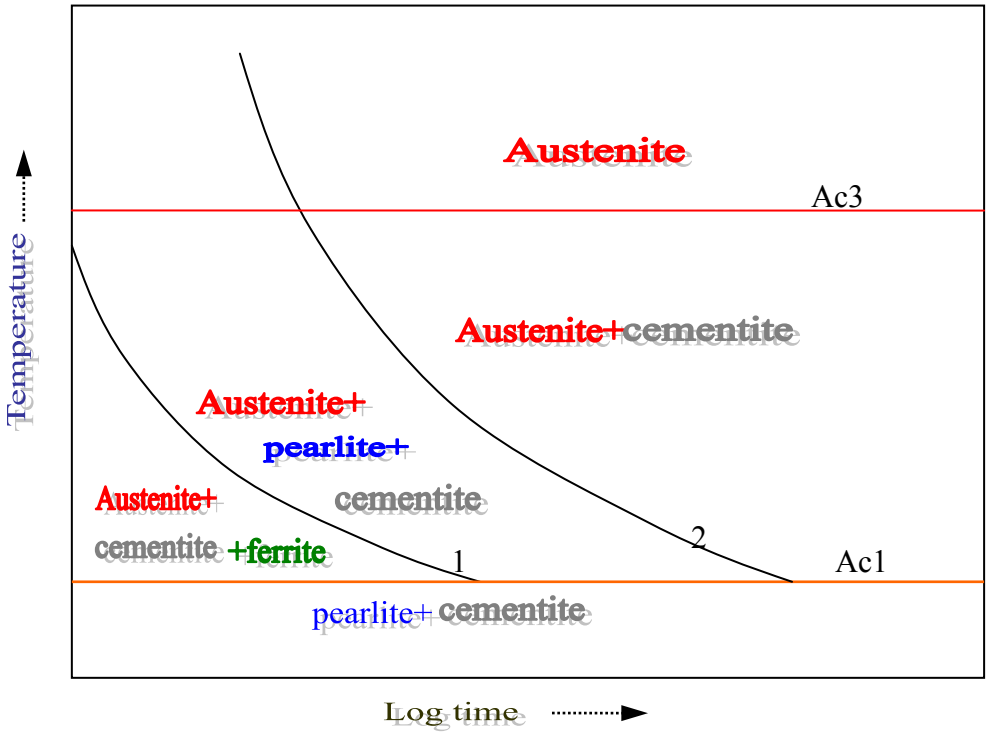

Figure 3.17 Isothermal Transformation diagram for a hyper-eutectoid steel (for heating) [SHIG63]

3.7.2 Cooling

After heating to an austenitizing temperature, cooling has to take place at various cooling rates to allow the material transformation into different phases. The carbon atoms previously dissolved in the austenite remain in their interstitial lattice positions and distort the corresponding body-centred cubic lattice into different lattice structures, depending mainly upon cooling rate and temperature. If the transformation process proceeds slowly (slow cooling rate), carbon has the opportunity to diffuse more or less into the iron lattice. This is called a diffusion controlled transformation. If the transformation process proceeds rapidly (high cooling rate), the face-centred cubic iron lattice shears without diffusion into a face-centred cubic iron lattice, the dissolved carbon is 'captured' in the iron lattice and distorts the body centred lattice tetragonal; as it forms. The material so produced is termed martensite (hard). This is called a diffusionless transformation through shearing.

For the phase transformation calculations during cooling, the model used is based on the knowledge of continuous cooling transformation (CCT) diagram for the steel (AISI 52100 steel), as illustrated in **Figure 3.5.** For diffusion-dependent phase transformation calculations (pearlite, bainite), equation 3.19 is used, while for the diffusionless transformation calculations (martensitic transformation) which do not depend directly on time but only on temperature, the Koistinen-Marlburger [KOIS59] equation is used:

$$z_M = z_\gamma \left\{1 - \exp\left[-\beta(M_S - T)\right]\right\} \tag{3.25}$$

where z_M and z_γ are martensitic and austenitic phase proportions, respectively, β is a material constant typically chosen in the order of 0.01 for plain carbon steel. M_S is the temperature at which the martensitic transformation starts, and T the temperature.

3.7.3 Verification of the proposed phase transformation model

3.7.3.1 Numerical Example:

The numerical implementation of the proposed model was carried out through a FORTRAN subroutine called PHASE using the FEM commercial software Abaqus®/standard. A series of FEM simulations were performed for a 2D single element (0.001×0.001 m^2). The element type CPE4T (4-node plane strain thermally coupled quadrilateral bilinear displacement and temperature) was used for the analysis.

3.7.3.2 Initial conditions, assumptions and boundary conditions

It was assumed that heating is uniform and the maximum temperature is sufficient to initiate austenite phase transformation. The component can therefore be assumed to be stress-free and 100% austenitic. The simulation starts with no stress at an initial temperature and above Ac3 with 100% austenite. The cooling characteristics in relation to phase transformations are given by the CCT diagram. The martensitic start temperature is given by Ms and the final temperature is the ambient one. Other critical transformation temperatures are given by Ps (pearlitic start temperature) and Bs (bainitic start temperature). Four metallurgical phases are assumed for the simulation: austenite, pearlite, bainite, and martensite.

The initial temperature was set to 20°C. A convective heat transfer was applied at the walls. The thermal and mechanical boundary conditions are shown in **Figure 3.18**.

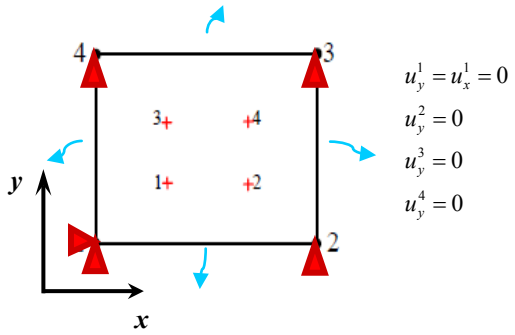

Figure 3.18 Mechanical and thermal boundary conditions for the single element analysis

The material used was AISI 52100 (100Cr6) steel. A detailed description of the material properties is given in section 4.4.2

The analysis was performed in two steps. The element was first heated to 1000°C at a constant heating rate and then cooled down to room temperature at different cooling rates. The different temperature histories used are shown in **Figure 3.19**. During cooling the heat source was removed and convective cooling was applied to all four sides of the specimen. The phase transformation calculations are done with the subroutine PHASE. Micro-structural constituents are defined as state variables. They are computed and updated inside the subroutine PHASE.

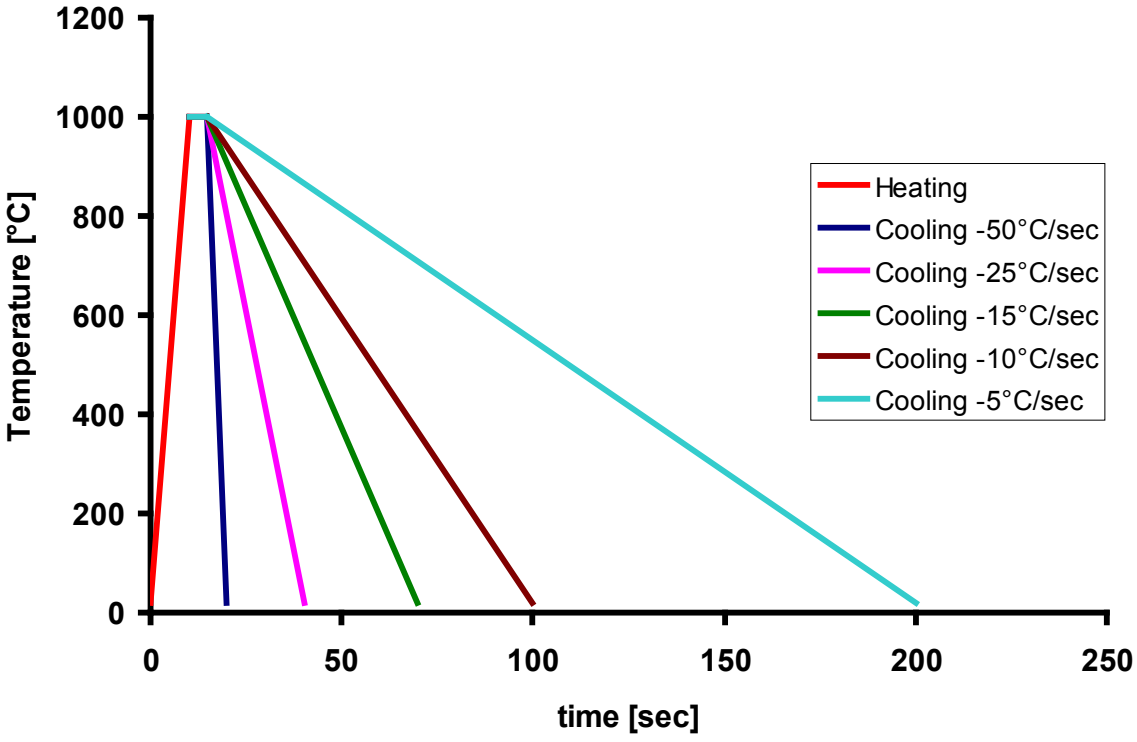

Figure 3.19 Different temperature histories used

3.7.3.3 Results and discussion

Figure 3.20 shows the CCT diagram for the material AISI 52100 (100Cr6) steel, which has been divided in four regions according to the number of transformations that may occur during cooling. The phase transformation calculations are made according to the cooling rate lines falling in the specified regions. For instance Region 1 corresponds to slow cooling rate where the only phase formed is pearlite due to very slow cooling rates. Regions 2 and 3 correspond to medium cooling rates where more than one phase (pearlite, bainite and martensite) may be formed. In Region 4 high cooling rate leads to the formation of martensite. The transformation product emerging from austenite during the continuous cooling process may be determined by only two factors, the transformation temperatures *(T_s,* and *T_f),* and the cooling rate from the CCT diagram, see **Figure 3.20**. Another important characteristic associated with the continuous cooling transformation is that each transformation product can only be formed within a certain cooling rate range, i.e., for a specific product ***i,*** there is a lower critical cooling rate $\dot{T}_L^i$, and an upper critical cooling rate, $\dot{T}_U^i$ **(Figure 3.20)** within which it is formed during cooling. For this case only pearlite phase may be formed within a cooling rate < 8 $K.s^{-1}$ and an overall cooling rate ranging between $\dot{T}_L^P = \sim 0$ $K.s^{-1}$ and $\dot{T}_U^P = \sim$ $K.s^{-1}$. The bainitic transformations occur within the range of cooling rate from $\dot{T}_L^B = \sim 8$ $K.s^{-1}$ and $\dot{T}_U^B = \sim$ 40 $K.s^{-1}$, and the martensite transformations in the cooling rate range between $\dot{T}_L^M = \sim 23$ $K.s^{-1}$ and $\dot{T}_U^M$ =≥ 40 $K.s^{-1}$. Similarly we may have combined pearlitic-bainitic-martensitic transformations in the cooling rate range from $\dot{T}_L^{PBM} = \sim 8$ $K.s^{-1}$ to $\dot{T}_U^{PBM} = \sim 22$ $K.s^{-1}$, and bainitic-martensitic transformations between $\dot{T}_L^{BM} = \sim 23$ $K.s^{-1}$ and $\dot{T}_U^{BM} = \sim 40$ $K.s^{-1}$.

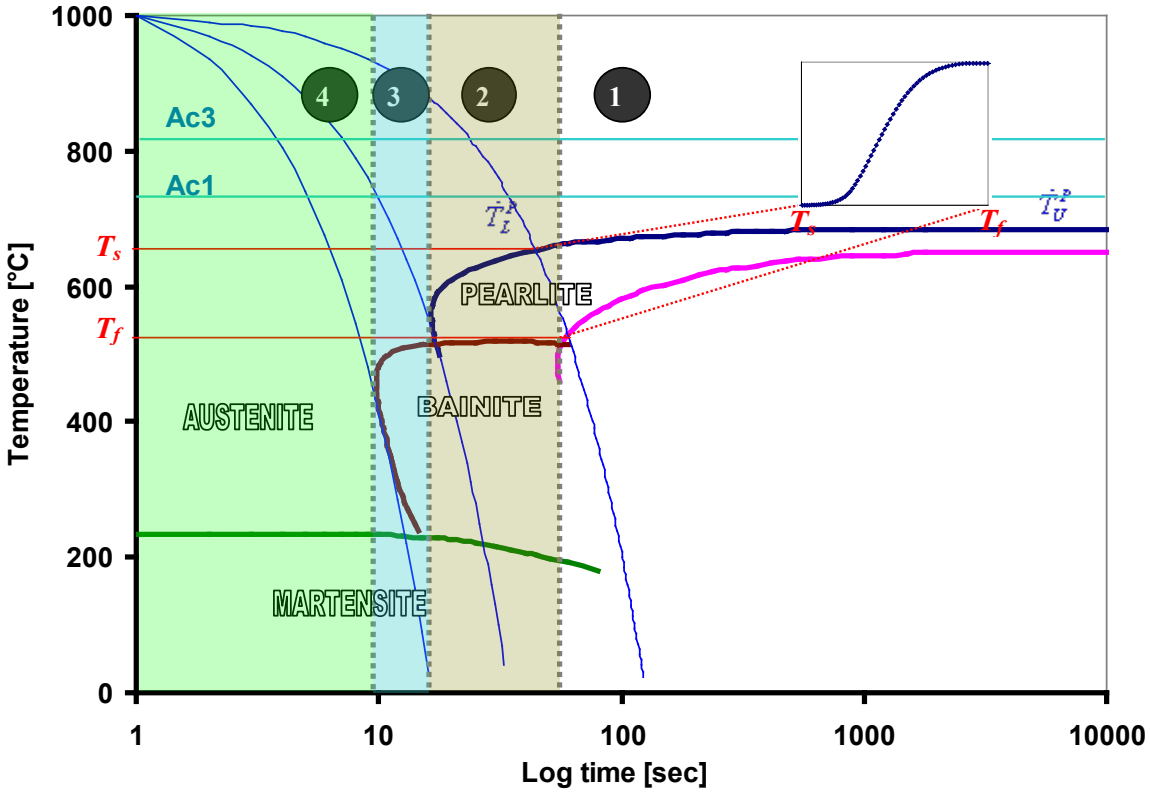

Figure 3.20 CCT diagram of AISI 52100 steel showing regions of possible phase transformations according to different cooling rates

Figures 3.19 to 26 show the phase transformation calculations from initial ferrite state to austenite during heating for constant heating rate, and austenite to pearlite, bainite and martensite phases during cooling according to different cooling rates. Similarly the evolutions of different phase fractions with cooling rate are shown in **Figures 3.27 to 29**.

The transformation products for a complete heating and slow cooling cycle are shown in **Figure 3.22**, only pearlitic phase transformation has occurred due to a slow cooling rate ($\dot{T}$=5 K.s^{-1}), which corresponds to region-1 in **Figure 3.20**. The combined transformation of pearlite, bainite and martensite phases from austenite at a cooling rate $\dot{T}$=10 K.s^{-1} is presented in **Figure 3.22** (region-2 in **Figure 3.20**). **Figure 3.23** shows transformation of bainite and martensite from austenite at a cooling rate of 20 K.s^{-1}, it may be observed that no more pearlite has been transformed as for region 3 in **Figure 3.20**. **Figure 3.24** shows that austenite has directly converted into martensite due to the high cooling rate (40 K.s^{-1}) corresponding to region 4 in **Figure 3.20**.

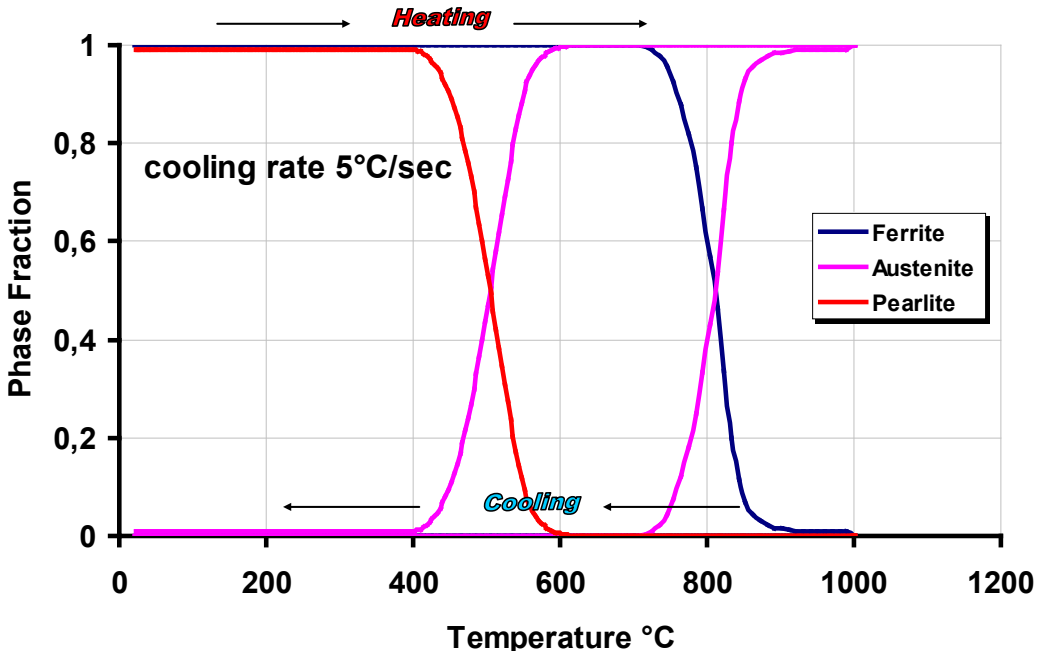

Figure 3.21 Phase transformation at slow cooling rate (Pearlite phase transformation)

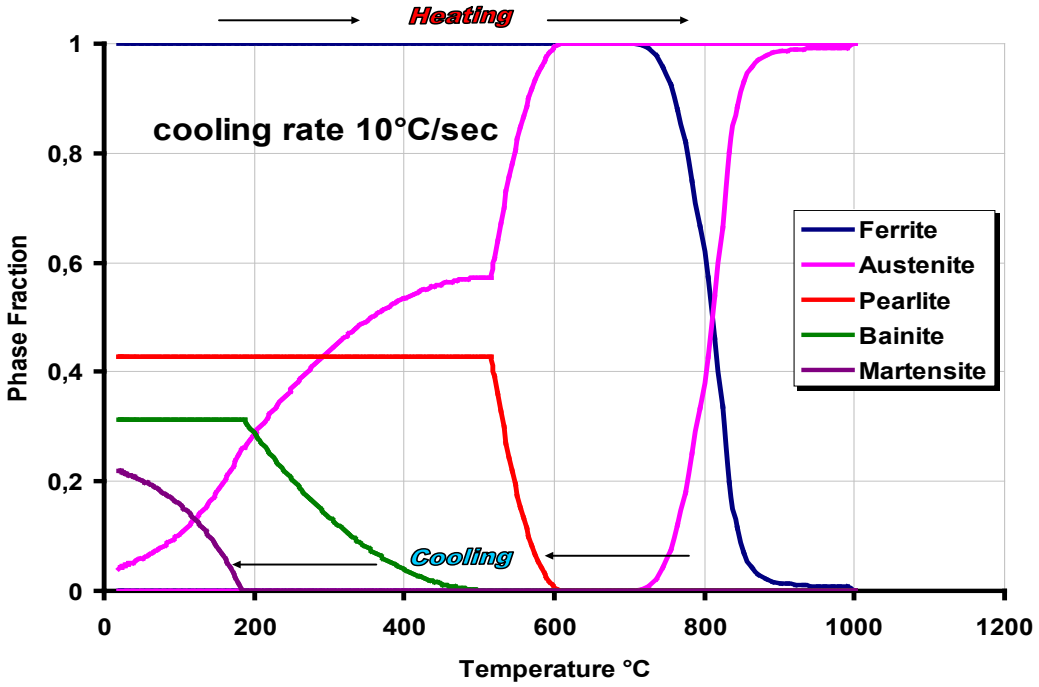

Figure 3.22 Evolution of different phases at medium slow cooling rate

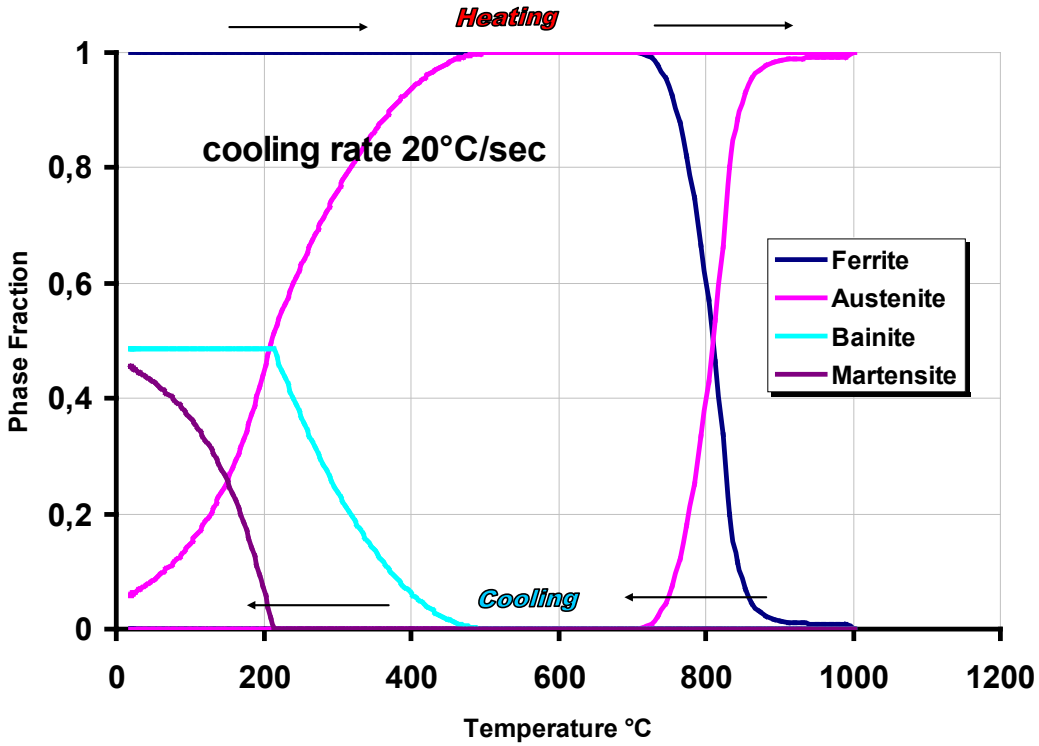

Figure 3.23 Evolution of phases at medium cooling rates

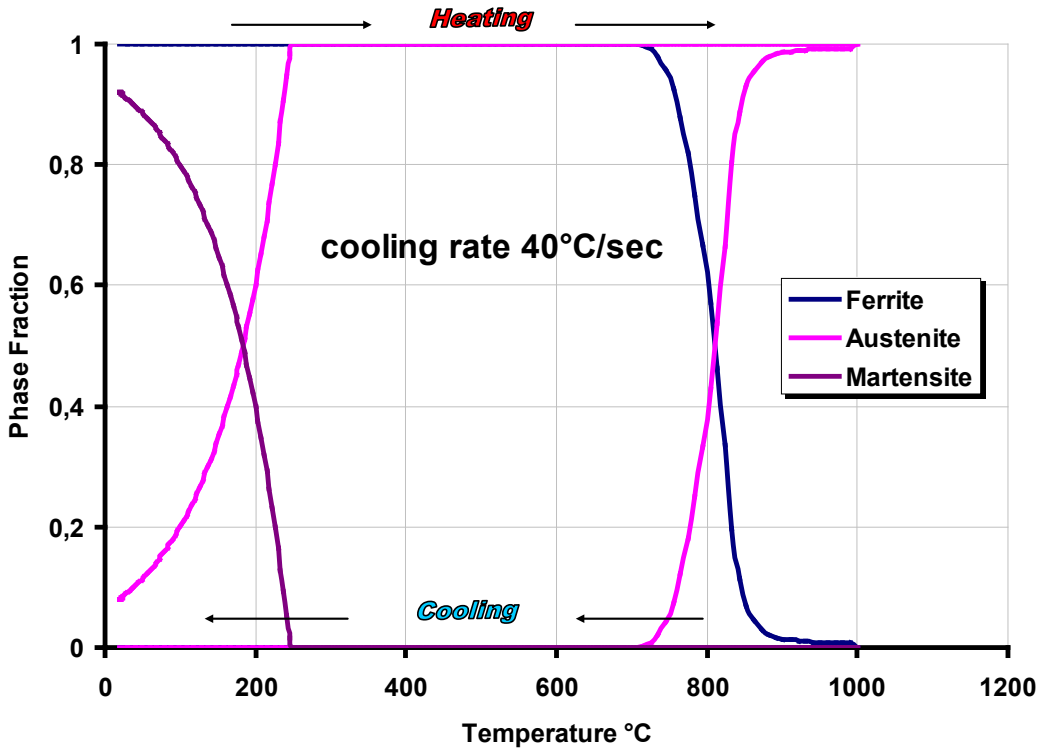

Figure 3.24 Evolution of different phases at high cooling rate (Martensite phase transformation)

The predicted percentages of different individual phases transformed at different cooling rates are presented in **Figures 3.25, 3.26** and **3.27**. **Figure 3.25** describes the evolution and percentage of the residual pearlite phase at the end of the cooling process for different cooling rates. At low cooling rates we can have high percentage of pearlite phase when the material is heated and cooled to ambient temperature. The formation of pearlite can be suppressed or completely eliminated by using higher cooling rates. The formation of individual bainite phase is shown in **Figure 3.26** which normally appears at medium cooling rates. In contrast to pearlite phase, bainite has low or zero percent content at slow and high cooling rates, see **Figure 3.28**. Similarly the evolution and percentage of martensite is described in **Figure 3.27**. At high cooling rates a maximum content of martensite is observed.

The overall transformation mechanism of the material AISI 52100 (100Cr6) steel for different cooling rates is presented in **Figure 3.28**. The percentage of phases that can be obtained with respect to time, required to cool the material to the ambient temperature is shown in **Figure 3.29**. The results of the simulated phase transformations for the material AISI 52100 (100Cr6 steel) are compared with experimental results of [WEVE59] and simulated results of [HUNK04] (**Figure 3.30)** and have been found in a very good agreement.

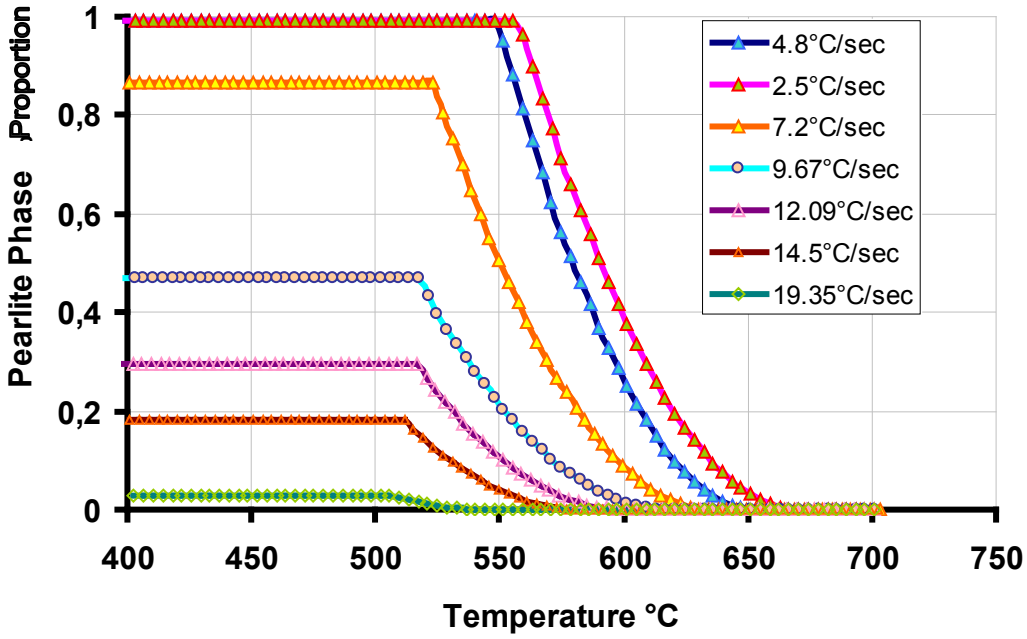

Figure 3.25 Predicted evolution and phase fraction of Pearlite after different temperature histories

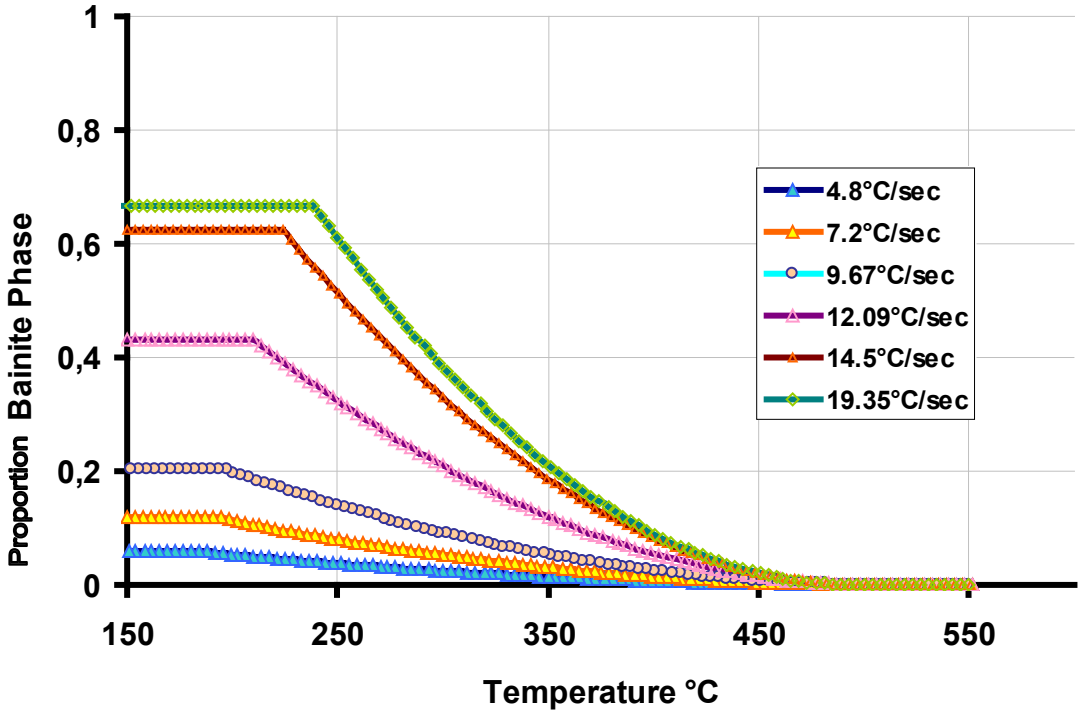

Figure 3.26 Predicted evolution and phase fraction of Bainite after different temperature histories

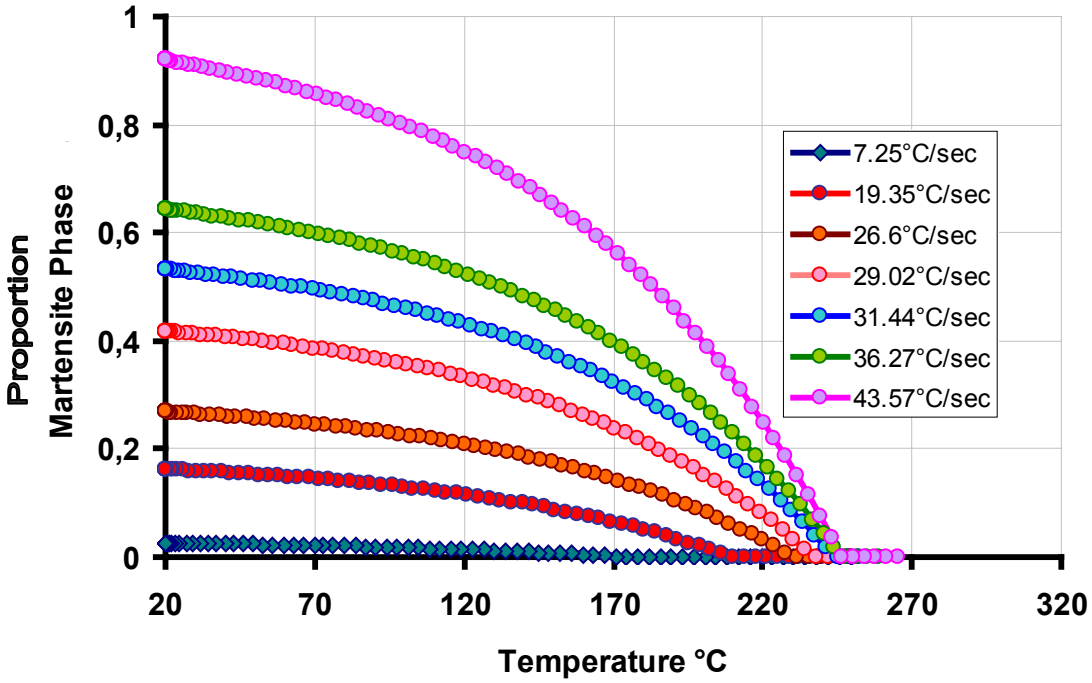

Figure 3.27 Predicted evolution and phase fraction of Martensite phase after different temperature histories

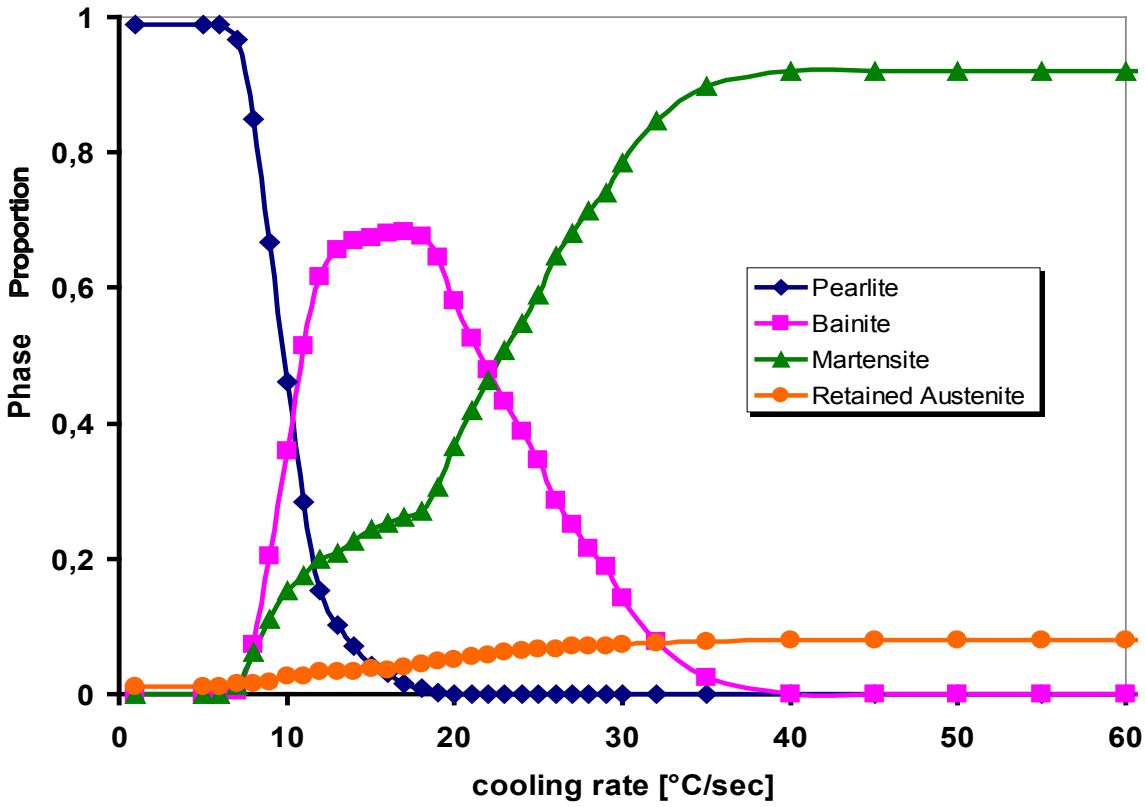

Figure 3.28 Prediction of volume fraction versus cooling rate for AISI 52100 (100 Cr6) steel

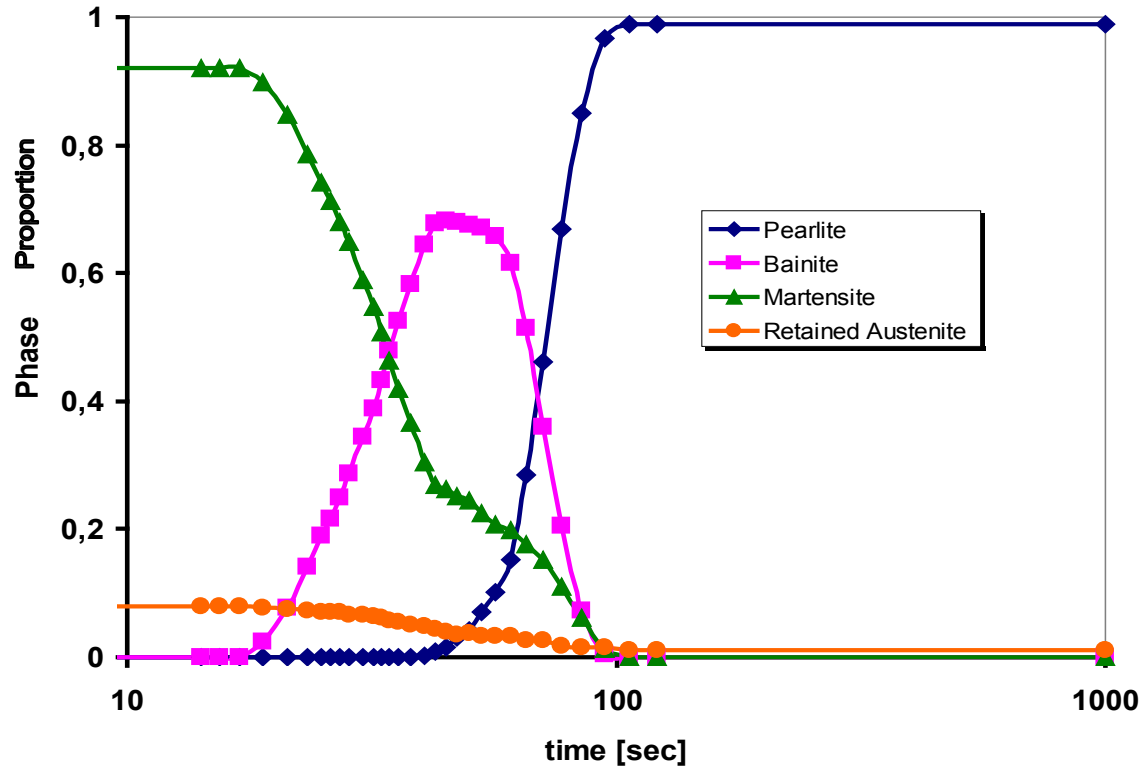

Figure 3.29 Prediction of volume fractions versus time for AISI 52100 (100Cr6) steel

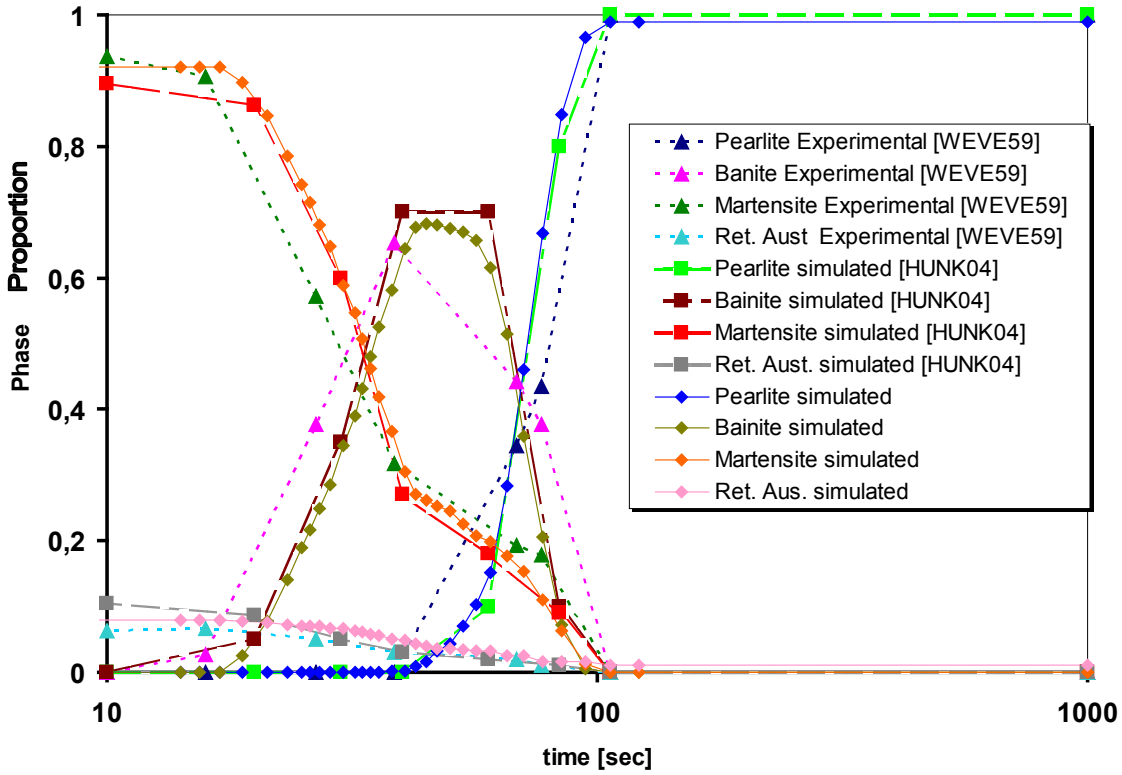

Figure 3.30 Comparison of simulated and experimental results of phase proportions for AISI 52100 steel

An alternative way to describe the continuous cooling transformation kinetics is to plot the transformation temperature, T_t (including T_s and T_f), directly against the cooling rate $\dot{T}$ creating a T_t-$\dot{T}$ diagram Figure 3.31. A T_t-$\dot{T}$ diagram is equivalent to a CCT diagram in terms of the continuous cooling transformation kinetics. The main difference between the two diagrams is that a CCT diagram employs the cooling time but a T_t-$\dot{T}$ diagram uses $\dot{T}$ as the horizontal axis. Thus, the right-hand side (low cooling rate, long cooling time) of a CCT diagram corresponds to the left-hand side of a T_t-$\dot{T}$ diagram (low cooling rate). For the CCT diagram under discussion it can be shown that Ms and B_s, are almost independent of $\dot{T}$ in most of the $\dot{T}$ range but the percentage of the phase fractions of bainite and martensite formed are dependent of the cooling rate.

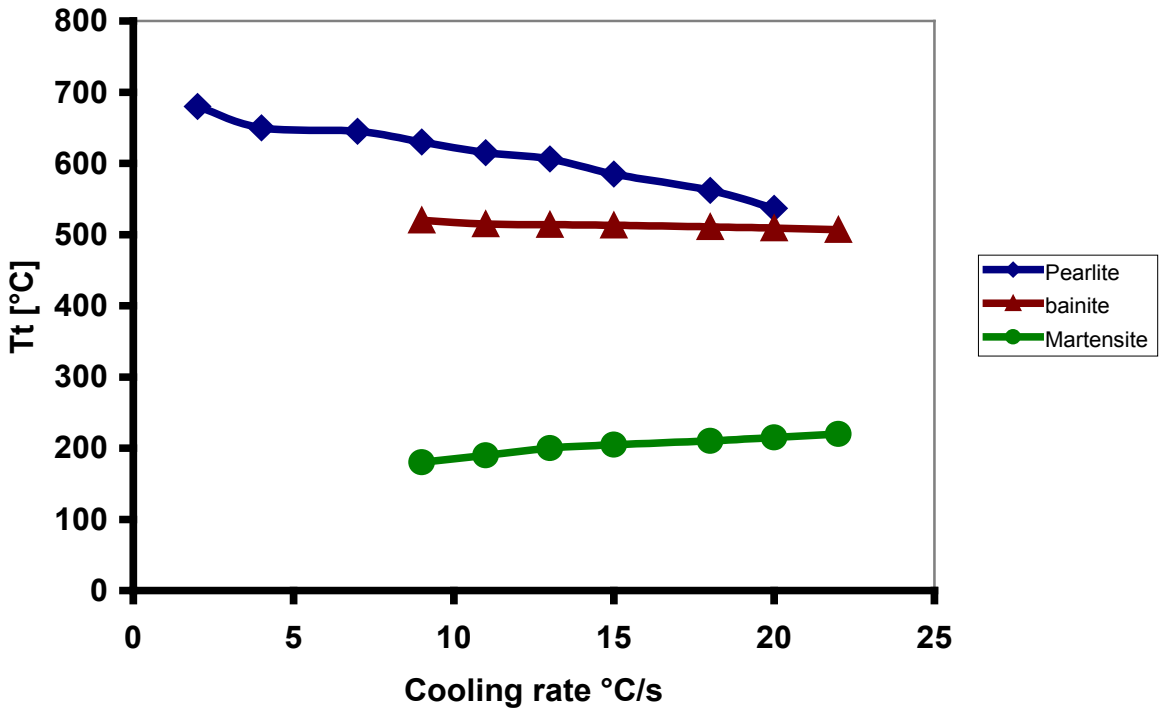

Figure 3.31 Tt-$\dot{T}$ diagram (cooling rate diagram and Transformation temperature)

3.7.3.4 Dilatometric curves

At room temperature, AISI 52100 steel has a body-centred cubic (BCC) iron lattice (see **Figure 3.1**). During austenitization, it shears into a face-centred cubic (FCC) structure, during cooling it returns to a body-centred cubic (BCC) lattice. The body-centre cubic and face centred cubic lattices have different specific volumes, which can be measured in a dilatometer test (see **Figure 3.2**). The simulated dilatometric curves obtained for different cooling rates are presented in **Figure 3.32** which shows a volume change after each phase transformation. The volume changes arising from transformation of the crystalline structure have a decisive effect on dimensional changes and distortion, and on the residual stresses. The overall thermal expansion comprises the classical thermal expansions of the respective phases. The thermal constitutive behaviour of the material and thermal strains $\boldsymbol{E^{therm}}$ $\boldsymbol{(T,z)}$ with volumetric changes are introduced through subroutine UEXPAN which is described in details in section 4.6.1.

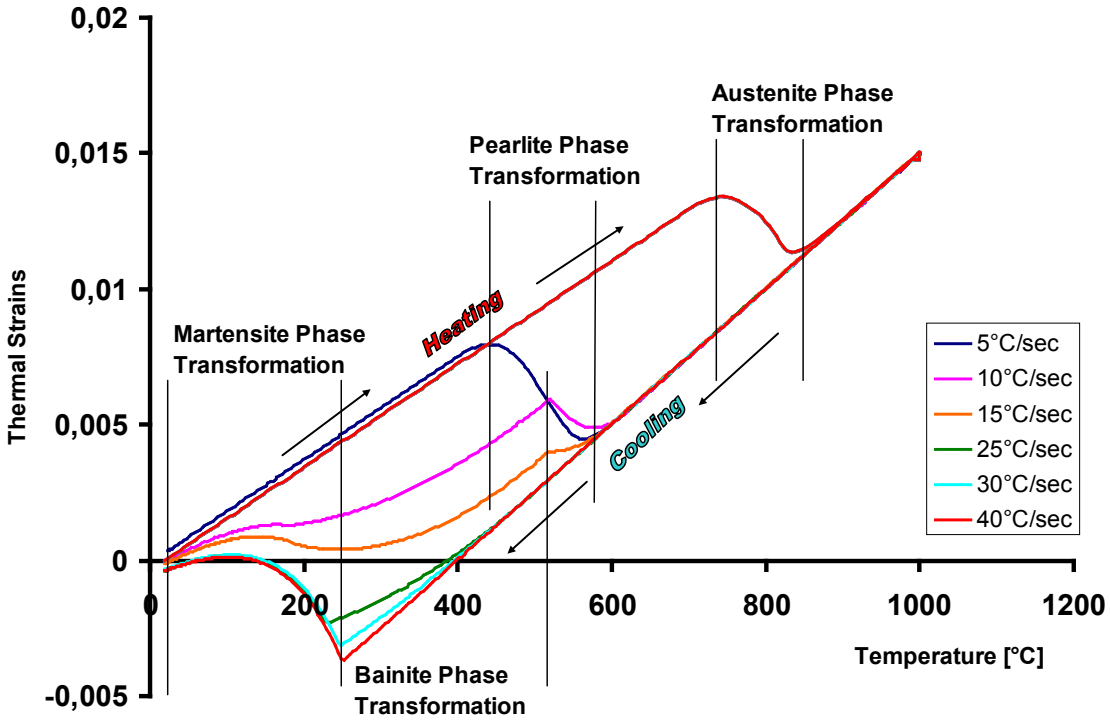

Figure 3.32 Thermal strains and phase transformation for different cooling conditions

3.8 Summary

A detailed account of phase transformation has been presented in order to give some brief theory to understand the phase transformation phenomena in steels. An overview of phase transformation modelling has also been presented including some coupled thermo-metallo-mechanical models presented in the literature. A proposed model for phase transformation calculations was presented and in order to verify the validity of the model, a series of numerical analysis for a single 2D element in abaqus/standard were performed. The transformation products emerging from austenite during the continuous cooling process are determined considering two parameters i.e. the transformation temperatures ***(T_s,*** and ***T_f),*** and the cooling rate from the CCT diagram. It was discussed that for a specific product ***i,*** there is a lower critical cooling rate $\dot{T}_L^i$, and an upper critical cooling rate, $\dot{T}_U^i$ within which it is formed during cooling. An alternative way to describe the continuous cooling transformation kinetics by plotting the transformation temperature, T_t (including T_s and T_f), directly against the cooling rate $\dot{T}$ was presented. The simulated results were also compared with experimental results of [WEVE59] and simulated results of [HUNK04] and are found to be in a very good agreement.

CHAPTER 4

MODELLING AND SIMULATION OF GRINDING PROCESS

4

4.1 Introduction

In the past, a lot of numerical models for grinding were proposed, especially for the thermal aspect of the process. The obtained results show that simulation is a suitable tool for the determination of the impacts caused by grinding processes. The FEA simulation enables a better understanding of the process and helps the user to analyze complex experimental results. With the FEA, an optimized combination of grinding parameters could be found to minimize the adverse affects imparted due to grinding.

The FE simulations, which are being presented in this chapter, focus on the development of macroscopic 2D coupled model on FE code Abaqus®/Standard. The efforts are made to simulate the grinding process for the investigation of residual stresses in ground components by considering the full coupling of mechanical (elastic and plastic) strains, thermal strains and phase transformations during grinding. In this regards the workpiece is considered as 2D semi-infinite plate with an insulated bottom surface and convective cooling is applied to the top and side surfaces to represent coolant application.

4.2 Grinding Process Modelling

Figure 4.1 shows a schematic representation of the surface grinding process. Here a rotating wheel with surface speed V_s is simultaneously translated at the surface of a workpiece with a relative velocity V_w, a_p is the depth of cut, i.e. the depth of material removed after one pass of the wheel against the workpiece. If the process of material removal is not considered, then surface grinding can be essentially thought of as the traversal of normal pressure, tangential traction and heat flux distributions, of finite length in the direction of motion and of infinite width perpendicular to this direction, over the solid surface (**Figure 4.2**). As to the technique developments for the solution of the heat source problem, Jaeger [JAEG42] and Carslaw and Jaeger [CARS59] presented solutions for uniform moving rectangular heat sources and a uniform stationary heat source using the heat source method. Similar approximate equations

based on Jaeger's solution were developed in several studies [BOWD53] [BARB67] [CAME64] [GECI85] for a stationary heat source to estimate the sliding contact temperature. Several seminal contributions to the analysis of a moving heat source problems have been made by several authors [JAEG42] [ROSE41,46] [BLOK37,55], and their results became the basis for many developments as discussed below.

As a first step towards the modelling of the grinding process, the mechanical effects of a grinding wheel can be assumed to be a combination of normal pressure and tangential surface traction whereas the thermal effect can be represented by a moving heat source of elliptical shape, see **Figure 4.2**. The velocity V_w would represent the workpiece velocity in surface grinding. The geometrical contact length, between the wheel and workpiece for surface grinding is assumed to be equal to the heat source length.

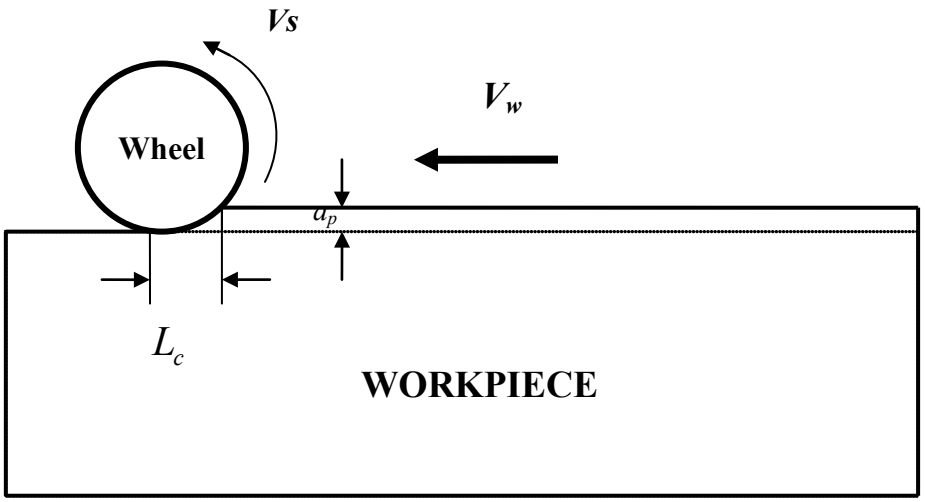

Figure 4.1 Schematic representation of surface grinding

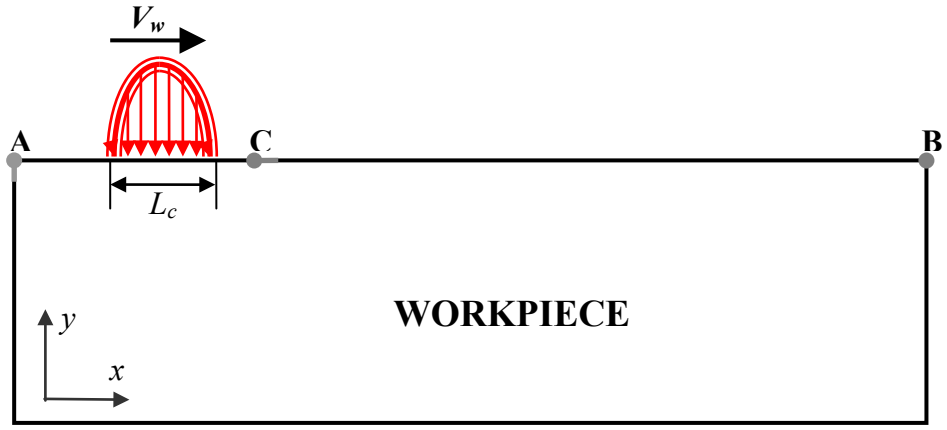

Figure 4.2 Model for thermal analysis of grinding

Numerical simulations were performed using the commercial finite element software Abaqus®/Standard and the material behavior was defined in subroutines, PHASE, PROP, UEXPAN and UMAT. Moreover, UMAT and UEXPAN are special purpose routines available in Abaqus for defining the material constitutive behavior and user expansion coefficient, respectively. PHASE and PROP user subroutines were written separately to calculate the time and temperature dependent phase proportions and their effect on the thermo-mechanical properties, respectively. The temperatures arising due to a moving heat source are obtained with the user subroutine DFLUX in order to predict phase transformation and subsequently the depth of martensite. The whole analysis is described in **Figure 4.3**

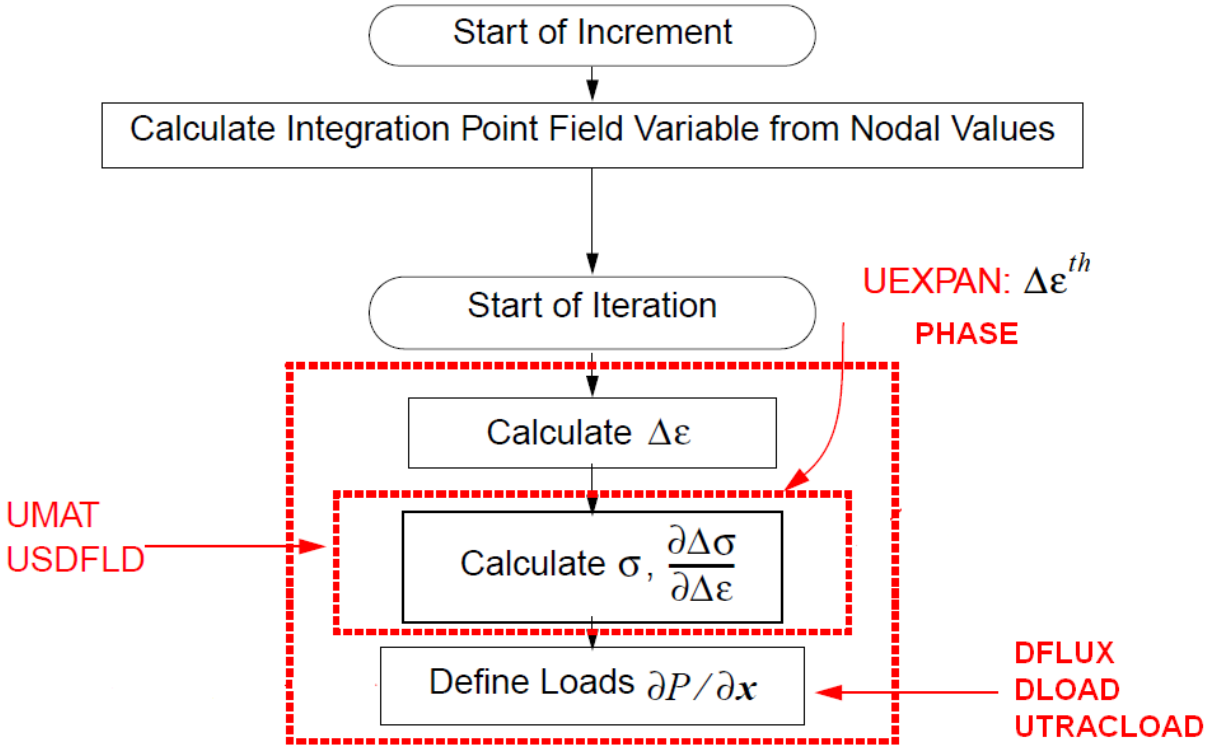

Figure 4.3 Figure showing the Abaqus analysis

4.3 Principle of Finite Element Analysis

The principle of numerical simulation of grinding entails the know-how of a comprehensive database with reference to geometry, thermo-mechanical properties, initial conditions, boundary and loading conditions. The essentials of numerical simulation of grinding are shown in **Figure 4.4**. The more the information regarding these parameters is accurate, the more the simulation is robust. Once the input database is furnished FE simulation may now be performed, however, an experimental database is almost always required to establish the comparison with simulation results and validate the numerical model.

A coupled temperature-displacement analysis is performed for all the cases. Here, it is assumed that the mechanical response of the test specimen depends upon the thermal loading; while there is no inverse dependency. This is because the amount of heat dissipated by plasticity, if any, is negligibly small as compared to the heat energy supplied by the heat source. The description of thermal models has already been presented in chapter 2 in detail. In some cases, the boundary conditions are also temperature-dependent; while, in some other cases, they are assumed independent of temperature.

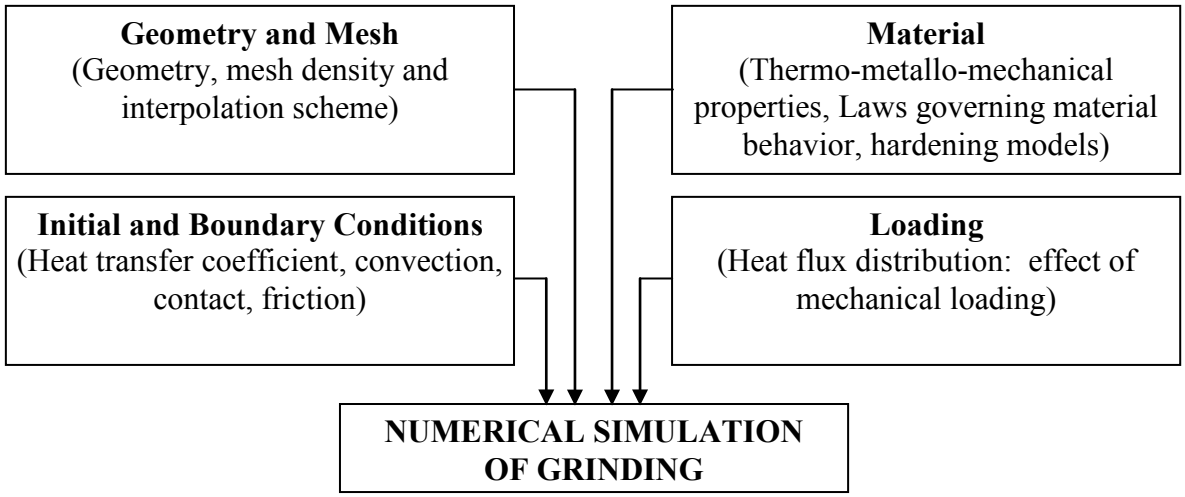

Figure 4.4 Essentials of the numerical simulation of grinding

4.3.1 Finite Element Mesh

The mesh density is generally controlled by the applied loading and/or boundary conditions. Since grinding processes involve high temperature gradient in and near the grinding zone, a fine mesh is required to capture the grinding zone boundary and temperature distribution in the vicinity of the contact. However, a too fine mesh should be avoided to keep the computation time reasonable. An optimum mesh density is, therefore, used without compromising the quality of results. As the temperature gradient is considerably low outside the grinding zone, a relatively coarser mesh is deemed sufficient for the analysis. The mesh is organized so that its density is progressively reduced when the depth from the grinding surface is increased; as an abrupt increase in mesh size may lead to discontinuous contours and poor interpolation of temperatures, displacements and stresses.

The general 2D thermal model setup is illustrated in **Figure 4.5** along with the elliptical heat flux distributions. In this study the workpiece is considered as a 2D semi-infinite plate of 0.1

m length and 0.03 m width with an insulated bottom surface and convective cooling to the top surface and side walls. The wheel is treated as a heat source equal to the contact length and considered to be the integration of a number of moving line sources, of infinite length in the z direction and infinitesimal width along the contact line direction. The heat source is assumed to be moving along the surface at a velocity V_w. The finite element (FE) mesh (**Figure 4.6**) consists of CPE4T (4-node plane strain thermally coupled quadrilateral bilinear displacement and temperature) elements totalling over 3216 nodes and 3000 elements. The mesh size increases progressively across the test plate from very fine at the surface to a coarser mesh at the bottom (**Figure 4.6**). The FE code Abaqus®/standard is used to perform the simulation.

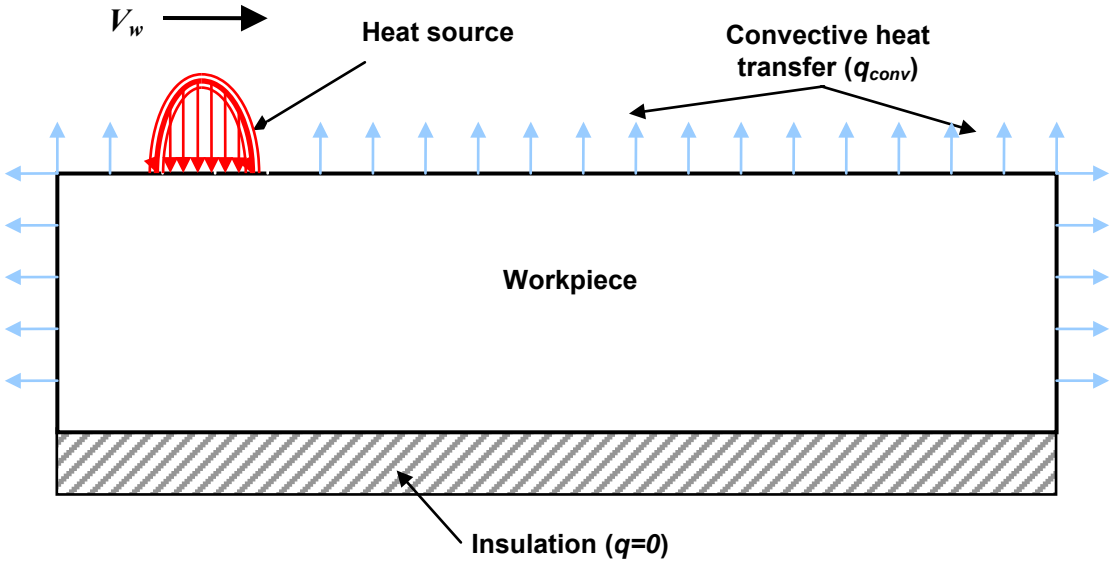

Figure 4.5 Finite element thermal model setup

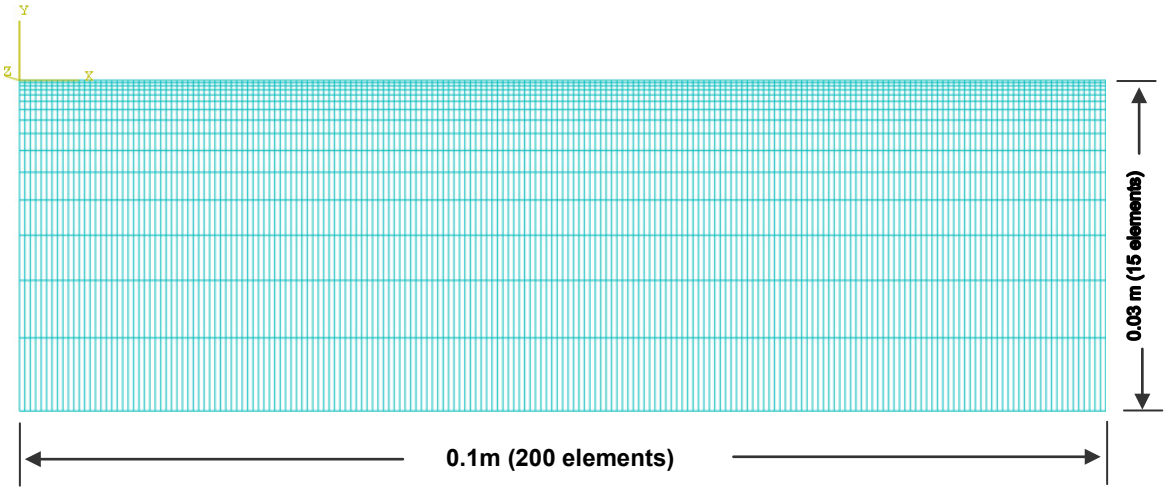

Figure 4.6 Finite element mesh

4.3.2 Material Properties (Bearing steel AISI 52100 (100 Cr6))

AISI 52100 (commonly, 100Cr6 in Europe) is a high carbon-chrome-manganese through hardening steel which finds applications in several components like anti-friction bearings, cams, crank shaft, etc for its good resistance to corrosion and fatigue. Over low-carbon steels high-carbon steels can carry higher contact stresses, such as those encountered in elliptical point contact loading in ball bearings [GUOY02]. The temperature dependent thermal and mechanical material properties are crucial to the successful development of numerical models. The thermo-mechanical properties, which are used for Abaqus simulations, are being summarized in this section. The chemical composition and the key physical and mechanical properties of AISI 52100 (100Cr6) steel are listed in Annex A1

4.3.3 Initial and Boundary Conditions

All FE analysis problems are defined in terms of initial and boundary conditions. A typical type of initial conditions for a grinding application is the initial temperature that, in most cases, is set to room temperature. Initial conditions for these simulations are as follows:

$$\text{At} \qquad t = 0 \text{ sec} \qquad T(t=0) = 20°\text{C} \tag{4.1}$$

The heating and cooling cycle is a transient heat conduction problem with convective boundary conditions. The convective heat transfer boundary conditions are applied on the surface and side walls.

$$q_{conv} = h_{conv}(T - T_0) \tag{4.2}$$

where T, T_0, are the temperature of the semi-infinite solid and the ambient temperature, respectively, and h_{conv} (W/°C.m^2) is the convective heat transfer coefficient of the cooling media. Imposed temperature values are obtained using the moving heat source model (**Figure 4.2**). **Figure 4.5** shows a schematic representation of thermal boundary conditions.

4.3.4 Loading condition

4.3.4.1 Thermal Loading

The thermal loading is used by applying either a temperature distribution on nodes through a moving heat source or a heat flux. The heat source model plays a critical role in achieving the precise application of heat flux, which in turn helps acquiring required thermal histories. The

selection of an appropriate model is, therefore, a matter of great concern. In the past most of the thermal models were based on Carslaw and Jaeger's early work of a sliding heat source model [CARS59] [JAEG42]. In Carslaw and Jaeger's model, a uniform heat flux is assumed for the flat heat source, which moves with a constant velocity along the surface of a semi-infinite solid, under an assumed quasi steady state heat transfer condition. Recently, Jin et al. [JINT99] developed an analytical thermal model for an oblique or circular moving heat source for deep grinding. Mahdi and Zhang [MAHD97] investigated the temperature field of surface grinding process using a triangular profile with an adjustable apex to accommodate the effect of different grinding operations. There are differing views amongst researchers on which distribution method is best to use for grinding. Some researchers [SATO61] [MALK74] [DESR70] have used a rectangular (uniform) distribution, mostly to simplify subsequent calculations. However, due to the localised "spike" temperatures of a very short time as previously discussed, some researchers [SNOE78, DEDE72, MARR77] have argued that the assumption of a uniform heat flux field may not lead to accurate predictions. Keeping in view the contact mechanism of grinding process, theoretically the pressure and corresponding temperature distribution should be modelled according to a sliding/rolling contact approach. Also by recalling the Hertz contact pressure distribution between a cylinder and a plane is elliptical in shape, similarly in consideration of different grinding conditions where the heat flux varies along the contact length; the choice of model closer to the practice should assume an elliptical distribution of heat flux. A heat source with elliptical distribution has, therefore, been integrated for numerical simulation in this work. **Figure 4.7** shows the presence of a schematic heat source moving with velocity V_w on the top surface of the FE model. Here, the length of heat source is equal to the contact length (L_c) of the grinding wheel with the workpiece. $q(x)$ (in J/m² s) is the heat-liberation intensity of the heat source, which is a function of the distance x . The larger is the value of x, smaller the value of $q(x)$. When $x = 0$, $q(x)$ has its maximum value. When $x = a$, $q(x)$=0. The functional relationship is given by

$$q(x) = q_o \sqrt{\left(1 - \frac{x^2}{a^2}\right)} \tag{4.3}$$

Where q_o is the maximum heat entering the workpiece and can be obtained by integrating the equation (4.3) and equating it to the net heat entering to the workpiece.

$$Q = \int_{-a}^{a} q_o \sqrt{\left(1 - \frac{x^2}{a_o^2}\right)} dx \tag{4.4}$$

it leads that

$$q_o = \frac{2Q}{\pi a} \tag{4.5}$$

Substituting in equation (4.3) for q_o we get

$$q(x) = \frac{2Q}{\pi a} \sqrt{\left(1 - \frac{x^2}{a^2}\right)} \tag{4.6}$$

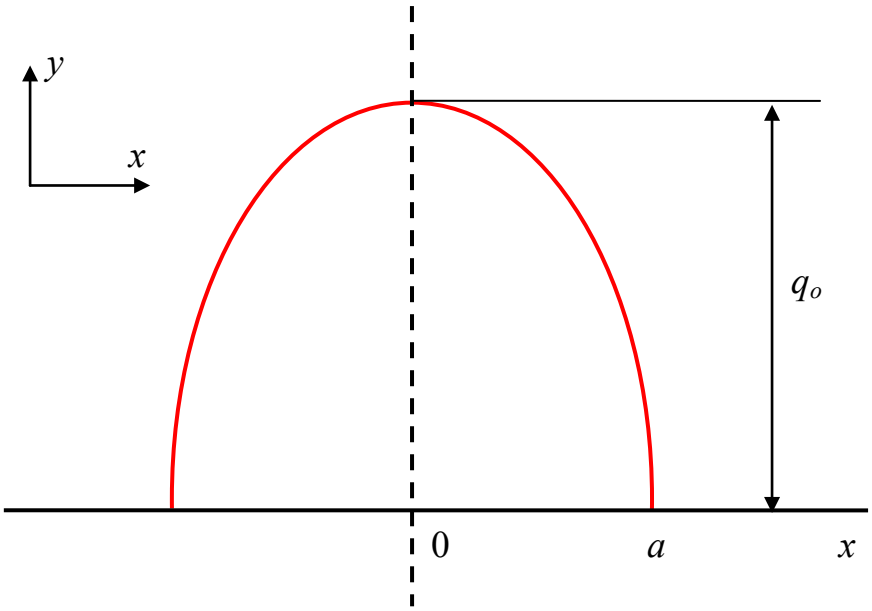

Figure 4.7 Elliptical heat distribution model

In Abaqus®/Standard, the moving heat source is integrated in the finite element model through a FORTRAN subroutine, called DFLUX. The heat source is moved along the axis of symmetry where it travels with respect to the nodal coordinates.

Before carrying out a complete thermo-mechanical analysis, a few heat-transfer simulations were run to perform the sensitivity analysis of various types of heat source distributions. An elliptical, a triangular and a uniform heat source were used in each simulation run. The temperature distribution as a function of distance for all three cases were compared (**Figure 4.8**).

It was found that the peak temperatures in all three cases were identical, however, the distribution of temperatures over the surface varies to some extent. An interesting observation was that the flux distribution with an elliptical source lies almost midway between the triangular and the uniform heat sources, which, in-turn indicates that the elliptical heat source is an appropriate choice from the perspective of flux distribution.

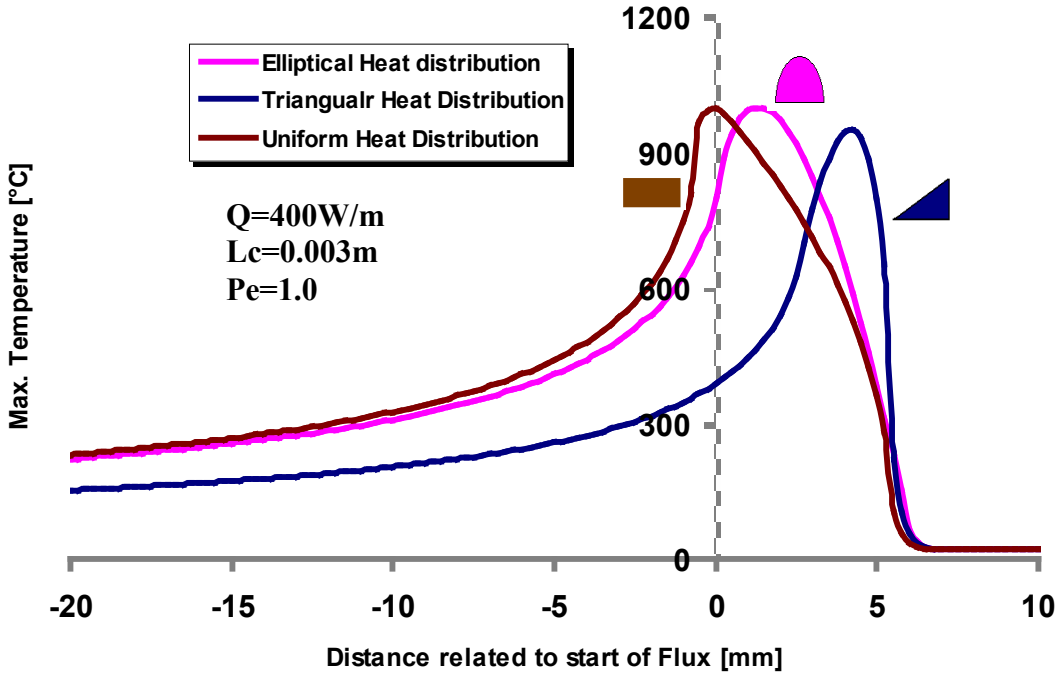

Figure 4.8 Temperature evolution with different heat source models

4.3.4.2 Mechanical Loading

The mechanical loading in the grinding process modelling requires the application of an equivalent normal surface pressure and a tangential traction to represent the best approximate contact problem of the grinding wheel and workpiece. The purpose of this whole process is to integrate the possible non linearity arising from the contact problem and to reduce the computing time.

The equivalent normal load (here an equivalent normal distributed pressure P in N/m^2 with an elliptical profile) and tangential traction (here an equivalent distributed moving traction P_α in N/m^2 on the surface of the workpiece with an elliptical profile) are applied on the surface elements through user subroutines. For the grinding process the modelling of the distribution of mechanical loading is a complex function of time and/or position therefore the mechanical

loads are defined in the user subroutine DLOAD and UTRACLOAD to have the required pressure distribution and tangential traction respectively.

4.4 Thermal Analysis

In order to compute the temperature histories, the heat transfer analysis is performed using temperature dependent thermal properties. The transient temperature field (T) in time (t) and space (x, y) is achieved by solving the following heat transfer equation:

$$\frac{\partial}{\partial x}\left(K(T)\frac{\partial T}{\partial x}\right)+\frac{\partial}{\partial y}\left(K(T)\frac{\partial T}{\partial y}\right)Q_w = \rho(T)C_p(T)\left(\frac{\partial T}{\partial t}\right) \quad (4.7)$$

Here, $K(T)$ is the thermal conductivity as a function of temperature in $W.m^{-1}.K^{-1}$, $\rho(T)$ is the density as a function of temperature in $kg.m^{-3}$, $C_p(T)$ is the specific heat as a function of temperature in $J.kg^{-1}.K^{-1}$ and Q_w is the heat flux in $W.m^{-1}$.

Abaqus®/Standard uses an iterative scheme to solve non-linear heat transfer problems. This scheme is based on the Newton iterative method. In Abaqus®/Standard, time integration in transient problems is done with the backward Euler method (sometimes also referred to as the modified Crank-Nicholson operator). This method is unconditionally stable for linear problems. Automatic time incrementation is used for the analysis. The analysis is performed in two steps as follows:

- *Step 1*: meant to integrate the heat flux through a Fortran subroutine DFLUX.
- *Step 2*: intended to incorporate cooling due to thermal boundary conditions.

The heat source is moved along the axis where it travels with respect to the nodal coordinates. For automatic incrementation, Abaqus®/Standard chooses the time step such as to keep the largest temperature change at every integration point less than an allowed value, ΔT_{max}. At the very beginning of the cooling, the temperature drops rapidly due to the conduction within the work-piece. Restrained by maximum allowable temperature change (ΔT_{max}), the time increment is very small at this stage. However, as the cooling progresses, the time step grows up to the maximum allowed value defined by the user.

4.5 Mechanical Analysis

For the grinding process modelling with phase transformation, the mechanical analysis indeed requires an accurate calculation of the temperature fields and the related phase

transformations during thermal analysis. Various mechanical analyses are performed in order to calculate the affect of thermal and phase transformation on the stress state induced during the grinding process, while taking care of mechanical loading and boundary conditions. The phase transformation calculations are performed using the nodal temperature values calculated during the thermal analysis. For all the simulations, the material is assumed to follow either the elasto-plastic (EP) or elasto-viscoplastic (EVP) behaviour with isotropic hardening law (von Mises plasticity model).

4.5.1 Stress-Strain Constitutive Relation

Stress/strain state in the process incorporating phase transformation is complicated due to inhomogeneous temperature distribution and a gradient varying with time, thus inducing thermal and phase transformation strains. Such strains are at the origin of stresses often exceeding the yield stress, therefore an elasto-plastic stress analysis considering the temperature-dependent material parameters is needed. Strain and strain rate (or the increment) are generally assumed to be divided into recoverable elastic part $\dot{\varepsilon}_{ij}^{e}$ and irrecoverable plastic (inelastic) one $\dot{\varepsilon}_{ij}^{p}$

$$\dot{\varepsilon}_{ij} = \dot{\varepsilon}_{ij}^{e} + \dot{\varepsilon}_{ij}^{p} \tag{4.8}$$

4.5.2 Elastic Strain

In the case of a complicated coupling of mechanical field with temperature and phase change, the relation for the elastic strain can be expressed by:

$$\varepsilon_{ij}^{e} = \frac{1+\nu}{E}\sigma_{ij} - \frac{\nu}{E}\sigma_{kk}\delta_{ij} + E^{thm}\delta_{ij} \tag{4.9}$$

$$E^{thm}\left(T,z\right) = \left(1-z\right)\varepsilon_{\gamma}^{th}\left(T\right) + z\cdot\varepsilon_{\alpha}^{th}\left(T\right) \tag{4.10}$$

$$\varepsilon_{\alpha}^{th}\left(T\right) = \alpha_{\alpha}\cdot\left[T - T_{ref}\right] \tag{4.11}$$

$$\varepsilon_{\gamma}^{th}\left(T\right) = \alpha_{\gamma}\cdot\left[T - T_{ref}\right] - \Delta\varepsilon_{\alpha\gamma}^{25°C} \tag{4.12}$$

where

T_{ref} is the reference temperature

$\Delta\varepsilon_{\alpha\gamma}^{25°C}$ is thermal strain difference between the two phases

α_γ is the thermal expansion coefficient of the austenite Phase

α_α is the thermal expansion coefficient of the ferrite phase

E, and *v* are Young's modulus and Poisson's ratio of the constituent, respectively. A temperature dependent Young's modulus E(T) and a constant Poisson's ratio are used for this particular case.

4.5.3 Yield Function and Plastic Strain Rate.

Subsequent yielding as well as initial yielding of material with plastic strain ε_{ij}^{p}, hardening parameter H_m at temperature T under multiaxial stresses is controlled by a criterion using the yield function expressed in stress space as:

$$F = F\left(\sigma_{ij}, \varepsilon_{ij}^{p}, H_m, T, z_i\right) = 0 \tag{4.13}$$

with existing plastic strain ε_{ij}^{p}, hardening parameter H_m, to be discussed later, temperature T, and volume fraction of phases z_i. The yield function F necessitates a simple mathematical structure and is adequately capable to fit the experimentally observed yield condition. One of the most widely used yield functions in engineering practice is the von Mises type, taking the form:

$$\sqrt{\frac{3}{2}S_{ij}S_{ij}} - \sigma_y^g\left(\bar{\varepsilon}^{pl}, T, z\right) = 0 \tag{4.14}$$

$\sigma_y^g\left(\bar{\varepsilon}^{pl}, T, z\right)$ being the global yield stress of material depending on strain, temperature and microstructure of the material and calculated by

$$\sigma_y^g = (1-z)\sigma_y^\alpha\left(\bar{\varepsilon}^{pl}, T, z\right) + z\sigma_y^\gamma\left(\bar{\varepsilon}^{pl}, T, z\right) \tag{21}$$

σ_y^α and σ_y^β are the yield stresses of ferrite and austenite phases, respectively.
The equivalent plastic strain is given by:
S_{ij} is the deviatoric stress such that:

$$S_{ij} = \sigma_{ij} - \frac{1}{3}\delta_{ij}\sigma_{kk} \tag{4.15}$$

The equivalent plastic strain is given by:

$$\bar{\varepsilon}^{pl} = \int_0^t \dot{\bar{\varepsilon}}^{pl} dt \tag{4.16}$$

$$\dot{\bar{\varepsilon}}^{pl} = \sqrt{\frac{2}{3}\dot{\varepsilon}_{ij}^{pl}\dot{\varepsilon}_{ij}^{pl}} \tag{4.17}$$

The framework for developing the flow stress model is shown in **Figure 4.9**. The flow stresses which take into account hardening, thermal and viscous effects uses a kind of Johnson-Cook model proposed by [DOME04] is modified for multiphase material.

The basic approach is to build step by step the influence of the effective strain, effective strain rate, temperature and phase transformation on the flow stress. In developing the flow stress model, the influence of the temperature and the strain rate are considered as multiplier factors of the work hardening for each individual phase. For the temperature effects a factor (ζ_{fact}) is introduced, which is a best fit for the temperature data obtained from published results [MAMA00]. The temperature factor ζ_{fact} is an exponential function which includes a 5th order polynomial exponent. The details of procedure for the material flow stress model are explained in the following sections.

4.5.4 Work hardening

The work hardening curves as a function of plastic strain for each phase of the material AISI 52100 (100Cr6) bearing steel at room temperature 20°C are shown in **Figure 4.10**. The reference curves are adopted from the work of Brosse [BROS09]

By using a numerical regression of the data reported these flow curves can be best expressed by the power law,

$$\sigma_{z_i} = C_{z_i}\varepsilon^{n_{z_i}} \tag{4.18}$$

where C_{z_i} is the strength multiplier of the phase z_i, n_{z_i} is the strain hardening coefficient of the respective phase and ε is the effective strain. The values of C_{z_i} and n_{z_i} obtained for each phase from the curves of figure 4.10 are given in table 4.1

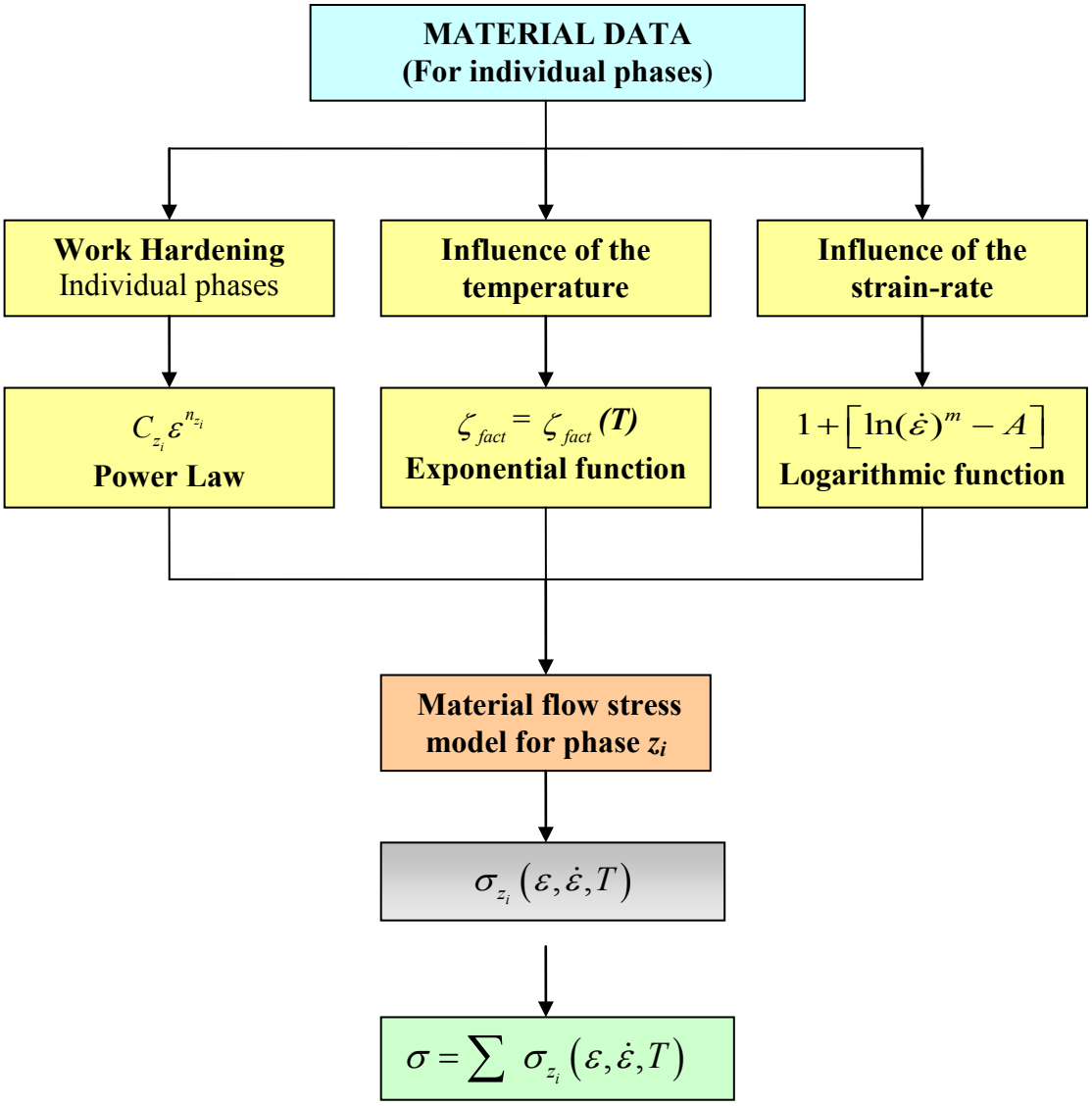

Figure 4.9 General framework used to build the new material flow stress model for individual phase and their combined effect on the material

Table 4.1

Description	Value	Description	Value
C_{aust}	206 MPa	n_{aust}	0.15
C_{pearl}	1350 MPa	n_{pearl}	0.4
C_{bain}	2100 MPa	n_{bain}	0.347
C_{mart}	3244 MPa	n_{mart}	0.235

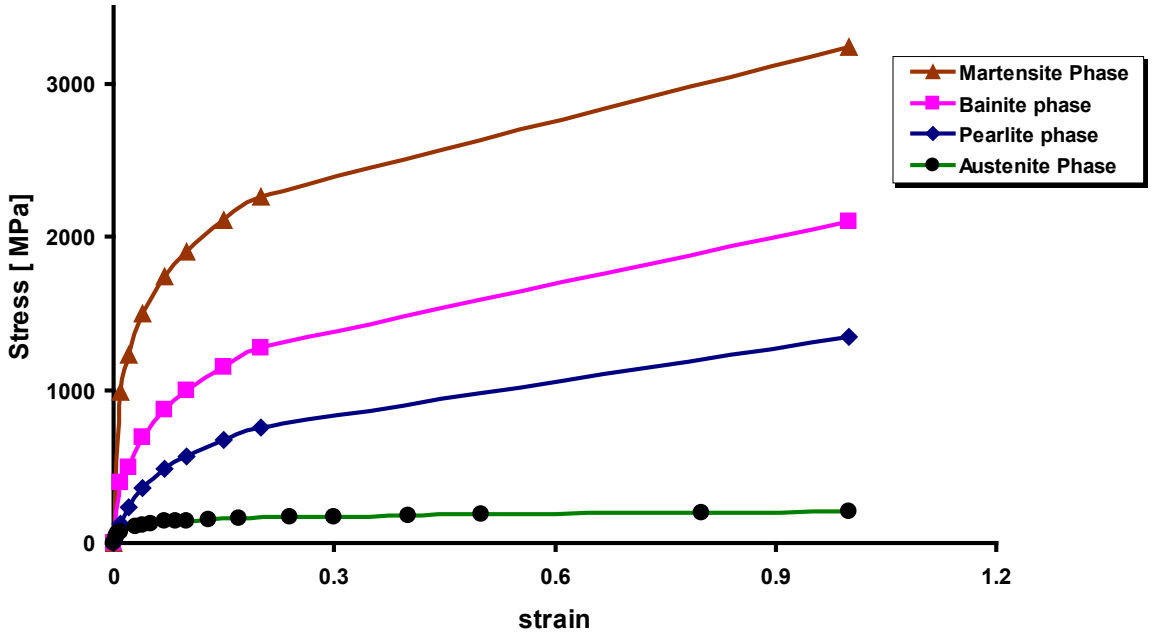

Figure 4.10 Stress-strain flow curve for each phase at 20°C for AISI 52100 (100Cr6) steel [BROS09]

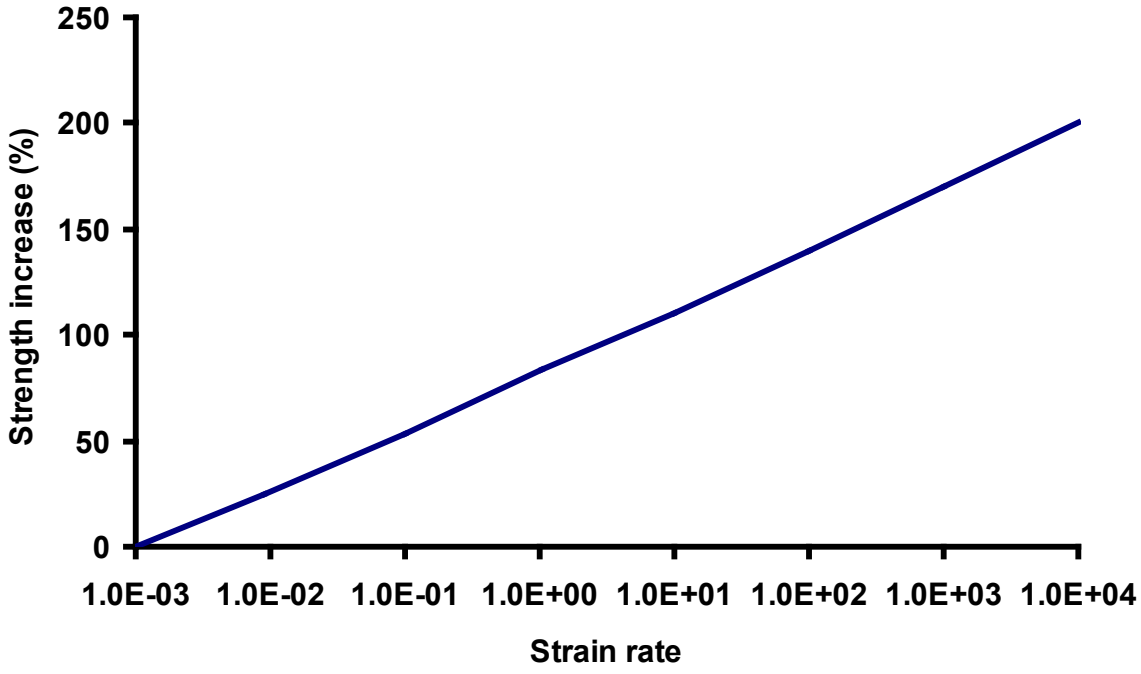

Figure 4.11 Strength increase as a function of increase in strain rate [KONT93]

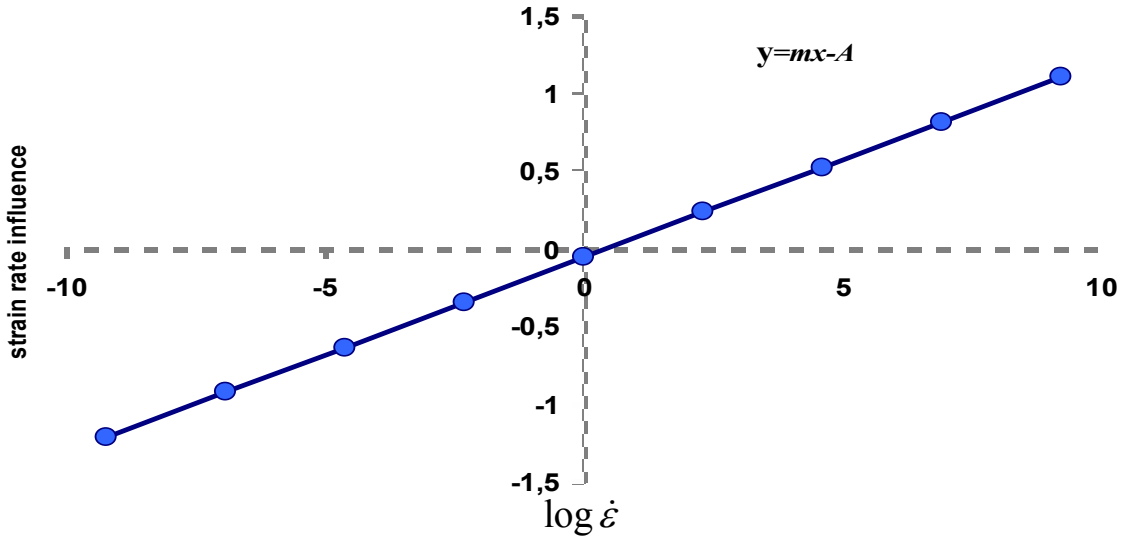

Figure 4.12 Strain rate influence on strength as a function of logarithmic strain rate

4.5.4.1 Influence of the strain rate on the reference curve

The influence of the strain rate on the flow stress for the 52100 bearing steel is adopted from [KONT93]. **Figure 4.11** shows a logarithmic relationship between the yield stress and the strain rate. In order to find a relationship between the flow stress value and different strain rates, a numerical adjustment is performed, so that at the reference strain rate of 1.0 s^{-1} the effect of strain rate is not zero (unity multiplier). The strength line in **Figure 4.12** represents the increment of the flow stress at different strain rates, described as follow:

$$\text{Strain rate hardening multiplier} = \ln(\dot{\varepsilon})^m - A \tag{4.19}$$

Where $\dot{\varepsilon}$ is the effective strain rate, m the strain rate sensitivity factor and A a material constant (m=0.1259 and A=0.0567 [DOME04]).

4.5.4.2 Influence of the temperature on the reference curve

Typically, in grinding, the workpiece is initially at room temperature, and the heat is generated at the contact zone between the wheel and the workpiece due to friction. This heat raises the temperature of the material being ground, resulting in lower flow stress due to recovery processes, as shown in **Figure 4.13**. In finite element description of the process, this physical behaviour is represented by treating the effect of strain, strain rate and temperature of flow stress separately. Temperature relationship is shown in **Figure 4.13**. In the proposed model,

a single 5th order polynomial exponent was found to best fit the influence curve for the entire temperature range, with the average influence factor ζ_{fact}

$$\textit{Temperature softening multiplier} = \zeta_{fact} = Exp\left(aT^5 + bT^4 + cT^3 + dT^2 + eT + f\right) \qquad (4.20)$$

Where T is the temperature in degree Celsius and the coefficients a to f are material constants (Table 4.2).

Table 4.2

Description	**Value**
a	3.81 × E-15
b	-4.29 ×E-12
c	-6.91× E-9
d	5.50 × E-6
e	-1.60 × E-3
f	2.44 × E-02

The temperature dependent reference flow curve for the phase z_i is then expressed by the equation:

$$\sigma_{z_i} = C_{z_i}\left(\bar{\varepsilon}_p\right)^{n_{z_i}} .\zeta_{fact} \qquad (4.21)$$

Using equation 4.21 and data from figure 4.10 the stress-strain flow curves for different temperatures are then obtained for each phase (**Figure 4.14, 4.15 and 4.16**).

The generic expression for flow stress as a function of effective strain, effective strain rate, and temperature for the material can be written as follows

$$\sigma_{eq}^{g} = \sum_{i=1,z} \sigma_{z_i} .\left[1 + \ln(\dot{\varepsilon}^{pl})^m - A\right] \qquad (4.22)$$

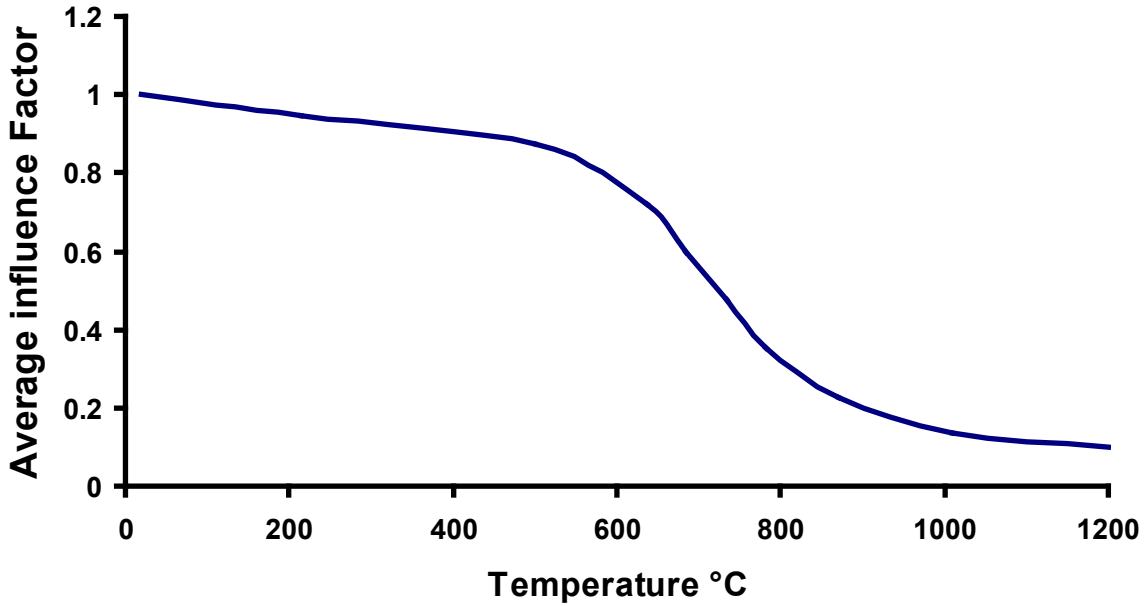

Figure 4.13 Average influence of the temperature on the flow stress [BOUZ99] [KONT93]

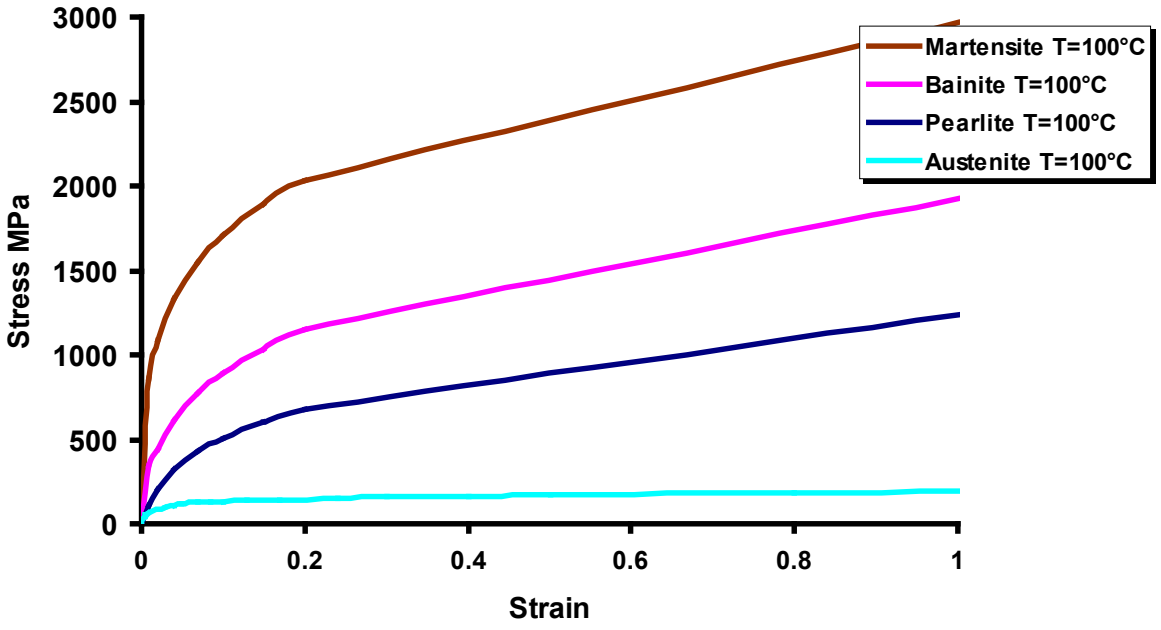

Figure 4.14 Stress-strain flow curve for each phase obtained using equation 3.2 for T=100°C

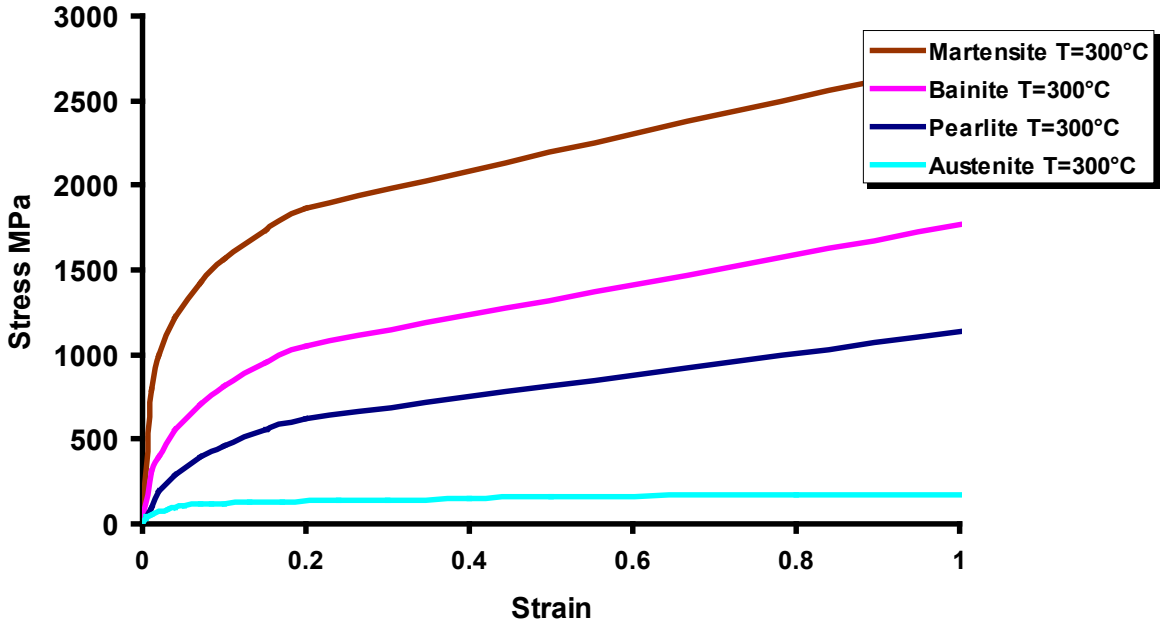

Figure 4.15 Stress-strain flow curve for each phase obtained using equation 3.2 for T=300°C

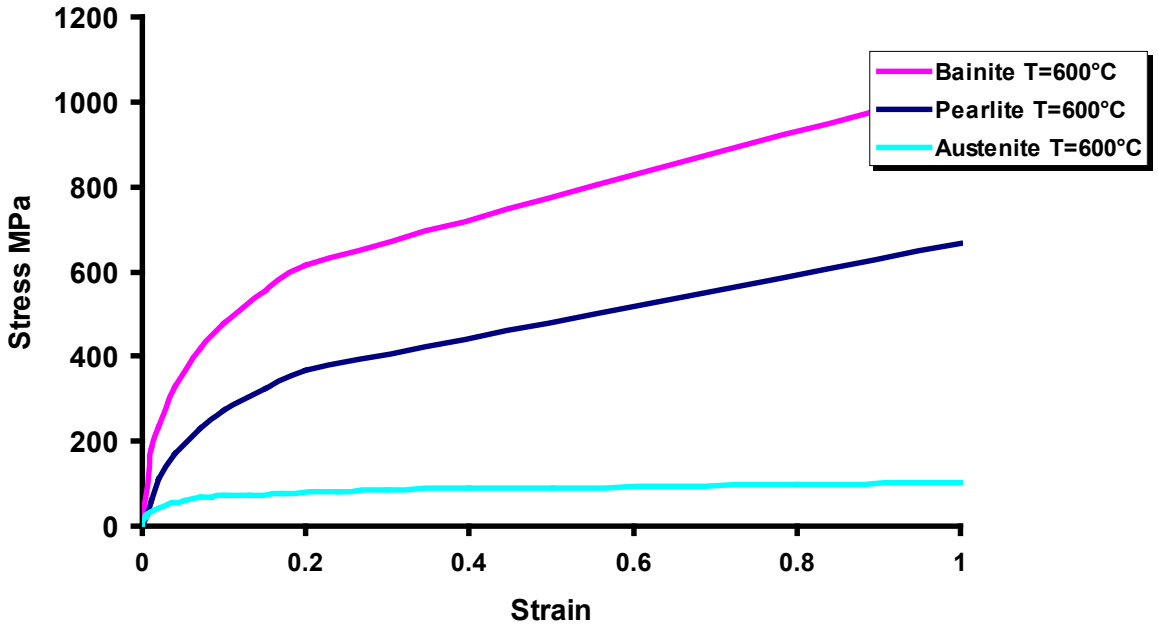

Figure 4.16 Stress-strain flow curve for each phase obtained using equation 3.2 for T=600°C

The default plasticity models used for calculations in Abaqus® are termed as rate independent models which essentially imply that the yield stress depends only upon the plastic strain and temperature only, i.e.

$$\sigma_y = \sigma_y(\varepsilon^p, T)$$

However, in order to take into account the viscoplastic effects, a rate-dependent model may be incorporated, where in addition to plastic strain and temperature the yield strength also depends upon the strain rate such that

$$\sigma_y = \sigma_y(\varepsilon^p, \dot{\varepsilon}^p, T)$$

In Abaqus®, the rate-dependent stress strain data can be provided in tabular form with yield stress values versus equivalent plastic strain at different equivalent plastic strain rates. Owing to this capability of Abaqus®, the viscoplastic material parameters *K* and *n* are not required to be calculated separately.

Summary:

A comprehensive numerical model to simulate the grinding process for the investigations of residual stresses in the ground components is presented. The essentials of finite element modelling are reviewed. The full coupling of mechanical strains, thermal strains and phase transformations during grinding were considered. The contact nonlinearity was simplified by removing the grinding wheel and substituting an equivalent grinding force profile. The grinding wheel was modelled as combination of normal pressure and tangential surface traction and the temperatures produced by friction at the contact between the grinding wheel and the workpiece is presented. The moving heat source has elliptically distributed heat intensity over a 2D semi-infinite solid (half-space) in plane strain. Numerical simulations were performed using the commercial finite element software Abaqus®/Standard along with the user subroutines UMAT, PHASE, UEXPAN, and PROP so as to model the thermal, metallurgical and mechanical behaviour of the material. The grinding wheel was modelled as a normal pressure and tangential traction moving on the workpiece through subroutines DLOAD and UTRACLOAD, respectively. Numerous simulations are performed to see the effects of the Peclet number, non dimensional heat transfer coefficient, different magnitudes of input heat flux and Poisson's ratio on the residual stresses were analyzed. The results are presented and discussed in details in the next chapter.

CHAPTER 5

RESULTS AND DISCUSSION

5

5.1 Results and Discussion

The results of the simulations are being presented and discussed in this chapter. In order to simplify the problem a step by step procedure is followed for the analysis where each phenomenon in the grinding process (thermal, phase transformation and mechanical) is described separately first. How these phenomena interact is then presented in a coupled analysis. The variations of the residual stresses and strains at the integration points have been examined, and the effects of the Peclet number (*Pe*), the non dimensional heat transfer coefficient (*H*) and different magnitudes of the input heat flux (*Q*) on both the microstructure and the residual stress state were analyzed. The Peclet number (*Pe*) is a convenient non-dimensional expression used to express the relative sliding velocity of motion of the heat source considering the thermal properties of the conduction medium which determines the speed of dissipation of heat in the medium [HOUZ00][ROWE01].

$$Pe = \frac{V_w L_c}{4\alpha_w} \tag{1}$$

Similarly *H* is a non-dimensional expression used to express the relative heat coefficient of the cooling media for a grinding process considering thermal properties of the conduction medium and velocity of the heat source [MAHD97].

$$H = \frac{2h_{conv}\alpha_w}{KV_w} \tag{2}$$

where α_w is the thermal diffusivity of the workpiece material calculated from the expression:

$$\alpha_w = \left(\frac{K}{\rho c_p}\right)_w \tag{3}$$

Other non dimensional parameters used are:

Non-dimensional time $t' = \frac{V_w^2 t}{2\alpha}$

t=time (sec)

Non-dimensional temperature $T' = \dfrac{T}{\left(\dfrac{QL_c}{2k}\right)}$

Q is heat input (W/m²)

Non dimensional coordinate $X = \dfrac{V_w x}{2\alpha}$

Non dimensional distance across x-axis related to workpiece $= \dfrac{2x}{L_c}$

Non dimensional depth across y-axis related to workpiece $= \dfrac{2y}{L_c} = \dfrac{2d}{L_c}$

x and y are the (x,y) coordinates related to the workpiece whereas d here refers to the depth of the workpiece across y-axis

5.2 Residual Stresses due to thermal loading

5.2.1 Grinding Temperature

Grinding is an expensive operation because the specific energy consumed is considerably higher than in other cutting processes [KALP97], to a degree exceeding the melting energy of materials [MALK74]. Virtually, almost all of the grinding energy is converted into heat [MALK89]. The accumulation of heat within the abrasives-workpiece contact zone (grinding zone) will result in a local elevation of temperature. Such excessive temperature rise, in addition to high stresses creates plastic strains and wear. It may also be at the origin of thermal damage at the surface of the ground component [SNOE78]. Furthermore, most stress-induced failures of a machine component (fracture, fatigue, stress corrosion cracking and wear) are associated with tensile residual stresses [SHAW96]. Such stresses, according to several researches, are reported to be of thermal origin [MAHD97].

To study residual stresses due to thermal loading, the grinding-induced temperature field needs to be investigated carefully in relation to grinding conditions. A surface temperature history under specified conditions and its variation with respect to depth is given in **Figure 5.1**. Temperature fields calculated during grinding (i.e. heating) at a given time instance (t′=33.61; non-dimensional time) as a function of non-dimensional depth ($2y/L_c$) are shown in **Figure 5.1** for the specified values of parameters Q, L_c, H and Pe. From the values of peak temperatures,

it is found that up to a certain depth ($2y/L_c$ =0.30) the temperature goes beyond Ac1 (755°C [ZHAN02]) for the material AISI 52100 and then the regions behind the heat source cool down below Ms (250°C [ZHAN02]). A high cooling rate thus results in transformation of austenite to martensite in the top most surface.

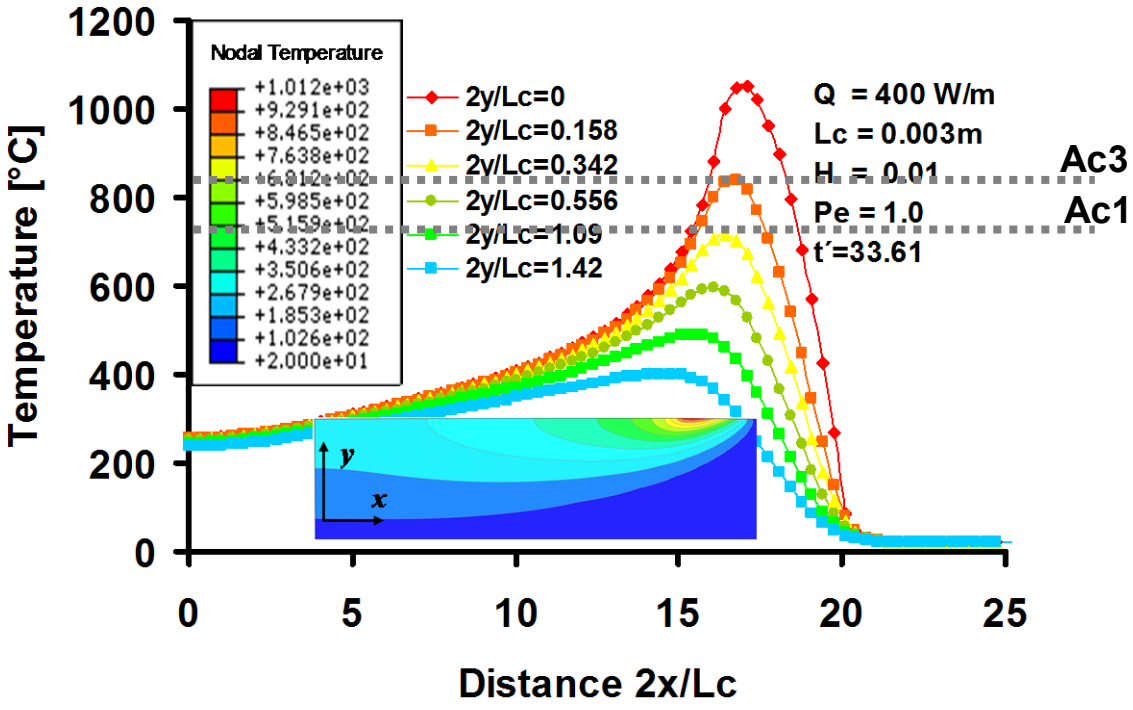

Figure 5.1 Temperature profiles at various depth to a moving heat source

Similarly typical surface temperature profiles at various Peclet numbers (i.e. grinding speeds) are shown in **Figure 5.2, Figure 5.3** and **Figure 5.4**. The grinding temperature develops much faster ahead of the heat source than that behind it as more time is required for thermal energy to diffuse through the workpiece. Moreover, for higher Peclet number the grinding temperature profile approaches its steady state much faster than for lower Peclet numbers. Theoretically, the time required to achieve steady conditions is very long. Steady state conditions are reached only when the grinding temperature profile relative to the heat source movement becomes hardly changed. **Figure 5.2, Figure 5.3** and **Figure 5.4** exhibits the maximum grinding temperature history in terms of non-dimensional time t'. It shows that for a given grinding condition (e.g. Pe=0.5), t' should exceed 4 if more than 95 % of the grinding temperature needs to be reached.

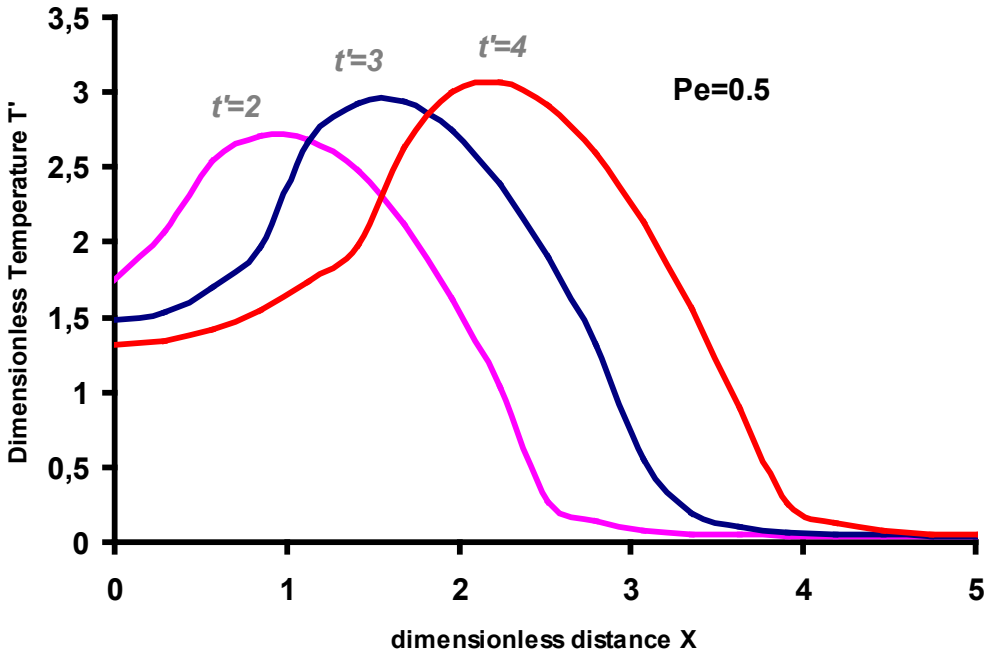

Figure 5.2 Dimensionless surface temperature profiles at various dimensionless time t′, Pe=0.5

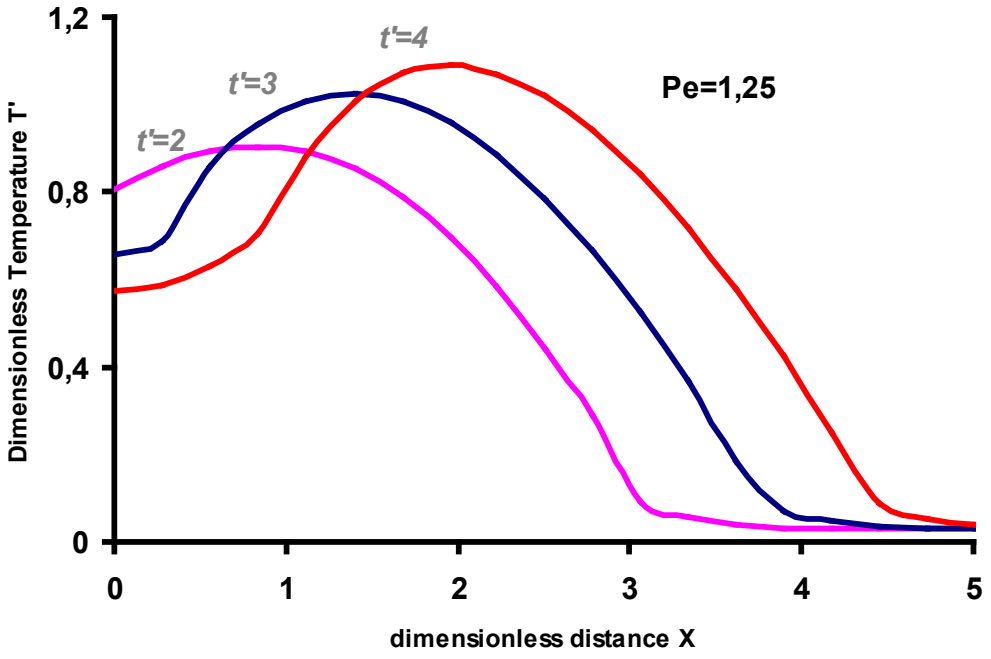

Figure 5.3 Dimensionless surface temperature profiles at various dimensionless time t′, Pe=1.25

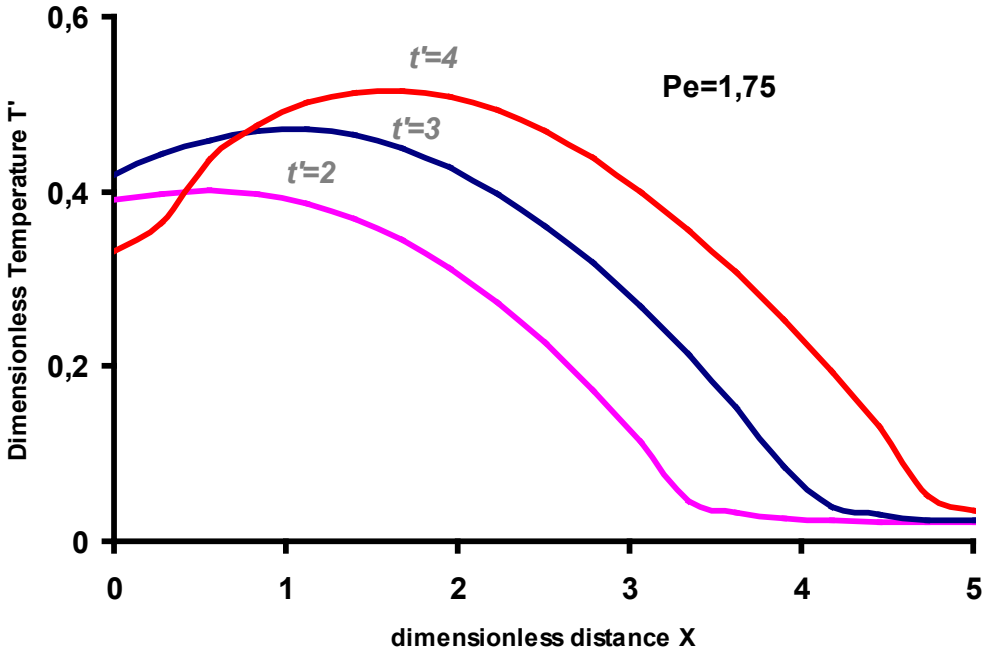

Figure 5.4 Dimensionless surface temperature profiles at various dimensionless time t′, Pe=1.75

Figure 5.5 describes the distribution of temperature within the workpiece depth (non dimensional depth *2y/Lc*) for different Peclet numbers. For a given set of grinding conditions higher *Pe* results in lower temperature distribution into the workpiece. The maximum surface temperature versus the Peclet number is shown in **Figure 5.6**. For a given heat source length L_c and intensity *Q*, the peak temperature decreases when increasing the Peclet number (*Pe*). This is because a large *Pe* shortens the duration of heat accumulation into the workpiece. A comparison with the analytical solution of Blok [BLOK55] is also provided and a good agreement is found, which validates the numerical model. The difference can be attributed to the heat exchange by convection that we have in the FE model, whereas Blok does not consider it. If the non-dimensional heat transfer coefficient (*H)* or the contact length (L_c) between the grinding wheel and the workpiece increases, the grinding temperature decreases (**Figure 5.7**). It can be seen from **Figure 5.7** that the parameter *H* and L_c have a very significant effect on the maximum surface grinding temperature for a given Peclet number.

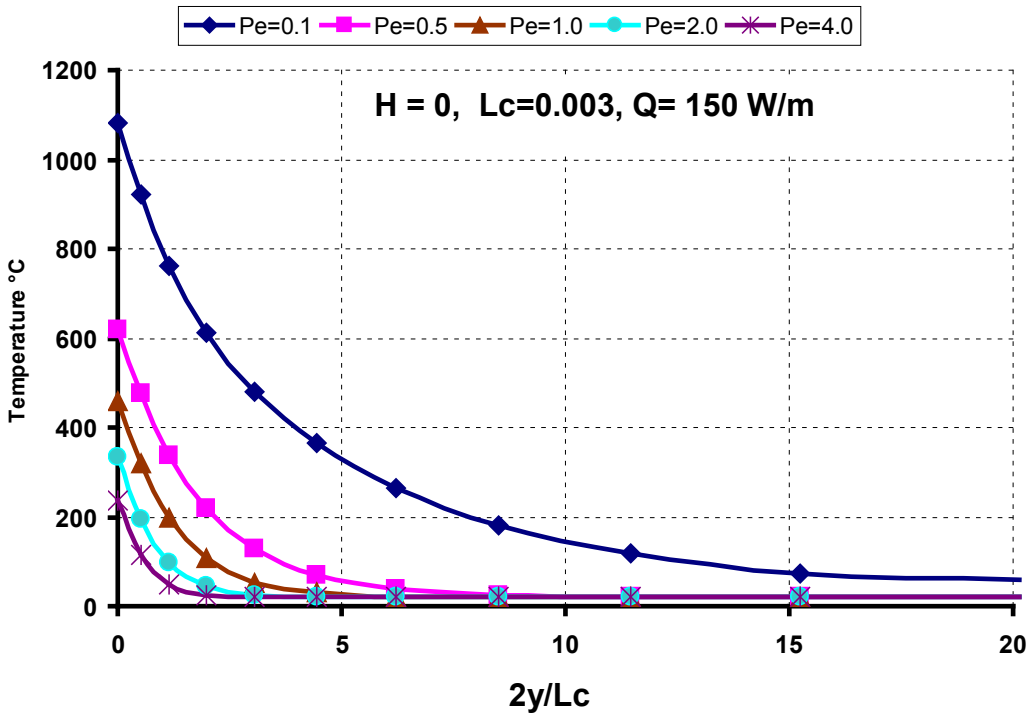

Figure 5.5 Temperature distribution versus dimensionless depth for various Peclet numbers Pe

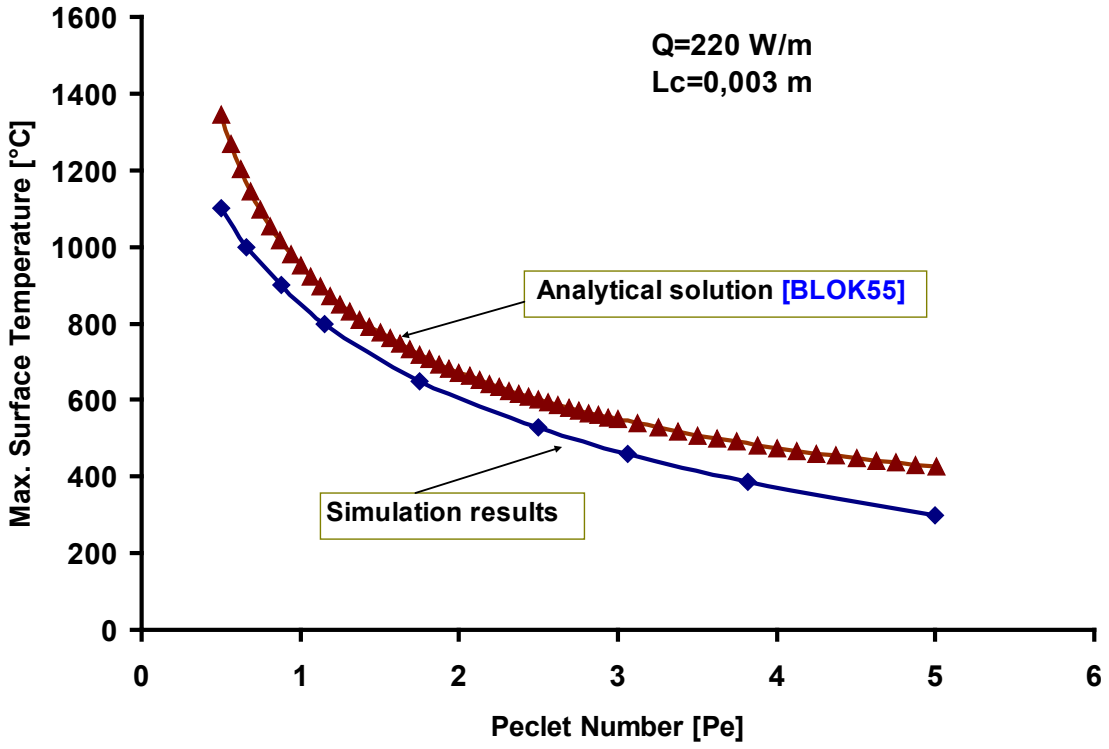

Figure 5.6 Effect of the Peclet number Pe on the maximum surface temperature

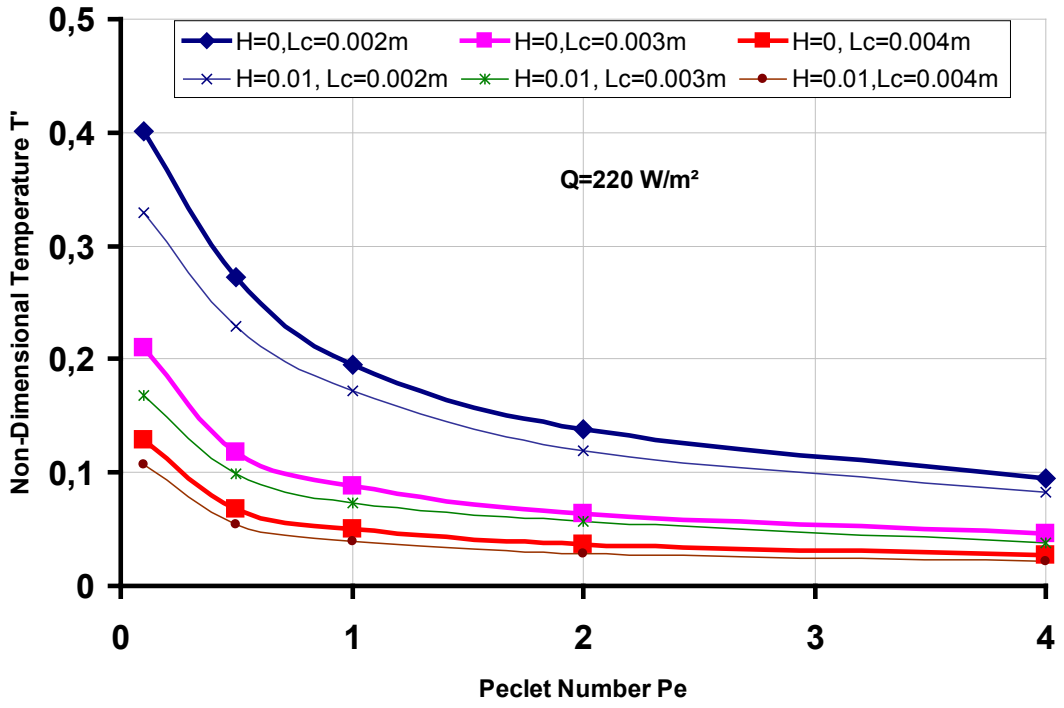

Figure 5.7 Effect of Pe, H and L_c on the maximum surface temperature

5.2.2 Effect of grinding conditions on the onset of plastic strain

Since the grinding temperature is directly proportional to the input heat flux, Q, it is also useful to express the critical grinding conditions directly in terms of Q. A series of analysis was performed to see the effect of Q, Pe and H on the onset of plastic strains for thermal loading conditions. **Figure 5.8** shows that plastic strains may appear if the input heat flux, Q, is above the Q-Pe curves. Very low heat input may cause plastic strains if Pe is very low (e.g. 15 W/m² for Pe=0.1). More input heat flux is needed to initiate plastic strain when increasing the convection heat transfer coefficient H or the Peclet number Pe. For high Pe and H the material may remain in elastic region even for large values of Q. It can also be seen that for high values of Pe and H the elastic domain increases significantly.

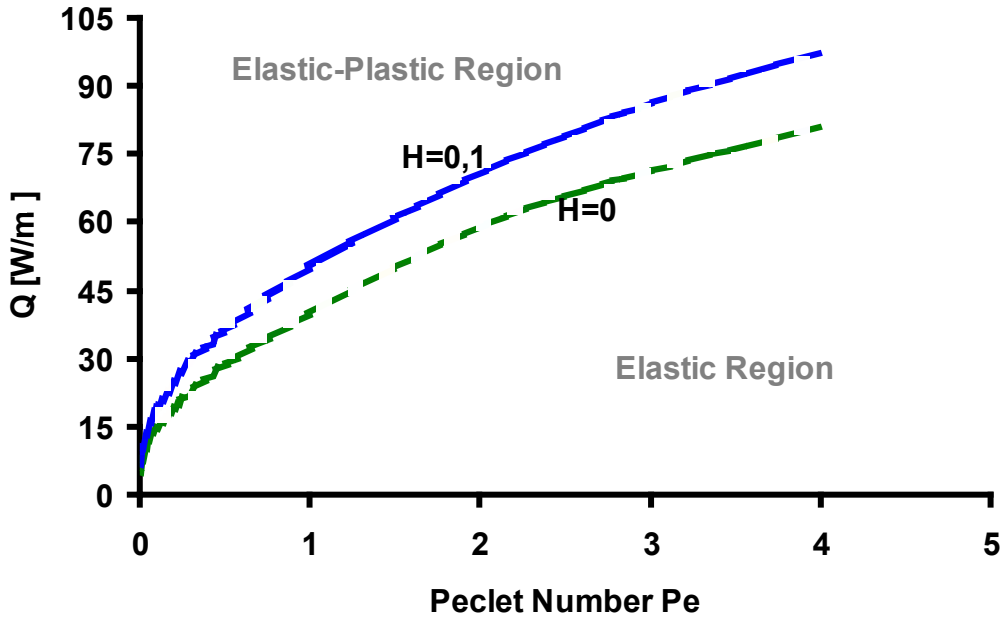

Figure 5.8 Effect of grinding conditions on onset of plastic strains

5.2.3 Mechanism of Residual Stresses due to Thermal Loading

The mechanisms of residual stresses as a result of thermal loading can be best understood if the grinding stresses and strains are studied in relation to grinding temperature. The history of the longitudinal thermal strain, $(\varepsilon_{xx})_T$, is plotted in **Figure 5.11**. It is noted that the longitudinal compressive strains start to develop first followed by surface stretching which in turn results in permanent surface strain. To reveal the link between surface stresses due to the thermal loading, the stress history associated with the grinding temperature is examined in **Figure 5.10**. It shows that the ground surface is in compression ahead of the heat source whereas it switches to tension behind the center of the heat source. Moreover, the occurrence of irreversible plastic strains prevents the geometric recovery of the workpiece and hence tensile residual stresses are developed. Similar residual stresses are observed below the surface but attenuated as the depth increases (**Figure 5.11**).

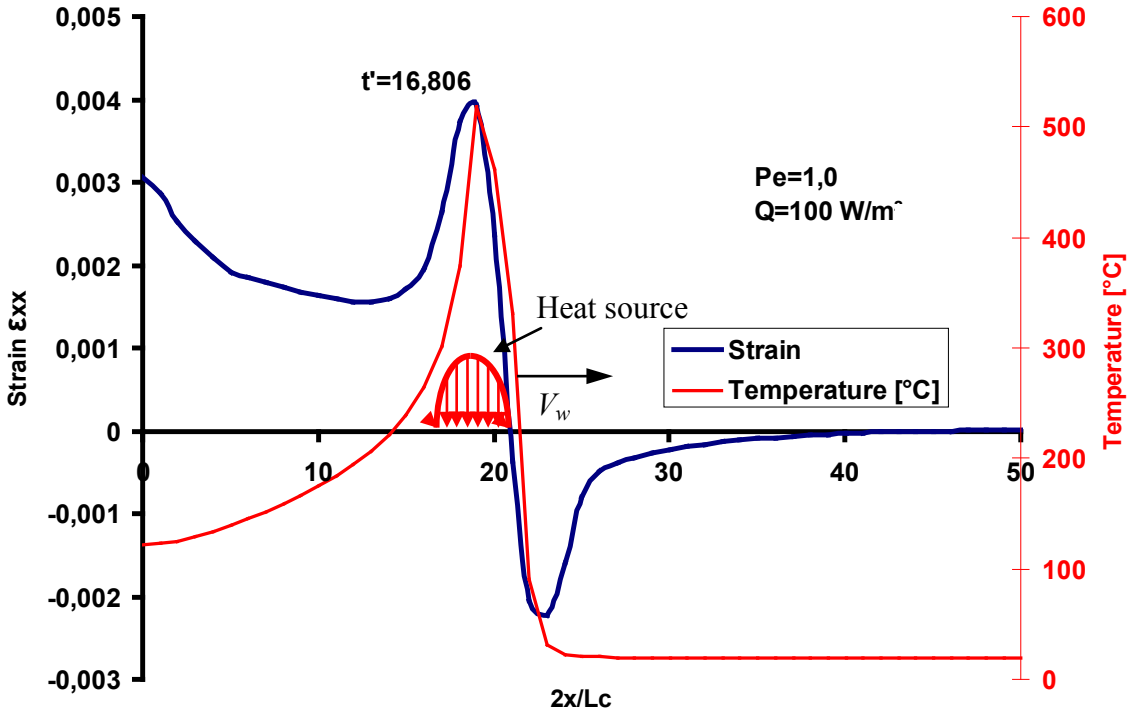

Figure 5.9 Distribution of the longitudinal surface strain ε_{xx} and temperature at non dimensional time t´=16.806

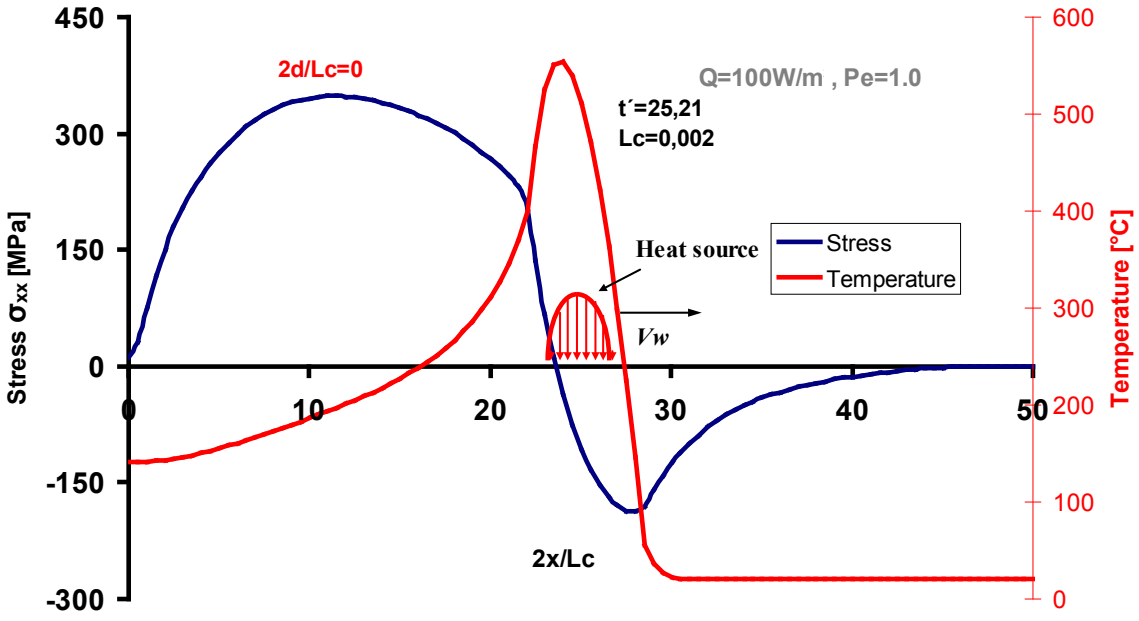

Figure 5.10 Distribution of the longitudinal surface stress σ_{xx} and temperature at non-dimensional time t'=25.21

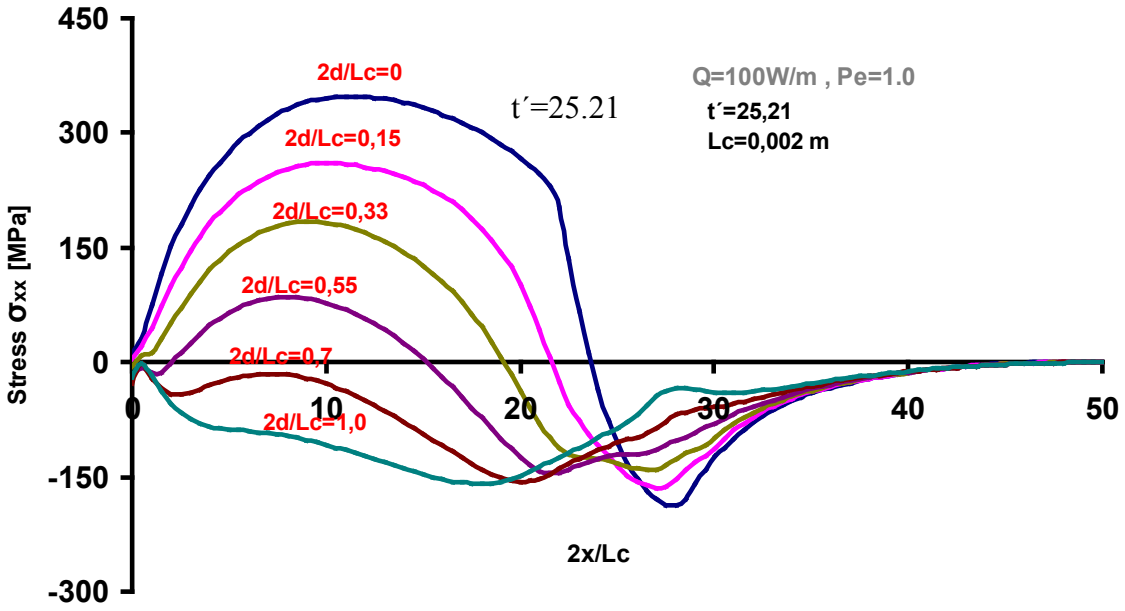

Figure 5.11 Distribution of the longitudinal stress σ_{xx} at various depths

5.2.4 Effect of Grinding Conditions on Residual Stresses due to Thermal loading

To decrease the level of residual stresses due to thermal loading the grinding temperature should be lowered by either enhancing the cooling power of the cooling fluid or by increasing the heat source velocity (table speed) with all other conditions maintained the same. The influence of the cooling fluid is shown in **Figure 5.12** which illustrates the effect of convection heat transfer on the residual stress distribution. It is observed that a stronger cooling decreases the magnitude of the longitudinal residual stresses at the surface, also reducing the thickness of the layer where tensile longitudinal stress is found, providing that other parameters are kept the same and for a given set of grinding conditions. It is also found that a more powerful cooling increases the residual stress gradient along depth.

Another way to decrease the grinding residual stresses due to heating and cooling consists in increasing the Peclet number (i.e. the heat source velocity), see **Figure 5.13**. It is observed that a higher heat source speed produces a decrease of residual stresses if the heat flux intensity is maintained constant. The effect of the input heat flux intensity is shown in **Figure 5.14**, with similar trends on the residual stresses.

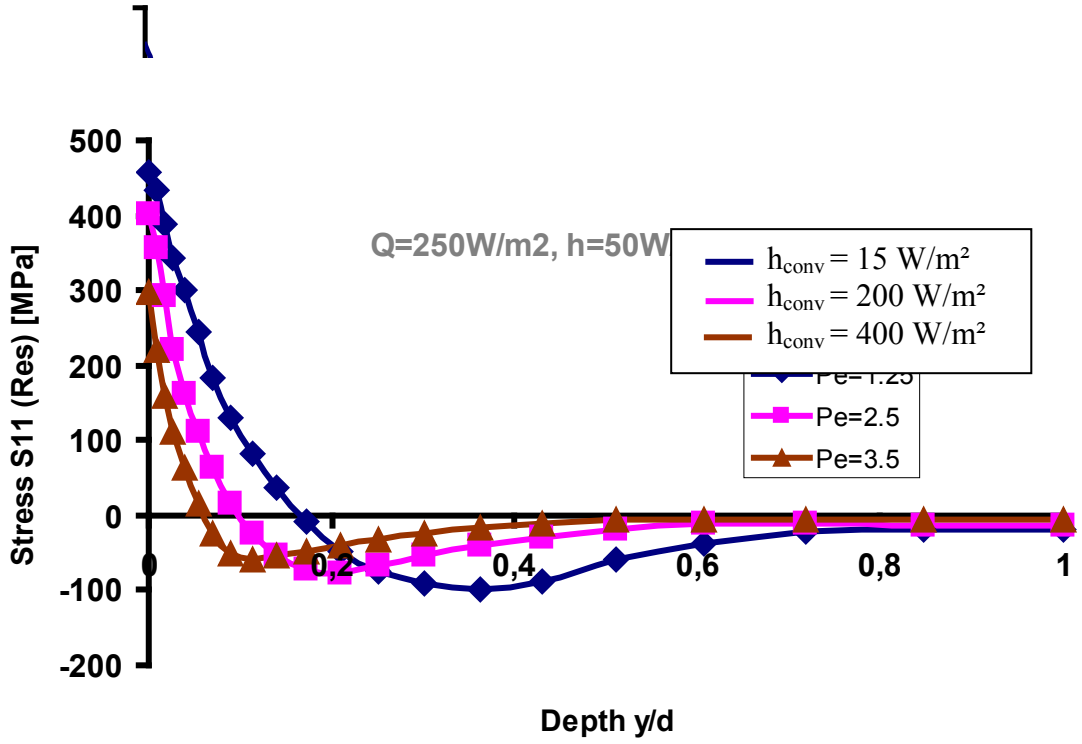

Figure 5.12 Effect of cooling on the distribution of the longitudinal residual stress versus depth

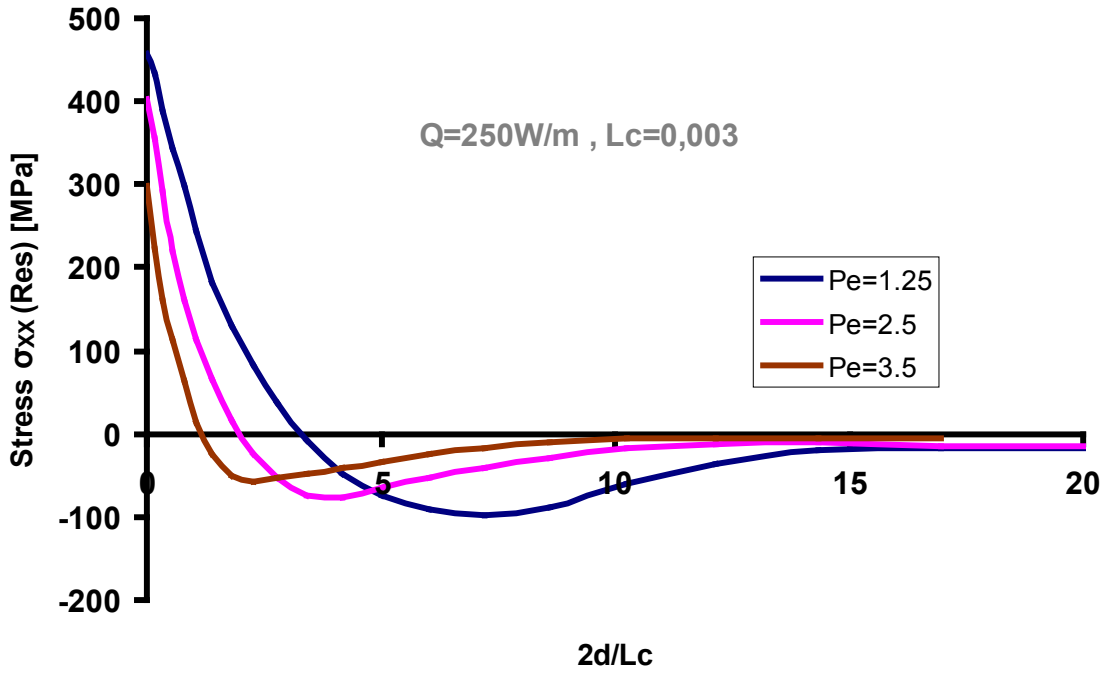

Figure 5.13 Effect of the Peclet number on the distribution of the longitudinal residual stress versus depth

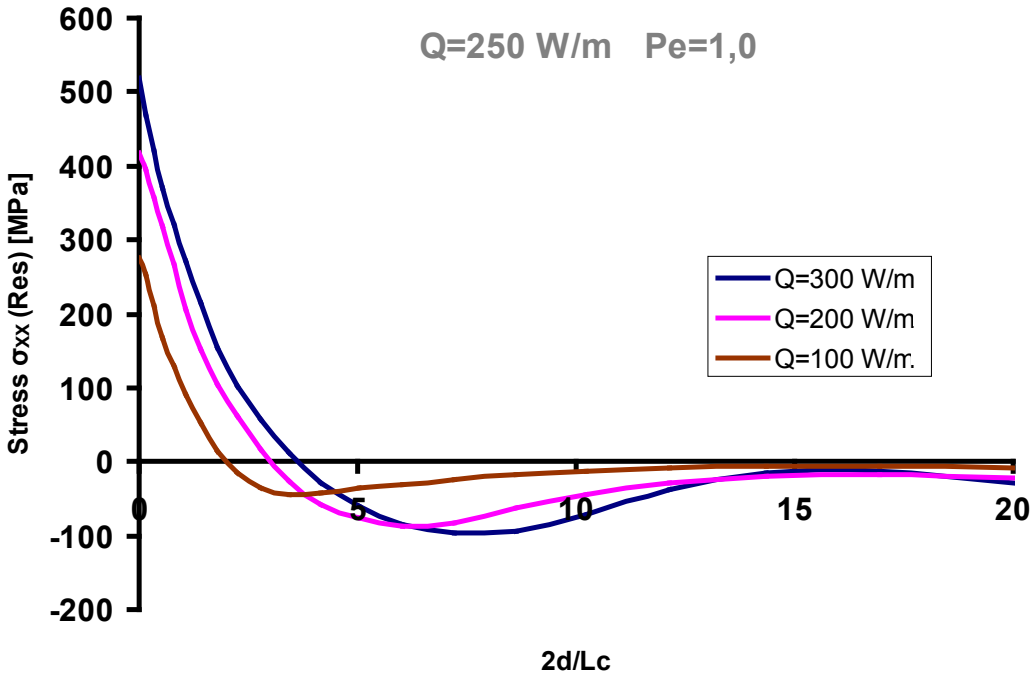

Figure 5.14 Effect of the input heat flux intensity on the longitudinal residual stress profile along depth

5.3 Phase Transformation and Residual Stresses

5.3.1 Critical Grinding Conditions

The temperatures at which phase transformation occurs are usually referred as critical temperatures (section 3.2.1). Critical temperatures are observed by measuring changes in heat transfer or volume as specimens are heated or cooled. When the workpiece experiences a critical temperature change in grinding, phase transformations will take place. During heating, heat is absorbed and specimen contraction occurs as ferrite and cementite are replaced by the close-packed structure of austenite. During cooling, heat is exhausted and specimen expansion occurs as austenite transforms to other phases (pearlite, bainite, martensite etc). For AISI 52100 (100Cr6) steel, at the austenitizing temperature (750^{o}C), the workpiece surface undergoes phase change to the apparition of an austenitic phase. During cooling that follows, another phase change can take place depending on the cooling rate. The number of phases present during cooling are purely cooling rate dependent and are obtained from CCT diagram of the given material as discussed in details in section 3.5.2.

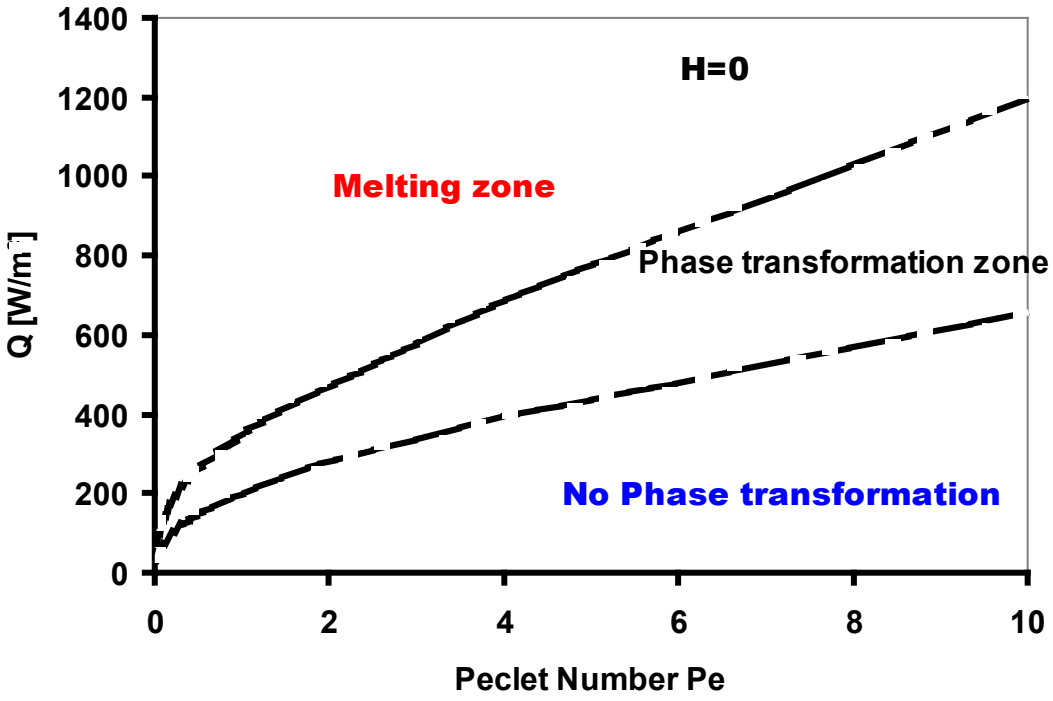

Figure 5.15 Critical grinding conditions for the onset of phase transformation (H=0)

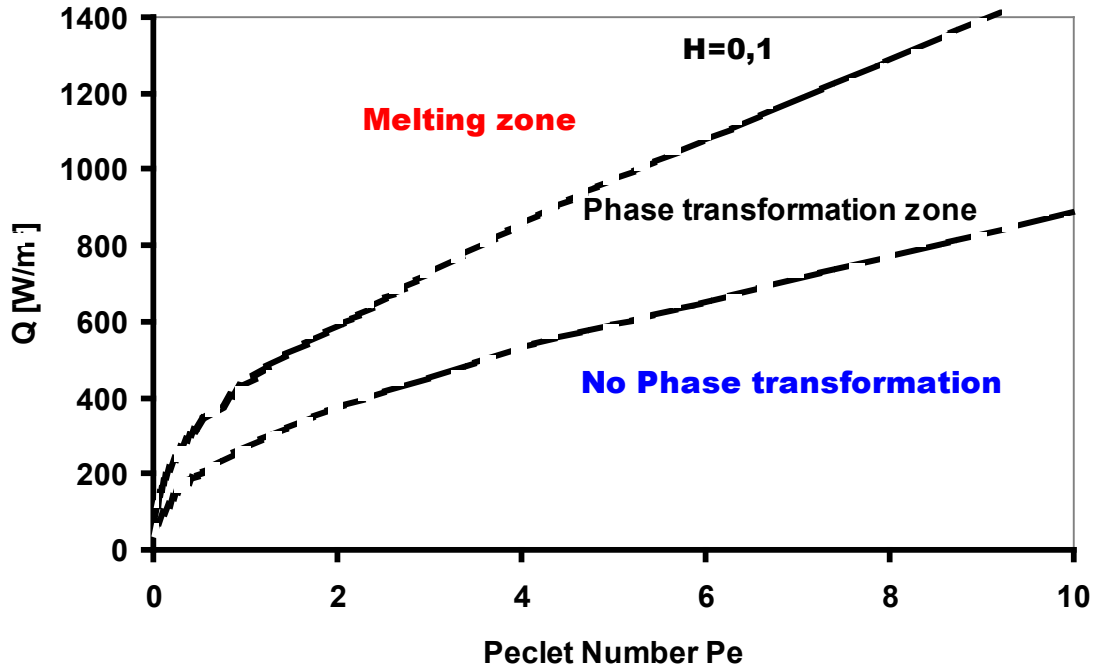

Figure 5.16 Critical grinding conditions for the onset of phase transformation (H=0.1)

In order to have an idea about the critical grinding conditions resulting in austenitization

temperatures during heating, a series of analyses was performed and the results shown in **Figure 5.15** and **Figure 5.16** which reveal the onset of phase transformation in relation with the heat flux intensity Q and Peclet number Pe. As shown in **Figure 5.15**, there exists a wide range of grinding conditions that can initiate phase transformation; therefore it is sufficient to bring the grinding temperature above an austenitizing temperature for the phase change to take place. For a given contact length (for example L_c = 0.002 m) the minimum Peclet number required to initiate phase transformation is very small and in the order of 0.01 which in turn corresponds to a very low heat source velocity (table speed). It is obvious that a higher convection heat transfer coefficient increases the input heat flux required to initiate phase transformation for the same grinding conditions, see **Figure 5.16**. The critical input heat flux intensity is changing rapidly at a lower Peclet number. At higher Peclet numbers, however, the change can be considered as linear in terms of Peclet number.

5.3.2 Phase transformation

The most common transformation products that may be formed (from austenite during cooling process) in the workpiece experiencing a critical grinding temperature history are in order of formation with decreasing cooling rate: martensite, bainite, pearlite, ferrite and cementite. However, since the heat source and convection act on the surface, different parts of the workpiece material must experience a different heating and cooling history. It is therefore understandable that at a certain depth in the subsurface, heating and cooling cannot activate phase transformation even though it does take place near the surface. The depth of the layer with the transformed phase must therefore be a function of the material properties of the workpiece and grinding conditions, including the heat source velocity, depth of cut, cooling rate and so on. For the highest cooling rates only martensite phase transformation occurs.

5.3.3 Residual Stress Distribution - Effect of Phase Transformation

5.3.3.1 Stress evolution

The change of workpiece properties associated with phase change plays a major role in residual stress distribution. Therefore, a close understanding of the ground surface properties in relation to the heat source speed is necessary to explore the residual stress mechanisms when phase transformation is likely to take place. The mechanisms of residual stresses due to phase transformation can be best understood if the grinding stresses and strains are studied in

relation to the thermal history. A typical case study is given in **Figure 5.17**, which illustrates the von Mises stress history of the ground surface in relation to heat source movement. It is found that the von Mises stress rises shortly after the heat source passes the grinding zone due to surface cooling and martensite transformation.

The history of the longitudinal stress $\sigma_{xx}(z_i, T)$ is plotted in **Figure 5.18** for a surface point, where the maximum temperature T_{max} reaches 1000°C. It is noted that with an increase in temperature the element tends to expand in all direction, however, restricted by the cooler surrounding material it develops compressive stresses which keeps on increasing with increasing temperature. These stresses are initially elastic in nature, but with further increase in temperature plastic compressive stresses develop and a stress reversal is observed. When the temperature exceeds the austenitizing temperature (Ac_1), an almost free stress state is developed because of the low yield stress of the austenitic phase at high temperatures. Having crossed Ac_3, the element develops tensile stresses of low magnitude due to lattice contraction. When the heat source moves away the element starts to cool down, another stress reversal occurs due to contraction / shrinkage and thus compressive stresses develop once again. Beyond Ms, compressive stresses grow rapidly due to lattice dilatation. This volumetric expansion finally results in very high longitudinal compressive stresses.

The evolution of stresses with and without phase transformation is illustrated in **Figure 5.19**. For the case when the temperature is high enough to initiate phase transformation during heating, small tensile stresses localized within the heat source are observed as the result of austenite formation which has a low yield stress. During fast cooling, the martensite transformation results in an increase in volume at the surface and nearby subsurface of the material. The expansion of a surface layer is resisted by the subsequent unchanged volume in the depth resulting in compressive stresses. During phase transformation the surface stresses exceed the yield strength of the material, which is plastically deformed, resulting in thermally induced dimensional changes and surface hardening. Thus it is justified to conclude that surface hardening would result in a higher magnitude of residual stresses regardless of their nature. Note that tensile longitudinal residual stresses appears below the surface, so as to equilibrate the residual stress state, as shown in **Figure 5.20**.

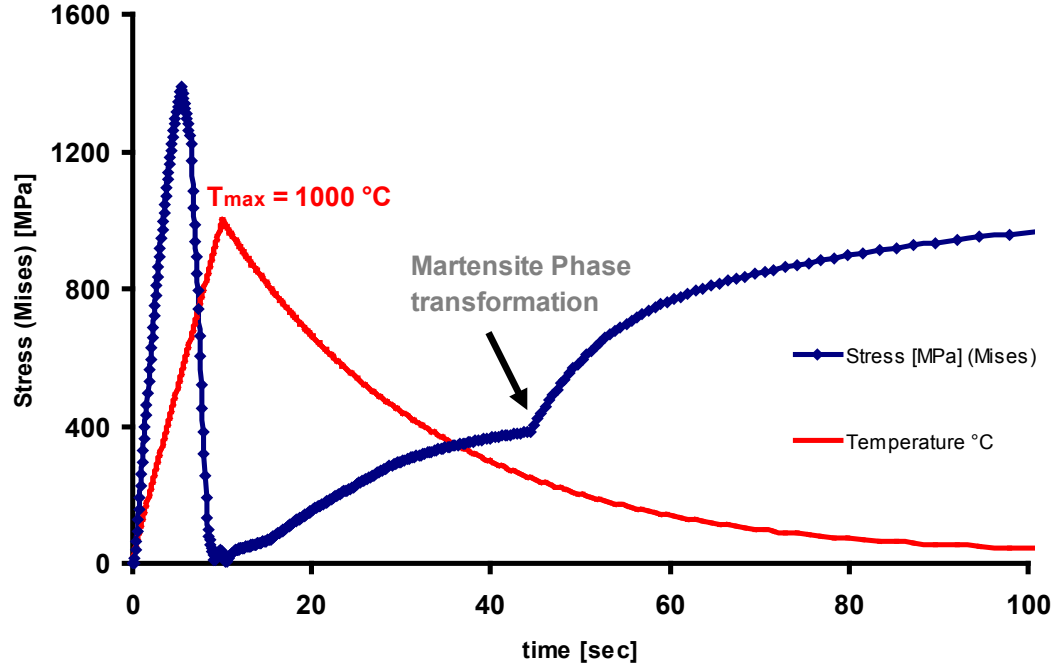

Figure 5.17 Evolution of the von Mises stress at a surface point and during one pass of the heat source (Pe=1, Q=200W/m, Lc=0.002m)

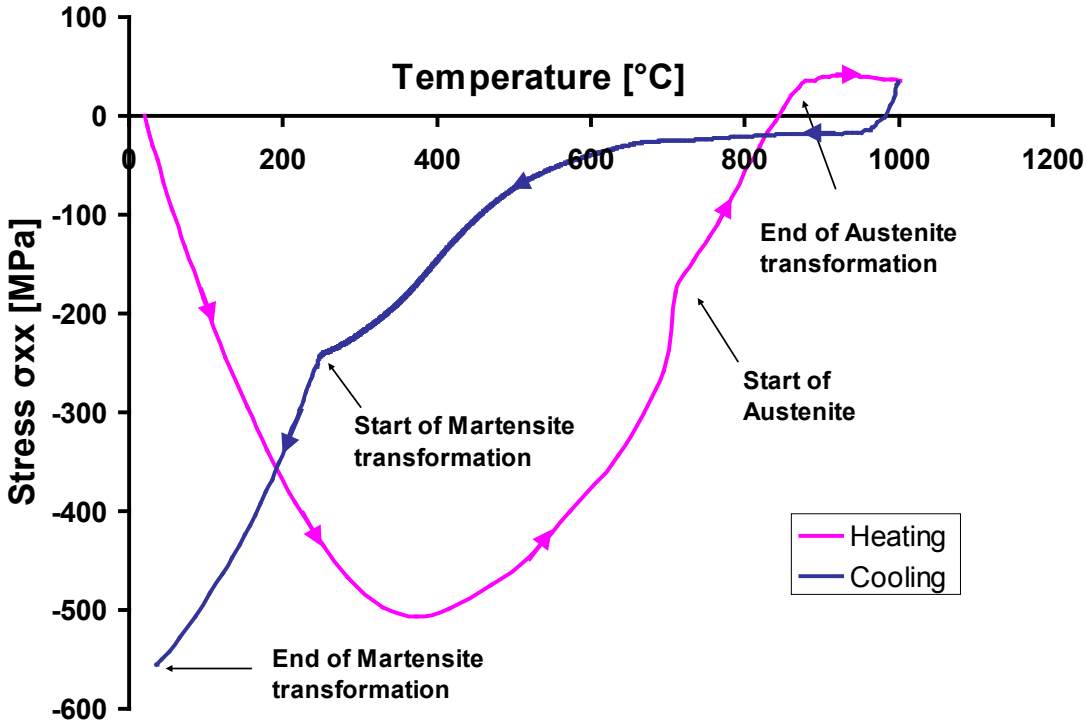

Figure 5.18 Evolution of the longitudinal stress σ_{xx} at a surface point during heating and cooling (Pe=1, Q=200W/m, Lc=0.002m)

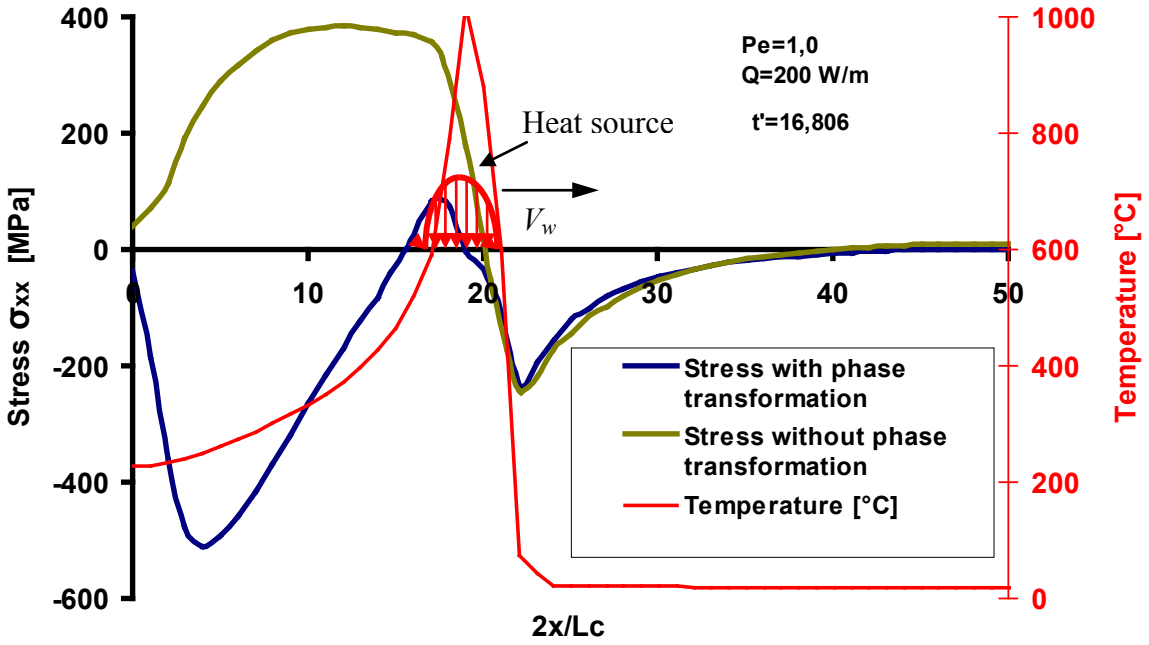

Figure 5.19 Distribution of the longitudinal stress σ_{xx} with and without phase transformation

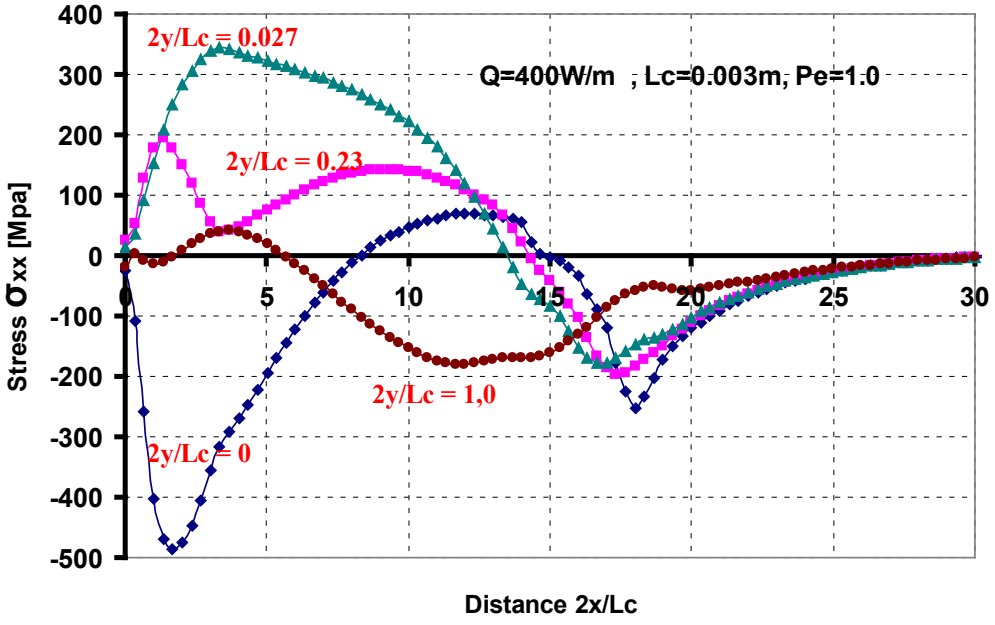

Figure 5.20 distribution of longitudinal stress σ_{xx} at different depths

5.3.3.2 Residual stresses

Figure 5.21 shows the distribution of the longitudinal residual stress with and without phase transformation. The residual stress distribution after a certain depth is almost identical with and without phase transformation, whereas the surface layer exhibits significant compressive stresses in presence of phase transformation (up to -700 MPa in Figure 5.21).

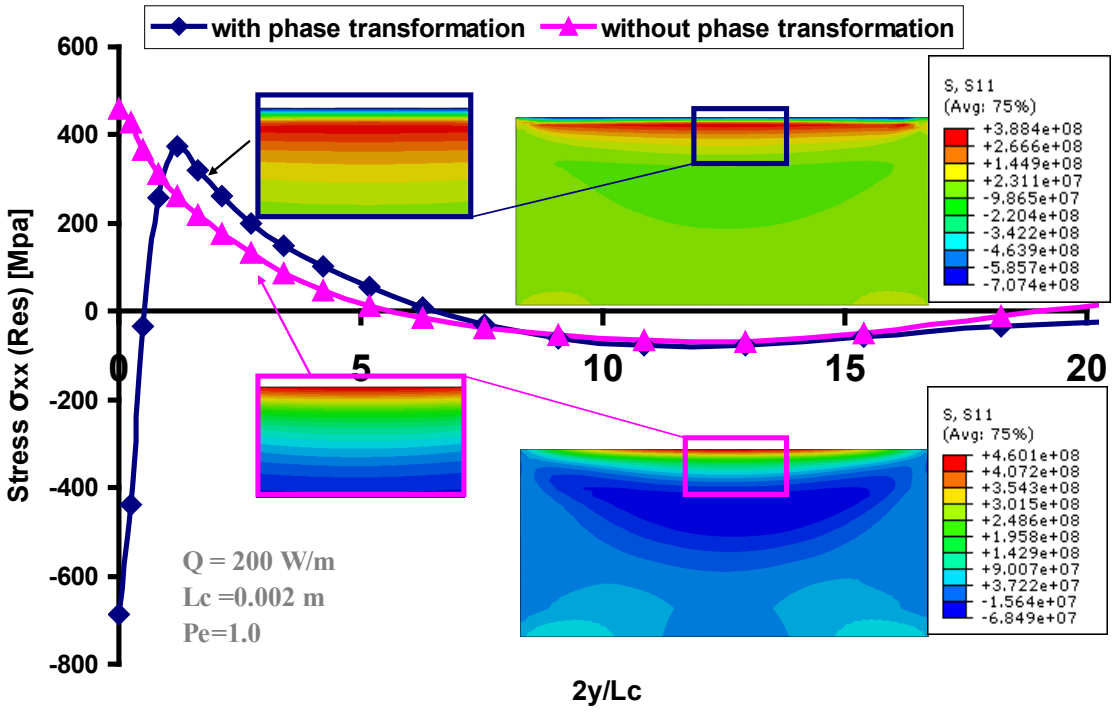

Figure 5.2 1 Distribution of the longitudinal residual stress versus depth with and without phase transformation

5.3.4 Effect of grinding parameters on phase transformation and residual stress distribution

A parametric study was carried out to find the effect of the variation of various grinding parameters on phase transformation and subsequent effects on the residual stress distribution in the workpiece.

5.3.4.1 Effect of Cooling

The cooling mechanism relies on convection heat transfer throughout the ground surface and the heat energy diffused into the workpiece material. Cooling has a significant effect on the formation of residual stresses since it lowers the grinding temperature, influences the grinding temperature history and in turn dominates the critical grinding conditions for phase

transformation. The volume growth associated with phase transformation also plays an important role in the formation of residual stresses. In this regards the cooling has a significant impact on the nature of residual stresses. Generally speaking; when the steel is slowly cooled; it undergoes a crystal (size) change as it transforms from a less densely packed austenite (face-centered cubic or *fcc*) to a more densely packed body centered cubic (*bcc*) structure of ferrite (a relatively soft transformation product). At faster cooling rates the formation of ferrite is suppressed and martensite (a relatively hard transformation product) which is an even less densely packed body centered (*bcc)* structure than austenite is formed. This results in volumetric expansion at the Ms Temperature as shown in **Figure 5.22**. If these volume changes cause stresses that are constrained by the surrounding material, a residual stress system is created. The effect of the cooling rate on the formation of longitudinal stress is shown in **Figure 5.23**. If the temperature is enough to initiate phase transformation (Austenite) the evolution of the longitudinal stress is strongly dependent on the cooling rate, see **Figure 5.23 and Figure 5.24**. This is explained by the transformation product that are less dense (volume increase) at high cooling rates than those obtained at low cooling rates ($\rho_{mart} < \rho_{bain} < \rho_{pearl}$).

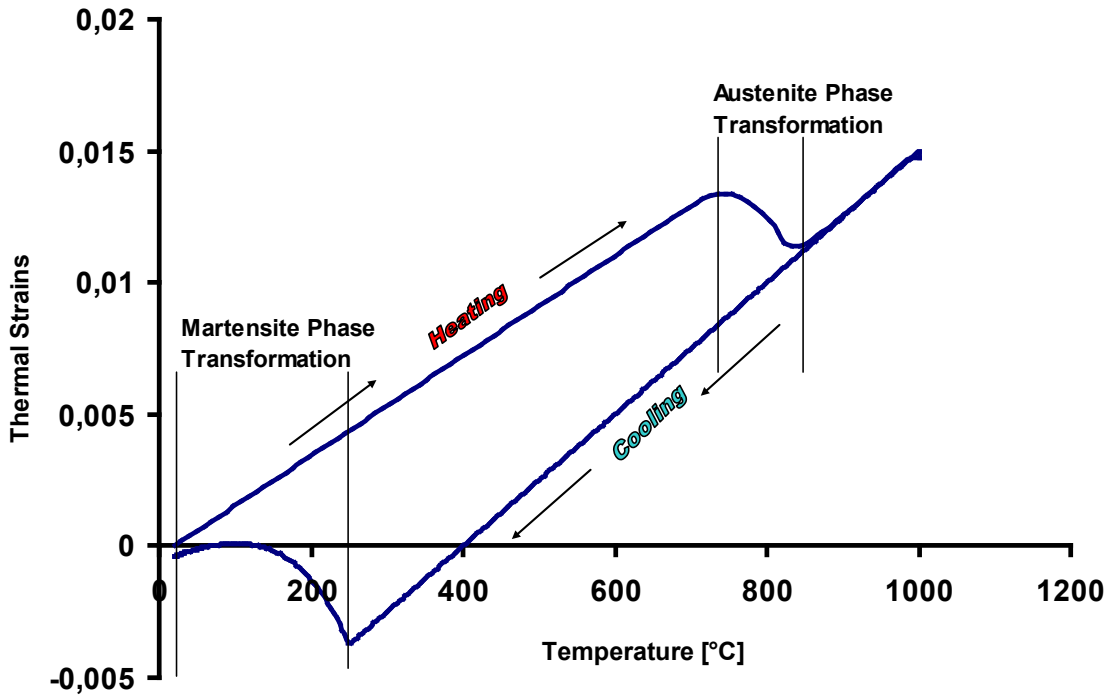

Figure 5.22 Dilatometric curve - Evolution of thermal strains with temperature

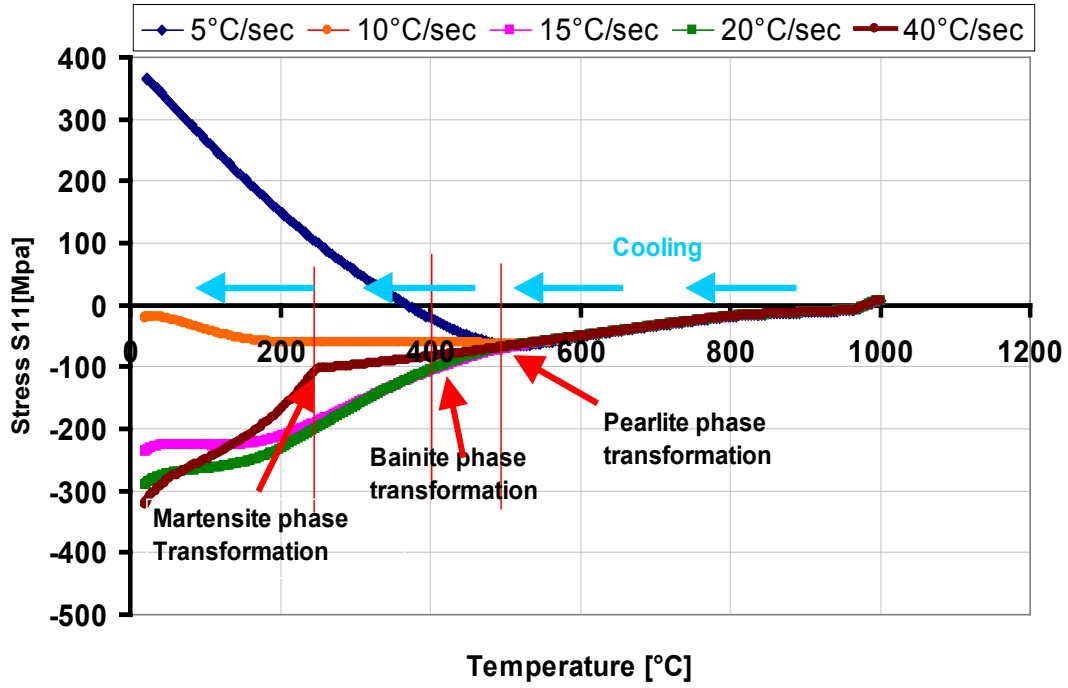

Figure 5.23 Evolution of the longitudinal stress at different cooling rates

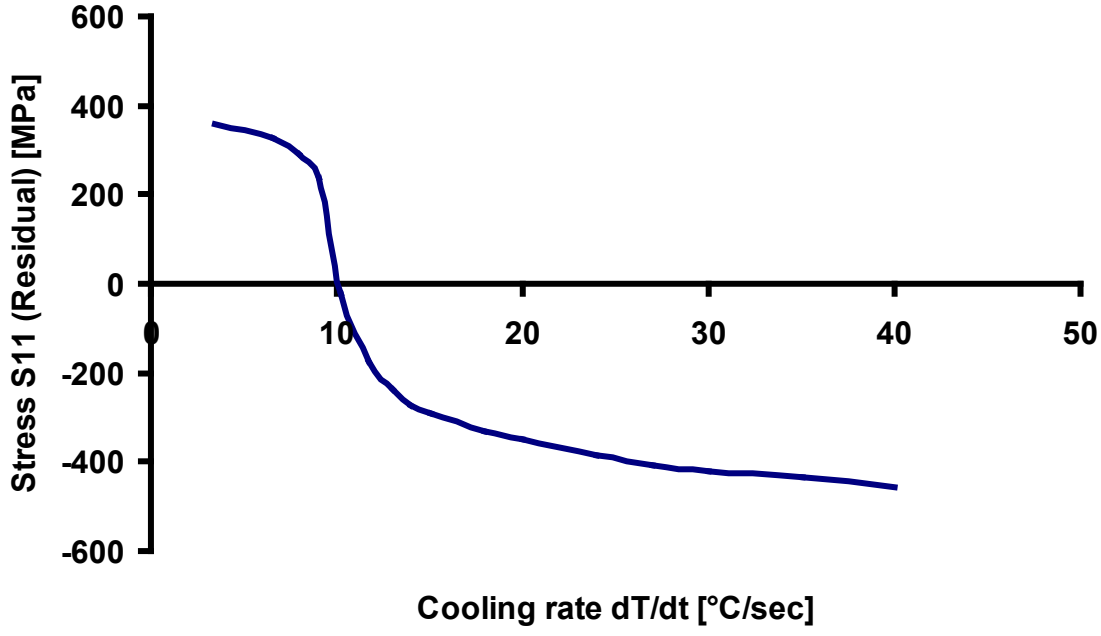

Figure 5.24 Prediction of the longitudinal residual stress at a surface point and function of the cooling rate

At high cooling rates, Martensite is the only phase to be formed. Above the Ms temperature,

the stresses that are formed are mostly elastic due to thermal expansion. Upon further cooling, the stresses found at the surface exceed the yield strength and plastic strain occurs. Subsequent martensitic transformation at the surface provides a substantial stress component due to volumetric increase. The transformation-induced volume increase of the surface layer brings compressive stresses at the surface which is balanced by a sub-surface in tension. The permanent volume growth of martensite is restrained by the surrounding part without transformation. That is why the martensite volume growth results in compressive residual stresses **(Figure 5.21)**. The tendency towards more compressive stresses increases as the martensite volume increases. Beyond the martensite layers, a rapid change to tensile residual stresses occurs due to lack of volume growth **(Figure 5.21)**. This means that in spite of the surface compressive residual stresses induced by volume growth it exists a risk of rapid change of the stress nature from compressive to tensile at the onset of martensite depth.

Figure 5.25 clearly demonstrates the effect of convection heat transfer on the distribution of residual stress. At higher cooling rate, a lower grinding temperature is generated and thus leads to a thinner martensite layer, see **Figure 5.26**. If the grinding temperature is below the austenizing temperature, martensite will not form and residual stresses in a workpiece in this case are only those associated with yielding during cooling in absence of phase transformation. When a martensite layer appears, the residual stresses vary almost linearly with depth. The maximum of the residual stress is not really affected by the convection heat transfer coefficient when sufficiently low. For a higher convection heat transfer coefficient, the effect of cooling becomes more dominant as the martensite depth becomes much thinner. The power of the mechanisms of cooling can be enhanced by either increasing the Peclet number or enlarging the convection heat transfer coefficient. It is apparent that both mechanisms result in a different grinding temperature history and thereby cause different cooling rates in the temperature range of interest.

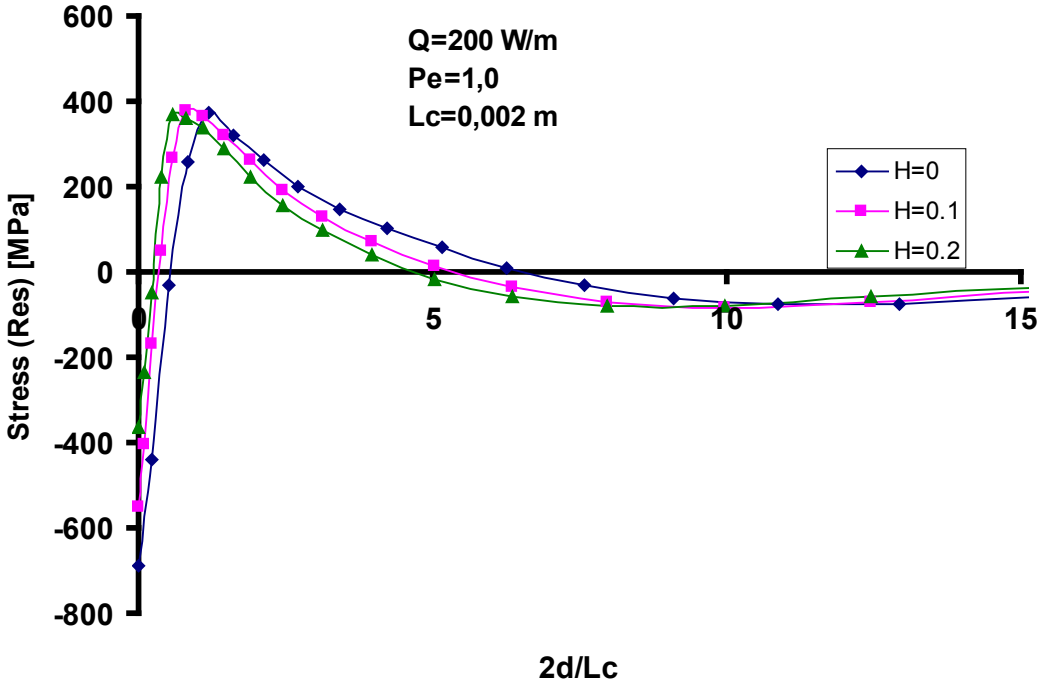

Figure 5.25 Effect of the convection heat transfer coefficient H on the longitudinal residual stress along depth

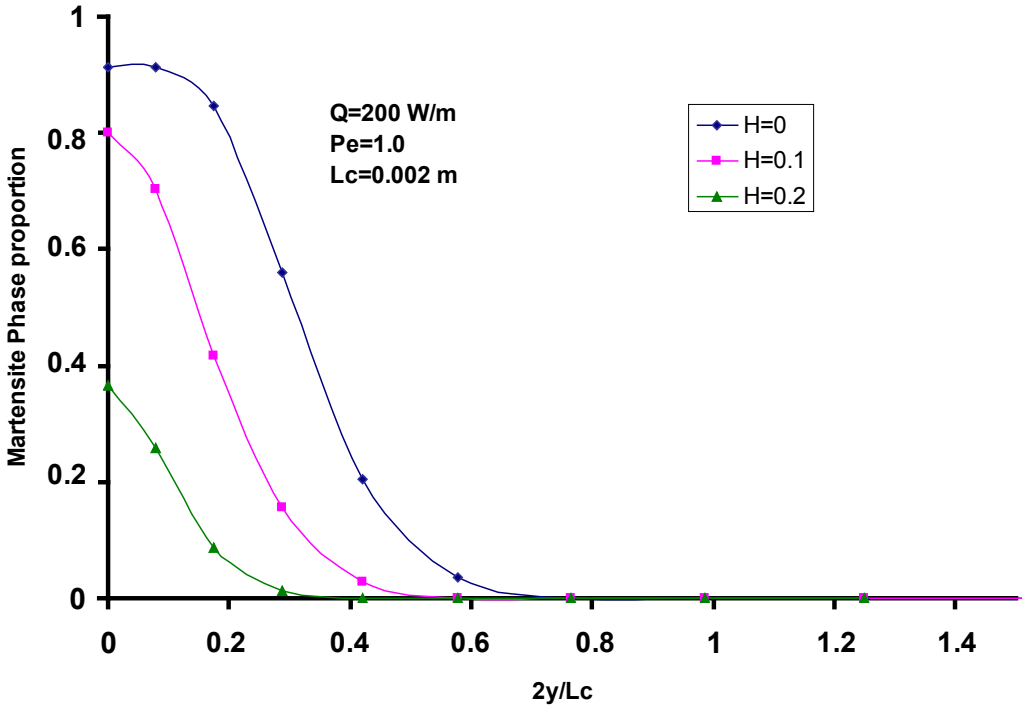

Figure 5.26 Effect of the convection heat transfer coefficient on the proportion of martensite

5.3.4.2 Effect of the Peclet number

The Peclet number of a grinding process, *Pe*, reflects the variation of the grinding table speed (i.e. the heat source speed) and thus the thermal energy diffusion rate through the ground surface. An increase of *Pe* results in a decrease of the grinding temperature and an increase of the cooling rate, if all the other grinding conditions remain the same. Therefore to maintain the same grinding temperature and martensite depth a higher input of heat flux is needed compared with the cases of low table speeds (**Figure 5.27** and **Figure 5.28**). **Figure 5.29** demonstrates the variation of the martensite depth with the Peclet number *Pe* which is attributed to the variation of the maximum grinding temperature at the surface of the workpiece. The variation of residual stresses versus the heat flux intensity is also function of the Peclet number *Pe* as illustrated in **Figure 5.30** and **Figure 5.31**.

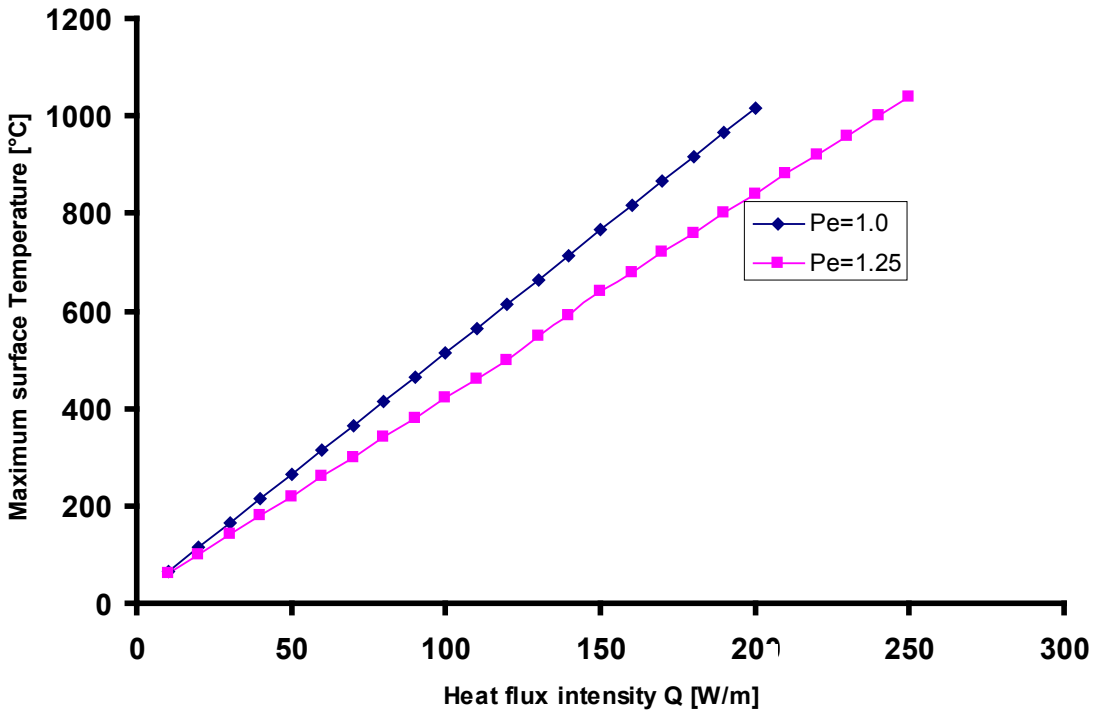

Figure 5.27 Effect of the Peclet number Pe on the maximum surface temperature function of the heat flux intensity Q

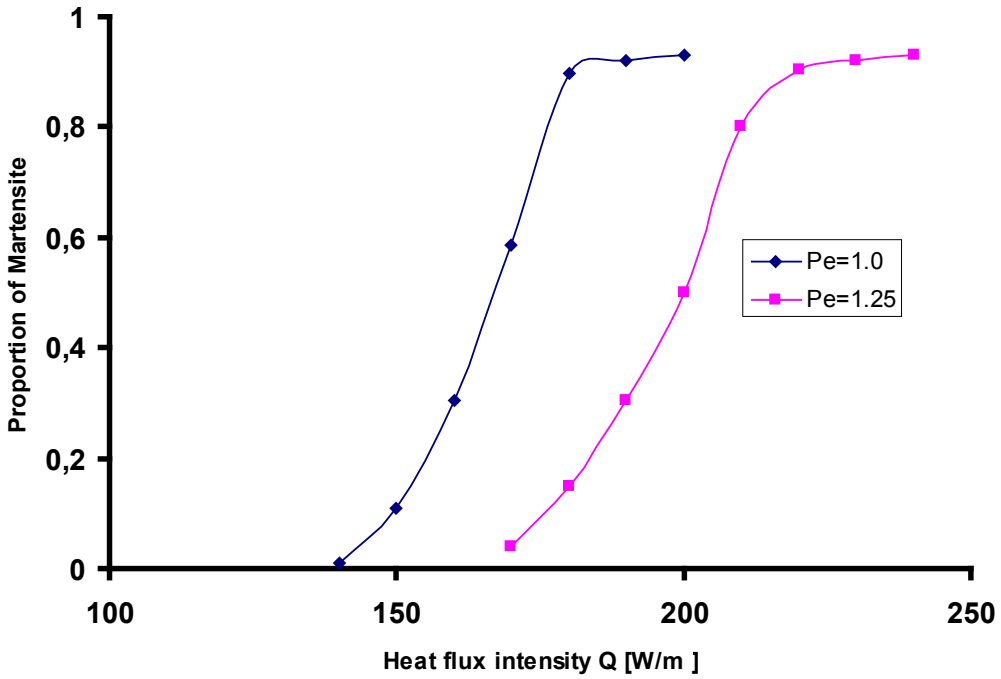

Figure 5.28 Effect of the Peclet number Pe on the proportion of martensite function of the heat flux intensity Q

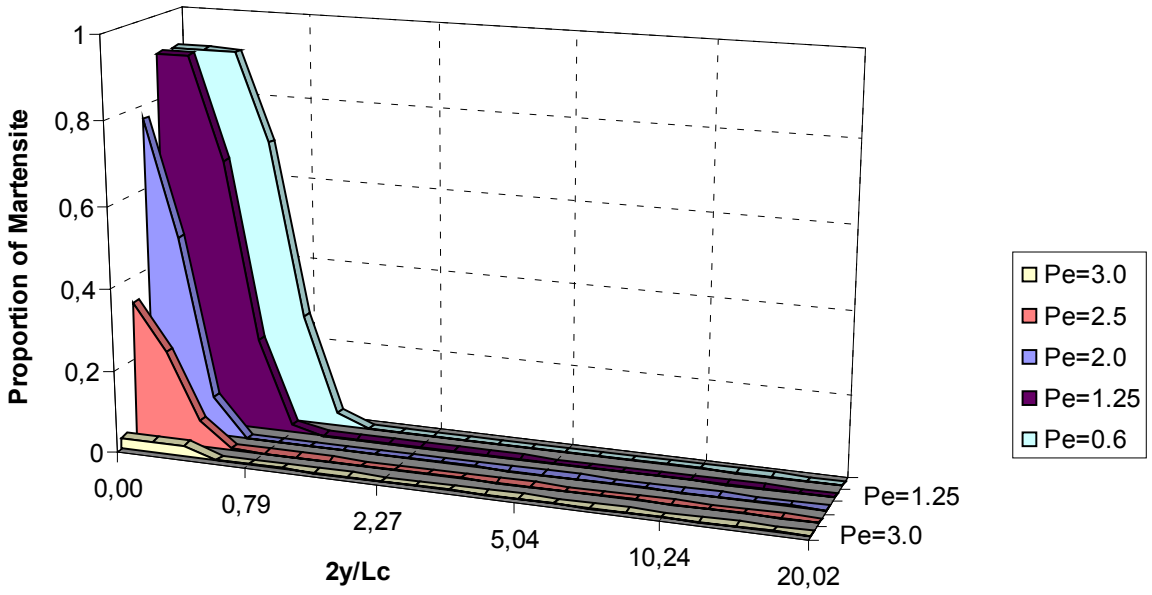

Figure 5.29 Variation of Martensite depth with the Peclet number Pe

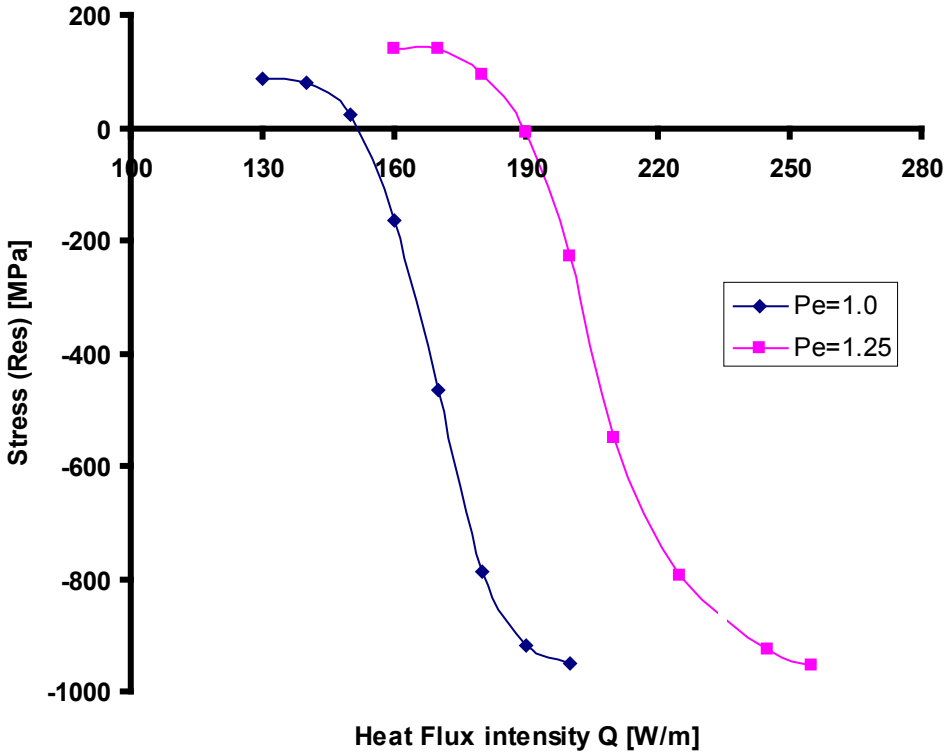

Figure 5.30 Effect of the Peclet number Pe on the longitudinal residual stress at the surface versus the heat flux intensity

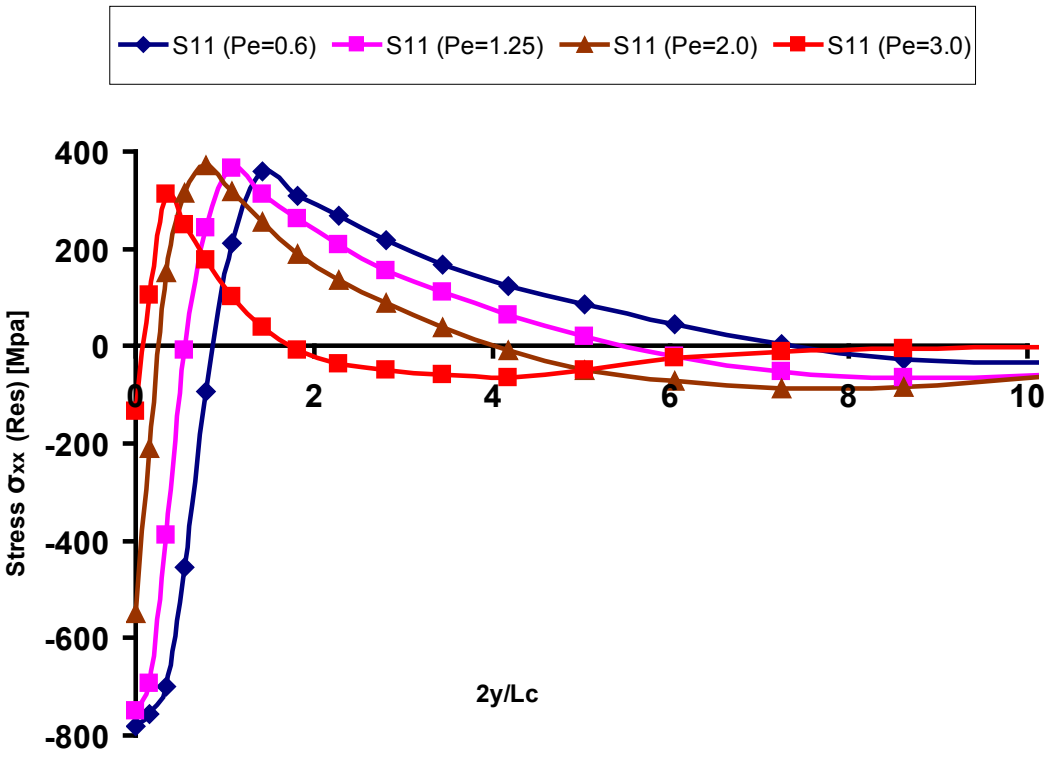

Figure 5.31 Effect of Peclet number Pe on distribution of the longitudinal residual stress with depth

5.3.4.3 Effect of the heat flux intensity

An investigation on the influence of the heat flux intensity on residual stresses is also carried out and the results are shown in **Figure 5.32** and **Figure 5.33**. In contrast to cooling role, an increase of heat generation within the grinding zone raises the grinding temperature thereby increasing the tendency of martensite formation. The depth of the hardened layer increases with the heat flux intensity as a higher grinding temperature is produced (**Figure 5.32**). Conversely, a lower heat flux results in a lower grinding temperature and therefore a thinner martensite depth. Thus with a lower heat flux, a lower residual stress will be generated, see **Figure 5.33**. As observed earlier, the magnitude of the longitudinal residual stress is directly related to the martensite depth.

It should be noted that after cooling it remains between 5 and 15% of austenite. The amount of retained austenite may affect the magnitude of compressive stresses formed. Note also that a higher austenite content in a thicker layer will be more detrimental in terms of dimensional changes to be expected if the workpiece is stored a long time before use.

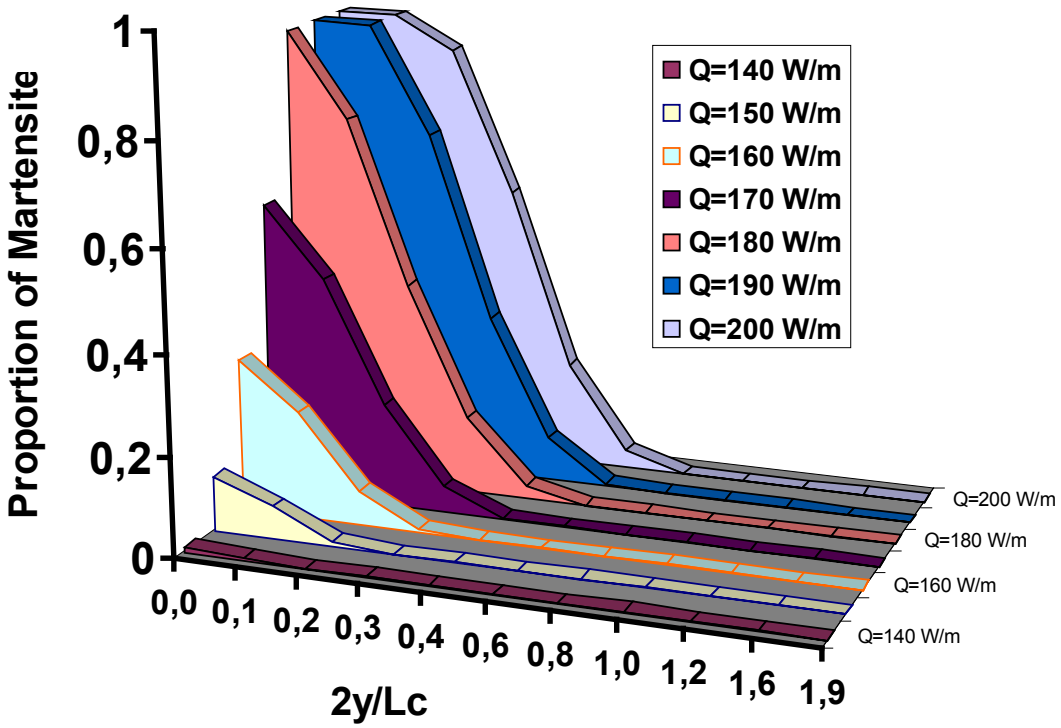

Figure 5.32 Proportion of Martensite versus depth for different heat flux intensities

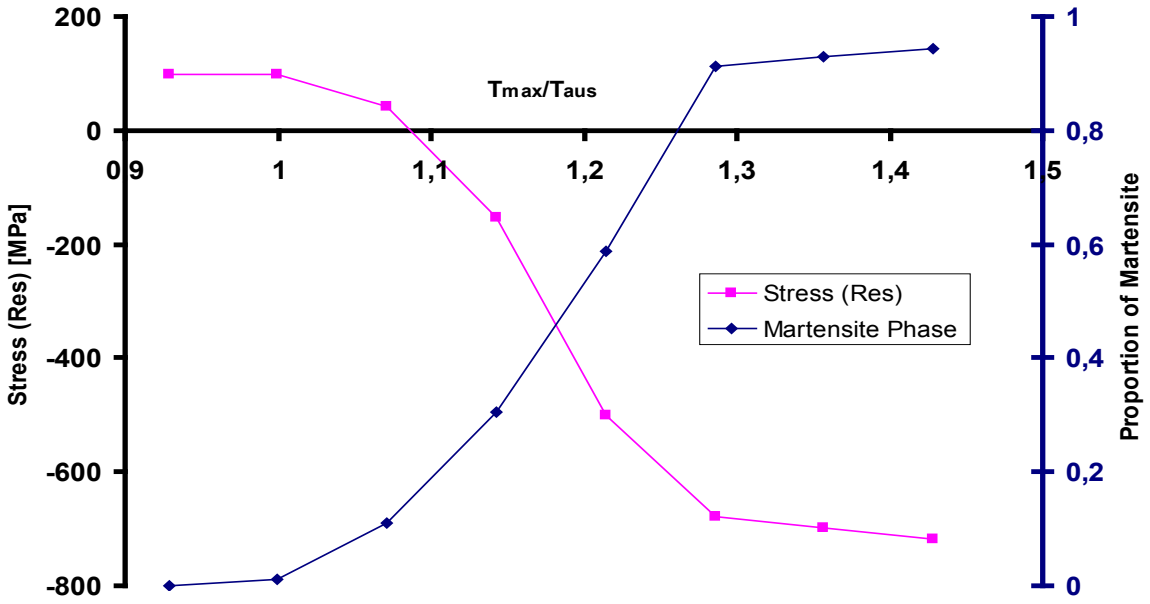

Figure 5.33 Variation of the longitudinal residual stress and proportion of martensite versus the maximum temperature reached by the surface

5.4 Mechanical Residual Stresses

5.4.1 Onset of Isothermal Mechanical Residual Stresses

During grinding, a thin layer of material is removed by mechanical abrasion and cutting. Although heating and possibly associated phase transformation may change the properties of the workpiece material, isothermal mechanical cutting and the induced residual stresses need to be understood before the mechanisms of residual stresses with a full coupling of all the causes can be explored.

To initiate plastic strain in a grinding process, the level of effective stress at a point should be beyond the initial yield stress of the workpiece. As the grinding stresses rely on the complex nature of the contact mechanisms between a grinding wheel and a workpiece, it is important to consider the effect of the grinding surface traction components and their related stresses. The equivalent normal load (here an equivalent normal distributed pressure P in N/m^2) and tangential traction (here an equivalent distributed surface traction P_α in N/m^2) are applied on the surface elements through user subroutines. Keeping in view the contact mechanism between the grinding wheel and the workpiece an elliptical profile for the applied mechanical loadings can be assumed. The ratio of the horizontal to vertical grinding forces, μ, known as the friction coefficient is another dominant factor leading to the onset of plastic strain. At a larger friction coefficient, much less grinding forces are needed to initiate plastic strains.

To reveal the stress field associated with traction distribution, the von Mises stress of the workpiece prior to yielding are examined in **Figure 5.34**(a, b and c). It shows that the maximum von Mises (effective stress) is found below the surface when μ <0.3 and at the surface itself when the μ is higher than 0.3.

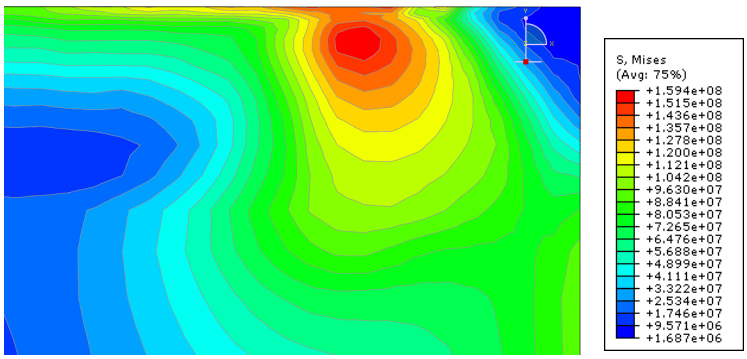

(a) Pe=1.0, μ=0.01

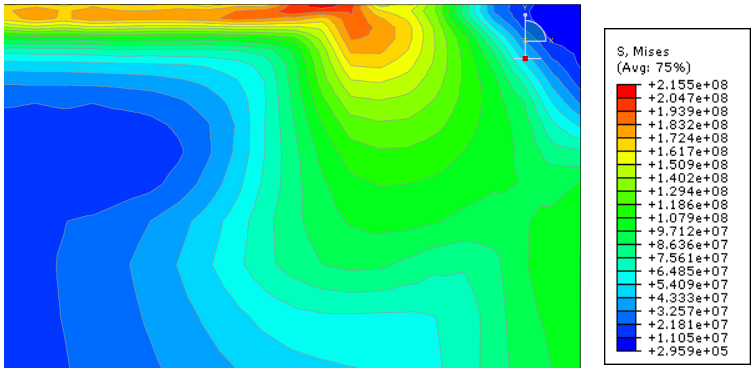

(b) Pe=1.0, μ=0.3

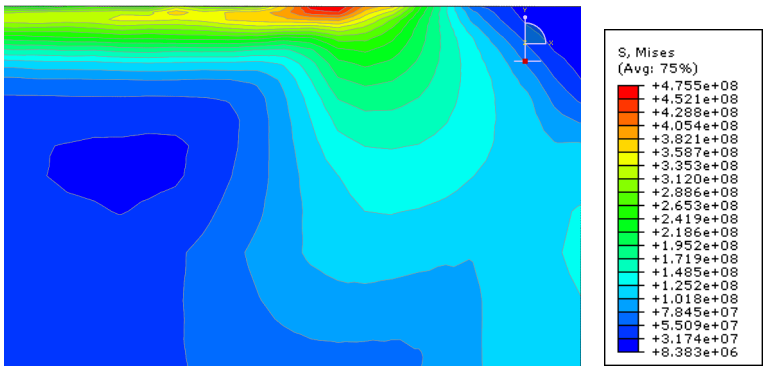

(c) Pe=1.0, μ=0.6

Figure 5.34 Distribution of the von Mises stress for various friction coefficients

5.4.2 Isothermal Grinding Residual Stresses

The first step towards understanding the mechanisms of isothermal mechanical residual stresses is to investigate the effects of both the normal and tangential loading components. The surface stress history of a grinding operation is shown in **Figure 5.35.** A compressive longitudinal stress σ_{xx} is found ahead of the distributed contact load, followed by a tensile state as the consequence of the tangential loading and localized plasticity. The effect of the μ on the longitudinal residual stresses σ_{xx} is shown in **Figure 5.36.** It can be observed that the magnitude and the depth of residual stresses increase with the friction coefficient.

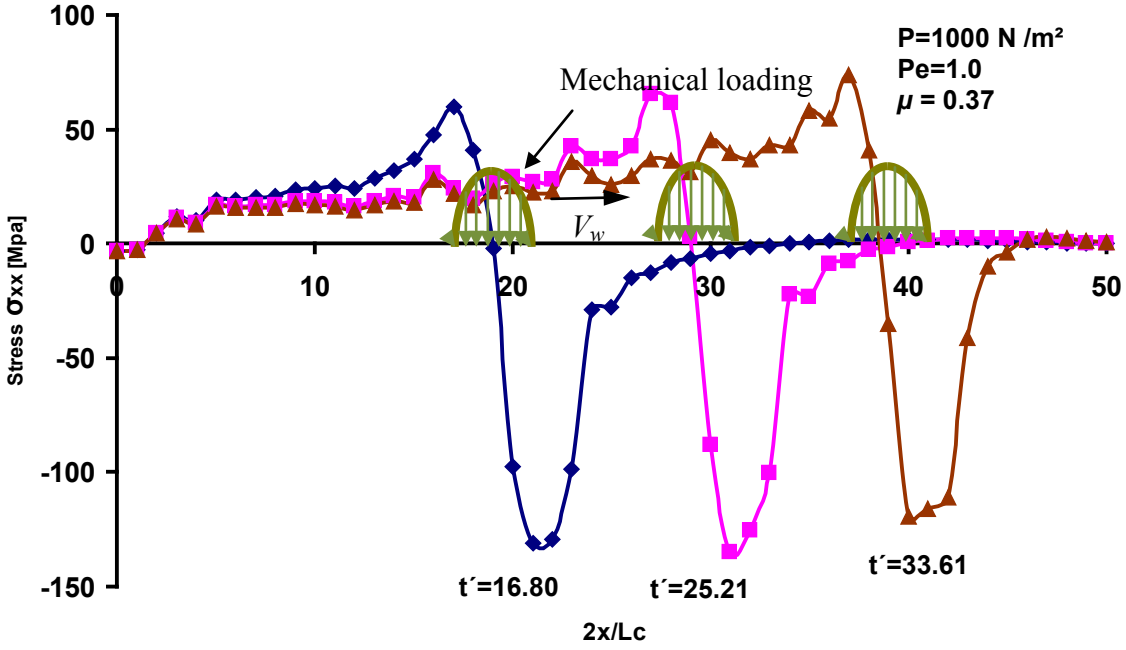

Figure 5.35 Longitudinal stress profile as the consequence of the mechanical loading

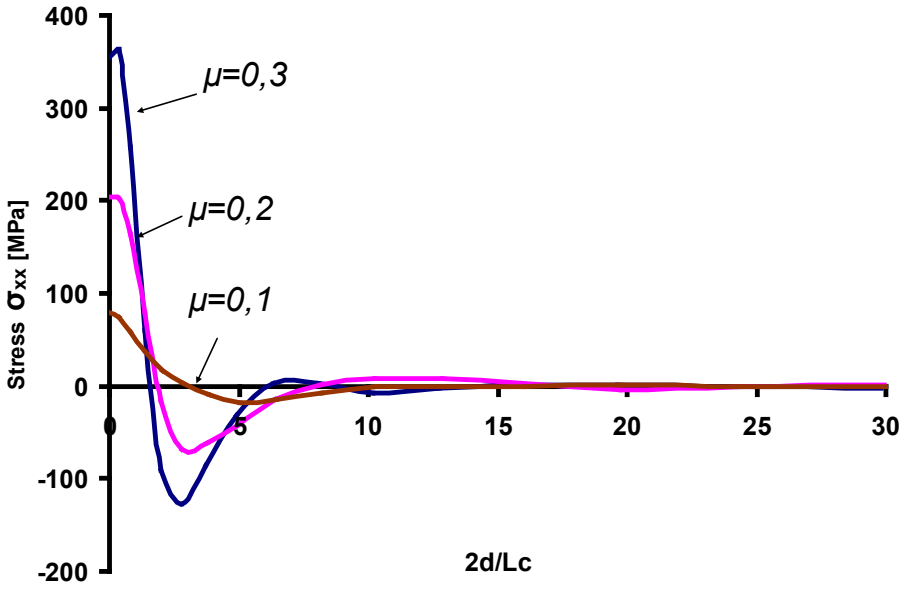

Figure 5.36 Effect of the friction coefficient on the residual stress profile along depth (Pe=1)

5.5 Coupling of Thermal and Mechanical Loadings

5.5.1 Critical thermal and mechanical grinding conditions

The term critical thermal and mechanical grinding conditions means that a combination of thermal and mechanical grinding conditions required to initiate plastic flow in the workpiece in the steady-state regime is reached. For an elastic material with constant thermal and mechanical properties the stress solution due to the mechanical load and the thermal load can be superimposed to yield thermo-mechanical effective stress [MOFID], but for an elastoplastic material with temperature dependent properties the stress solution with thermo-mechanical loading is not as simple. To understand the mechanism of irreversible strain for a combined thermal and mechanical loading, the stress field associated with a given set of grinding parameters needs to be explored. **Figure 5.37** presents the stress field associated with different grinding conditions. The effective stress (von Mises) distributions show sharp gradients at some points near the workpiece surface. It is clear that a local maximum effective stress can be developed at different locations relative to the surface loading position.

There exists a local maximum effective stress zone near **(Figure 5.37** (c)) or at **(Figure 5.37** (a) and (b)) the surface of the workpiece. The location of the plastic region – i.e. where the residual stress is the highest - is very sensitive to the combination of thermal and mechanical loadings. It moves from the surface to a deeper layer when the normal load increases **(Figure 5.37** (c)).

The critical thermo-mechanical grinding condition, defined as the set of parameters at the onset of yielding for the most loaded point, is presented in **Figure 5.38, Figure 5.39** and **Figure 5.40**. The effect of the input heat flux intensity, Q, the heat convection coefficient, H, the Peclet number, Pe, and the friction coefficient μ is investigated. It can be seen that plastic strains may be developed at a low heat flux intensity ($Q < 5$ MW/m^2) when the value of peak normal distributed pressure P (N/m²) is sufficiently high (i.e. when the ratio between the P and the yield stress of the material at 20°C $\sigma_{y(20°C)}$ is in the order of 1), see **Figure 5.38**. The convection heat transfer coefficient, H, has a reversed role in critical grinding conditions as a higher convection heat transfer coefficient requires higher levels of critical heat flux intensity and normal traction pressure (see **Figure 5.40**) to meet the same grinding temperature as above. The heat source velocity has a similar role to that of the convection heat transfer coefficient since a higher velocity results in a lower grinding temperature if the heat flux intensity is kept the same, see **Figure 5.39**.

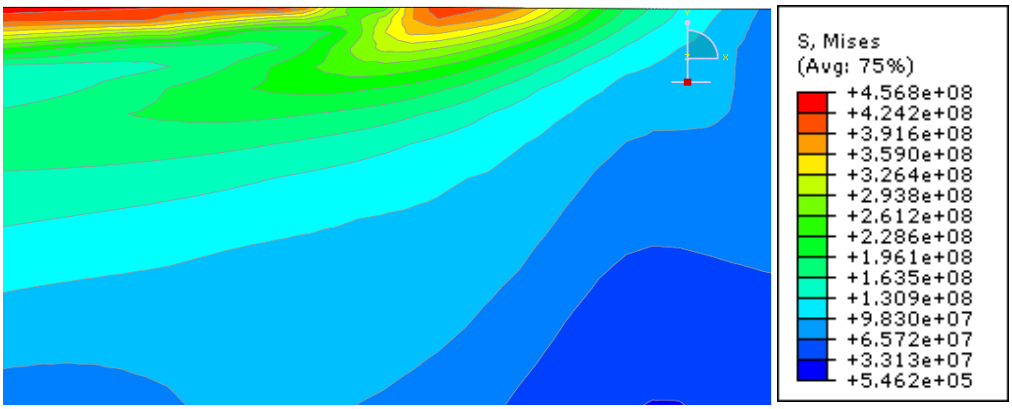

(a) Pe=1.0 P/ $\sigma_{y\,(20°C)}$=0.0, Q=100 W/m, μ=0.0

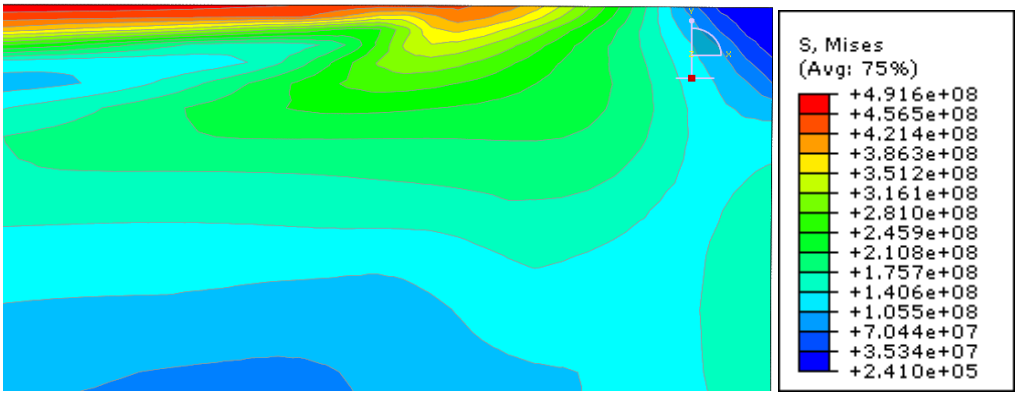

(b) Pe=1.0 P/ $\sigma_{y\,(20°C)}$=0.95, Q=100 W/m, μ=0.1

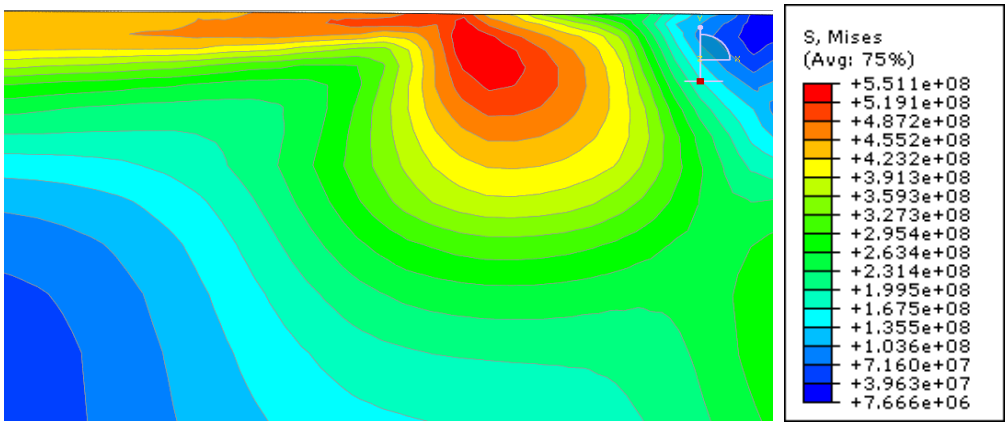

(c) Pe=1.0 P/ $\sigma_{y\,(20°C)}$=2.5, Q=15 W/m, μ=0.1

Figure 5.37 Onset of thermo-mechanical stresses (von Mises stress) for different grinding conditions. $\sigma_{y\,(20°C)}$ is the yield stress of the material at 20°C

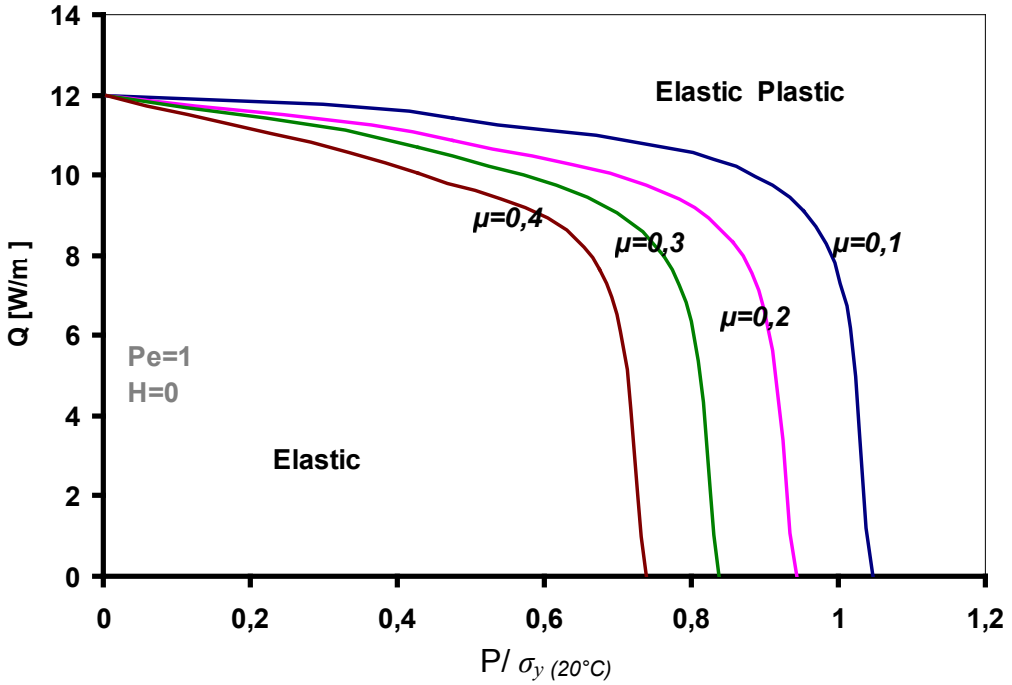

Figure 5.38 Critical grinding conditions to initiate plastic strains for different friction coefficients. $\sigma_{y\,(20°C)}$ is the yield stress of the material at 20°C

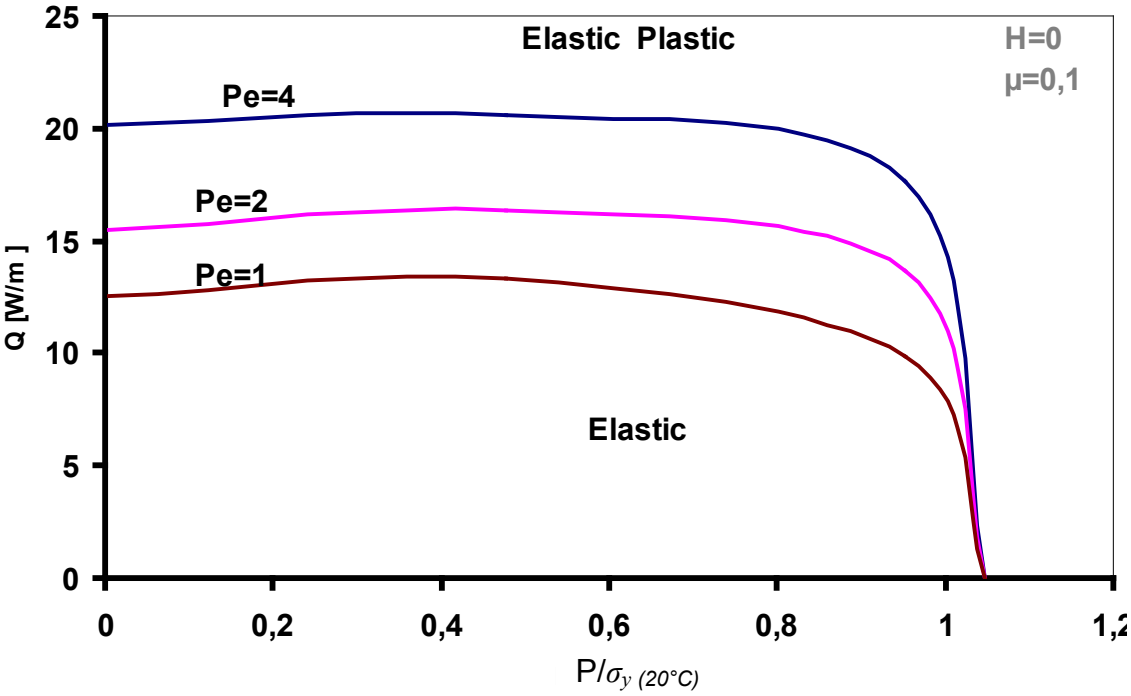

Figure 5.39 Critical grinding conditions for different Peclet numbers.

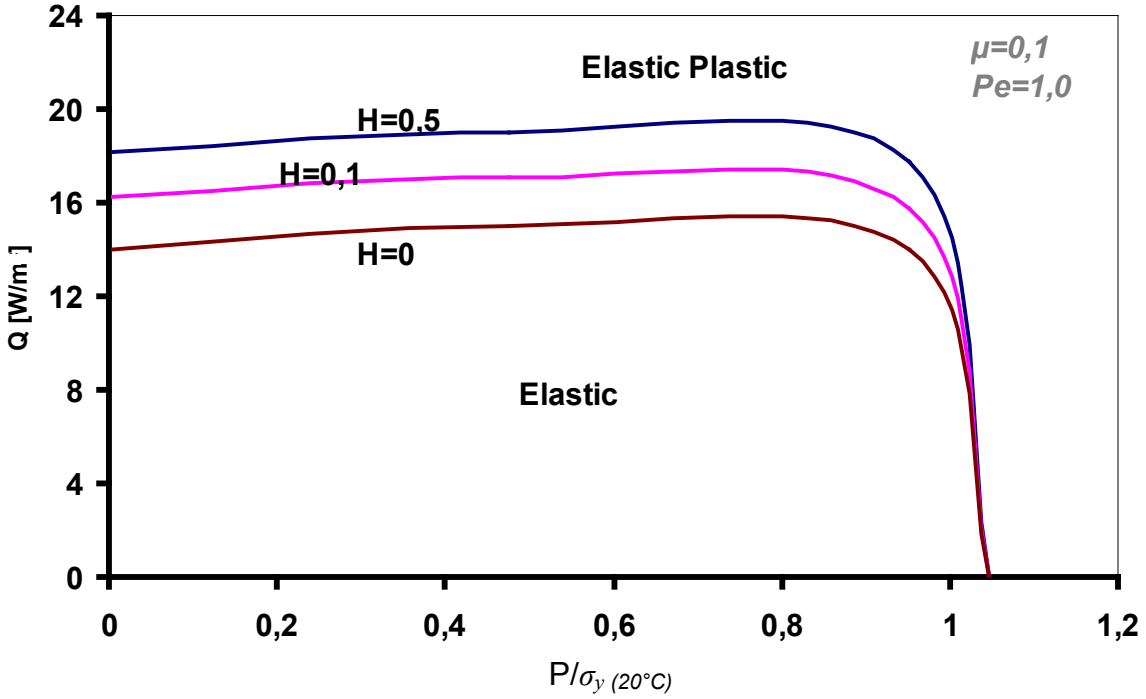

Figure 5.40 Critical grinding conditions for different heat convection factors

5.5.2 Grinding Stress History

During the grinding process the workpiece is subjected to moving thermal and mechanical loads with their magnitudes relying on the grinding conditions. This will result in irregular thermal and mechanical deformations of the ground surface layer which in turn lead to a complex stress field history. Therefore, it is important to trace the grinding stress history in terms of loading conditions and workpiece properties.

5.5.3 Grinding Surface Strain History

Figure 5.41, **Figure 5.42** and **Figure 5.43** presents the longitudinal strain, ε_{xx}, at the surface of the workpiece and at three different time steps for a purely thermal loading, a mechanical loading only, and a coupled thermal-mechanical loading, respectively. First it can be observed that the strain distribution approaches the steady-state regime shortly after the load movement has started. Under thermal loading conditions of grinding, the ground surface exhibits compressive strains in front of the thermal load followed by a rapid increase up to tensile strains (**Figure 5.41**). The thermal strain history indicates that as the grinding zone is heated it tries to expand but is restricted by the surrounding material (colder ahead), which is experiencing a lower temperature rise, so that a compressive stress forms. The iso-thermal

mechanical loading conditions, on the other hand, result in a local compressive strain with a sharp gradient away from the grinding zone. This is obvious as surface traction presses the ground surface of the grinding zone. A stretched surface is developed behind the (mechanical) load in a manner similar to the results under purely thermal loading (see **Figure 5.42**). **Figure 5.43** presents the effect of the combined thermo-mechanical loading. The combination of thermal and mechanical loading shows a somewhat intermediate state of strain with similar trends to that of thermal grinding conditions but with more compressive strains (see also a comparison of the steady-state solutions in **Figure 5.44)**.

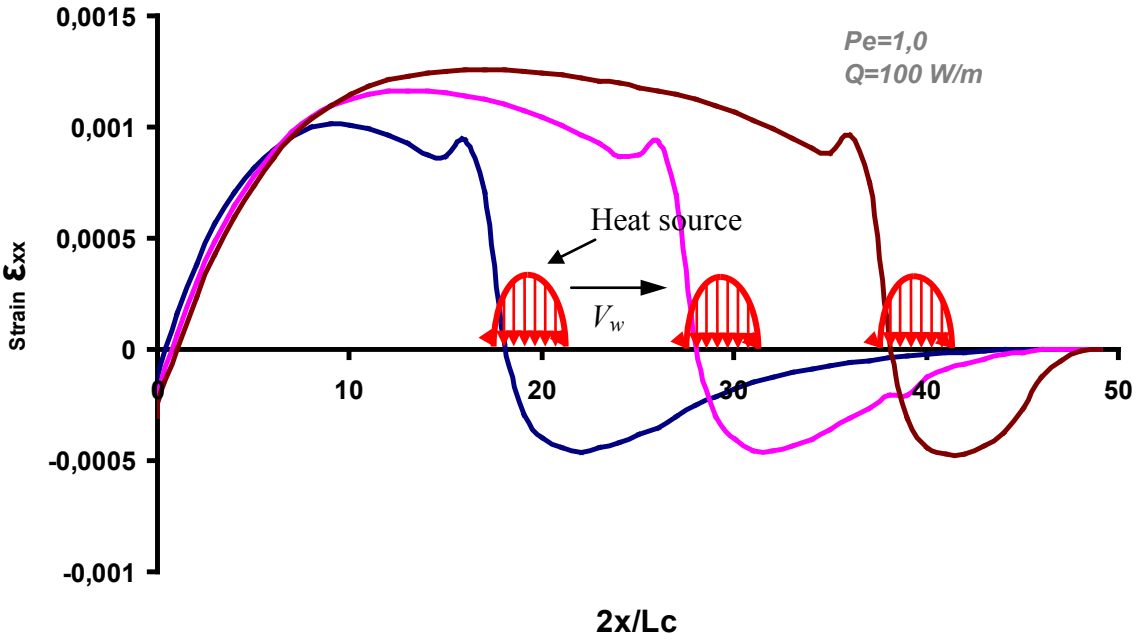

Figure 5.41 Distribution of the longitudinal strain due to the thermal loading only

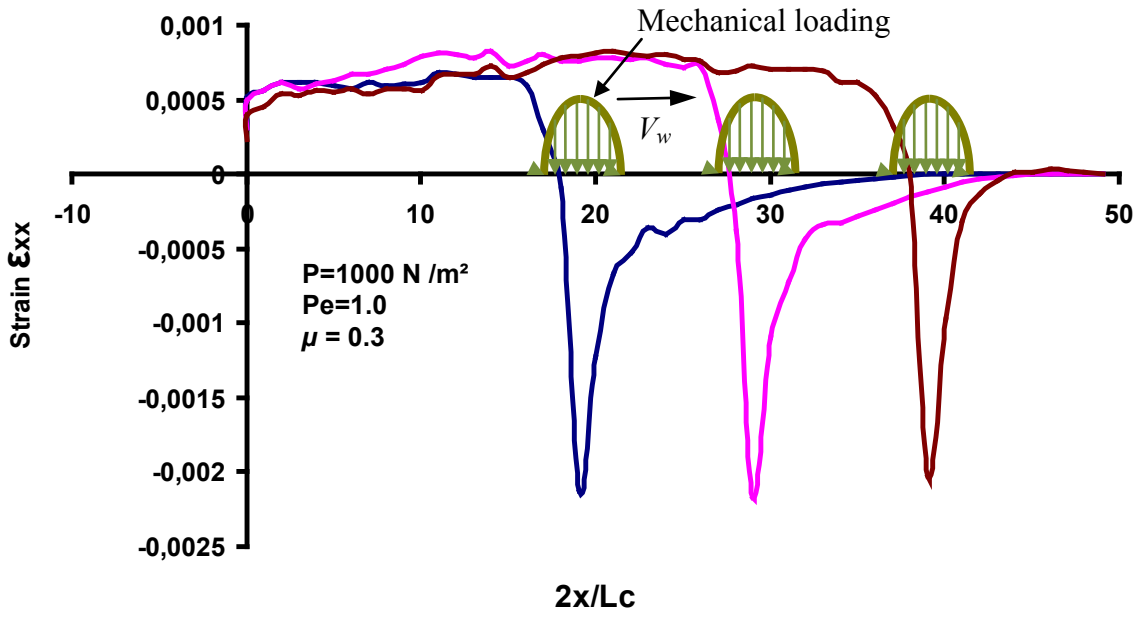

Figure 5.42 Distribution of the longitudinal strain due to the mechanical loading only (normal + tangential)

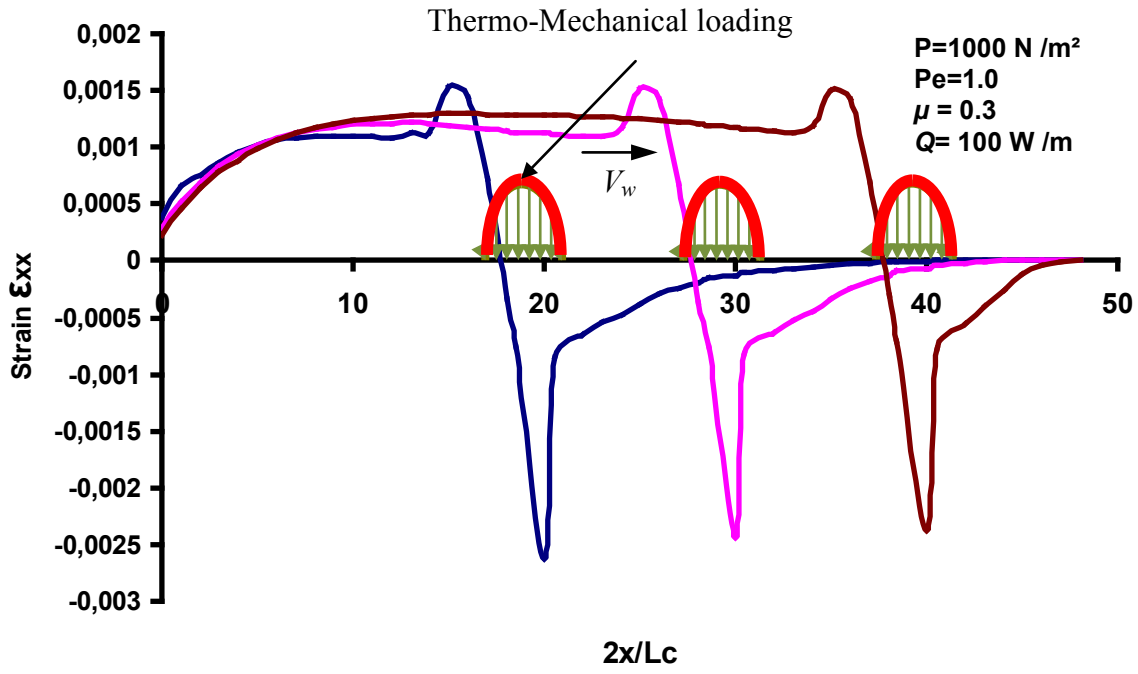

Figure 5.43 Distribution of the longitudinal strain due to the thermo-mechanical loading

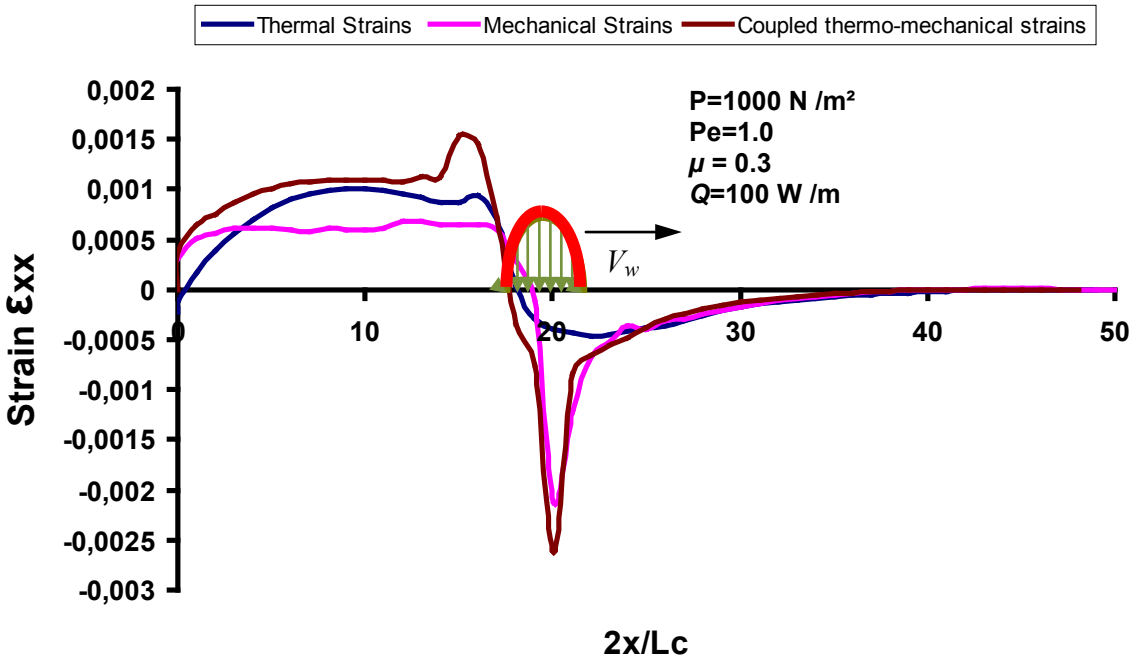

Figure 5.44 Comparison of the longitudinal strain (total strain) due to different loading conditions

5.5.4 Grinding Surface Stress History

Figure 5.45 and **Figure 5.46** show the history of the longitudinal stress for a purely thermal loading and a purely mechanical loading, respectively. For the two types of loadings the stress σ_{xx}, is characterized by an initial growing compressive stress followed by a progressing tensile stress. The remaining stress is of tensile nature. Given the thermal condition being constant (e.g. Q=100 W/m), for low values of ratio of peak normal pressure P to yield stress at 20°C $y_{(20°C)}$, i.e. $P/y_{(20°C)}$=0.45 here, the mechanical load has a little effect on the evolution of stress compared when the coupled thermo-mechanical loading is applied (see **Figure 5.47 for comparison**). For higher mechanical loading, i.e. $P/y_{(20°C)}$=1.5 in **Figure 5.48,** the contribution of normal and tangential tractions is no more negligeable. All these indicate that residual grinding stresses and strains are sensitive to both thermal and mechanical loadings.

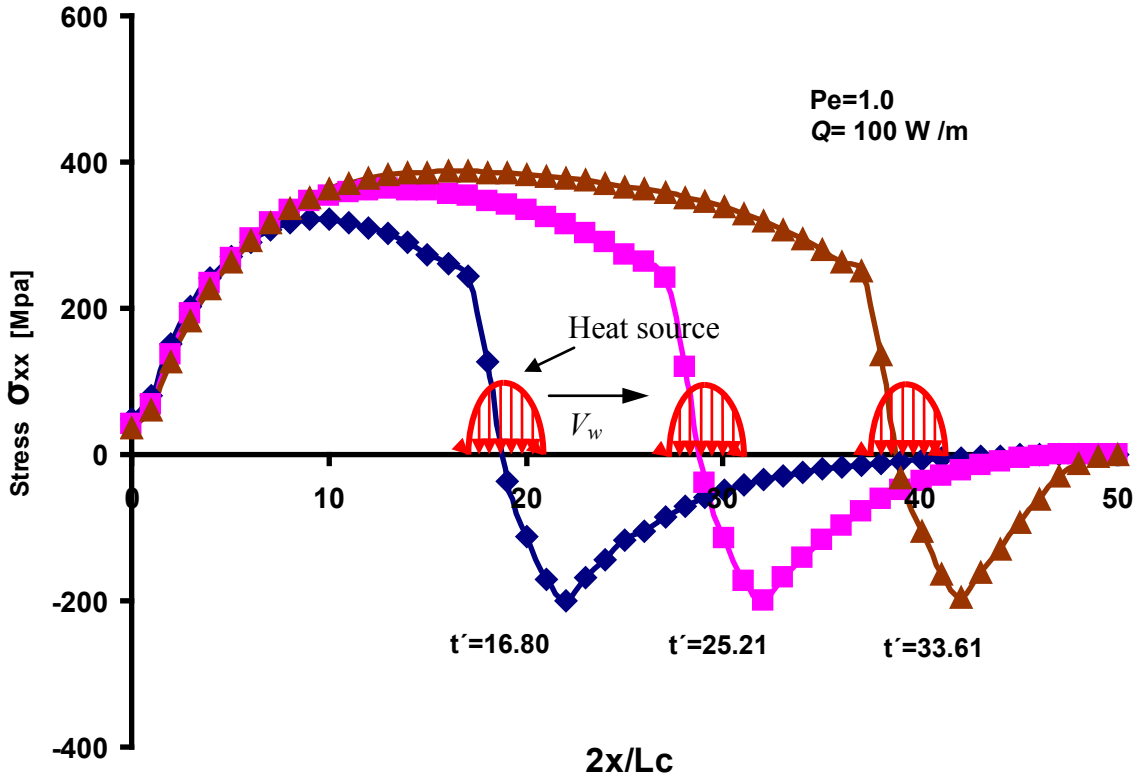

Figure 5.45 Evolution of the longitudinal stress due to thermal loading only

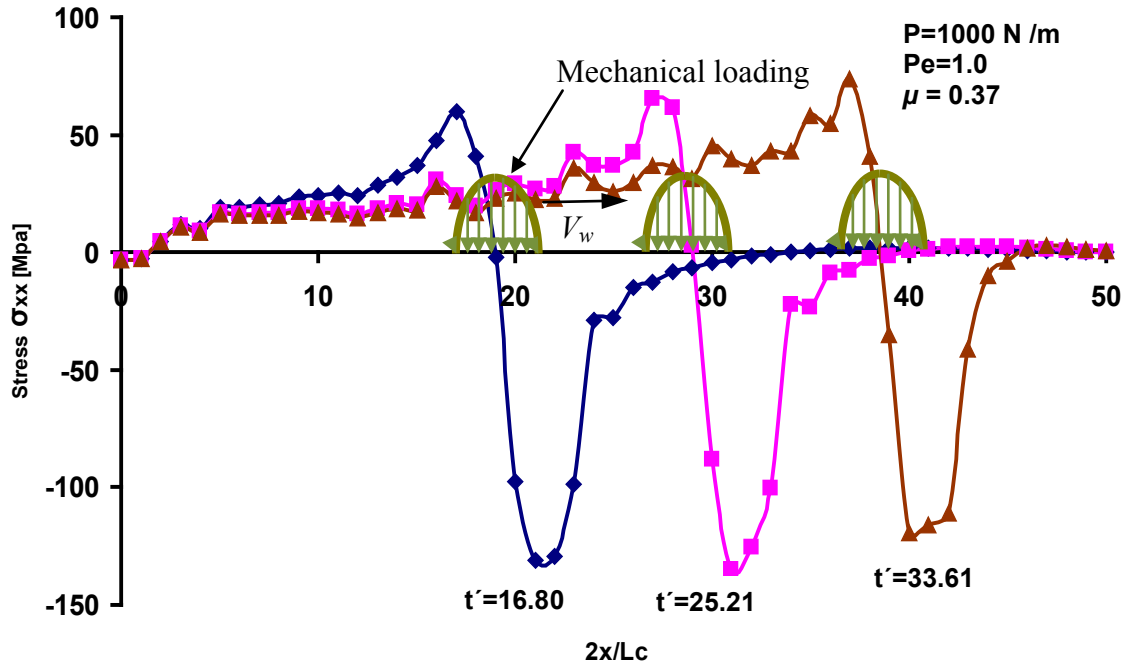

Figure 5.46 Evolution of the longitudinal stress due to purely mechanical loading

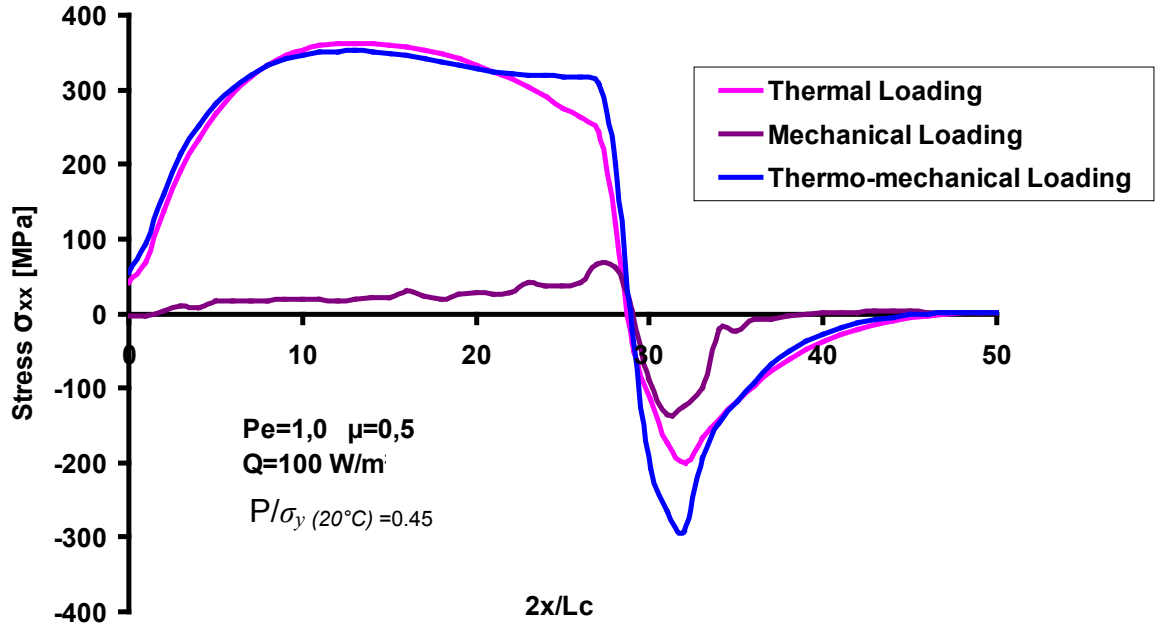

Figure 5.47 Comparison of the longitudinal stress due to different loading conditions (Pe=1, μ=0.5, Q=100W/m, P/$\sigma_{y(20°C)}$=0.45)

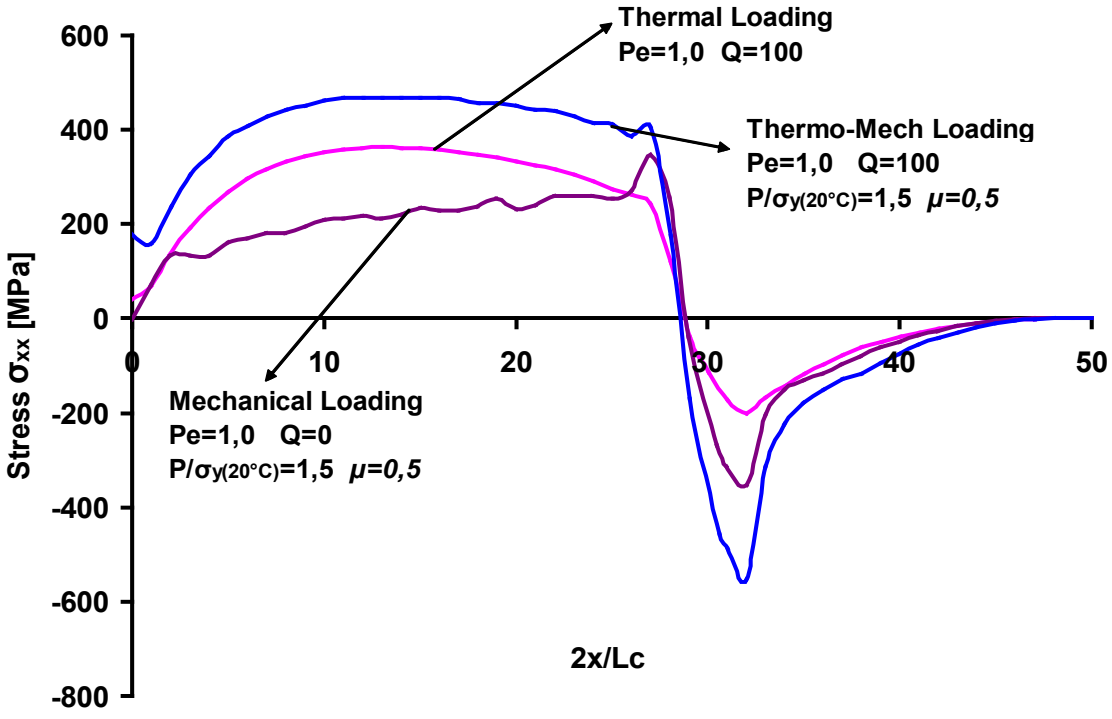

Figure 5.48 Comparison of the longitudinal stress due to different loading conditions (Pe=1, μ=0.5, Q=100W/m, P/$\sigma_{y\,(20°C)}$=1.5)

5.5.5 Thermo-Mechanical Residual Stresses without phase transformation

The magnitude of the surface longitudinal residual stresses, σ_{xx}, is directly related to the grinding conditions. The coupling of mechanical traction with low heat input has very remarkable effect on the residual stress as shown in **Figure 5.49**. However the coupling of mechanical traction with a high input of heat flux has comparatively less effect because the increase of the heat flux intensity elevates the grinding temperature and in turn enlarges the thermal strains and stresses. In the thermo-mechanical analysis, the lower values of normal surface traction (i.e. $\frac{P}{\sigma_{y(20°c)}} < 1$) have almost no effect on the residual stresses when the friction coefficient is small (e.g., μ = 0.1 or less). This is because at lower tractions the thermal stresses become dominant when $\frac{P}{\sigma_{y(20°c)}} < 1$. For a low to moderate heat flux intensity (Q=30W/m) and a moderate friction coefficient (e.g., μ=0.3), an increase of the normal surface traction would lead to an undesirable residual stress distribution with high tensile stress at the surface (see **Figure 5.50**). This is because the surface workpiece in the grinding zone experiences a greater initial surface stretching and thus a larger tensile stress σ_{xx} during grinding. At high heat flux values, similar effect to that of pure thermal loading conditions is produced due the evolution of greater surface residual stresses. It is apparent according to **Figure 5.50** that an increase of the normal loading increases the longitudinal residual stress, σ_{xx} at the surface if the heat flux intensity and the heat source velocity are kept constant.

For a deeper understanding of the above mechanism, the longitudinal residual stresses is plotted along depth in **Figure 5.51** to show the contribution of thermal and mechanical loadings. It can be observed that, in absence of phase transformation, the coupling of thermal and mechanical effects results in higher longitudinal residual stresses at the surface than when each effect is taken individually.

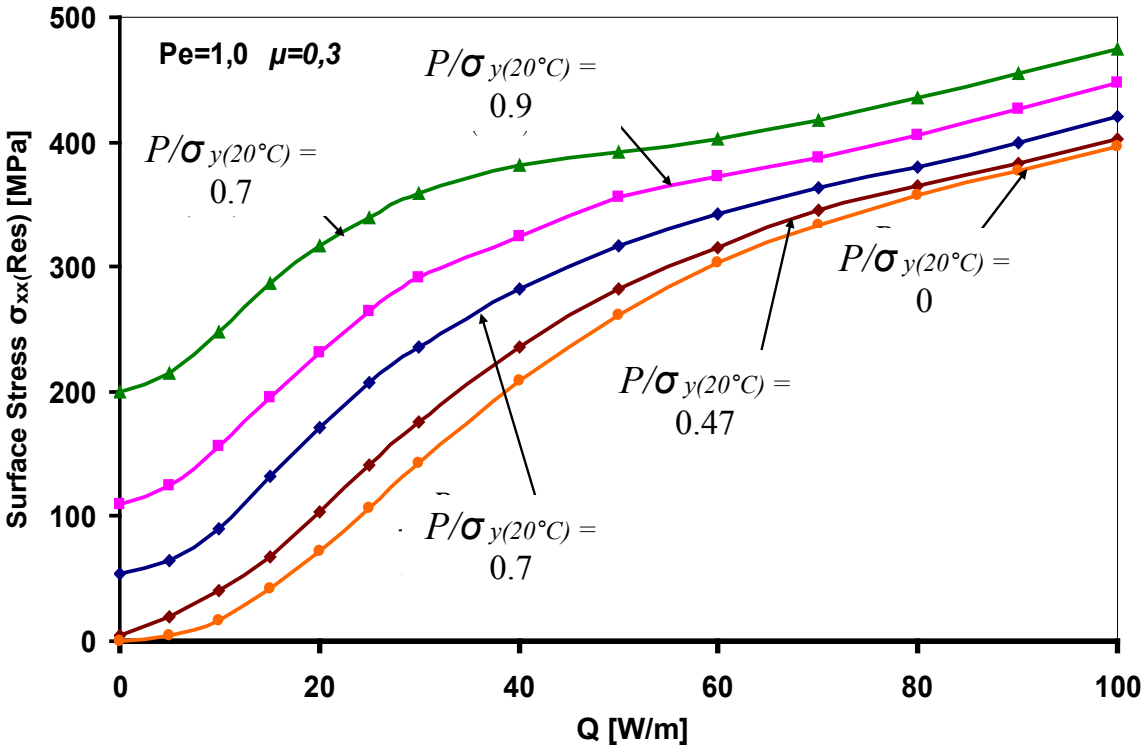

Figure 5.49 Coupled thermal and mechanical effects on the longitudinal residual stresses at the surface

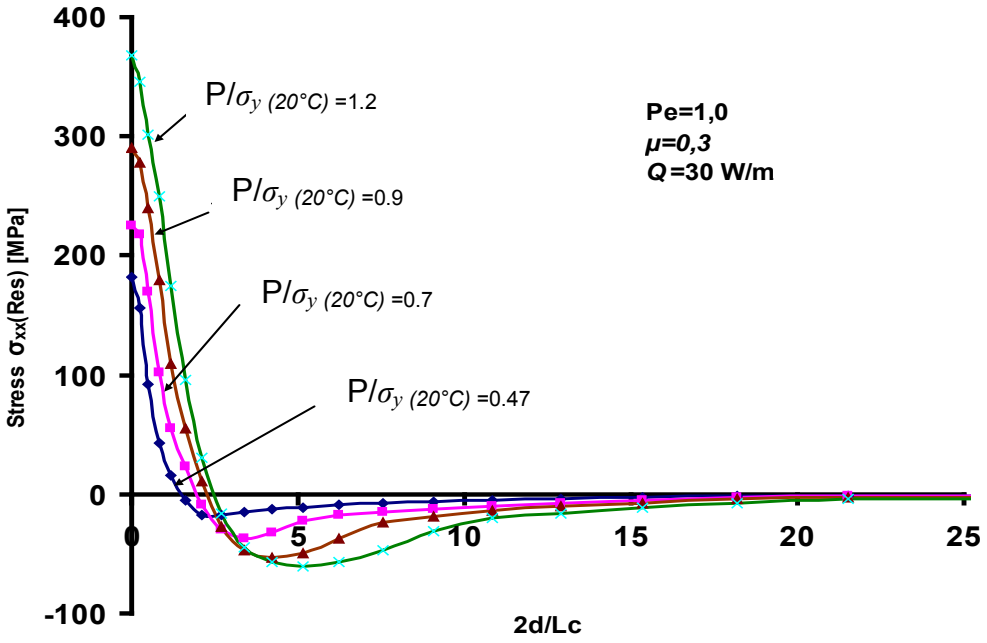

Figure 5.50 Distribution of the longitudinal residual stress versus depth for various normal loadings

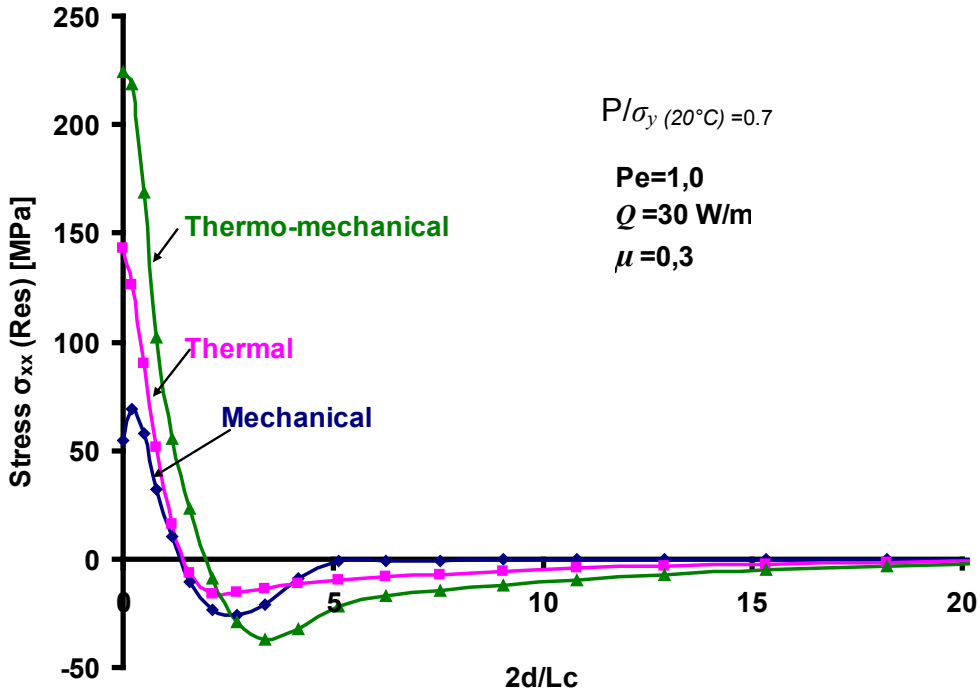

Figure 5.51 Effects of the purely thermal, purely mechanical and thermo-mechanical loadings on the distribution of the longitudinal residual stress versus depth

5.5.6 Thermo-Mechanical Residual Stresses with Phase Change

When a workpiece experiences a critical temperature variation in grinding due to temperature rise, austenite phase transformation occurs in the vicinity of the grinding zone and the martensite phase change occurs up to a certain distance away from the grinding zone depending on the cooling process applied; as demonstrated by **Figure 5.52** (a) and (b)

The coupling of mechanical loading with thermal loading – when no phase transformation occurs – has a minor influence on the distribution of residual stresses for low to moderate surface traction as described above (mostly when $\frac{P}{\sigma_{y(20°c)}} < 1$) and low values of the friction coefficient (e.g., $\mu = 0.1$ or less). However, associated with high mechanical traction, thermal strains become considerably higher and strains due to phase transformation also contribute remarkably to the deformation of the workpiece. Thus compared with thermal effects and phase transformations, the effect of mechanical traction becomes less important. In the case of martensitic phase transformation, the strain mismatch at the austenizing grinding temperature plays a central role in the formation of compressive residual stresses. The evolution of longitudinal residual stresses at the surface of the workpiece when increasing the maximum temperature reached by the surface (i.e. by increasing the heat flux) are plotted in **Figure 5.53**

with and without mechanical loading. It explains that beneficial compressive residual stresses are mostly produced by phase transformation. At low heat flux intensities i.e. when the maximum surface temperature remains small (**Figure 5.53** zone 1), one may observed a significant effect of the mechanical loading (when coupled with the thermal loading) compared to the purely thermal loading, whereas the mechanical loading has a negligible effect at moderate heat flux intensities (**Figure 5.53** zone 2). As soon as the workpiece experiences the critical temperature (T ≥ Ac1), a volume increase due to the martensitic phase transformation occurs within a surface layer which in turn forces the ground surface to expand and thus a compressive surface stress develops (**Figure 5.53** zone 3). At the same time the results indicate that higher surface traction can decrease the residual stress level up to a state where no residual stresses can be achieved (it corresponds to a specific set of grinding conditions, for example $\frac{T_{\max}}{T_{aus}} = 1.07$, $\frac{P}{\sigma_{y(20°C)}} = 0.47$, μ=0.3, Pe=1), see **Figure 5.53** and **Figure 5.54**. This is because the increase of the contact loading may slightly decrease the longitudinal surface residual stress σ_{xx}.

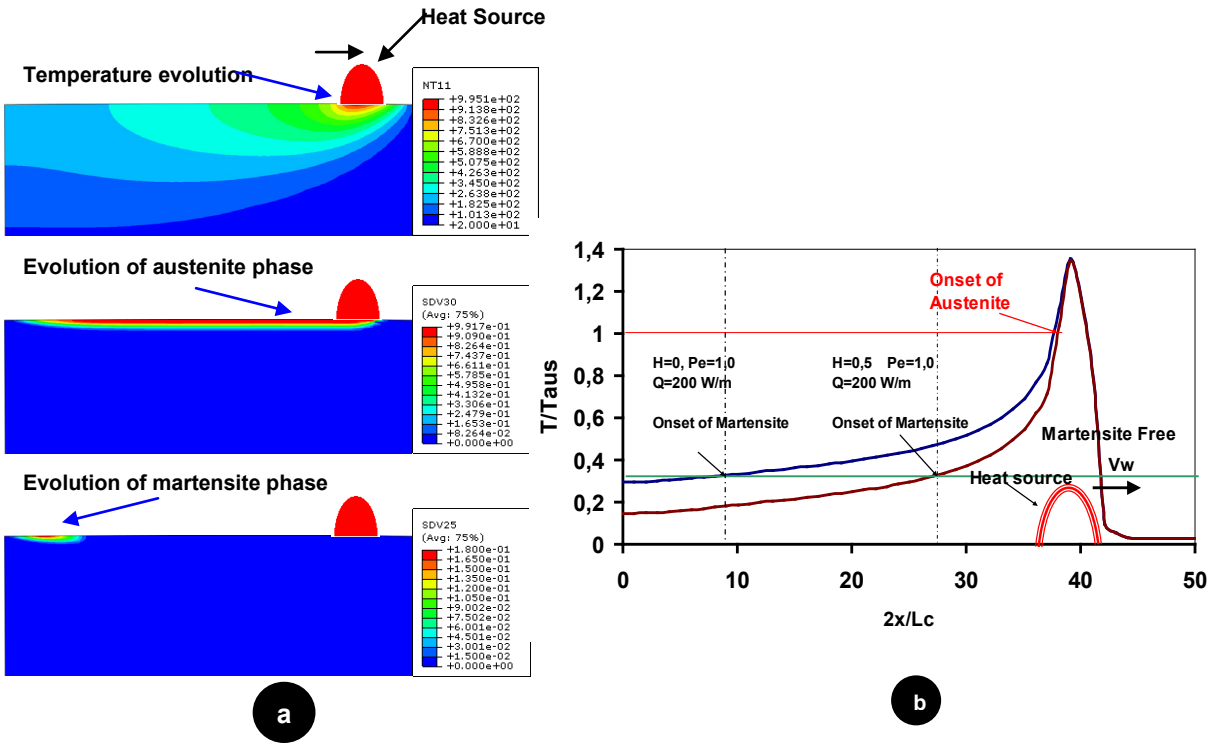

Figure 5.52 (a)Distributions of temperature (top left), austenite (left middle) and martensite (left bottom)
(b) Effect of cooling on onset of martensitic phase

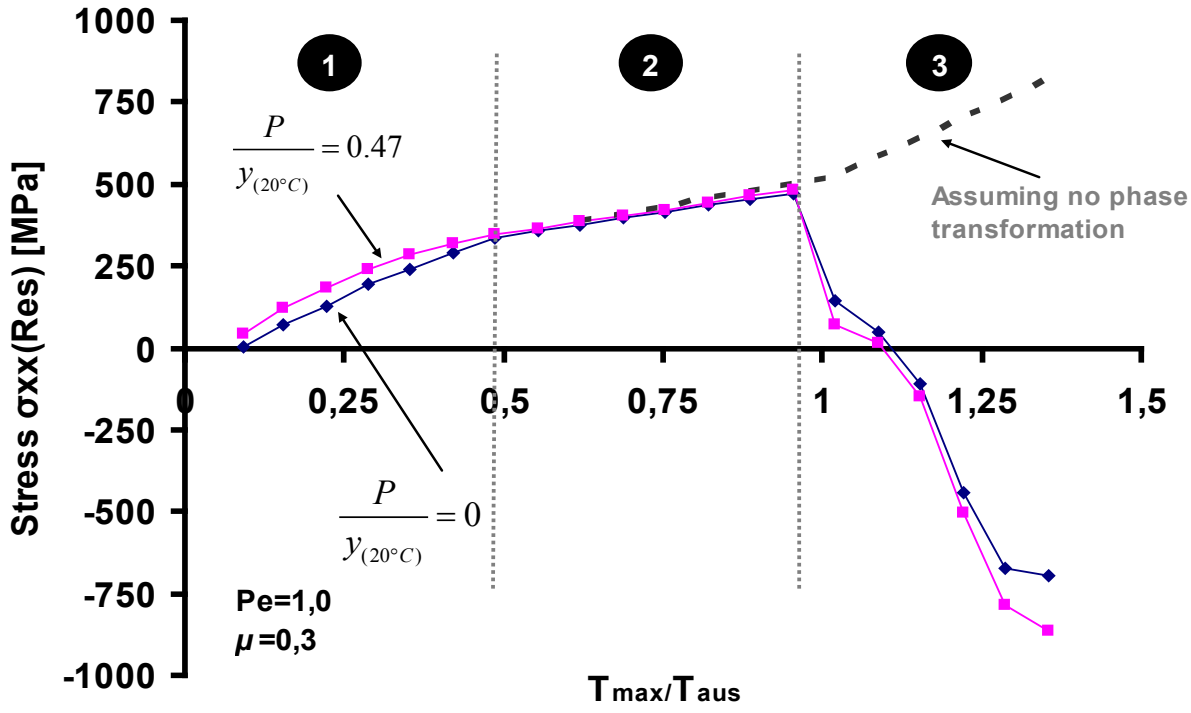

Figure 5.53 Effect of an increasing heat flux (i.e. increasing surface temperature) on the occurrence of phase transformation and longitudinal residual stresses with ($P/_{(20°C)}$ =0.47) and without ($P/\sigma_{y(20°C)}$=0) mechanical loading

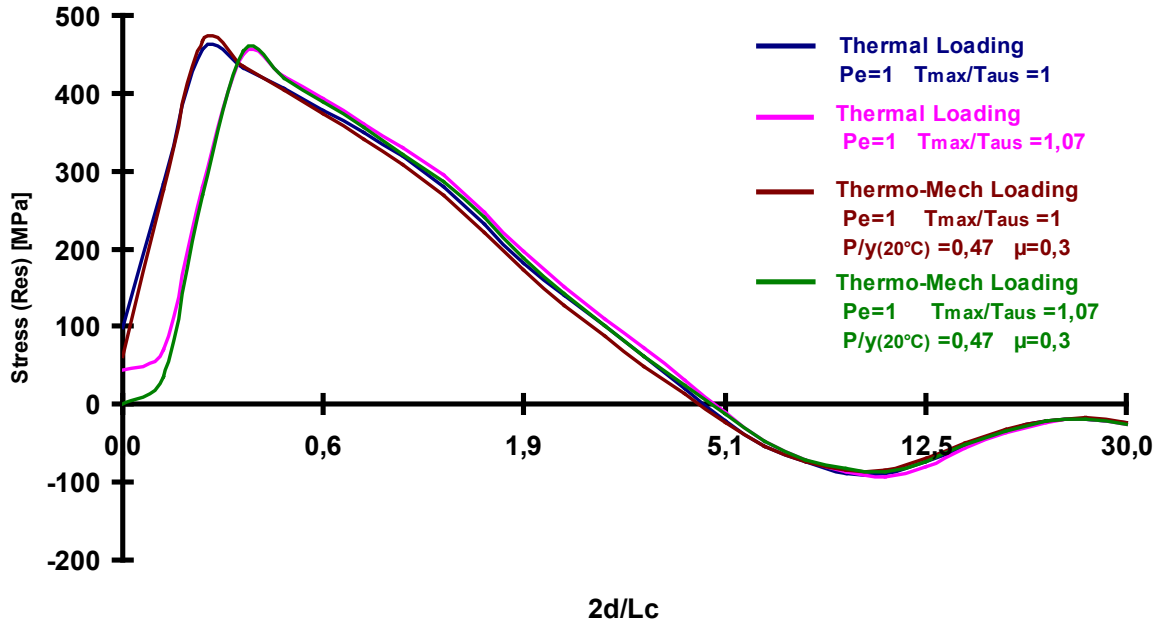

Figure 5.54 Effect of the loading conditions on the residual stress

The residual stresses produced by the martensitic phase transformation are proportional to the percentage of martensite phase transformed. Furthermore, the depth of the zone with large residual stresses is directly related to the thickness of the hardened martensite layer that is characterized by a higher yield stress (**Figure 5.55** and **Figure 5.56**).

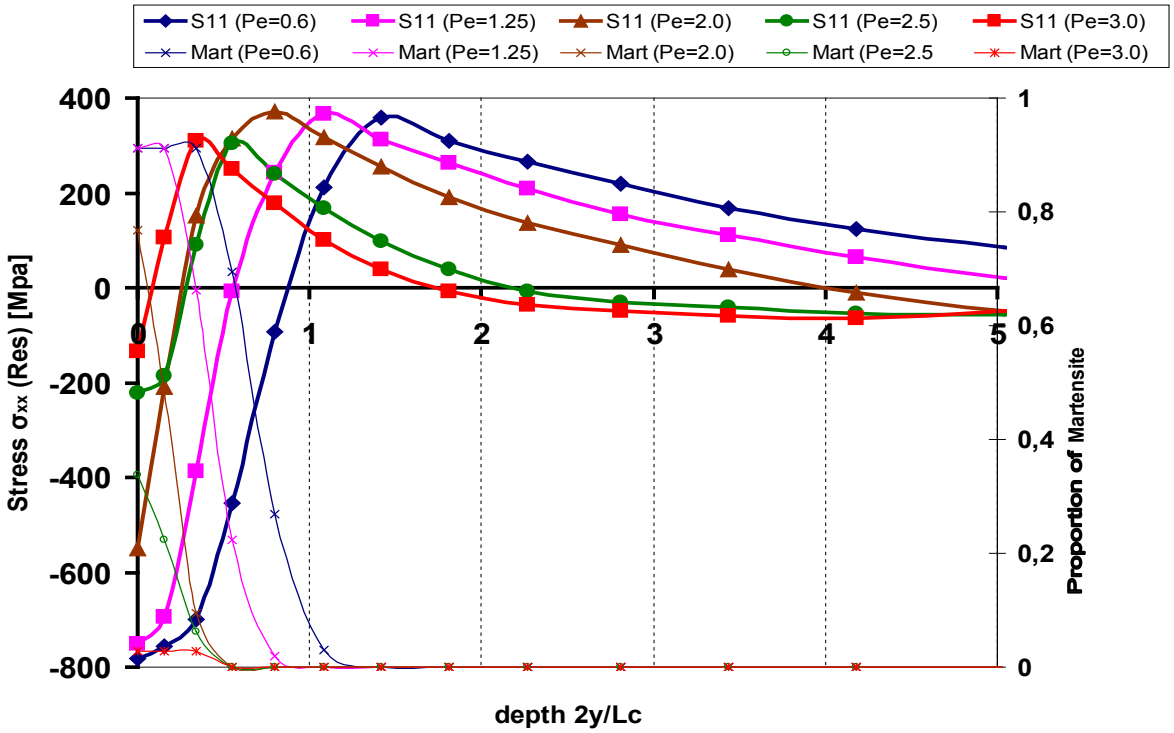

Figure 5.55 Proportion of martensite and longitudinal stress versus depth for various Peclet numbers

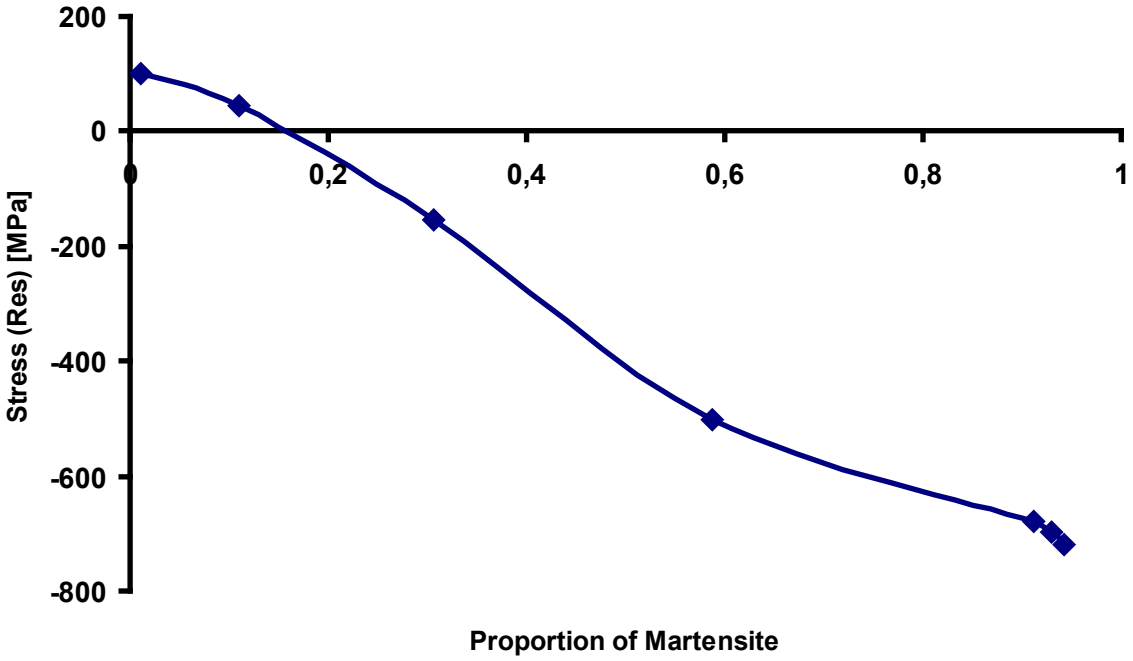

Figure 5.56 Relationship between the proportion of martensite and the longitudinal residual stresses

The effect of grinding conditions on the nature of residual stresses can be understood more deeply by comparing the influence of the causes individually and with different combinations. **Figure 5.57** shows the role of each mechanism for different grinding conditions on the longitudinal residual stress, σ_{xx}. Under purely mechanical loading (**Figure 5.57**), a very small, almost negligible, residual stress is developed. A purely thermal loading without surface hardening (no phase transformation) leads to tensile residual stresses, which decreases gently with depth. When phase transformation takes place, however, a surface layer with a greater compressive residual stress is generated.

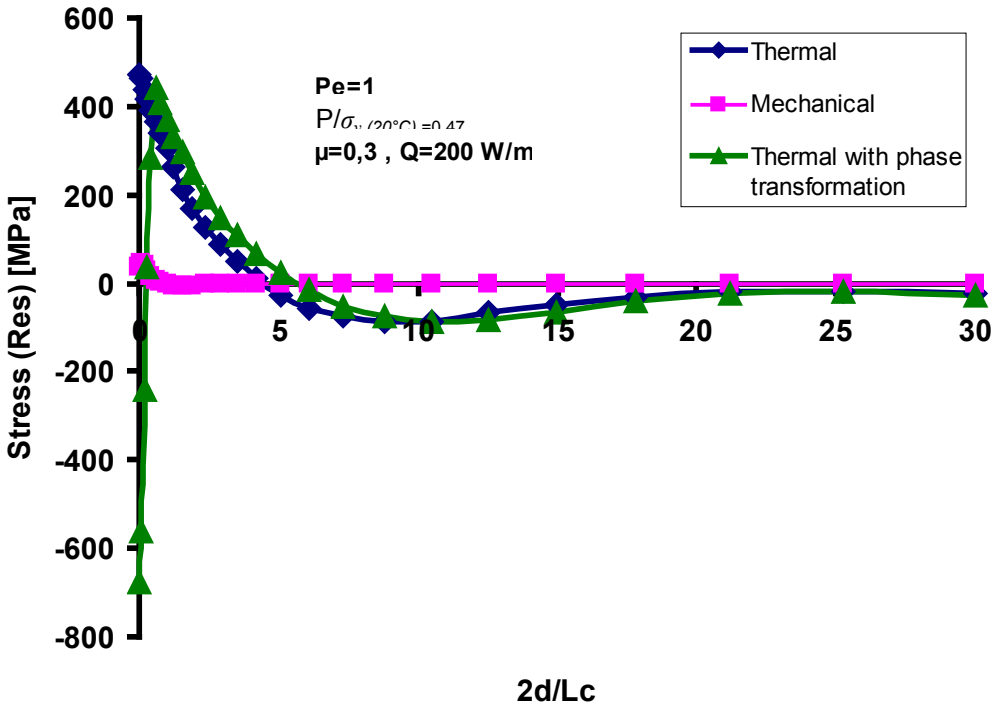

Figure 5.57 Effect of the loading conditions on the longitudinal residual stress along depth

CHAPTER 6

CONCLUSION AND PROSPECTIVES

Conclusion and Perspectives

General Summary

The work presented provides a solid foundation for the prediction of residual stresses due to grinding. It also offers a comprehensive understanding of the mechanisms that govern the grinding process which eventually are useful to optimize the process.

In the ***first chapter*** the context and the historical background is described. The development of residual stresses in the ground components is explained and a brief introduction about the motivations and needs for a reliable numerical model to simulate the grinding process is given.

The ***second chapter*** of this thesis presents the grinding process as a whole. A description of the process is presented globally and the different physics involved in the process are discussed. Two critical points appear in the literature about the surface integrity of ground workpieces: the occurrence of metallurgical transformations and the presence of either compressive (beneficial) or tensile (detrimental) residual stresses on the surface of the workpiece. The temperature reached during grinding may be considered as the critical point of the process affecting the surface integrity of ground parts. From the modelling point of view, a review of different analytical and numerical modelling approaches mostly addressing the thermal aspects of grinding process is presented. In this regard, the modelling of the contact between the grinding wheel and the workpiece and the resultant energy dissipation in the form of heat are found to be one of the major difficulties to be addressed in the modelling of the process. From the literature review it was found that predictive techniques like numerical simulations are regarded as the very useful tools to analyze the mechanical and/or the thermal strains and subsequent residual stresses associated with a grinding process thus providing in advance useful guidelines for defining the optimum grinding parameters.

In the ***third chapter*** a detailed account of phase transformation has been presented. An overview of phase transformation modelling has also been presented including some coupled thermo-metallo-mechanical models found in the literature. A model for phase transformation was proposed and the numerical implementation of the model was carried out through the Fortran subroutine PHASE using the FEM commercial package Abaqus®/standard. A series of FEM simulations were performed for a single 2D element. Phase transformations were simulated for different thermal histories and the results compared to those in the literature.

A comprehensive FE model of the grinding process is proposed in ***chapter four***. The essentials of the FE model are reviewed in this section. The full coupling of mechanical, thermal and metallurgical (phase transformations) effects occurring during grinding is analyzed. The nonlinearity due to the contact problem is removed by assuming an hertzian pressure (and shear) distribution instead of solving the contact between the grinding wheel and the workpiece. The temperature field produced by the sliding between the grinding wheel and the workpiece has been obtained by considering a moving heat source of elliptical shape. Numerical simulations were performed using the commercial finite element software Abaqus®/Standard along with the user subroutines UMAT, PHASE, UEXPAN, and PROP so as to model the thermal, metallurgical and mechanical behaviour of the material. The grinding wheel was modelled as a normal pressure and tangential traction moving on the workpiece through subroutines DLOAD and UTRACLOAD, respectively. Numerous simulations are performed to observe the effects of the Peclet number, the heat transfer coefficient, and the magnitude of the input heat flux on the residual stresses.

In the ***fifth chapter*** the results of the simulations are being presented and discussed. In order to simplify the problem a step by step procedure is followed for the analysis where each phenomenon involved in the grinding process (thermal, phase transformation and mechanical) is described separately and then sequentially coupled.

Main results

A comprehensive numerical model taking into account the phase transformations occurring during the grinding process has been presented for the material AISI 52100 (100Cr6) steel. Investigations carried out in the present thesis include:

- Thermal analyses of the grinding process using an elliptical heat source distribution
- Multi-phase transformation which occur when the critical grinding temperature is reached, according to CCT diagram for the given material
- The correlation of critical grinding conditions with the onset of the irreversible strains due to plasticity and phase transformations
- Residual stresses introduced by normal and tangential traction at the contact surface under isothermal grinding conditions,
- Residual stresses due to thermal loading and with phase change,
- Residual stresses due thermo-mechanical loading when the maximum grinding temperature is below the austenitizing temperature

- Residual stresses introduced by combined thermo-mechanical loading with phase transformation

The investigation led to the following findings and conclusions:

✓ For the case of thermal analysis with phase transformation:

⇒ the structural balance promoted by the microstructural change results in compressive residual stresses within the induced martensite layer.

⇒ The maximum surface residual stress is sensitive to cooling conditions; for very slow cooling conditions tensile stresses are likely to be present due to the formation of pearlite and/or bainite phases (less volume growth, more dense phase) and compressive stresses for fast cooling rates when martensite transformation occurs.

⇒ Surface hardening and volume growth due to martensite phase transformation dominate the transition of residual stresses from tensile to compressive.

⇒ Residual stresses in the no-martensite zone are nearly unaffected by surface hardening and volume change.

⇒ The residual stresses within the martensite zone are directly related to the depth of the martensitic layer.

⇒ To decrease the level of residual stresses due to thermal loading the grinding temperature may be lowered by either enhancing the cooling power of the cooling fluid or more efficiently by increasing the table speed (i.e. the heat source velocity) with all other conditions maintained the same.

✓ Under a pure mechanical loading due to the contact between the grinding wheel and the workpiece:

⇒ the normal load and the friction coefficient have a critical role in changing the nature of residual stresses.

✓ With thermo-mechanical grinding conditions when the maximum temperature is below the austenitizing temperature (low heat flux intensity, no phase transformation and for a given set of grinding conditions):

⇒ at high surface temperatures, the effect of the thermal loading becomes dominant compared to the mechanical loading.

⇒ If the maximum grinding temperature is kept the same and a low input heat flux intensity is maintained, the surface tensile residual stresses can be reduced when a

higher cooling rate is imposed by either increasing the table speed of grinding or by enlarging the convection heat transfer coefficient of the coolant.

- ✓ With fully coupled thermal, mechanical and metallurgical analysis:
  - ⇒ the mechanical grinding conditions may have stronger effects on the residual stresses when combined with thermal conditions and phase transformation, particularly at a lower Peclet number.
  - ⇒ For a given set of grinding conditions, higher values of residual stresses are obtained when the mechanical effects are not negligible.

Perspectives

Although the work presented performs well in terms of capturing trends and magnitudes of the residual stresses produced from a variety of grinding conditions, there are still areas for improvement. The following areas for future research will help to address limitations in the current work and improve the prediction of residual stresses.

The current modelling approach for the phase transformation does not account for the effect of heating rate, the mechanical loading effects on the critical grinding conditions for phase transformation and the effect of retained austenite on residual stresses. A method to incorporate these effects and their influence on the residual stress production needs to be developed.

In the present application, the friction coefficient was considered as an independent parameter. The influence of the friction coefficient on residual stresses was discussed in details but the effects on the temperature distribution were not taken into account. Conversely the effect of the temperature on the friction coefficient was not considered either. A physics-based model for determining the effect of temperature on the friction coefficient could be used to better understand the role of friction.

The assumptions regarding the interaction between the workpiece and the grinding wheel need to be refined in the light of non-linear contact mechanisms including material removal and heat generation. For this purpose there is a need to

- ✓ establish a more realistic model that accounts for the contact between the grinding wheel and the workpiece,
- ✓ introduce the material removal in the model.

It should be noted that the above suggestions for further improvements of the FE model may not be enough unless some critical experiments are conducted to verify the outcomes of the

numerical investigations. To achieve this, the following experimental work should be performed simultaneously:

1. temperature measurements in the workpiece during grinding
2. determination of phase transformation
3. observation of plastic strain using experimental techniques like transmission electron microscope (TEM), and scanning electron microscope (SEM)
4. measurement of residual stresses using X-ray diffraction (XRD)

Bibliography

[AGUI05] **Aguiar A., Monteiro, A., Natal, R., Lages**, **M.P.,** Experimental and FEM study of the influence of the grinding stone one the temperature field during superficial grinding, COMPLAS VIII (2005) 1–4.

[ALDE14] **Alden G.I.**, Operation of grinding wheels in machine grinding. *ASME Trans.* 36 (1914), pp. 451–460.

[ALI97] **Ali Y.M., Zhang**, **L.C.,** Estimation of residual stresses induced by grinding using a fuzzy logic approach. Journal of Materials Processing Technology, 63(1-3):875–880, January 1997.

[ALIA98] **Aliaga, C., Massoni, E., Treuil, J.L**., 3D numerical simulation of thermo-elastovisco-plastic behaviour using stabilized mixed f.e. formulation: application to 3D heat treatment, In IV World Congress on Computational Mechanics, Buenos Aires, Argentina, June-July 1998

[ANDE08] **Anderson D., Warkentin A., Bauer R**., Experimental validation of numerical thermal models for shallow and deep dry grinding, Journal of Materials Processing Technology 204 (2008) 269–278.

[ANDR65] **Andrews, K.W**., Empirical Formulae for the Calculation of Some Transformation Temperatures, *JISI,* Vol 203, 1965, p 721–727

[ANON60] **Anon,** Grinding Stresses - Cause, Effect and control, Collected Papers, grinding Wheel Institute, Cleveland, Ohio, 1960.

[ARRA05] **Arrazola, P.J., Villar, A., Ugarte, D., Meslin, F., Le Maitre, F., Marya, S**., Serrated Chip Prediction in Numerical Cutting Models, Proceedings: 8th CIRP International Workshop on Modelling of Machining Operations, Chemnitz, Germany: 115-122, 2005.

[AVRA39] **Avrami, M.,** Kinetics of phase change i: general theory, Journal of Chemical Physics, 7: 103–112, 1939.

[AVRA40] **Avrami, M**., Kinetics of phase change ii: transformation-time relations for random distribution of nuclei. Journal of Chemical Physics, 8: 212–224, 1940.

[BACK52] **Backer, W.R., Marshall., E.R., Shaw, M.C.**, *The size effect in metal cutting.* Transactions of ASME, 1952: p. 61 - 72.

[BADG00] **Badger, J., Torrance, A**., 2000, A comparison of two models to predict the grinding force from wheel surface topography, Int. Journal of Machine Tools and Manufacture, 40: 1099-1120.

[BAIN61] **Bain, E.C., Paxton, H.W**., *Alloying Elements in Steel,* 2nd ed., American Society for Metals, 1961

[BALI98] **Baliga, B., Doyle, E.D., Hodgson, P.D**, Thermal modelling of punch grinding, in Materials 98. 1998: Wollongong. p. 227 - 232.

[BARB67] **Barber, J.R.**, Distribution of heat between sliding surfaces, Journal of Mechanical Engineering Science 9 (1967) 351–354

[BECK04] **Becker, J.-C**., 2004, *Bahngesteuertes Schleifen von Kurbelwellen,* Dissertation IFW Hannover.

[BELA91] **Belak, J., Stowers, I.F.**, The Indentation and Scraping of a Metal Surface: A Molecular Dynamics Study, Fundamentals of Friction: Macroscopic and Microscopic, Eds.: Singer, Pollock, ASI Series E, 220:1-10, 1991.

[BESS93] **Besserdich, G**. Dissertation, Universitat Karlsruhe, Germany,1993.

[BHAD01] **Bhadeshia, H.K.D.H**., *Bainite in steels*, The Inst. of Meter, 2nd Ed., 2001.

[BHAD91] **Bhadeshia, H.K.D.H, David, S.A., Vitek, J.M., Reed, R.W**., *Mater. Sci. Technol.,* Vol 7, 1991, p 686–698

[BIER97] **Biermann, D., Schneider**, **M.** Modeling and simulation of workpiece temperature in grinding by finite element analysis, Machining Science and Technology 1 (1997) 173–183.

[BLOK37] **Blok, H**., Theoretical study of temperature rise at surfaces of actual contact under oiliness lubricating conditions. Proceedings of the General Discussion on Lubrication and Lubricants, Institute of Mechanical Engineers 2(1937) 222–235, London

[BLOK55] **Blok, H**. The dissipation of frictional heat. Applied Scientific Research Section A5:151–181(1955)

[BOUZ99] **Bouzakis, K.D, Vidakis, N.** "Superficial plastic response determination of hard isotropic materials using ball indentations and a FEM optimization technique", *Int.Journal of Materials Characterization*, vol. 42, p.1-12, 1999.

[BOWD53] **Bowden, F.P., Thoma**, **P.H.** Surface temperatures of sliding solids, Proceedings of Royal Society NSW, 223 (1953) 29–39.

[BRAC88] **Brach, K., Pai., D.M**., **Ratterman, E., Shaw, M.C.,** *Grinding forces and energy.* Journal of Engineering for Industry, 1988. 110(February): p. 25 - 31.

[BRINK06] **Brinksmeier, J., C. Aurich, E. Govekar, C. Heinzel1, H.-W. Hoffmeister, F. Klocke, J. Peters, R. Rentsch1, D. J. Stephenson, E. Uhlmann, K. Weinert, M. Wittmann**; Advances in Modeling and Simulation of Grinding Processes *Annals of the CIRP Vol. 55/2/2006*

[BROS09] **Brosse A**.; Modélisation expérimentale et numérique des effets induits par la rectification. Application à la rectification haute productivité, Ph.D. thesis ENS des Mines Saint Etienne France 2009

[BUSC68] **Busch, D.M.,** *Ritz und verschleissuntersuchungen an sproden werkstoffen mit einzelkornbestuckten hartstoffwerkzeugen*. 1968, Technische Hochschule: Hannover, West Germany.

[CAME64] **Cameron A., Gordon**, **A.N.** Contact temperatures in rolling/sliding surfaces. Proceedings of Royal Society NSW (1964) 45–61

[CARS59] **Carslaw, H., Jaeger, J. C.,** 1959, *Conduction of heat in solids, Oxford Science Publications,* Oxford University Press.

[CARS65] **Carslaw H. S. and Jaeger, J. C**. (1965), Conduction of Heat in Solids, 2nd Edn. *Oxford University Press, Great Britain*, (1965).

[COLO92] **Colonna F., Chenot J.L**., Wendenbaum J., Denis S., and Gautier E., On thermoelastic-viscoplastic analysis of cooling processes including phases changes, Jal. Mater. Proc. Tech., Vol 34: 525–532, 1992.

[CONS92] **Constant, A., Henry, G., and Charbonnier, J.C**., Principes de bases des traitements thermiques, thermomecaniques et thermochimiques des aciers, PYC ed. 1992.

[COOK71] **Cook, N.H**., *Manufacturing Analysis*. 1966: Addision-Wesley. Chapter 3.

[CORE01] **Coret, M**., Etude experimentale et simulation de la plasticite de transformation et du comportement multiphase de l'acier de cuve 16MND5 sous chargement multiaxial anisotherme, Ph.D Thesis, LMT Cachan, Paris, France, 2001.

[COSM84] **Cosmano, R.J., Abrahamson, G.R., Duwell, E.J**., *Energy dissipation in grind interface - heat distribution in the chip and workpiece*, in *International Grinding conference papers*, S.o.M. Engineers, Editor. 1984, Society of Manufacturing Engineers: Dearborn, Michigan. p. mr84-548.

[COST04] **Costes** :**F.** Modélisation thermomécanique tridimensionnelle par éléments finis de la coulée continue d'aciers. Thèse de doctorat, Ecole des Mines de Paris, 2004.

[COUE05] **Couey, J.A., Marsh, E.R., Knapp, B.R., Vallance, R.R.**: Monitoring force in precision cylindrical grinding. Precision Engineering, 29(3):307–314, July 2005.

[DALG08] **Dalgic M., Lowisch G.**, Transformation plasticity at different phase transformations of bearing steel International Journal of Microstructure and Materials Properties 2008 - Vol. 3, No.1 pp. 49 - 64

[DAUD66] **Daude**, Untersuchung des schleifprozesses. 1966, T.H. Aachen.

[DEDE72] **Dederichs, M**., *Untersuchung der warmebeeinflussing des werkstuckes beim flachschleifen*. 1972, T.H. Achhen.

[DENG87] **Denis S., Gautier E., and Sjostrom S**., Influence of stresses on the kinetics of pearlitic transformation during continuous cooling, Acta. Metall., 35: 1621–1632, 1987.

[DENI96] **Denis S**., Considering stress-phase transformation interactions in the calculation of heat treatment residual stresses, Jal. Ph., 6: 159–174, 1996.

[DENS87] **Denis S., Sjostrom S., and Simon A**., Coupled temperature, stress, phase transformation calculation model, numerical illustration of the internal stresses evolution during cooling of a eutectoide carbon steel cylinder, Metall., 18A: 1203–1212, 1987.

[DESR70] **Des Ruisseaux, N.R., Zerkle, R.D**., *Thermal analysis of the grinding process.* Journal of Engineering for industry, 1970(May): p. 428-434.

[DEVA98] **Devaux, J**., Comportement plastique des aciers en cours de transformations de phases- Etude numerique des lois de melange et de la plasticite de transformation. Rapport Systus International LDEW98/235, 1998.

[DREW01] **Drew S. J., Mannan M. A., Ong K. L. and Stone J.** : The measurement of forces in grinding in the presence of vibration. International Journal of Machine Tools and Manufacture, 41(4):509–520, mars 2001.

[ESHG68] **Eshghy, S**., Thermal aspects of the abrasive cutoff operation. Part 2 -Partition functions and optimum cutoff. Journal of Engineering for Industry, 1968(May): p. 360-364.

[FERN85] **Fernandes F.B.M., Denis S., and Simon A**., Mathematical model coupling phase transformation and temperature evolution during quenching of steels, Material science and technology, 1(10): 838–844, 1985.

[FIEL64] **Field, M. and Kahles, J. N**., DMIC, *report to usa air force*, (1964).

[FISC90] **Fischer F. D**., Acta Metall. Mater. 1990, 38, 1535 – 1546.

[FOLK88] **Folkhard E**., Welding Metallurgy of Stainless Steels. Springer-Verlag, Wien, New York, 1988.

[GAUT94] **Gautier E., Denis S., Liebaut C., and S. Sjostrom**, Mechanical behaviour of fe-c alloy during phase transformations, Jal. Ph. IV, C3(4): 279–284, 1994.

[GECI85] **Gecim B., W.O.Winer**, Transient temperatures in the vicinity of an asperity contact, Journal of Tribology, Trans ASME 107(1985) 333–342

[GREE65] **Greenwood, G.W., and Johnson, R.H**. The deformation of metals under small stresses during phase transformation, Proc Roy Soc, 283: 403–422, 1965.

[GUES15] **Guest J.J** (1915)., *Grinding Machinery*, Edward Arnold.

[GUOC00] **Guo, C., Malkin, S**., 2000, Energy partition and cooling during grinding, Journal of Manufacturing Processes, 2/3: 151-157.

[GUOC95] **Guo, C., Malkin, S**., 1995, Analysis of Transient Temperatures in Grinding, Journal of Engineering for Industry 117: 571-577

[GUOY02] **Guo Y.B, C. R. Liu**., Mechanical Properties of Hardened AISI 52100 Steel in Hard Machining Processes; Journal of Manufacturing Science and Engineering 124(2002) 1-9.

[HABR92] **Habraken A.M**., and Bourdouxhe M., Coupled thermo-mechanical-metallurgical analysis during the cooling process of steel pieces, E. J. Mech. A./Solids, 11(3): 341–402, 1992.

[HAHN62] **Hahn, R.S**. On the nature of the grinding process. in Proceedings of the 3rd MTDR conference. 1962.

[HAHN66] **Hahn, R.S.**, On the mechanics of the grinding process under plunge cut conditions. Transactions of ASME, 1966(February): p. 72 - 80.

[HAHN71] **Hahn, Robert. S., Lindsay, Richard. P**., *Principles of grinding*, in *Grinding: Theory, Techniques and troubleshooting*, C.L. Bhateja, Richard., Editor. 1971, Society of Manufacturing Engineers: Dearborn, Michigan. p. 3-41.

[HAHN86] **Hahn, R.S.,** *Precision grinding cycles*, in *Handbook of modern grinding technology*, R.I.H. King, Robert. S., Editor. 1986, Chapman and Hall: New York, London. p. 170-190.

[HAMD00] **Hamdi H.** : Contribution à l'étude de la physique de l'interface meule-pièce dans le cadre de la rectification traditionnelle et à grande vitesse. PhD Thesis (2000), Ecole centrale Lyon,.

[HAMD04] **Hamdi H., Zahouani H., J.-M. Bergheau**, Residual stresses computation in a grinding process, Journal of Materials Processing Technology 147 (2004) 277–285.

[HONG00] **Hong, K. K., Lo, C. Y**., , An inverse analysis for the heat conduction during a grinding process, Journal of Materials Processing Technology 105 (2000): 87-94.

[HOU03] **Hou Z. B., Komanduri R.:** On the mechanics of the grinding process - part I. stochastic nature of the grinding process. International Journal of Machine Tools and Manufacture, 43(15):1579–1593, December 2003

[HOUZ00] **Hou Z.B., Komanduri R.** General solutions for stationary/moving plane heat source problems in manufacturing and tribology; International Journal of Heat and Mass Transfer 43 (2000) 1679-1698

[HUNK04] **M. Hunkel, Th. Lübben, F. Hoffmann and P. Mayr**, Using the jominy end-quench test for validation of thermo-metallurgical model parameters *J. Phys. IV France* 120 (2004) 571-579

[INOU78] **Inoue T., and Raniecki B**., Determination of thermal-hardening stress in steels by use of thermal-plasticity theory. Jal. Mech. Sol., 26: 187–212, 1978.

[INOU85] **Inoue T., Wang Z.**, Coupling between stress, temperature and metallic structures during processes involving phase transformations, Journal of Material Science and Technology, 1(1985) 845-849

[JAEG42] **Jaeger J.C**., Moving sources of heat and the temperature at sliding contacts, Proceedings of Royal Society NSW, 76(1942) 203–224.

[JINT99] **Jin T. D. J. Stephenson**, Three dimensional finite element simulation of transient heat transfer in high efficiency deep grinding, Annals of the CIRP 53 (1) (1999) 259–262.

[JOHN39] **Johnson W.A. and Mehl R.F**., Reaction kinetics in process of nucleation and growth, Transactions of the A.I.M.E., 135: 416–45, 1939.

[JOHN62] **Johnson R.H. and Greenwood G.W.**, *Nature,*Vol 195, 1962, p 138–139

[KALP97] **Kalpakjian, S.,** *Manufacturing process for engineering materials*, 3rd ed., 1997, Addison-Wesley, Menlo Park, California.

[KIMN97] **Kim, N.K., Guo, C., Malkin, S**., Heat flux Distribution and energy partition in creep-feed grinding. Annals of the CIRP, 1997. 46(1): p. 227-232.

[KIMP00] **Kim P.J., Lee D.G., Choi J.K**., Grinding characteristics of carbon fiber epoxy composite hollow shafts, Journal of Composite Materials 34 (2000) 2016–2035.

[KIRK78] **Kirkaldy J.S. and E.A. Baganis**, Thermodynamic Prediction of the Ae3 Temperature of Steels with Additions of Mn, Si, Ni, Cr, Mo and Cu, *Metall. Trans. A,* Vol 9A, 1978, p 495–501

[KLOC03] **Klocke, F**., 2003, Modelling und simulation in grinding, 1st European Conference on Grinding,Aachen, 6.-7. November, Fortschritt- Berichte VDI Reihe 2 Fertigungstechnik: 8.1-8.27.

[KOHL95] **Kohli, S., Guo, C., Malkin, S**., *Energy partition to the workpiece for grinding with aluminum and CBN abrasive wheels.* ASME Journal of Engineering for Industry, 1995.

[KOIS59] **Koistinen D.P. and Marburger R.E**., A general equation prescribing extent ofaustenite-martensite transformation in pure Fe-C alloys and plain carbon steels, Acta Metallurgica, 7: 59–60, 1959.

[KOMA71] **Komanduri, R**., *Some aspects of machining with negative rake tools simulating grinding.* Int. J. Mach. Tool Des. Res., 1971. **11**: p. 223 - 233.

[KOND99] **Kondo K., Ueda M., Ogawa K., Amaya H., Hirata H., and Takabe H**., Alloy Design of Super 13 Cr Martensitic Stainless Steel (Development of Super 13 Cr Martensitic Stainless Steel for Line Pipe-1). In Supermartensitic Stainless Steels, 99: 11–18, Belgium, 1999.

[KONT93] **Konter A.W.A.,** FEM analysis of contact problems in metal form-ing and rubber application, MARC Analysis Research Corporation, Europe, Zoetermeer, April 1993.

[KWAK06] **Kwak J-S., S-B. Sim et Y-D. Jeong** : An analysis of grinding power and surface roughness in external cylindrical grinding of hardened scm440 steel using the response surface method. International Journal of Machine Tools and Manufacture, 46(3- 4):304–312, mars 2006.

[LACO93] **Lacombe P., Baroux B., and Beranger G**., Stainless Steels, Les Editions de Physique Les Ulis, 1993.

[LAVI91] **Lavine, A.S., von Turkovich, B.F**., Thermal aspects of grinding: the effect of heat generation at the shear planes. Annals of the CIRP, 1991. 40(1): p.343-345.

[LEBL84] **Leblond J.B. and Devaux J**., A new kinetic model for anisothermal metallurgical transformations in steels including effect of austenite grain size. Acta Metal., 32(1): 137–146, 1984.

[LEBL85] **Leblond J.B., Mottet G., Devaux J., Devaux J.C**., Mathematical models of anisothermal phase transformations in steels, and predicted plastic behaviour, Mater. Sci. Tech, 1: 815–822, 1985.

[LEBL89] **Leblond J.B., Devaux, J., and Devaux, J.C**., Mathematical modelling of transformation plasticity in steels - I: Case of ideal-plastic phases, International Journal of Plasticity, 5:551–572, 1989.

[LEED71] **Lee, D.G**., An experimental study of thermal aspects of grinding. 1971, University of Cincinnati.

[LIEB88] **Liebaut C., Gautier E., and Simon A**., Etude reologique d'un acier fe-0,2%c durant sa transformation de phase. Memoire et etude scientifique Revue de metallurgie, 571–579, 1988.

[LIND71a] **Lindsay, R.P., Hahn, R.S.,** On the basic relationships between grinding parameters. Annals of the CRIP, 1971. **XVIV**: p. 657 - 666.

[LIND71] **Lindsay, R.P**., On the material removal - and wheel removal parameters -surface finish, geometry and thermal damage in precision grinding. 1971,Worchester Polytechnic Institute.

[LIND75] **Lindsay, Richard. P**., *Principles of grinding: four years later*, in *Grinding: Theory, Techniques and troubleshooting*, C.L. Bhateja, Richard., Editor 1975, Society of Manufacturing Engineers: Dearborn, Michigan. p. 42-60.

[LIND86] **Lindsay, R.P.,** *Principles of grinding*, in *Handbook of modern grinding technology*, R.I.H. King, Robert. S, Editor. 1986, Chapman and Hall: New York, London. p. 30-71.

[LITT67] **Littman W. E**., The Influence of Grinding on Workpiece Quality, ASTME Paper, MR67-593, 1967.

[LIU08] **Liu Q., X. Chen, Y. Wang et N. Gindy** : Empirical modelling of grinding force based on multivariate analysis. Journal of Materials Processing Technology, 203:420–430, 2008.

[LIUW02] **Liu W.J., Z.J. Pei, X.J. Xin**, Finite element analysis for grinding and lapping of wire-sawn silicon wafers, Journal of Materials Processing Technology 129 (2002) 2–9.

[LOWI80] **Lowin, R**., 1980, Schleiftemperaturen und ihre Auswirkungen im Werkstück. Dissertation, University of Aachen.

[MACG46] **MacGregor, C.W., J.C. Fisher**: *A Velocity-Modified Temperature for the Plastic Flow of Metals.* Journal of Applied Mechanics 1946. March A-11-A-16.

[MAGE70] **Magee C.L**., Nucleation of martensite, Phases transformations, ASM, Metals Park, 1970.

[MAHD00] **Mahdi M., L Zhang**., A numerical algorithm for the full coupling of mechanical deformation, thermal deformation, and phase transformation in surface grinding, Computational Mechanics 26 (2000) 148–156.

[MAHD95] **Mahdi M., L. Zhang**, The finite element thermal analysis of grinding processes by ADINA, Computers and Structures 56 (1995) 313–320.

[MAHD97] **Mahdi M., Zhang L**., Applied mechanics in grinding—V: thermal residual stresses, International Journal of Machine Tools and Manufacture 37 (1997) 619–633.

[MAHD98] **Mahdi M., Zhang L**., Applied mechanics in grinding—VI. Residual stresses and surface hardening by coupled thermo-plasticity and phase transformation, International Journal of Machine Tools and Manufacture 38 (1998) 1289–1304.

[MAHD99] **Mahdi M.,. Zhang L.C**, Residual stresses in ground components caused by coupled thermal and mechanical plastic deformation, Journal of Materials Processing Technology 95 (1999) 238–245.

[MALK71] **Malkin, S., Cook, N.H**., The wear of grinding wheels (Part 1). Transactions of asme, 1971. **93**: p. 1102 - 1128.

[MALK74] **Malkin, S., Anderson, R.B**., *Thermal aspects of grinding.* Journal of Engineering for Industry, 1974. 96: p. 1177-1191.

[MALK78] **Malkin, S., Lenz, E.**, Burning limit for surface and cylindrical grinding of steels. Annals of the CIRP, 1978. 27(1): p. 233-236.

[MALK89] **Malkin S.**, *Grinding Technology: Theory and Application of Machining with abrasives* United States of America, Ellis Horwood, Wiley, Chichester, 1989.

[MALK89a] **Malkin, S., Kovach, J. A**., *Grinding fundamentals and applications*. Vol. PED-Vol. 39. 1989, San Francisco, California: The American Society of Mechanical Engineers. 405

[MAMA00] **Mamalis A.G., A.S. Branis, D.E. Manolakos, J. Mater**. Process. Technol. 123 (2000) 464–475.

[MAMA03] **Mamalis A.G., J. Kundra´k, D.E. Manolakos, K. Gya´ni**, A. Markopoulos, Thermal modelling of surface grinding using implicit finite element techniques, International Journal of Advanced Manufacturing Technology 21 (2003) 929–934.

[MARI04] **Marinescu, I.D., Rowe, W.B.,and Inasaki**, 2004, *Tribology of abrasive Machining process.* William Andrew Publishing Norwich, NY.

[MARI07] **Marinescu I.D., Hitchiner M., Uhlmann E. Rowe, W.B.,and Inasaki**, 2007 *Handbook of Machining with Grinding Wheels*, CRC Press NY

[MARR77] **Marris, M**., Thermische aspekten van de oppervlakteintegriteit bij het slijpen, in Kath. 1977, University Leuven.

[MART99] **Martinez M**., Jonction 16MND5-INCONEL 690-316LN par soudage-diffusion, PhD Thesis, ENSMP, Paris, France, 1999.

[MARU01] **Maruyama K., Sawada K., and Koike J.I**., Strengthening mechanisms of creep resistant tempered martensitic steel. ISIJ international. 41(6): 641–653, 2001.

[MATS87] **Matsumoto Y., Barash M.M., C.R**. Liu, Mater. Sci. Technol. 3 (1987) 299–305.

[MOUL01] **Moulik P.N., Yang H.Y.T., Chandrasekar S**., Simulation of thermal stresses due to grinding, International Journal of Mechanical Sciences 43 (2001) 831–851.

[NAND04] **Nandi A. K. et D. K. Pratihar** : Design of a genetic-fuzzy system to predict surface finish and power requirement in grinding. Fuzzy Sets and Systems, 148(3):487–504, December 2004.

[OKAM67] **Okamura, K.**, Study on the cutting mechanism of abrasive grain (4th Report).Bull. Japan Soc. of Prec. Eng., 1967. **33**(3): p. 161.

[ONOK61] **Ono, Koji**., *Analysis on the grinding force.* Bulletin of J.S.G.E.,1961. 1: p19 -22.

[ORYN99] **Orynski F. et W. Pawlowski** : The influence of grinding process on forced vibration damping in headstock of grinding wheel of cylindrical grinder. International Journal of Machine Tools and Manufacture, 39(2):229–235, février 1999

[OSMOND] **Osmond F**., *Transformation du Fer,* Baudoin and Co., Paris, 1888

[OUTW52] **Outwater, J.O., Shaw, M.C**., *Surface temperatures in grinding.* Transactions of asme, 1952. 74(Januray): p. 73 - 86.

[OVAKO] **Ovako steels** http://www.ovako.com (Last time accessed on 28-03-2011)

http://www.matml.org/pub/Production/TechStreet/AlloyDigestDec2010/Dec2010/sa582.pdf

http://www.ovako.com/applications/ovako_search_new/ovako_search/pdf/100Cr6%20v5.pdf

http://www.ovako.com/Data/r3249/v1/Steels_for_bearing_production_from_Ovako.pdf

[PATE53] **Patel J.R. and Cohen M**., Criterion for the action of applied stress in the martensite transformation. Acta Mater., 1: 531–538, 1953

[PAUL95] **Paul S., A.B. Chattopadhyay,** A study of effects of cryo-cooling in grinding, International Journal of Machine Tools and Manufacture 35 (1) (1995) 109–117.

[PEKL57] **Peklenik, J**., Ermittlung von geometrischen und physikalischen kenngrossen fur die grundlagenforschung des schleifens. 1957, T.H. Aachen.

[PETE80] **Peters, J., Aerens, R.,** Optimization procedure of three phase grinding cycles of a series without intermediate dressing. Annals of the CIRP, 1980. **29**(1): p.195 - 200.

[PETE83] **Peters, J., Vanservenant, E., Leuven, K.U**., *A thermal model covering pendulum grinding and creep feed grinding.* Annals of the CIRP, 1983. 32(1): p. 491-494.

[POUL01] **Poulachot G., Moison A.L., Jawahir I.S.**, Ann. CIRP 50 (1) (2001) 31–36.

[POUL99] **Poulachon G.** : Aspects phénoménologiques, mécaniques et métallurgiques en tournage c-BN des aciers durcis. PhD Thesis (1999), École nationale supérieure d'arts et métiers de Cluny.

[QIAO00] **Qiao G. Y., Zhang K.Q., and Xiao F. R**., Effect of cooling rate on martensite microstructure of Fv520 (B) steel, China Journal of Heat Treatment of Metals, No.2P: 31–32, 2000.

[RAYN88] **Raynor G.V., V.G. Rivlin**, *Phase Equilibria in Iron Ternary Alloys,* Inst. Met., London, 1988, pp. 378-388.

[REIC56] **Reichenbach, G.S., Mayer, I.E., Kalpakcioglu, S., Shaw, M.C.,** The role of chip thickness in grinding trans. ASME, 1956. **18**: p. 847 - 850.

[ROSE41] **Rosenthal D**., Mathematical theory of heat distribution during welding and cutting, Weld Res Supplement, (1941) 220–234

[ROSE46] **Rosenthal D**., The theory of moving sources of heat and its application to metal treatments, Transaction of ASME 80(1946) 849–866

[ROWE01] **Rowe W.B.,** Thermal analysis of high efficiency deep grinding, International Journal of Machine Tools and Manufacture 41 (1) (2001) 1–19.

[ROWE88] **Rowe, W.B., Pettit, J.A., Boyle, A., Moruzzi, J.L**., *Avoidance of thermal damage in grinding and prediction of the Damage threshold.* Annals of the CIRP, 1988. 37(1): p. 327-330.

[ROWE90] **Rowe, W.E., Pettit, J.A., Morgan, M.N., Lavine, A.S**., *A Discussion of thermal models in grinding.* Technical paper, Society of manufacturing engineers, 1990: p. MR90-516-1 to MR90-516-15.

[ROWE91] **Rowe, W.B., Morgan, M.N., Allanson, D.A**., An advance in the modelling of thermal effects in the grinding process. Annals of the CIRP, 1991. 40(1): p.339-342.

[ROWE92] **Rowe, W.B., Morgan, M., Allanson**, D., *The tribology of grinding from energy considerations.* Tribology in metal cutting and grinding, 1992: p. 19-31.

[ROWE95] **Rowe, W.B., Black, S.C.E., Mills, B., Qi, H.S., & Morgan, M.N**., *Experimntal investigation of heat transfer in grinding.* Annals of the CIRP, 1995. 44(1): p. 329-322.

[ROWE96a] **Rowe, W.B., Black, S.C.E., & Mills, B. & Qi, H.S**., *Analysis of grinding temperatures by energy partitioning.* Journal of Engineering Manufacture, 1996. 210(b6): p. 579 - 588.

[ROWE96b] **Rowe, W.B., Morgan, M.N., Black, S.C.E., Mills, B**., *A Simplified approach to control of thermal damage in grinding.* Annals of the CIRP, 1996. 45(1): p.299-302.

[ROWE97] **Rowe W. B., Black S. C. E., Mills B., Morgan M. N. and Qi H. S.** : Grinding temperatures and energy partitioning, volume 453, Proceedings de Royal society of London, 1997.

[SALJ53] **Salje, E., Ing,** Von., *Grundlagen des Schleifvorganges.* Werkstatt und betrieb, 1953. **86**(4): p. 177-182.

[SATO61] **Sato, Kenji.**, Grinding temperature. Bulletin of the Japan Society of Grinding Engineers, 1961: p. 31-33.

[SAUE71] **Sauer, J. Wolfgang**., *Thermal aspects of grinding*. 1971, Carnegie-Mellon University.

[SAUE72] **Sauer, Wolfang. J**., Thermal aspects of surface grinding, in New developments in grinding, M.C. Shaw, Editor. 1972, Carnegie Press:Pittsburgh, Pennsylvania. p. 391-411.

[SHAW93] **Shaw, M.C., Vyas, A**., Heat-affected zones in grinding steel. Annals of the CIRP, 1993. 43(1): p. 279-282.

[SHAW96] **SHAW, M. C**., (1996), *Principles of Abrasive Processing,* Oxford University Press (1996).

[SHIG63] **Shigeo O., Hideo A**. Time-Temperature-Austenitization diagram of hypereutectoid steel; Journal of the Japan institute of metals; 173-178 (4) 1963

[SJÖS85] **Sjöstrom S**., Interactions and constitutive models for calculating quench stresses in steel. Mat. Sci. Tech., 1: 823–829, 1985.

[SNOE71] **Snoeys, R., Decneut, A.,** Review of results of the co-operative research program of the CIRP grinding group. Annals of the CIRP, 1971. **19**: p. 507-512.

[SNOE74] **Snoeys, R., Peters, J.,** voor Werktuigkunde, Inst., Decneut, A., The significance of chip thickness in grinding. Annals of the CIRP, 1974. **23**(2): p. 227-237.

[SNOE78] **Snoeys, R., Leuven, K. U., Maris, M., Peters, B.J**., *Thermally induced damage in grinding*, in *Grinding: Theory, Techniques and troubleshooting*, C.L. Bhateja, Richard., Editor. 1978, Society of Manufacturing Engineers:Dearborn, Michigan. p. 206-216.

[STAR03] **Starostin, N. P., Kondakov, A. A**., 2003, Calculation of non-stationary temperature field in disk-block friction pair at smaller engagement coefficients, Trenie i iznos 24/3: 260-265.

[TAKA72] **Takazawa, K**., *Thermal aspects of the grinding operation.* Industrial diamond review, 1972(April): p. 143.

[TALE03] **Taleb L., and Sidoroff. F**., Micromechanical modelling of greenwood-johnson mechanism in transformation induced plasticity, Int. Jal. Plas., 19: 1821–1842(22), 2003.

[TANG85] **Tanguy J. C.** : Rectification : Connaissances de base et données pratiques. ISBN 2-85400-048-X, 1985

[TÖNS80] **Tönshoff H.K., Rohr G. and Althaus P.G.** : Process control in internal grinding. CIRP Annals - Manufacturing Technology, 29(1):207–211, 1980.

[TÖNS92] **Tönshoff H.K., Peters J., Inasaki I. and Paul T.** : Modelling and simulation of grinding processes. CIRP Annals - Manufacturing Technology, 41(2):677–688, 1992.

[TÖNS95] **Tönshoff H.K., Wobker H.-G., Brandt D.**, Trans. NAMRI/SME XXIII (1995) 215–220

[TSAI98] **Tsai, H. H., Hocheng, H**., 1998, Investigation of the transient thermal deflection and stresses of the workpiece in surface grinding with the application of a cryogenic magnetic chuck, Journal of Materials Processing Technology 79: 177-184.

[VERK76] **Verkerk, J**., *Wheel wear control in grinding*. 1976, T.H. Delft.

[VINC02] **Vincent Y**., Simulation numerique des consequenes metallugriques et mecaniques induites par une operation de soudage: acier 16MND5, These de Doctorat, INSA de Lyon, 2002.

[WAEK94] **Waeckel F**., Une loi de comportement thermo-metallurgique des aciers pour le calcul mecanique des structures (A thermo-metallurgical constitutive law of steels for structural mechanics), These, ENSAM, 1994.

[WAEK96] **Waeckel F., Dupas P., and Andirieu S**., A thermo-metallurgical model for steel cooling behavioue : proposition, validation and comparison with the sysweld's model, J. Ph., C1, III(6): 255–263, 1996.

[WANG03] **Wang L.,Y. Qin, Z.C. Liu, P.Q. Ge, W. Gao**, Computer simulation of a workpiece temperature field during the grinding process, Proceedings of the Institution of Mechanical Engineers—Part B: Journal of Engineering Manufacture 217 (7) (2003) 953–959.

[WARN99] **Warnecke G., Barth C**., Optimization of the dynamic behavior grinding wheels for grinding of hard and brittle materials using the finite element method, Annals of the CIRP 48 (1) (1999) 261–264.

[WEBE99] **Weber T**., Simulation of grinding by means of the finite element analysis, in: Third International Machining and Grinding Conference, 1999.

[WEBS01] **Webster G.A., and Ezeilo A.N**., Int. J. Fatigue 23, 2001.

[WERN71] **Werner, G.,** *Kinematik und mechanik des schleifprozesses*. 1971, TH Achhen.

[WEVE59] **Wever,F. A. Rose, W. Peter, W. Strassburg, L. Rademacher**: *Atlas zur Wärmebehandlung vonStählen*; Verlag Stahleisen (1959)

[WOOD59] **Robert S.Woodbury** 1959 History of the Grinding Machine: A Historical Study in Tools and Precicion Production MIT Press

[YUXX94] **Yu X.X., Lau W.S**., A finite element analysis of residual stresses in stretch grinding, Journal of Materials Processing Technology 94 (1999) 13–22.

[ZHAN02] **Zhang J. G.** et al ,Microstructure and continuous cooling transformation thermograms of spray formed GCr15 steel; Materials Science and Engineering A326 (2002) 20–25

[ZHAN95] **Zhang L., Mahdi M**., Applied mechanics in grinding-IV: the mechanism of grinding induced phase transformation, International Journal of Machine Tools and Manufacture 35 (1995) 1397–1409.

[ZHOU04] **Zhou S. F**., et al, Microstructure and mechanical properties in simulated HAZ of 0Cr13Ni5Mo martensitic stainless steel, Transactions of the china welding institution, 25(5): 63–66, 2004.

[ZHUB95] **Zhu, B., Guo, C., Sunderland, J.E., Malkin, S**., *Energy partition to the workpiece for grinding of ceramics.* Annals of the CIRP, 1995. 44(1): p. 267 -271.

Annex A1

Properties of Material AISI 52100 (100Cr6) steel

Table A.1 Chemical composition of AISI 52100 (100Cr6) bearing steel

Element	C	Si	Mn	S	Cr	Mo	P
Mass %	0.95-1.10	0.15-0.35	0.20-0.40	≤0.025	1.35-1.60	≤0.10	≤0.030

Table A.2 Mechanical and Thermal properties of AISI 52100 (100Cr6) steel at room temperature [GUOY02]

Description	Value
Young's modulus (GPa)	210
Poisson's ratio	0.30
Mass density (kgm^{-3})	7827
Specific heat (Jkg^{-1}per °C)	458
Thermal conductivity (Wm^{-1}per°C)	43

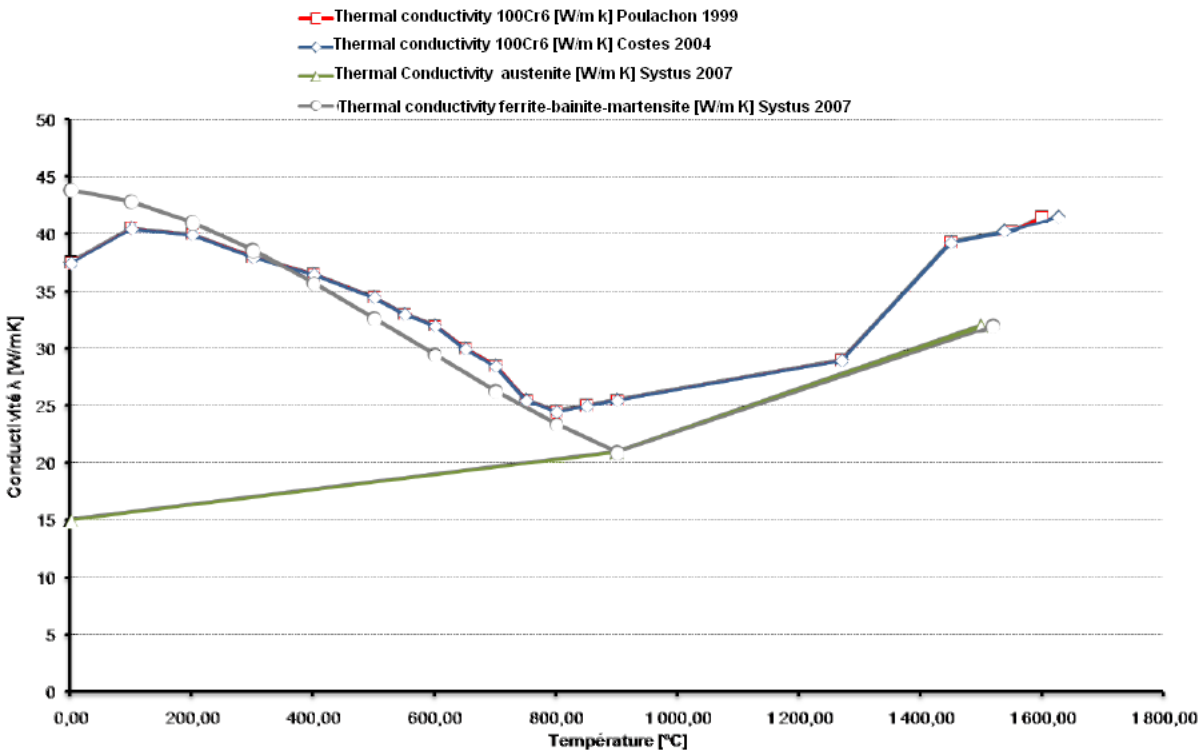

Thermal conductivity

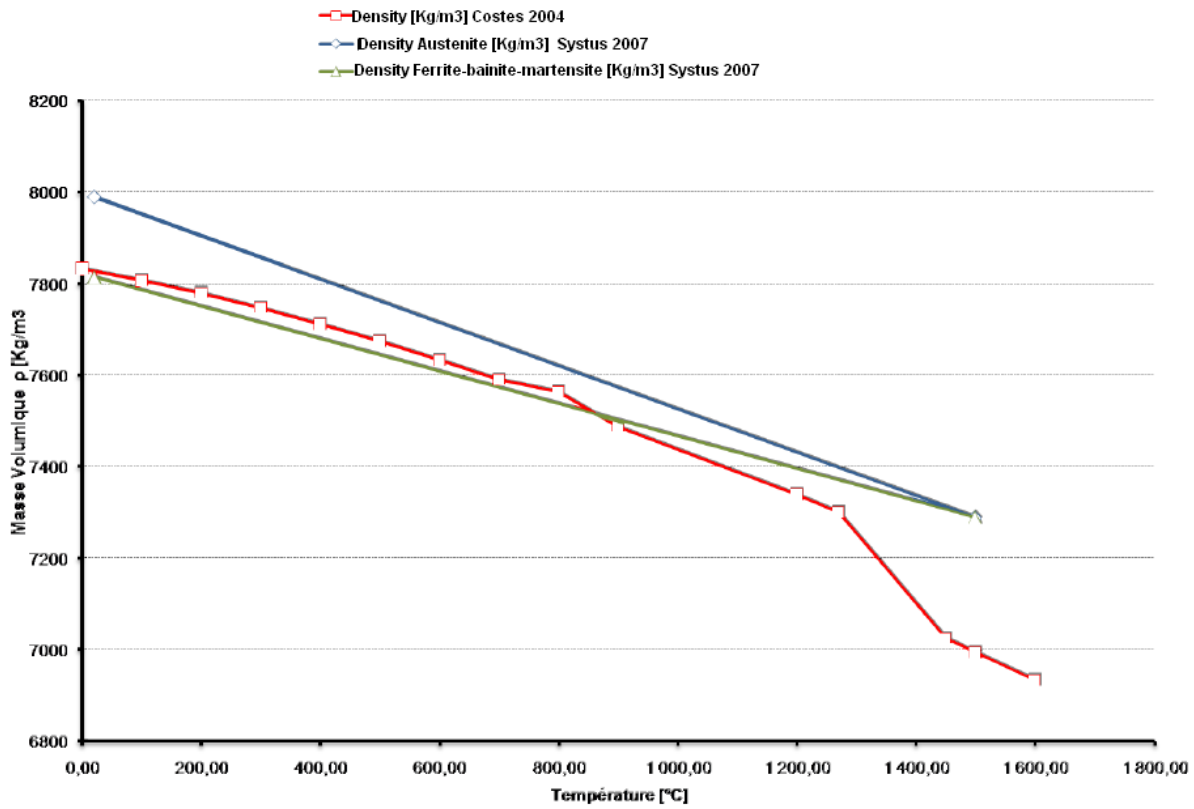

Density

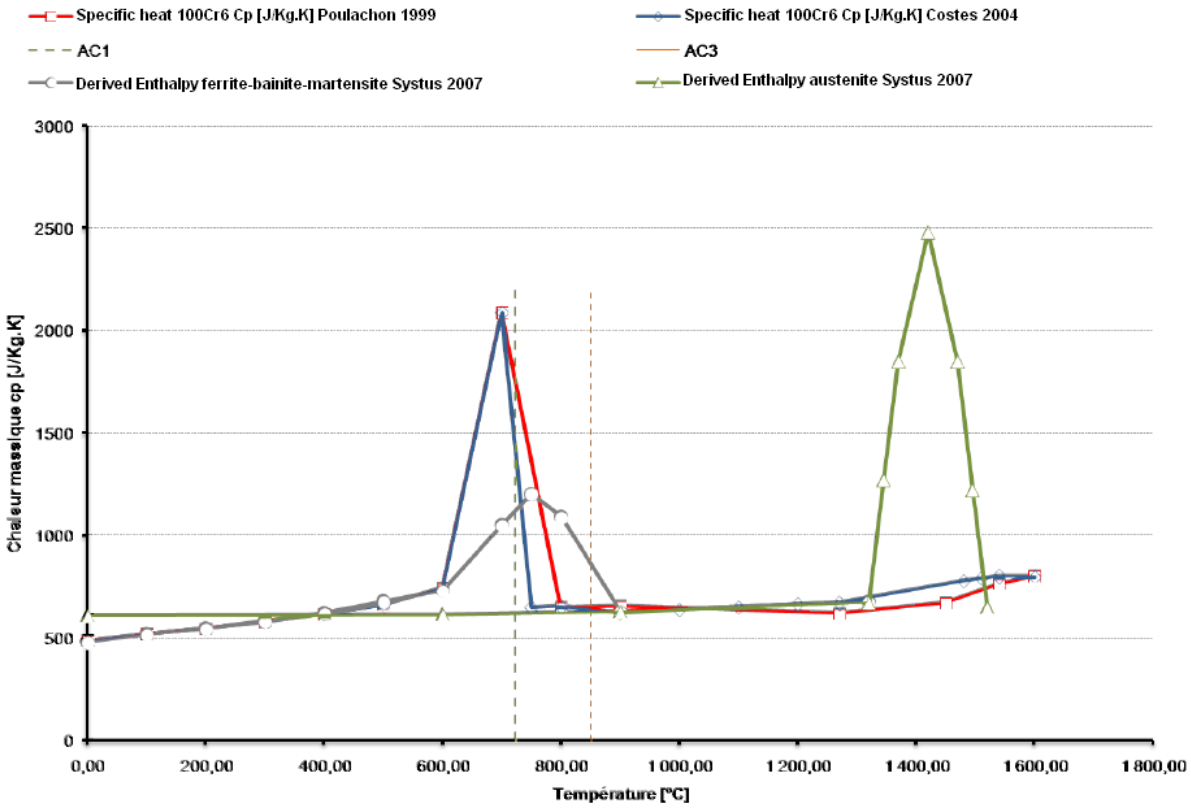

Specific heat

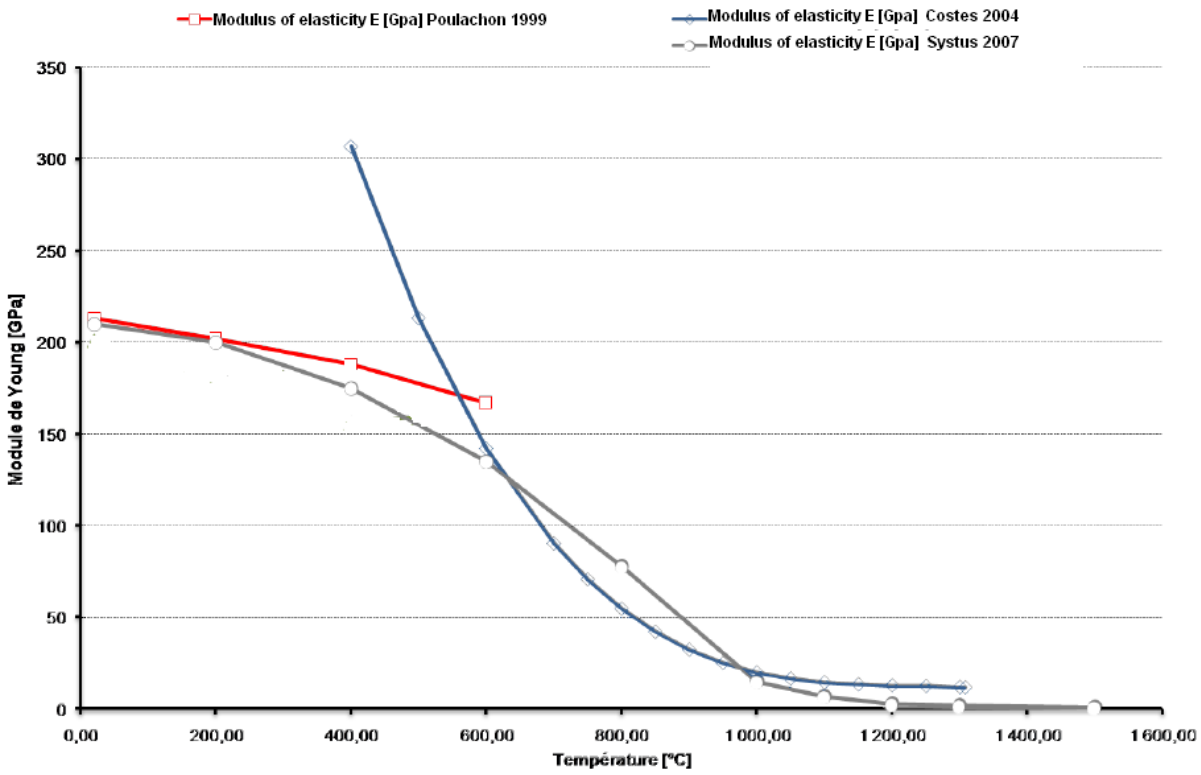

Modulus of elasticity

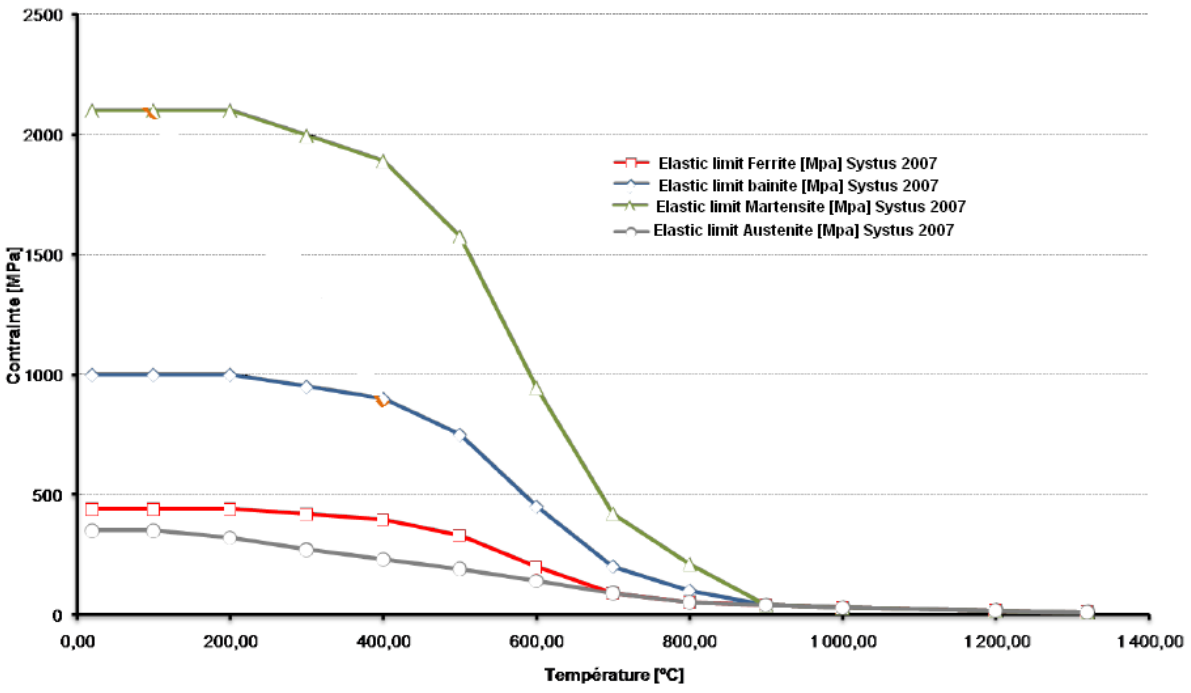

Elastic limit

FOLIO ADMINISTRATIF

THESE SOUTENUE DEVANT L'INSTITUT NATIONAL DES SCIENCES APPLIQUEES DE LYON

NOM : SHAH DATE de SOUTENANCE : 20 juin 2011

Prénoms : Syed Mushtaq Ahmed

TITRE : Prediction of residual stresses due to grinding with phase transformation

NATURE : Doctorat Numéro d'ordre :

Ecole doctorale : MEGA

Spécialité : Mécanique- Génie Méchanique

Cote B.I.U. – Lyon . T 50/210/19 / et bis CLASSE :

RESUME :

La rectification est un procédé couramment utilisé dans l'industrie pour la finition de surface. L'optimisation du procédé consiste à trouver un compromis entre la qualité des pièces, minimiser les temps d'usinage et augmenter l'efficacité économique grâce au choix judicieux des paramètres de rectification. Par ailleurs le taux de production des pièces rectifiées est souvent limité par la topographie de la surface et l'endommagement des pièces par des brûlures de rectification ou des micro-fissures liées aux transformations de phase. Ces défauts d'aspect engendrent généralement, lorsqu'ils concernent une surface fonctionnelle, une réduction de la durée de vie du composant ainsi rectifié.'effet des conditions de rectification et des propriétés des matériaux sur la nature des contraintes résiduelles a été analysé par modélisation numérique. Le modèle élément finis permet la prédiction non seulement des contraintes résiduelles, mais aussi des phases en présence et des déformations associées. Ces déformations sont induites par un couplage entre quatre phénomènes : (1) la non linéarité du comportement du matériau (viscoélastoplasticité), (2) la non linéarité géométrique en raison des grandes déformations locales, (3) la non linéarité introduite par le contact entre la meule et la pièce, et (4) la dépendance des propriétés des matériaux à la température. L'objectif de cette étude est de construire un modèle numérique fiable en se basant sur la méthode des éléments finis pour analyser les contraintes résiduelles induites par la rectification et d'explorer, par conséquent, les mécanismes en termes de conditions de rectification. Plus précisément, les points suivants sont abordés :

1. étudier la distribution de la température en fonction des paramètres thermiques liés au procédé de rectification et des propriétés thermiques du matériau rectifié (100Cr6 ici),
2. prédire les différentes transformations de phase en fonction de l'histoire thermique vue par le matériau,
3. étudier les contraintes résiduelles pour les conditions de chargement thermique, y compris l'effet du changement de phase,
4. analyser les contraintes résiduelles induites mécaniquement sous des conditions isothermes de rectification,
5. couplage des effets thermiques, mécaniques et métallurgiques dans la prédiction des contraintes résiduelles et
6. proposer les conditions optimales pour la rectification, notamment en terme de contraintes résiduelles.

Le modèle éléments finis a été construit avec le logiciel commercial, Abaqus ® / Standard. Le comportement du matériau étudié (100Cr6) a été défini dans les routines utilisateurs PHASE, PROP, UEXPAN et UMAT. Les routines UMAT et UEXPAN sont disponibles de base dans Abaqus. Elles permettent de définir la loi de comportement des matériaux et le coefficient de dilatation thermique, respectivement. Les routines utilisateurs PHASE et PROP ont été développées pour calculer la proportion des phases en fonction du temps et de la température et leurs effets sur les propriétés thermomécaniques, respectivement. Les températures dues à une source de chaleur en mouvement sont obtenues avec la sub-routine utilisateur DFLUX qui est exploitée pour prévoir la transformation de phase et ensuite la profondeur de la couche martensitique. Afin de résoudre le problème de non linéarité provenant du contact de la meule avec la pièce, un chargement normal et tangentiel de type contact de Hertz a été ajouté aux travers des routines DLOAD et UTRACLOAD. Pour simplifier le problème, deux étapes ont été adoptées. La première consiste à suivre une procédure étudiant séparément les trois phénomènes apparaissant dans le processus de rectification (effets thermiques, les transformations de phase et les effets mécaniques). Les effets ont ensuite été couplés.

La variation des contraintes résiduelles et des déformations aux points d'intégration a été analysée. Les effets du coefficient de frottement (μ), du nombre de Peclet (Pe), de la conductance de paroi (H) et du flux de chaleur (Q) sur la microstructure et l'état de contraintes résiduelles ont été analysés. Enfin, sur la base des nouveaux résultats de ce travail de recherche, une méthodologie plus complète est proposée pour la suite.

MOTS CLES : Rectification, simulation numérique, éléments finis, analyse thermique, analyse mécanique, transformation de phase, paramètres de rectification, contraintes résiduelles, subroutine utilisateur UMAT, acier AISI 52100 (100Cr6)

Laboratoire(s) de recherche : Laboratoire de Mécanique des Contacts et des Structures

Directeur de thèse : Daniel Nelias

Président de jury : Jean Francois RIGAL

Composition du jury Joël RECH, Claire LARTIGUE, Pierre LAGARRIGUE, Michel CORET, Jean François RIGAL, Daniel NELIAS